NEUTRALIZATION MECHANISMS OF HUMAN ANTI-ALPHAVIRUS MONOCLONAL ANTIBODIES

By

Lauren E. Williamson

Dissertation

Submitted to the Faculty of the

Graduate School of Vanderbilt University

in partial fulfillment of the requirements

for the degree of

DOCTOR OF PHILOSOPHY

in

Microbe-Host Interactions

March 31st, 2021

Nashville, Tennessee

Approved By:

Mark R. Denison, M.D. (Chair)

Ivelin S. Georgiev, Ph.D.

Julián F. Hillyer, Ph.D.

Kristen M. Ogden, Ph.D.

James W. Thomas, M.D.

James E. Crowe, Jr., M.D.

To my parents for their unconditional love and support.

ACKNOWLEDGEMENTS

The body of work described here would not have been possible without the financial support from the U.S. Defense Threat Reduction Agency-Joint Science and Technology Office for Chemical and Biological Defense (Grant no. HDTRA1-13-1-0034), CTSA awards UL1 TR000445 and UL1 TR002243 from the U.S. National Center for Advancing Translational Sciences, NIAID grant U19 AI142790, and NIH grants T32 HL069765 and F31 AI145189. Financial support from collaborators was funded from U.S. Defense Threat Reduction Agency-Joint Science and Technology Office for Chemical and Biological Defense (Grant no. HDTRA1-15-1-0047), NIH grants R01 AI095436, S10OD020011, and T32 AI007163. The contents of this document are solely the responsibility of the author and do not reflect the official views of any of these agencies.

Most importantly, I would like to thank Dr. James E. Crowe, Jr. for obtaining the funding sources supporting this body of work and for his mentorship. I am extremely grateful for the support but also freedom he has given me to grow as an independent thinker and a critical scientist. I look up to Dr. Crowe as a role model and he inspires me every day through his humbleness, leadership, and commitment to improving public health through scientific achievement.

Additionally, I would like to thank the mentorship I received from my current and previous committee members: Drs. Mark R. Denison (chair), Ivelin S. Georgiev, Julián F. Hillyer, Kristen M. Ogden, James W. Thomas, and Karen C. Bloch (clinical mentor). I am grateful for the support from each of you and for pushing me forward in my graduate

school career to become a better scientist. I would also like to thank the Department of Pathology, Microbiology, and Immunology at Vanderbilt University and the Vanderbilt Program in Molecular Medicine for providing me with additional training opportunities and clinical experience outside of the laboratory.

During my graduate studies, I interacted with many exceptional collaborators that made the work described in the following chapters a collaborative effort. Throughout this document, I use the pronoun ‘we’ to highlight studies performed by others or in collaboration. I would like to thank Dr. Melanie D. Ohi’s group (including Drs. Pramod Yadav and Clarrisa Durie) at the University of Michigan, Dr. Richard Kuhn’s group (including Dr. Abhishek Bandyopadhyay), and Dr. Elad Binshtein at Vanderbilt University for their expertise, discussion, and work on the cryo-electron microscopy (EM) structural studies described in this document. I’d also like to thank Dr. William B. Klimstra’s group (including Theron Gilliland, Jr.) at the University of Pittsburgh, Dr. Justin G. Julander’s group (including Kevin Bailey) at Utah State University, and Dr. Michael S. Diamond’s group (including Dr. Arthur S. Kim, Dr. Julie M. Fox, Emma Winkler, and Natasha Kafai) and at Washington University for their expertise, providing murine antibody (Ab) and virus reagents, BSL-3 neutralization studies, and/or performance of the animal studies described here in the following chapters. I would like to thank Drs. Edgar Davidson and Benjamin J. Doranz at Integral Molecular (including Mallorie E. Fouch) for testing human anti-alphavirus E1-specific monoclonal Abs (mAbs) for loss-of-binding phenotypes in a chikungunya virus (CHIKV) alanine-mutagenesis library. I would like to thank Dr. Galit Alter’s group (including Vicky Roy) for testing Fc activity of human anti-Eastern equine encephalitis virus (EEEV) and anti-alphavirus E1-

specific mAbs described in chapter IV. I am also grateful for the Vanderbilt University Flow Cytometry Shared Resource facility and the Center for Structural Biology Cryo-EM facility at Vanderbilt University for help with hybridoma cell sorting and EM studies, respectively.

I would like to thank everyone in Dr. Crowe's laboratory and the Vanderbilt Vaccine Center for their mentorship, help, support, and friendship during my graduate studies. I want to personally thank a few people and I apologize in advance for missing anyone since each member of Dr. Crowe's laboratory has contributed in some way to my graduate studies. First and foremost, I would like to thank Dr. Robert H. Carnahan for his administrative help, for pushing me to get out of my comfort zone, and helping me to serve as a role model for women in STEM even before joining the laboratory during my first year in the IGP. Many thanks to Merissa Mayo for her administrative help, project management, and answering all of my questions. Thanks to current and past members Drs. Pavlo Gilchuk, Iuliia Gilchuk, Seth Zost, Matthew Vogt, Elad Binshtein, and Andrew Flyak for your mentorship, expertise, and discussions. Many thanks to members of TechCore, iCore, and Ryan Irving for laboratory management, assistance with Ab and antigen sequencing, or Ab and protein expression. Special thanks to Rachel Nargi and Megan Vodzak for always being there to support me when I needed it the most, not only scientifically but in life. Thanks to Rachel Sutton as well for always making me laugh, brightening my day, and keeping life interesting. A huge shout out to Kristen Reeder for swooping in towards the end of my graduate studies and helping me reach the finish line. A huge thanks to Nurgun Kose for your mentorship on human hybridoma generation, assay development, friendship, and advice. I would also

like to thank my current and previous fellow graduate students (*i.e.*, Nate Chapman, Mike Doyle, Helen Parrington, Monique Bennett, Sandhya Bangaru, Jessica Finn, and Laura Powell) in Dr. Crowe's laboratory for your advice, friendship, and support.

I would like to thank the friends I made during graduate school for an adventure full of great memories. I look forward to the future ones. I would also like to thank my friends back home, especially Kelly, that have supported me and reminded me that there is a reality outside of the scientific community. Lastly, I would like to thank my parents for supporting my decision to go to graduate school and for always allowing me to follow my passions and curiosity. I owe it to you both for teaching me the importance of hard work, perseverance, and that "knowledge is power".

TABLE OF CONTENTS

LIST OF TABLES

LIST OF FIGURES

LIST OF ABBREVIATIONS

Ab	Antibody
Abs	Antibodies
ADCC	Antibody-dependent cellular cytotoxicity
ADCD	Antibody-dependent complement deposition
ADCP	Antibody-dependent cellular phagocytosis
ADE	Antibody-dependent enhancement
ADNKA	Antibody-dependent natural killer cell activation
ADNP	Antibody-dependent neutrophil phagocytosis
BBB	Blood-brain barrier
BLI	Biolayer interferometry
$CCID_{50}$	Cell culture infectious doses
CDC	Centers for Disease Control and Prevention
CDR	Complementary-determining region
CNS	Central nervous system
CHIKV	Chikungunya virus
CPE	Cytopathic effect
Cryo-EM	Cryo-electron microscopy
Cryo-ET	Cryo-electron tomography
DARPA	Defense Advanced Research Projects Agency
DC-SIGN	Dendritic cell-specific intercellular adhesion molecule-3 grabbing non-integrin

D-PBS	Dulbecco’s phosphate buffered saline
D-PBS-T	D-PBS Tween 20
EBOV	Ebola virus
EBV	Epstein-Barr virus
EC_{50}	Half-maximal effective concentration
EEE	Eastern equine encephalitis
EEEV	Eastern equine encephalitis virus
ELISA	Enzyme-linked immunosorbent assay
EVD	Ebola virus disease
EVD68	Enterovirus D68
Fab	Fragment antigen-binding
Fc	Fragment crystallizable
FFA	Focus-forming assay
FFU	Focus-forming units
FRNT	Focus-reduction neutralization test
FSC	Fourier shell correlation
GFP	Green fluorescent protein
GM-CSF	Granulocyte-macrophage colony-stimulating factor
GP	Glycoprotein
Hp	Heparin
HS	Heparan sulfate
IACUC	Institutional animal care and use committee
I.c.	Intracerebral

IC_{50}	Half-maximal inhibitory concentration
IFN	Interferon
IgA	Immunoglobulin A
IgG	Immunoglobulin G
IgM	Immunoglobulin M
I.n.	Intranasal
IND	Investigational New Drug
I.p.	Intraperitoneal
IRF	Interferon regulatory factor
ISG	Interferon-stimulating gene
I.v.	Intravenous
IVIS	*In vivo* imaging system
LDLRAD3	Low-density lipoprotein receptor class A domain-containing 3
L-SIGN	Liver-specific intercellular adhesion molecule-3 grabbing non-integrin
mAb	Monoclonal antibody
mAbs	Monoclonal antibodies
MADV	Madariaga virus
MARV	Marburg virus
MAYV	Mayaro virus
Mxra8	Matrix remodeling associated 8
NHP	Non-human primate
NIH	National Institutes of Health

NPC1	Niemann-Pick C1 protein
NRAMP2	Natural resistance-associated macrophage protein 2
nsP	Nonstructural protein
OD	Optical density
PAMP	Pathogen-associated molecular pattern
PBMC	Peripheral blood mononuclear cells
PBS	Phosphate buffered saline
PFU	Plaque-forming units
PRNT	Plaque reduction neutralization test
PRR	Pathogen recognition receptor
RACE	Rapid amplification of cDNA ends
RBD	Receptor binding domain
RBS	Receptor binding site
RRV	Ross river virus
RT-PCR	Reverse-transcription polymerase chain reaction
RV	Rhinovirus
SARS-CoV	Severe acute respiratory syndrome-associated coronavirus
SARS-CoV-2	Severe acute respiratory syndrome coronavirus 2
S.c.	Subcutaneous
SF	Semliki Forest
SFV	Semliki Forest virus
sGP	Soluble glycoprotein
SIN	Sindbis

SINV	Sindbis virus
TF	Transframe protein
Treg	Regulatory T cells
USDA	United States Department of Agriculture
VEE	Venezuelan equine encephalitis
VEEV	Venezuelan equine encephalitis virus
VLP	Virus-like particle
VLPs	Virus-like particles
WEE	Western equine encephalitis
WEEV	Western equine encephalitis virus
WHO	World Health Organization
WT	Wild-type
ZAP	Zinc finger antiviral protein

CHAPTER I

INTRODUCTION

Dissertation Overview

The body of work described here is a culmination of my dissertation on the characterization of human monoclonal antibodies (mAbs) to several viruses, with particular focus on the neutralization mechanism(s) of human anti-EEEV antibodies (Abs). My dissertation is divided into seven chapters. In chapter I, I provide an overview of Ab isolation techniques and Ab-mediated mechanisms of action against viruses. As the main part of my dissertation, I provide more specific background to give an overview of alphaviruses, including their phylogenetic relationships, epidemiology, pathogenesis, replication cycle, and vaccine developments. I highlight the immune response towards alphaviruses, with an emphasis on the importance of Abs for alphavirus immunity and the mechanism(s) of action utilized by these molecules.

In chapter II, I describe the characterization of human mAbs to multiple virus targets, including Ebola virus (EBOV), Marburg virus (MARV), enterovirus D68 (EV-D68), and SARS-CoV-2 (COV2). In this chapter, I describe ELISA-based and epitope

mapping techniques utilized to characterize mAbs and gain technical expertise with these methods. First, I describe the studies I performed during my rotation project in Dr. Crowe's laboratory to characterize twenty-five previously isolated human anti-EBOV mAbs from early convalescent survivors treated for Ebola virus disease (EVD), in which a paucity of potent neutralizing mAbs was observed. Out of the panel, one mAb (EBOV237), displayed neutralization activity against EBOV and recognized the glycan cap, which may be an important epitope recognized for protection early in the human Ab response to EVD. My initial graduate studies in Dr. Crowe's laboratory focused on isolation of human anti-picornavirus mAbs, including rhinoviruses and enteroviruses. In this chapter, I also describe the ELISA-based optimization methods that contributed to isolation and characterization of human anti-EV-D68 mAbs by Dr. Matthew Vogt. Lastly, within this chapter, I describe the epitope mapping studies I performed to characterize human anti-SARS-CoV-2 mAbs during the COVID19 pandemic. Competition-binding studies revealed three neutralizing antigenic sites on the SARS-CoV-2 spike protein, a majority of which blocked binding of angiotensin-converting enzyme 2 (ACE2) to the receptor-binding domain (RBD).

In chapter III, I describe a panel of neutralizing human anti-Eastern equine encephalitis virus (EEEV) E2-specific mAbs. Potent neutralizing and protective mAbs against EEEV subcutaneous (s.c). and aerosol challenge were isolated from two natural survivors of EEEV infection. Additional mAbs with distinct phenotypes are also described in chapters IV and V. The neutralizing E2-specific mAbs target domains A and B of the EEEV E2 glycoprotein to stabilize trimeric spikes on the surface of intact

virions and inhibit virus entry into host cells. Two extremely potent mAbs, EEEV-33 and EEEV-143, protect against an extremely stringent mouse model involving EEEV aerosol challenge.

In chapter IV, I describe a panel of human E1-specific mAbs. The panel consists of two main groups of binding reactivity: EEEV-specific or cross-reactive (anti-alphavirus). 'Pan-alphavirus' cross-reactive mAbs recognize the highly conserved fusion loop of the E1 glycoprotein. Neutralizing E1-specific mAbs recognize cryptic epitopes on the surface of intact virions that become exposed during virus maturation. Recognition of these exposed epitopes can inhibit virus egress from infected cells. Neutralization and Fc-mediated effector functions may both contribute to protection from subcutaneous (s.c.) EEEV (EEEV-specific) and chikungunya virus (CHIKV) (anti-alphavirus)-induced disease.

In chapter V, I describe a panel of non-neutralizing human E2-specific mAbs. The panel recognizes distinct cryptic epitopes on the EEEV E2 glycoprotein that may account for the non-neutralizing phenotype observed for these mAbs. Two mAbs, EEEV-107 and EEEV-321, recognize EEEV and Venezuelan equine encephalitis virus (VEEV) subtypes. A non-neutralizing EEEV-specific mAb, EEEV-30, protected against highly stringent EEEV aerosol challenge. Studies are still ongoing for further characterization of the Ab-mediated mechanism(s) of action and the contribution these mAbs may have *in vivo*.

In chapter VI, I describe a panel of human anti-VEEV human monoclonal antibodies isolated from vaccinees. A potent neutralizing mAb, VEE-63, neutralized

VEE subtypes IAB and IC. This mAb recognizes domain B of the VEEV E2 glycoprotein and appears to form inter-spike cross-links of the trimeric spikes as a structural mechanism of neutralization. VEE subtype cross-reactivity was also observed by non-neutralizing E2- and E1-specific mAbs. Studies are still ongoing for further characterization of neutralizing epitopes recognized, mechanism(s) of neutralization against SINV/VEEV, and *in vivo* efficacy against SINV/VEEV and VEEV. VEE antigenic complex cross-reactive epitopes also warrant further characterization.

In chapter VII, I summarize the body of work I completed during my dissertation. I also discuss ongoing projects that aim to address additional questions about the human humoral response against alphaviruses. Furthermore, I consider future directions that could be performed either from the advancements I made throughout my dissertation studies or pertain to unanswered questions within the alphavirus human Ab field.

Antibody (Ab) isolation and production techniques

Immunization of mice for murine hybridoma generation

Mice are great tools to assess the immune response against viruses due to the ability to immunize mice with a variety of antigens, including live viruses. Boosting of the immune response against the virus of interest either through virus replication or frequent immunizations aids in the isolation and enrichment of specific B cells from mouse spleens (Crowe, 2017). Differences in the Ab repertoire and immunogenicity of murine

mAbs limits the use of these molecules for the study of natural immune responses and for clinical development against human viruses (Shi et al., 2014; Mestas and Hughes, 2004). The ability to generate transgenic mice with human Ab genes overcomes some of the limitations for Ab clinical use through humanization of mAbs (Lonberg, 2005; Shultz et al., 2011). However, differences still exist that make use of human-derived mAbs better suited for clinical Ab development, such as decreased likelihood of immunogenic responses, greater Ab diversity via more extensive somatic hypermutation, differences in animal pathogenesis and Fc receptor engagement (Shi et al., 2014; Akkina, 2014; Crowe, 2017; Mestas and Hughes, 2004; Corti and Lanzavecchia, 2015).

Human Ab phage display technologies

Phage display libraries are a versatile means to isolate human Abs (Hoogenboom, 2002). Through isolation of mRNA from B cells and cloning into phagemid plasmids through RT-PCR, human Abs can be expressed on the phage coat protein and screened through multiple rounds of functional analyses (Larrick et al., 1989; Clackson et al., 1991; Marks et al., 1991). Isolation of specific Abs can be amplified through *E. coli* infection and further cloned for mammalian expression (Sheehan and Marasco, 2015). Some limitations to the use of phage display libraries include unpaired heavy and light chain sequences and the primer specificity for

amplification of Ab genes (Crowe, 2017; Sheehan and Marasco, 2015; Corti and Lanzavecchia, 2015).

Human hybridoma generation

In the body of work described in the following chapters, the human anti-alphavirus mAbs were isolated through immortalization of immune memory B cells by Epstein-Barr virus (EBV). This approach takes advantage of naturally derived Abs and is target-agnostic. Through infection of B cells with EBV via CD21 and co-stimulatory molecules, such as TLR9-agonist CpG, B cells are maintained *in vitro* and secreting Ab is screened for recognition of many targets or functional analyses. Fusion with a non-secreting myeloma cell partner generates stable human mAb secreting hybridomas (Smith and Crowe, 2015; Traggiai et al., 2004; Lanzavecchia, 2018; Yu et al., 2008a).

Another approach to generate human mAbs involves enrichment of target derived B cells using a fluorescently labeled antigen to sort out these specific cells. This approach is not target-agnostic and has several limitations, including the conformation of the antigen, non-specific interactions, and lack of functional assessment (Corti and Lanzavecchia, 2015). Advances to address some of these concerns include technologies, such as linking B cell receptor to antigen specificity through sequencing (LIBRA-seq). LIBRA-seq enables assessment of multiple antigens through utilization of the diversity of DNA sequence tags to increase throughput and provide paired heavy and light chain sequences for downstream functional analysis (Setliff et al., 2019). All of

these approaches can be utilized to study memory B cells, plasma cells, or plasmablasts from naïve, immune, or infected individuals (Corti et al., 2011; Lanzavecchia, 2018; Crowe, 2017).

Ab-mediated mechanisms of action against viruses

Abs can inhibit viruses through direct recognition of virus particles by hypervariable domains and interact with immune effector cells through the Fc domain. These interactions can prevent virus infection, reduce viral load, and clear viral infection. The specificity, versatility, and *in vivo* efficacy of Abs enables the use of these molecules as useful tools and for clinical development of a number of diseases, including infectious agents, cancer, and autoimmunity (Marston et al., 2018; Lu et al., 2020; Forthal, 2014).

Virus neutralization

Abs can neutralize viruses through direct recognition of mature virus particles or at transitory stages during virus maturation (Forthal, 2014; Pierson and Diamond, 2009). A potential step in neutralization is to prevent virus infection of cells prior to entry. Abs can aggregate virus particles, which can reduce the number of free intact virions and target these immune complexes for clearance by the immune system (Zhang et al., 2020; Thomas et al., 1986). In addition, Abs can block virus engagement with cellular

attachment factors or receptors through direct binding to the receptor binding site or sterically hindering receptor binding (Smith et al., 1993; Lynch et al., 2012). Following virus attachment, Abs can also prevent conformational changes that occur during virus entry and fusion processes necessary for virus infection of host cells (Edwards et al., 2001; Barbey-Martin et al., 2002; Kaufmann et al., 2006). Abs can be internalized into host cells through direct binding to virus particles during virus entry or through Fc receptors (*i.e.,* FcRn) to inhibit virus processes and transcytosis within a cell (Forthal, 2014; Mazanec et al., 1995, Corthésy et al., 2006). Furthermore, Abs can inhibit virus egress through recognition of viral proteins on the surface of infected cells. Direct binding and cross-linking of these proteins by Abs can prevent conformational changes or enzymatic functions necessary for virus budding (Webster and Laver, 1967; Gilchuk et al., 2019). All of these mechanism(s) include some of the many ways in which Abs can neutralize virus infection.

Fc-mediated effector functions

Through the Fc domain, Abs can interact with molecules in circulation and Fc receptors on immune effector cells, such as neutrophils, monocytes/macrophages, and natural killer (NK) cells (Forthal, 2014). The affinity for this interaction depends on the Ab isotype, glycosylation patterns of the Fc domain (N297), and avidity interactions for cross-linking of Fc receptors (Lu et al., 2018; Jennewein and Alter, 2017). Downstream effects can result in lysis or phagocytosis of infected cells. Ab-dependent complement

deposition (ADCD) is one mechanism that involves interaction of Abs with complement molecules (*i.e.*, C1q, mannose-binding lectin), which leads to lysis of infected cells or opsonization of immune complexes for phagocytosis through complement (ADCD) or Fc (Ab-dependent cellular phagocytosis [ADCP]) receptors (Lu et al. 2018). Abs can also interact with Fc receptors on immune effector cells for Ab-dependent cellular cytotoxicity (ADCC). FcγRIIIA expressed on the surface of NK cells can lead to cytolysis of an infected cell through induction of perforin and granzyme production (Lu et al., 2018). Fc modifications, such as afucosylation of N297, increases FcγRIIIA engagement and subsequently enhance ADCC activity (Shields et al., 2002; Jennewein and Alter, 2017). Detrimental effects can also occur through sub-neutralizing Ab binding to virus particles and interactions with Fc receptors via the Fc domain. Incomplete neutralization of virus can result in replication within immune effector cells, which may increase disease severity through Ab-dependent enhancement (ADE) (Narayan and Tripathi, 2020).

Introduction to alphaviruses

Alphaviruses are positive-sense single-stranded RNA viruses that are members of the *Togaviridae* family. Within the *Alphavirus* genus, there are 29 virus species that cause a variety of diseases in humans, vertebrates, and fish (Weaver et al., 2012). The alphavirus genome is ~11.7 kb in length, 5′ capped, and contains a 3′ poly-A tail (**Figure 1**). Two open reading frames encode either the nonstructural or the structural proteins (Strauss and Strauss, 1994). The nonstructural proteins (nsP1-4) participate in

translation, polyprotein cleavage, minus-sense single-stranded RNA synthesis, formation of replication complexes, replication, RNA capping, and host protein shutoff (Weaver et al., 2012; Holmes et al., 2020; Jose et al., 2009). The structural proteins encode the capsid protein, E3 protein, E2 glycoprotein, 6K protein, transframe (TF) protein, and E1 glycoprotein (Yap et al., 2017; Holmes et al., 2020). The structural proteins engage in attachment factor and receptor interactions for virus entry, virus fusion, RNA genome interactions for packaging and assembly of nucleocapsids, and budding of mature virus particles (Holmes et al., 2020; Kielian et al., 2010; Mendes and Kuhn, 2018; Brown et al., 2018).

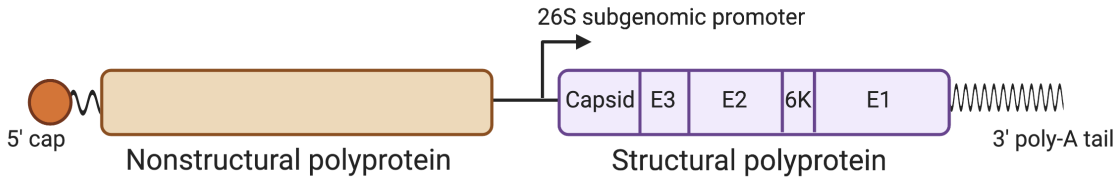

Figure 1. Alphavirus genome organization. Schematic of the ~11 kb alphavirus genome. The genome is a positive-sense single-stranded, RNA molecule that contains a 5' cap and 3' poly-A tail. Two open-reading frames encode either the nonstructural polyprotein (nsPs 1-4; orange) or the structural polyprotein (purple). The structural polyprotein is translated from a 26S subgenomic mRNA, which results from transcription starting at the 26S subgenomic promoter. The main structural proteins encoded include the capsid protein, E3 protein, E2 glycoprotein, 6K protein, and the E1 glycoprotein. During translation a frameshift within the 6K encoding region can result in expression of the transframe (TF) protein. Created with BioRender.com. Based on Leung et al., 2011.

Phylogenetic relationship of alphaviruses

Alphaviruses are taxonomically classified based on antigenic complex, historical geographic distribution (New or Old World), genetic relatedness, or disease state (encephalitic or arthritogenic) (Ronca et al., 2016).

Antigenic complex classification

Alphaviruses were originally taxonomically classified solely based on serologic assays (*i.e.*, neutralization, hemagglutinin inhibition, or complement fixation) as antigenic complexes, or a division of closely related viruses within a serogroup (Young and Johnson, 1969; Calisher, 1994; Calisher et al., 1980; Casals, 1963). Occasionally, mAb binding reactivities also defined antigenic varieties within the antigenic complexes (Rico-Hesse et al., 1988; Roehrig and Bolin, 1997; Broeck and Merrill, 1933; Roehrig et al., 1990). With the advent of genomic sequencing technologies, further classification was performed to complement the serologic assays, in which there are now at least eight antigenic complexes (Eastern equine encephalitis (EEE), Venezuelan equine encephalitis (VEE), Western equine encephalitis (WEE), Semliki Forest (SF), Barmah Forest, Middleburg, Ndumu, and Trocara (Weaver et al., 2005; Weaver et al., 2012). In the following chapters, I will focus on the EEE, VEE, WEE, and SF antigenic complexes in my characterization of the human Ab response to viruses (Eastern equine encephalitis virus (EEEV), Venezuelan equine encephalitis virus (VEEV), Western

equine encephalitis virus (WEEV), Chikungunya virus (CHIKV), and Mayaro virus (MAYV)) within these complexes, of which include some of the principal alphaviruses associated with human disease (**Figure 2**).

Old World alphaviruses

Alphaviruses were broadly defined based on geographic distribution, with the Old World alphaviruses including viruses, such as CHIKV, MAYV, Semliki Forest virus (SFV), and Sindbis virus (SINV), which are generally associated with an arthritogenic disease. Exceptions to this geographic classification include the recent emergence of CHIKV and MAYV in the New World due to global dispersal or divergence from an Old World ancestor, which confuses this classification scheme (Weaver et al., 2012; Powers et al., 2006; Weaver, 2014; Weaver and Forrester, 2015).

CHIKV and MAYV are within the SF antigenic complex. CHIKV consists of four lineages with respective endemic geographic distribution: Asian, Indian Ocean, ECSA: East, Central and South African (ECSA), and West African (Langsjoen et al., 2018; Powers et al., 2000; Powers, 2015; Schneider et al., 2019; Weaver, 2014). The Asian and Indian Ocean lineages are derived from the ECSA lineage. MAYV consists of three genotypes, D, L, and N. Genotype D is ‘dispersed’ throughout South America, while genotype L is ‘limited’ to Brazil, and genotype N is ‘new’ in Peru (Powers et al., 2006; Diagne et al., 2020).

New World alphaviruses

The New World alphaviruses primarily include EEEV, VEEV, and WEEV, which generally cause an encephalitic disease. The EEE complex consists of two viruses, EEEV and Madariaga virus (MADV). There originally were four genetic lineages of EEEV, with lineage I in North America and lineages II-IV in South America (Casals, 1963). However, more comprehensive genomic sequencing of the EEEV lineages led to recent reclassification of the South American lineages as a different virus species, MADV. The VEE complex contains six subtypes (I-VI) and several varieties of subtypes I (IAB and IC-IF) and III (IIIA-C) (Aguilar et al., 2011; Roehrig and Bolin, 1997; Weaver et al., 2012). VEE subtype I is further classified into several varieties (IAB, IC, ID, IE, and IF [Mosso das Pedras virus {IF}]). VEE subtypes II-VI are also classified as Everglades virus (II), Mucambo virus (IIIA-D [Tonate virus {IIIB}]), Pixuna virus (IV), Cabassou virus (V), and Rio Negro virus (VI) (Aguilar et al., 2004; Meissner et al., 1999). The WEE complex consists of WEEV, Highlands J, Buggy Creek, Fort Morgan, Aura, Sindbis, and Whataroa viruses (Weaver et al., 2012; Calisher et al., 1988). There are four lineages of WEEV with two lineages each in North America and South America (Bergren et al., 2014; Weaver et al., 1997).

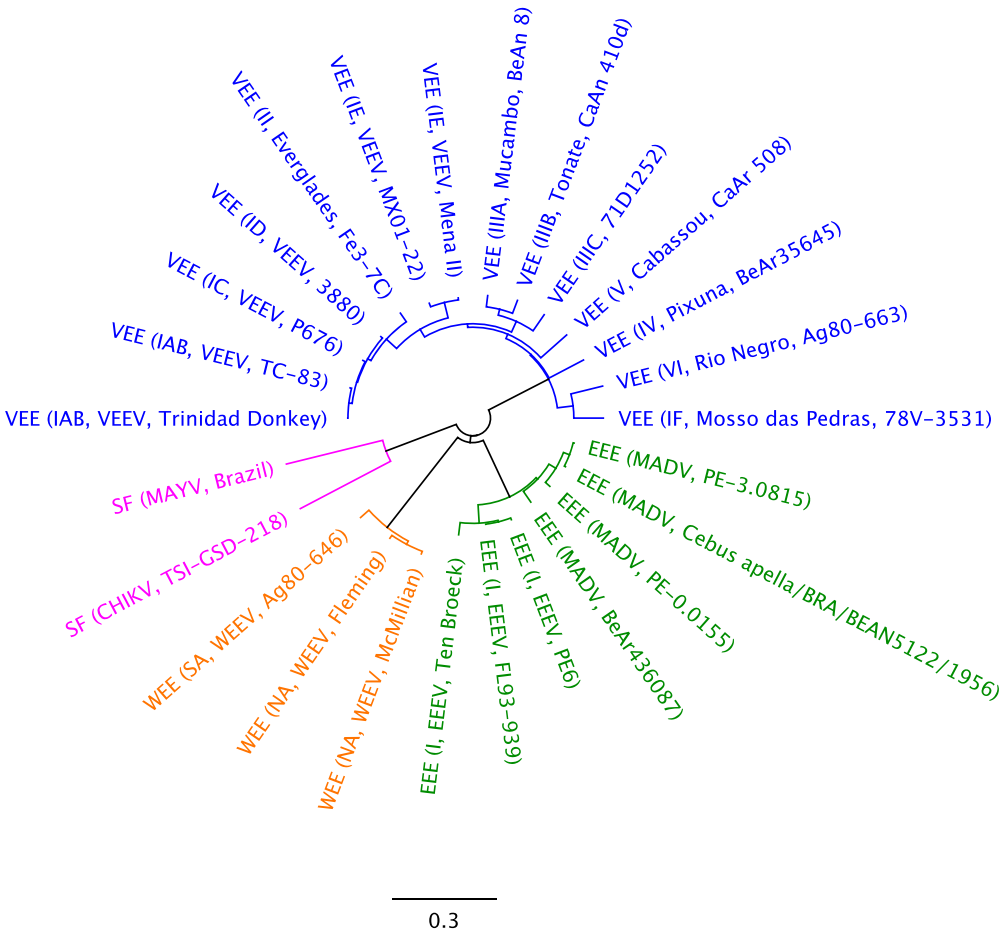

Figure 2. Alphavirus phylogenetic relationships. Phylogenetic tree derived from amino acid sequences of the structural polyproteins for the alphaviruses described in this document. A neighbor-joining method was used, and the scale bar shows 0.3% amino acid sequence divergence. Each node is labeled with antigenic complex (subtype, virus, and strain). Antigenic complex is colored accordingly: Eastern equine encephalitis virus (EEE; green), Venezuelan equine encephalitis (VEE; blue), Western equine encephalitis (WEE; orange), and Semliki Forest (SF; magenta). Created with Geneious version 2020.1 created by Biomatters. Available from https://www.geneious.com.

Epidemiology of alphaviruses

Enzootic and epizootic cycles

Alphaviruses are maintained through cyclic transmission of various susceptible hosts. During mosquito blood feeding, an infected mosquito can transmit the virus to a host via its salivary glands, in which following virus replication the host may establish viremia (Fong et al., 2018). As another mosquito feeds on the infected host, the virus may then be transmitted to the mosquito if the viremia titer is high enough (Calisher, 1994). The enzootic cycle for alphaviruses consists of this cyclic transmission among reservoir or amplifying hosts, such as avian, small mammal, or non-human primate (NHP) species, which helps maintain alphaviruses endemically in different geographical regions and environmental conditions (Weaver et al., 2012). Occasionally, a zoonotic spillover event occurs, such as infection of a bridge vector species (EEEV, MADV, WEEV, MAYV, and CHIKV), virus mutation (VEEV and CHIKV), or human encroachment in endemic areas, which leads to infection of larger mammals (*i.e.*, equines and humans). The resulting event may result in a large number of equine cases, which usually occurs first, or human cases, leading to an epizootic or epidemic (Weaver et al., 2012) (**Figure 3**).

Geographic distribution of alphaviruses corresponds with the patterns of respective mosquito vector species and reservoir hosts for each virus (Weaver et al., 2012; Weaver et al., 2006). In addition, genetic diversity may reflect geographic distribution, such that viruses transmitted by small mammals are less dispersed but are

genetically more diverse compared to virus transmission among avian reservoir hosts (Weaver et al., 2012).

Arthritogenic alphaviruses

The arthritogenic alphaviruses consist of six main viruses that cause human disease: Barmah Forest virus, CHIKV, MAYV, O'nyong-nyong virus, Ross River virus, SFV, and SINV (Mostafavi et al., 2019). These viruses cause an acute and chronic arthritogenic and musculoskeletal disease characterized by rash, arthralgia, myalgia, and joint swelling (Diagne et al., 2020; Mostafavi et al., 2019; Ganesan et al., 2017) (**Figure 3**).

Chikungunya virus (CHIKV)

CHIKV was first isolated in 1952 in East Africa (Robinson, 1955) and is endemic in Africa and Asia. Since 2004, several epidemics (2004: Kenya, 2005-2006: La Réunion island in the Indian Ocean; 2005: India; 2007: Italy; 2010: La Réunion island; 2013-2015: Europe and the Americas; 2016: Central and South America, Kenya, and Europe; 2017: Europe; 2018-2020: Africa and the Americas) have resulted in millions of human cases worldwide (Ganesan et al., 2017; WHO). CHIKV is maintained in the enzootic cycle between *Aedes africanus* and *Aedes furcifer* mosquitos and NHPs in Africa (Jupp et al., 1981; Jupp and McIntosh 1990). Transmission by other *Aedes*

species (i.e., *Aedes aegypti* and *Aedes albopictus*) to humans in urban and rural areas of Africa, India, and Asia can also occur. Humans develop a high enough viremia to continue transmission via mosquitos in these areas, which aids in global dispersal of CHIKV (Weaver et al., 2012). Furthermore, a mutation in the E1 glycoprotein (A226V) was associated with greater infectivity of *Aedes albopictus* mosquitoes, which is thought to play a role in greater transmission of CHIKV among Africa, Asia, Europe, and the Americas (Vazeille et al., 2007; Tsetsarkin et al., 2007; Tsetsarkin and Weaver, 2011). Globally, CHIKV is the most common alphavirus and has caused millions of human cases with <1% human case fatality rate (Mavalankar et al., 2008; Weaver et al., 2012; Jin and Simmons, 2019). CHIKV is normally associated with a debilitating and chronic arthritogenic disease in humans. However more recently, human cases of CHIKV induced encephalitis (~10% human case fatality rate) in children and the elderly have also been reported (Gérardin et al., 2016).

Mayaro virus (MAYV)

MAYV was first isolated in 1954 in Trinidad (Anderson et al., 1957) and has since emerged in the Caribbean and South America, including recent human cases in Brazil and Peru (Aguilar-Luis et al., 2020; Diagne et al., 2020). MAYV is maintained in the enzootic cycle between *Haemagogus* mosquito species and NHPs (Hoch et al., 1981; Diagne et al., 2020). Similar to CHIKV, epidemic potential is of concern as MAYV can infect mosquito species, such as *Aedes* and *Anopheles* (Brustolin et al., 2018). MAYV is

associated with severe athralgia and myalgia in a up to 90% and 75%, respectively, of infected persons (Diagne et al., 2020; Arenívar et al., 2019).

Encephalitic alphaviruses

The encephalitic alphaviruses consist of three main viruses that cause human disease: Eastern equine encephalitis virus (EEEV), Venezuelan equine encephalitis virus (VEEV), and Western equine encephalitis virus (WEEV). These viruses cause a febrile 'flu-like' (malaise, chills, etc.) illness that progresses to an onset of severe headaches, confusion, convulsions, seizures, and subsequently encephalomyelitis, or inflammation of the brain (encephalitis) and spinal cord (myelitis) (Lindsey et al., 2018; Weaver et al., 2012; Honnold et al., 2015; Griffin, 2010) (**Figure 3**).

Eastern equine encephalitis virus (EEEV)

EEEV is one of the most virulent human viruses that occurs geographically in the eastern part of North America and South America (MADV; see below). EEEV has a human case fatality rate of 30 to 75% and up to 90% of survivors develop neurological sequelae (Ronca et al., 2016, Armstrong and Andreadis, 2013; Ayres and Feemster, 1949; Lindsey et al., 2020; Lindsey et al., 2018). The incidence for encephalitis is <5% and on average, eleven human cases are reported each year in the United States since its initial isolation in 1933 (Lindsey et al., 2018; CDC 2020). EEEV is maintained in the

enzootic cycle between *Culiseta melanura* mosquitos and avian (passerine and wading birds) hosts within the eastern part of the United States (Morens et al., 2019; Sherwood et al., 2020; Allison and Stallknecht, 2009). EEEV is transmitted year-round in Florida, which serves as a reservoir for virus maintenance due to optimal weather conditions for mosquito and bird populations (Bigler et al., 1976). Occasionally, infection of a bridge vector mosquito species, (*i.e.*, *Aedes, Coquillettidia, Culex*) leads to transmission of EEEV to equines and humans (Armstrong and Andreadis, 2010; Crans et al., 1986). Humans and equines are considered dead-end hosts since little to no viremia is established upon infection (Lindsey et al., 2018; Weaver et al., 2012; Griffin, 2016). However, an increase in detection of EEEV in mosquito population pools that feed on humans (Mitchell et al., 1992; Sherwood et al., 2020), however, raises concern for zoonotic spillover events. As observed in 2019, an outbreak occurred with 38 reported human cases and 19 deaths with widespread geographical incidence, which lead to concern for EEEV as another potential emergent arbovirus in the United States (Lindsey et al., 2020; Morens et al., 2019; CDC 2020). Fortunately, in 2020, fewer reported human cases (9) were observed (CDC 2020).

Madariaga virus (MADV)

Madariaga virus (MADV) (formally the South American lineages II-IV of EEEV) occurs in Central and South America. Epizootics of equine disease have occurred since the 1930s (Weaver et al., 2012; Arrigo et al., 2010; Carrera et al., 2013). However, in

comparison to EEEV in North America, <12 human cases have been reported in South America, a majority of which occurred during an outbreak in Panama in 2010 (Aguilar et al., 2007; Carrera et al., 2013; Carrera et al., 2020). Additionally, human cases of MADV have been described in Haiti as well during 2015-2016 (Lednicky et al., 2019). The increase in MADV human cases suggests circulation of MADV with most cases asymptomatic as observed 2-5% seropositivity occurs to MADV (Aguilar et al., 2007; Carrera et al., 2013; Carrera et al., 2020). Not as much is known about the maintenance of MADV in mosquito populations and animal reservoir hosts. However, it is thought that MADV is maintained between *Culex* species and small mammals or birds in Central and South America (Weaver et al., 2012; Calisher, 1994).

Venezuelan equine encephalitis virus (VEEV)

VEEV is highly morbid and has a relatively low human case fatality rate (~1%) and incidence of encephalitis (up to 15%) (Hunt et al., 2010; Ronca et al., 2016; Weaver et al., 2012). VEEV was first isolated in 1938 and since then several epidemics and epizootics resulting in hundreds of thousands of VEEV human and equine disease cases, respectively, have occurred in North, Central, and South America due to the epizootic subtypes IAB and IC (Young and Johnson, 1969; Aguilar et al., 2011; Goodchild et al., 2011; Ronca et al., 2016; Weaver et al., 2004; Weaver et al., 2012; Aguilar et al., 2004). The enzootic subtypes (ID-F, II-VI) also cause animal and human disease, with a lower number of cases annually (tens of thousands), in Central and

South America (Aguilar et al., 2011; Forshey et al., 2010; Quiroz et al., 2009; Weaver et al., 2012; Aguilar et al., 2004).

VEEV is maintained in the enzootic cycle between *Culex* species and small mammals in Central and South America (Weaver et al., 2012; Calisher, 1994). In contrast to the other encephalitic alphaviruses, virus mutations can lead to adaptation of susceptibility in different mosquito species (*i.e.*, *Aedes*, *Psorophora*). This can result in greater widespread transmission of VEEV, increase mosquito feeding host range (*i.e.*, large mammals), and subsequently lead to an epizootic or epidemic of VEEV cases. Furthermore, large mammals, such as equine and humans, develop a high tittered viremia, which enables further transmission of VEEV from horses or humans to mosquitos (Walton et al., 1973; Walton and Grayson, 1988; Wang et al., 2001; Weaver et al., 2012).

Western equine encephalitis virus (WEEV)

WEEV is a recombinant virus of a Sindbis (SIN)-like virus and an EEE-like virus that occurs geographically in the western part of North and South America, from Canada to Argentina (Hahn et al., 1998; Calisher, 1994). WEEV is maintained in the enzootic cycle between *Culex tarsalis* mosquitoes and small mammals (rodents) or birds (Weaver et al., 2012; Calisher, 1994). WEEV was initially isolated in 1930 from infected horse brains during an epizootic outbreak of an estimated 6,000 horses in San Joaquin Valley, California (Calisher, 1994). Sporadic epizootics of WEEV have been

described since 1908 in Argentina. However, cases of WEEV in North America have seemingly disappeared, as the last documented human case was reported in 1994 and virus presence amongst mosquito pools has not been detected since 2008 (Bergren et al., 2014; Bergren et al., 2020). WEEV has a human case fatality rate of 3 to 15% and up to 30% of survivors may develop neurological sequelae (Bergren et al., 2014; Bergren et al., 2020; Ronca et al., 2016; Allison and Stallknecht, 2009). WEEV strains in North America are often more frequent and severe agents of human disease in comparison to South American strains (Calisher, 1994). Similar to EEEV, little to no viremia is established upon infection, suggesting infection of humans and equines are dead end hosts (Weaver et al., 2012; Griffin, 2016).

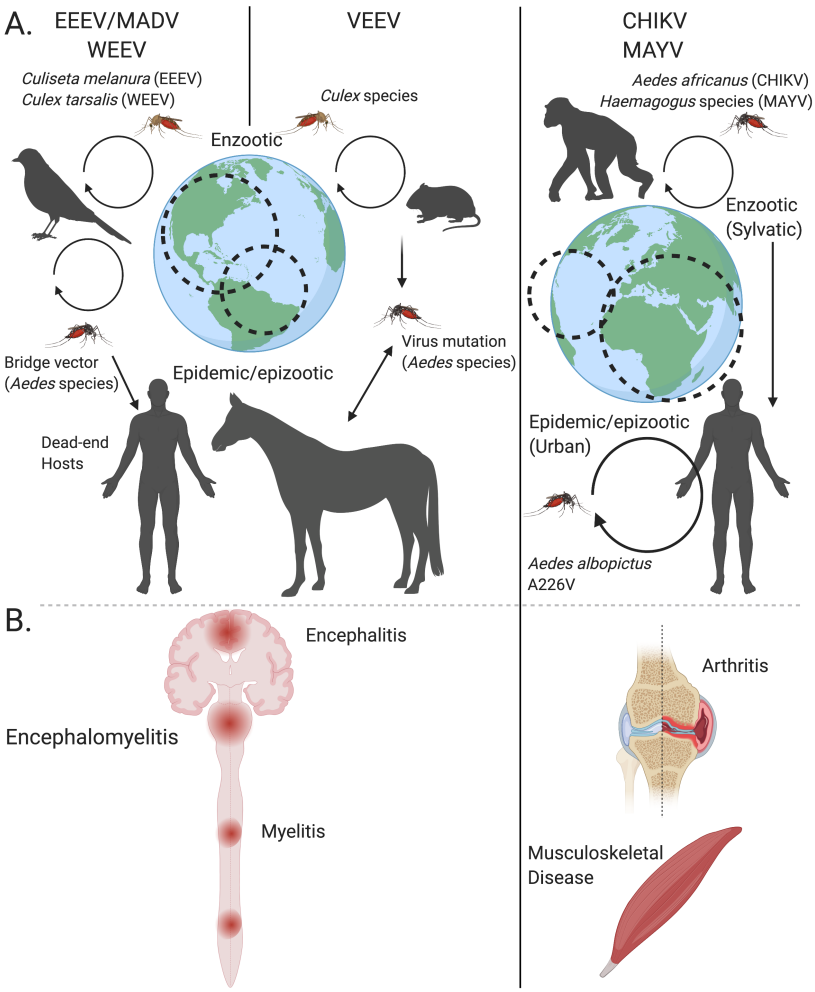

Figure 3. Epidemiology of alphaviruses. A. Transmission cycles for encephalitic (EEEV, MADV, VEEV, and WEEV) and arthritogenic (CHIKV and MAYV) alphaviruses. EEEV, MADV, WEEV, and VEEV are maintained in the enzootic cycle by mosquito (*i.e.*, *Culiseta melanura* and *Culex* species) transmission in primary reservoir hosts, such as birds (EEEV and WEEV) or small mammals (MADV, WEEV and VEEV). Transmission of EEEV, MADV, or WEEV to human-feeding mosquito species (*i.e.*, *Aedes* species) leads to greater transmission of the virus during an epizootic cycle. As a result, infection of equines and humans can occur, which are considered dead-end hosts. In contrast, greater transmission of VEEV by human-feeding mosquito species (*i.e.*, *Aedes* species) acquired by virus mutation can lead to infection of equine and humans with a high tittered viremia for further mosquito transmission. CHIKV and MAYV are maintained in the enzootic (or sylvatic) cycle via mosquito (*i.e.*, *Aedes* and *Haemogogus* species, respectively) transmission in rural areas and NHPs. Human presence in these rural areas or greater mosquito transmission (*i.e.*, E1 A226V mutation) can result in widespread dispersal and greater infection of humans (epidemic/epizootic/urban). Dotted circles on the globes indicate endemic areas for each virus (Eastern United States [EEEV]; Central and South America [MADV]; Western United States, Central, and South America [WEEV]; Central and South America [VEEV]; Africa, Southeast Asia, Europe, the Americas [CHIKV]; Europe, Central and South America [MAYV]). **B.** Cartoon depiction of human disease for the New World (EEEV, MADV, VEEV, and WEEV) or Old World (CHIKV and MAYV) alphaviruses. New World alphaviruses are associated with causing an encephalomyelitis disease, which can result in

inflammation of the brain (encephalitis) and spinal cord (myelitis). Old World alphaviruses are primarily associated with a debilitating arthritogenic and musculoskeletal disease. The figure was created with BioRender.com. Based on Weaver et al., 2012; Diagne et al., 2020.

Bioterrorism classification of alphaviruses

In addition to natural transmission by mosquito vectors, aerosolization of alphaviruses is of concern in the context of laboratory acquired infections and bioterrorism. During the cold war, VEEV was developed as a biological weapon (Hawley and Eitzen, 2001). The highly infectious nature of the encephalitic alphaviruses via the aerosol route (Reed et al., 2004; Phillpotts, 2006; Honnold et al., 2015; Hanson et al., 1967) and the absence of treatment options (Morens et al., 2019) is concerning for these viruses as bioterrorism agents, such that several alphaviruses are classified as NIAID Category B priority pathogens (*i.e.*, EEEV, VEEV, WEEV, and CHIKV) and USDA/CDC Select Agents (*i.e.*, EEEV and VEEV) (Weaver et al., 2012; Sidwell and Smee, 2003).

Alphavirus pathogenesis and immunity

Pathogenesis

Naturally, alphavirus pathogenesis begins after a mosquito bites a host and releases virus as it salivates. Infection then occurs at primary sites of replication, which involves multiple cell types, such as fibroblasts, epithelial cells, osteoblasts, or resident dendritic cells (Sourisseau et al., 2007; Gardner et al., 2008; Vogel et al., 2005). Alphavirus infection of dendritic cells leads to virus uptake to the draining lymph nodes. Replication within these primary tissues results in induction of a proinflammatory immune response that accounts for the clinical symptoms of malaise, fever, chills characteristic of prodromal disease. Eventually following virus replication at these primary sites, viremia is established, in which alphaviruses can spread throughout the body and infect secondary sites of replication specific to their host cell tropism (*i.e.*, skeletal and muscle cells for the arthritogenic alphaviruses and neurons of the brain and spinal cords for the encephalitic alphaviruses) (Schwartz and Albert, 2010; Kam et al., 2009). Animals, such as mice, hamsters, guinea pigs, and NHPs, can model natural infection through s.c. inoculation of alphaviruses (Honnold et al., 2015). In addition to natural infection, aerosolization is of concern for alphaviruses as bioterrorism agents and laboratory acquired infections. Aerosol or intranasal (i.n.) alphavirus inoculation of animals via these routes can serve as models for biodefense and are generally more virulent models than s.c. inoculation (Honnold et al., 2015; Phelps et al., 2019; Cirimotich et al., 2017).

Musculoskeletal Disease

Following dissemination to secondary sites of replication, arthritogenic alphaviruses can infect bone, muscle, synovial, and connective tissues leading to acute and chronic joint (arthralgia) and/or muscle (myalgia) pain. Acute disease appears to result from virus-induced cytolysis, induction of a proinflammatory cytokines, and infiltration of immune cells (*i.e.*, macrophages) to these sites (Suhrbier and Mahalingam, 2009; Assunção-Miranda et al., 2013; Gardner et al., 2010; Hawman et al., 2013). Similarly, chronic disease can result due to persistent virus presence, in which the continual induction of an inflammatory response results in tissue damage (Assunção-Miranda et al., 2013). Macrophage depletion studies did not show as severe disease symptoms or prominent levels of proinflammatory cytokines, which highlights the importance of macrophages in arthritogenic alphavirus pathogenesis (Lidbury et al., 2008). Furthermore, $CD4^+$ T cells contribute to greater inflammation and virus persistence in these tissues (Teo et al., 2013).

Neuropathology

The mechanism in which encephalitic alphaviruses enter the central nervous system (CNS) is not fully understood. This appears to depend on the route of infection and presence of the innate immune response (*i.e.*, type I interferons (IFN)) to limit virus replication in certain cell types (Cain et al., 2017; Salimi et al., 2020; Honnold et al., 2015; Gardner et al., 2008). The blood-brain barrier (BBB) serves as a blockade to prevent unwarranted molecules, including pathogens, to cross into the CNS (Cain et al.,

2017; Daneman and Prat, 2015). Integrity of the BBB is of importance to maintain this. However, it appears in studies with VEEV, virus can infect the CNS without directly affecting BBB permeability (Cain et al., 2017). Instead, BBB permeability becomes leaky as a result of an antiviral inflammatory response for recruitment and infiltration of immune cells (Cain et al., 2017). S.c. inoculation of mice with EEEV shows virus replication at the site of inoculation, such as fibroblasts and skeletal muscle cells, and is thought to spread via a hematogenous route to the CNS (Vogel et al., 2005; Honnold et al., 2015). In contrast, s.c. inoculation of mice with VEEV appears to result in CNS infection through the olfactory neuroepithelium (Charles et al., 1995; Ryzhikov et al., 1995). Aerosol and i.n. inoculation of mice with EEEV and VEEV suggests direct virus infection of the olfactory bulb through infection of olfactory neurons in the nasal cavity (Honnold et al., 2015; Cain et al., 2017; Phelps et al., 2019).

Similar to musculoskeletal disease, studies have also shown that neuronal damage that leads to clinical symptoms, such as headaches, seizures, confusion, and death, characteristic of encephalitic alphavirus pathogenesis is not only due to virus-induced cytolysis of neurons but from the immune response (*i.e.*, T-cell) itself (Rowell and Griffin, 2002; Griffin, 2016). One factor that attributes to neuronal cell death and disruption of the BBB involves infiltration of Th17 cells producing IL-17, GM-CSF, IL-22, and granzyme B (Kulcsar et al., 2014; Griffin, 2016). In addition, cytolytic $CD8^+$ T cells in the CNS can also contribute to neuronal damage (Kulscar et al., 2015). Absence of T regulatory cells (Tregs) producing IL-10, which can downregulate Th17 cells, leads to a more rapid onset of encephalomyelitis (Kulcsar et al., 2014; Kulscar et al., 2015).

Altogether, this suggests that regulation of the immune response is of key importance for survival and prevention of neurological damage during encephalitic alphavirus infections.

Innate immunity

The interferon response (IFN) plays a key role in the innate immune response to limit alphavirus replication early during infection (Carpentier and Morrison, 2018; Gardner et al., 2012) (**Figure 4**). This is supported by the observation that *Ifnar1*$^{-/-}$ mice develop more severe disease (Gardner et al., 2012; Couderc et al., 2008; Grieder and Vogel, 1999; Ryman et al., 2000). Cells respond to alphaviruses through recognition of pathogen-associated molecular patterns (PAMPs) by pattern recognition receptors (PRRs) (Carpentier and Morrison, 2018). PAMPs, such as single-stranded and double-stranded RNA, recognized by PRRs (*i.e.*, TLR-3 [Her et al., 2015], TLR-7 [Neighbours et al., 2012], TLR-8, RIG-I, and MDA-5 [Akhrymuk et al., 2016]) can activate interferon regulatory factors (IRFs; IRF3 and IRF7 [Schilte et al., 2012; Rudd et al., 2012]) for induction of type I interferon (IFNα/β) production (Carpentier and Morrison, 2018). IFNα/β in turn activate IFN-stimulated genes (ISGs), such as IFITM3, 2′3′-oligoadenylate synthetase, IFIT1, zinc finger antiviral protein (ZAP), and ISG-15 in response to infection (Carpentier and Morrison, 2018). IFITM3 interferes with virus fusion with the endosomal membrane (Poddar et al., 2016). Several IFN stimulated proteins (*i.e.*, 2′3′-oligoadenylate synthetase [Bréhin et al., 2009], IFIT1 [Reynaud et al.,

2015], and ZAP [Bick et al., 2003]) appear to inhibit alphavirus translation (Carpentier and Morrison, 2018).

In addition to the IFN response, proinflammatory cytokines (*i.e.*, IL-1, IL-6, IFNγ and TNF-α) are produced in response to alphavirus infection, which as previously mentioned can contribute to pathogenesis (Suhrbier and Mahalingam, 2009; Gardner et al., 2010). In addition to tissue damage, vascular and BBB permeability occurs in response to these cytokines to enable infiltration of effector cells, such as neutrophils, monocytes/macrophages (Salimi et al., 2020). These cells are targeted to the appropriate tissues through upregulation of chemokines (*i.e.*, IL-8, RANTES, MCP-1, IP-10, MIP-1) (Assunção-Miranda et al., 2013). CCL2 (MCP-1) is a key chemokine for recruitment of monocytes and macrophages to target tissues (*i.e.*, joints and brain) (Suhrbier and Mahalingam, 2009; Gardner et al., 2010). CXCL10 (IP-10) leads to recruitment of Tregs, B cells, and $CD4^+$ T cells into the CNS (Baxter and Griffin, 2016; Kulcsar et al., 2015). A balance between activation of immune effector cells to control virus replication and damage resulting from an inflammatory response is important.

Immune evasion

Alphaviruses also exhibit mechanisms to evade the innate immune response. Since alphaviruses infect a wide variety of cell types, differences in cell tropism may account for differences in pathogenesis, virulence, and ability to establish viremia (Griffin, 2016; Gardner et al., 2008). An example of this is observed by preferential

replication of EEEV and WEEV in mesenchymal lineage cells and limited replication in myeloid lineage cells (Gardner et al., 2008; Honnold et al., 2015; Vogel et al., 2005; Trobaugh et al., 2019). Infection of myeloid cells occurs but replication is halted, which in turn minimally induces type I IFN (alpha/Beta) stimulation as a potential mechanism to evade the innate immune response (Gardner et al., 2008). The presence of microRNA, miR-142-3p, in myeloid cells binds to the 3′ untranslated region (UTR) of the virus genome and limits replication of EEEV and WEEV in these cells (Trobaugh et al., 2019). In contrast, VEEV readily infects cells of both lineages, in which virus is brought to draining lymph nodes, and replication induces a substantial innate immune response (Gardner et al., 2008). VEEV exhibits partial resistance to IFN by the secondary structure of the 5' UTR of the RNA genome since mutations in this region increase virus susceptibility to IFN (White et al., 2001; Hyde et al., 2014). Virus evasion from the IFN response further implicates its importance in immunity against alphavirus infection.

Adaptive immunity

During the early stages (~1 day) of virus infection, a virus-specific IgM response can be detected in serum (Calisher et al., 1985; Schwartz and Albert, 2010). The presence of IgM is usually specific to homologous virus and thus, can be used to diagnosis disease (Calisher et al., 1985). IgG and IgA responses are induced ~7-14 days after infection and can be maintained for years (Calisher et al., 1985; Schwartz and Albert, 2010) (**Figure 4**). In addition to Abs, a T cell response aids in clearance of

virus and protection from infection (Yun et al., 2009). The T cell response generally involves a $CD4^+$ Th1 response, in which a proinflammatory response induces production of IFNγ to activate macrophages and stimulate B cell maturation (Lum et al., 2013; Paessler and Weaver, 2009). $CD8^+$ T cells are also involved in clearance of virus infected cells. However, cytolysis contributes to pathogenesis (Kulscar et al., 2015). To balance this response T-regs are also important to suppress the inflammatory response through production of IL-10 (Paessler and Weaver, 2009; Kulscar et al., 204; Kulscar et al., 2015).

The adaptive immune response aids in the clearance of infectious virus and maintenance of viral RNA (**Figure 4**). In synovial tissues, CHIKV can persist leading to chronic disease. Greater persistence is observed in *Rag1*$^{-/-}$ and μMT mice, which suggests the adaptive immune response (*i.e.*, B cells) helps control the continual replication of CHIKV in these tissues (Lum et al., 2013; Hawman et al., 2013). Furthermore, continual need for response is detected by induction of IgM during persistent infections (Lum et al., 2013).

Sindbis virus (SINV) is a prototypic alphavirus used to study alphavirus induced encephalomyelitis in mice (Levine et al., 1991; Schmaljohn et al., 1983; Griffin et al., 1997; Griffin, 2010; Griffin, 2016). Clearance of infectious virus was found to involve cooperation between IFNγ secreting $CD8^+$ and $CD4^+$ T cells and Ab production from B cells (Griffin, 2010). Further studies described the time course of persistent SINV infection of neurons (Griffin, 2010; Metcalf and Griffin, 2011). First, clearance of infectious virus from infected neurons is mediated by IFNγ secreting $CD8^+$ T cells and

IgM secreting B cells that infiltrate into the brain parenchyma within 3 to 7 days post-infection (Griffin, 2010; Metcalf and Griffin, 2011; Tyor and Griffin, 1993). Further clearance of viral RNA is mediated by infiltration of IFNγ secreting $CD4^+$ T cells and IgG secreting B cells (plasmablasts or memory B cells) approximately 5 to 60 days post-infection (Griffin, 2010; Metcalf and Griffin, 2011). Since neurons are terminally differentiated, survival depends on prevention of neuronal cell death. Thus, non-cytolytic mechanisms are essential to control virus replication in neurons (Griffin, 2016; Griffin, 2010). A caveat to non-cytolytic mechanisms is the persistence of viral RNA and continual need for an immune response (Griffin, 2010; Fragkoudis et al., 2018). To continue to inhibit reactivation of persistent viral RNA, immune cells, such as SINV-specific IgG and IgA secreting B cells, are retained in the brain parenchyma for at least one-year post-infection (Tyor et al., 1992; Metcalf and Griffin, 2011; Griffin, 2010).

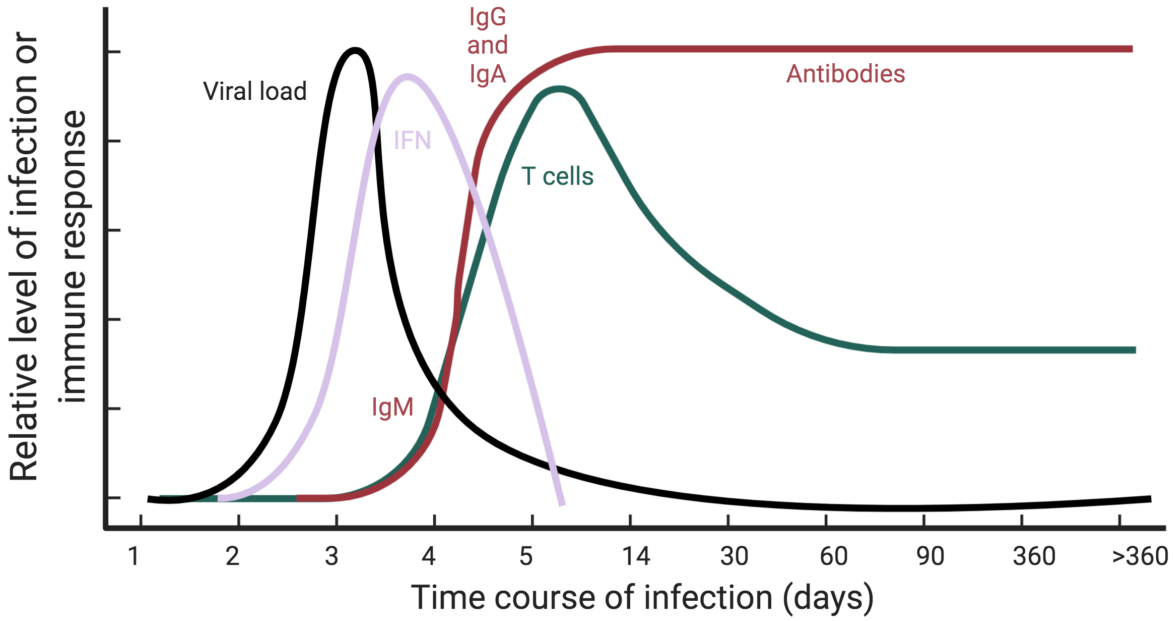

Figure 4. Time course of alphavirus pathogenesis and host immune response to infection. Viral load (black) increases as virus replication occurs in primary and secondary sites of infection. In response to replication, a type I IFN response (purple) is produced, which helps limit virus replication early during infection and while an adaptive immune response develops. IgM Abs can be detected 3-4 days after infection and $CD8^+$ T cells engage in cytolysis of infected cells. A $CD4^+$ Th1 response leads to production of IFNγ to activate macrophages and induce class switching and somatic hypermutation for production of an IgG and IgA response within 7-14 days. The Ab response persists for months to years following virus infection. In this case, viral load is reduced but may persist if immune mediated control were to decline. Created from BioRender.com. Based on Schwartz and Albert, 2010.

Vaccines for alphavirus prevention and treatment

To date, no human vaccines or antiviral drugs are approved for public use to protect or treat alphavirus infection (Morens et al., 2019; Trobaugh et al., 2019). Several approaches have been tried as potential candidates or are currently ongoing clinical trials. Experimental vaccines are available as investigational new drugs (INDs) through the U.S. Army Special Immunizations Program for at-risk laboratory workers and military

personnel but given reactogenicity and/or poor immunogenicity these vaccines are not approved for public use (Trobaugh et al., 2019; Ronca et al., 2016).

Live attenuated vaccines are immunogenic and protective for several alphaviruses, including CHIKV (TSI-GSD-218 [181/25]), VEEV (TC-83)) (McClain et al., 1998; Edelman et al., 2000; Levitt et al., 1986). Attenuation usually occurs through passaging in *in vitro* cell culture systems to acquire attenuating mutations. The vaccine strain for VEEV, TC-83 (IAB subtype), was attenuated following passage of the VEEV Trinidad Donkey strain (IAB subtype) in guinea pig heart cells (Berge et al., 1961). The VEEV TC-83 vaccine, however, is reactogenic and in 15 to 30% of vaccinees, they develop febrile symptoms (Ronca et al., 2016; McKinney et al., 1963). Another method of attenuation includes the generation of chimeric viruses, in which the nonstructural proteins are encoded by one virus (*i.e.*, SINV and the mosquito-host restricted Eilat virus [EILV]) and the structural proteins (*i.e.*, CHIKV, EEEV, VEEV, and WEEV) are encoded by another virus (Erasmus et al., 2017; Atasheva et al., 2009; Sun et al., 2014). This has been shown for several alphaviruses to elicit neutralizing Ab responses for protection of mice and NHPs against alphavirus infection (Wang et al., 2011; Atasheva et al., 2009; Wang et al., 2008; Roy et al., 2013). These viruses also serve as a great tool for use of these BSL-3 viruses under BSL-2 conditions as described in my studies on alphaviruses in the following chapters.

To decrease the risk of *in vivo* reactogenicity, *in vivo* reversion, or mosquito transmission (Pittman et al., 1996; Aguilar et al., 2011; Passler and Weaver, 2009), formalin-inactivated vaccines are another vaccination strategy. However, these

vaccines (VEEV [CA-84], CHIKV]) frequently require boosting and inactivation methods can disrupt the antigenic structures recognized by Abs (Jahrling and Stephenson, 1984; Tiwari et al., 2009; Trobaugh et al., 2019).

Another approach involves the use of virus-like particles (VLPs), which are non-infectious molecules that structurally resemble intact virions (Noranate et al., 2014; Ko et al., 2019). Transfection of the alphavirus structural polyprotein in mammalian expression vectors produces VLPs. CHIKV VLPs were shown to elicit immunogenic responses in NHPs for protection (Akahata et al., 2010; Metz et al., 2013) and were safe and tolerable in Phase I clinical trials (Chang et al., 2014). A trivalent VLP vaccine for EEEV, VEEV, and WEEV that protects all three viruses in NHPs recently completed Phase I clinical trials (Ko et al., 2019). Purified IgG from immunized animals with CHIKV, EEEV, VEEV, and WEEV VLPs, protected mice from challenge, which supports the immunogenicity of these vaccines (Akahata et al., 2010; Ko et al., 2019).

DNA and mRNA-based vaccination strategies through intramuscular administration have also been pursued. The feasibility of nucleic acid amplification greatly enhance the speed and readiness necessary to generate vaccines. DNA vaccines encoding the alphaviruses structural proteins can induce neutralizing Abs for protection in mice and NHPs against CHIKV infection (Muthumani et al., 2008; Mallilankaraman et al., 2011). Administration of multiple DNA vaccines together was shown to protect mice against EEEV, VEEV, and WEEV (Dupuy et al., 2018). A mRNA CHIKV vaccine has also been shown to be safe and immunogenic in Phase I clinical trials (Shaw et al., 2019). Furthermore, Abs can also be expressed in mRNA vectors for

administration. A potent neutralizing human anti-CHIKV mAb, CHKV-24, protects against CHIKV infection in mice expressed as either mAb or lipid-encapsulated mRNA (Kose et al., 2019), which during Phase I clinical trials was safe, tolerable, and showed significant expression of CHKV-24.

Alphavirus structure

Alphaviruses have *T* = 4 quasi-icosahedral symmetry, in which there are 60 quasi-threefold ("q3") and 20 icosahedral-threefold ("i3") trimeric spikes, with each spike consisting of three E1 and E2 glycoprotein heterodimers (Fox et al., 2015; Long et al., 2015; Porta et al., 2014; Voss et al., 2010; Li et al., 2010; Zhang et al., 2011; Chen et al., 2020). Each heterodimer interacts with the capsid protein underneath the viral membrane by the cytoplasmic tail of the E2 glycoprotein (Zhang et al., 2011; Brown et al., 2018; Byrd et al., 2019; Sun et al., 2013). The E2 glycoprotein projects radially from the viral surface and forms the tip of the trimeric spike, whereas the E1 glycoprotein lies tangential to the virus membrane (Mukhopadhyay et al., 2006; Zhang et al., 2011). Structural analyses, such as cryo-EM and X-ray crystallography, have elucidated the structural organization of the structural proteins (**Figure 5**).

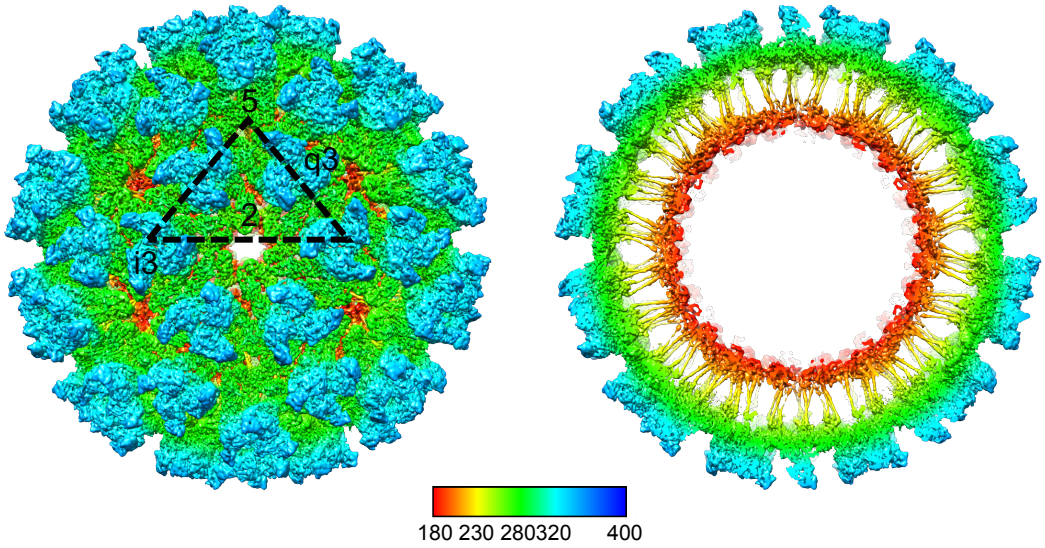

Figure 5. Alphavirus virion structure. Cryo-EM reconstruction of EEEV virus-like particle (VLP) (PDB ID: 6XO4) showing radially colored surface representation of full (left) and cross-section (right) of the map. Icosahedral symmetry is indicated on the left structure and labeled accordingly with the 5-fold, 3-fold ("q3 and i3"), and 2-fold axes. On the virus surface, 80 trimeric spikes can be observed, with 60 "q3" and 20 "i3" spikes. The E2 glycoprotein (relative color is light blue) projects out from these spikes, forms heterodimers with the E1 glycoprotein (relative color is green), and interacts with the capsid protein (relative color is orange) underneath the viral membrane (relative color is yellow). The E1 glycoprotein lies tangential to the viral membrane. Modified from Williamson et al., 2020.

E3 protein

The E3 protein is an α/β protein (β-hairpin with three α-helices) that makes contacts with the acid-sensitive β-ribbon connector region of the E2 glycoprotein via the α-helices to help stabilize E2 domains A and B (Voss et al., 2010). A N-linker helps tether the E3 protein to domain A of the E2 glycoprotein, further stabilizing the heterodimer (Voss et al., 2010).

E2 glycoprotein

The E2 glycoprotein contains three main Ig-like domains: domain A (a central domain thought to mediate receptor binding), domain B (a flexible domain that occludes the fusion loop at the distal tip of the E1 glycoprotein under neutral pH conditions), and domain C (connects to the transmembrane helices, may be involved in host recognition, and contains a cryptic glycosylation motif for EEEV) (Hasan et al., 2018; Voss et al., 2010; Li et al., 2010; Kielian et al., 2010) (**Figure 6**). A subdomain (D-loop), or the membrane-proximal or stem region, is also present and is implicated in virus budding (Zhang et al., 2011; Byrd and Kielian, 2017; Chen et al., 2018). Furthermore, an acid-sensitive β-ribbon connector region links domain A to domains B and C, which helps to aid stabilize domain B at neutral pH (Voss et al., 2010; Fields and Kielian, 2013).

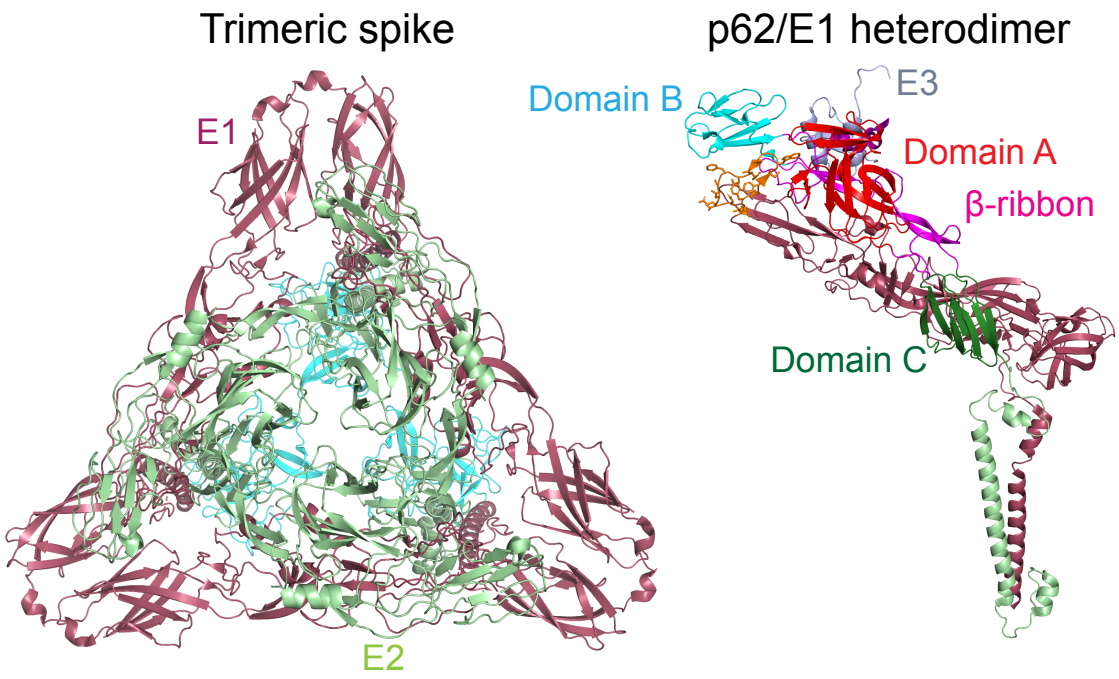

Figure 6. Alphavirus E2 glycoprotein structure. Cartoon representation of a SINV/EEEV (PDB ID: 6MX4) trimeric spike (left) and VEEV (PDB ID: 3J0C and 3J0G) p62E1 heterodimer (p62: E3E2; right) complex. In the trimeric spike, the E2 glycoprotein (green), E1 glycoprotein (red), and capsid protein (cyan) are indicated. The E2 glycoprotein projects out from the trimeric spike. In the p62E1 heterodimer, the E3 protein (lavender), E2 domains (domain A [red], domain B [cyan], domain C [dark green], and β-ribbon [magenta]), and the E1 fusion loop (orange) are colored to highlight these distinct regions. Based on Hasan et al., 2018 (open access); Zhang et al., 2011. Copyright permission from publisher John Wiley and Sons.

E1 glycoprotein

The E1 glycoprotein is a class II fusion protein and consists of three β-sheet structural domains: domain I (central domain), domain II (contains a highly conserved fusion loop at its distal tip), and domain III (Ig-like fold that connects to the stem region and transmembrane domain via C-terminus and contains an exposed glycosylation motif for EEEV) (Hasan et al., 2018; Gibbons et al., 2004; Lescar et al., 2001;

Mukhopadhyay et al., 2006; Roussel et al., 2006; Kielian, 2014). Two main interdomains are present, the flexible hinge region (connects domain I to domain II) and a linker region (connects domain I to domain III) (Lescar et al., 2001; Roussel et al., 2006; Sahoo et al., 2020; Kielian, 2014). The fusion loop is occluded between domains A and B of the E2 glycoprotein (Kielian, 2014; Voss et al., 2010) (**Figure 7**).

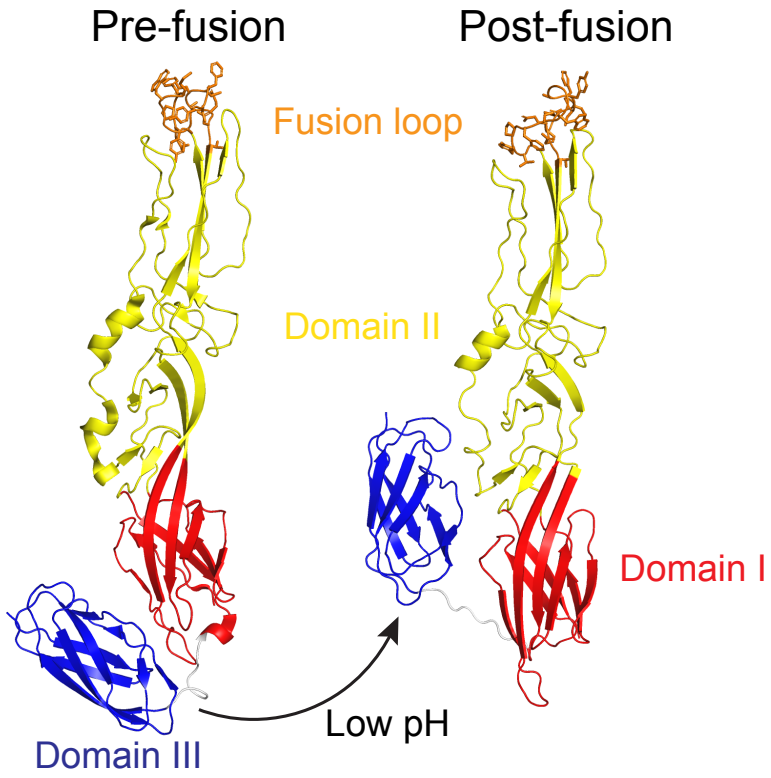

Figure 7. Alphavirus E1 glycoprotein structure. Cartoon representation of SFV E1 glycoprotein in the monomeric pre-fusion (left; PDB ID: 2ALA) or post-fusion (right; PDB ID: 1RER) form. The E1 domains (domain I [red], domain II [yellow], fusion loop [orange], and domain C [blue]) are colored to highlight these distinct regions. Upon low pH conditions within the endosome of host cells, the flexible hinge region, linker region, and domain C significantly move (black arrow) during E1 homotrimer formation and virus fusion with the endosomal membrane. Based on Roussel et al., 2006; Gibbons et al., 2004. Copyright permission from publishers Elsevier and Springer Nature.

Capsid protein

Two hundred and forty copies of the capsid protein make up the nucleocapsid core that lies underneath the viral membrane. The nucleocapsid core has icosahedral symmetry with 30 hexamers along the 2-fold axis and 20 pentamers at each 5-fold axis (Sun et al., 2013; Zhang et al., 2011; Hasan et al., 2018). The N-terminus of the capsid protein is positively charged and associates with the positive-sense single-stranded RNA genome (Mendes and Kuhn, 2018; Owen and Kuhn, 1996). The C-terminus of the capsid protein interacts with the cytoplasmic tail of the E2 glycoprotein via a hydrophobic pocket to tether the structural proteins across the viral membrane (Brown et al., 2018). The C-terminus of the capsid protein also functions as an autocatalytic proteinase to cleave itself from the structural polyprotein (Sun et al., 2013; Mendes and Kuhn, 2018; Choi et al., 1991).

Alphavirus replication cycle

Alphavirus attachment

During infection, alphaviruses first interact with attachment factors and entry receptors to enable virus entry into host cells. Virus interactions with attachment factors

allows for initial contact with cells, which may slow down virus movement, concentrate virus particles, and further enhance interactions at the host cell membrane for virus entry (Schnierle, 2019). Virus interaction with entry receptors helps induce conformational changes necessary for internalization into host cells (Schnierle, 2019; Holmes et al., 2020) (**Figure 8**).

Attachment factors

Several attachment factors have been implicated to increase alphavirus infectivity, including heparan sulfate (HS) (Gardner et al., 2011), dendritic cell-specific intercellular adhesion molecule-3-grabbing non-integrin (DC-SIGN) (Klimstra et al., 2003), liver-specific SIGN (L-SIGN) (Klimstra et al., 2003), and phosphatidylserine (PS) receptors (Jemielity et al., 2013).

HS, a negatively charged glycosaminoglycan, is an important attachment factor for many viruses (Cagno et al., 2019). For most alphaviruses, positively charged cell culture-adaptations of the E2 glycoprotein (SINV, SFV, CHIKV, RRV, VEEV; Smit et al., 2002; Ryman et al., 2007; Klimstra et al., 1998)) or natural dependence (EEEV; (Gardner et al., 2011)) on HS interactions leads to increased virus infectivity *in vitro* (Gardner et al., 2011). Route of inoculation appears to play a role in the *in vivo* efficacy of viruses with HS adaptations or dependence (Holmes et al., 2020). S.c. inoculation appears to result in reduced virulence *in vivo*, which may be due to increased clearance of the virus in circulation via HS interactions (Bernard et al., 2000; Holmes et al., 2020;

Byrnes and Griffin, 2000; Ryman et al., 2007). Intracranial (i.c.) inoculation, however, increased neurovirulence of cell culture-adapted (SINV) or natural isolates (EEEV) in a HS binding-dependent manner, which suggests HS may aid in infection of the central nervous system CNS (Ryman et al., 2007; Gardner et al., 2011; Chen et al., 2020; Holmes et al., 2020). The EEEV HS binding site on the E2 glycoprotein appears to correspond to residues 71-77, specifically 71K, 74K, and 77K, which when mutated show reduced binding, infectivity, and virulence (Gardner et al., 2011; Gardner et al., 2013). Cryo-EM reconstructions of EEEV in complex with low molecular-weight (6 kDa) heparin (Hp) showed four Hp binding sites, three “peripheral sites” and one “axial site” on each q3 and i3 spike (Chen et al., 2020). Positively charged residues of the E2 glycoprotein interacted with Hp electrostatically and these residues were found to be conserved amongst EEEV strains, supporting the involvement on HS dependence for EEEV pathogenesis (Chen et al., 2020). The residues identified were distinct from E2 71-77, which may be due to differences in the size of HS (Holmes et al., 2020).

DC-SIGN and L-SIGN are C-type lectins that bind high-mannose N-glycans. Viruses grown in mosquito cells contain high-mannose N-glycans, which may result in increased infectivity due to interaction with DC-SIGN or L-SIGN. In contrast, mammalian cells produce complex N-linked glycans (Hasan et al., 2018). PS receptors, such as T cell Ig mucin (TIM)-1, bind PS that becomes surface exposed during apoptosis. Alphaviruses may incorporate PS in the viral membrane during budding to take advantage of this receptor for virus entry (Hasan et al., 2018; Homes et al., 2020).

Entry receptors

Several receptors for alphaviruses have been identified (Holmes et al., 2020), such as matrix remodeling associated protein 8 (Mxra8) (Zhang et al., 2018), low-density lipoprotein receptor class A domain-containing 3 (LDLRAD3) (Ma et al., 2020), and natural resistance-associated macrophage protein 2 (NRAMP2) (Rose et al., 2011).

Mxra8 is expressed on the surface of epithelial, mesenchymal, and myeloid cells and is important for infection *in vitro* of fibroblasts, osteoblasts, chondrocytes, and skeletal muscle cells by several arthritogenic alphaviruses (CHIKV, RRV, MAYV, and ONNV) (Zhang et al., 2018). Infection of these cell types are important for the pathogenesis of arthritogenic alphaviruses. Blockade of Mxra8 reduced CHIKV pathogenesis *in vivo* in mouse models, further supporting the importance of Mxra8 as a receptor for these viruses (Zhang et al., 2018). Interaction of Mxra8 for the encephalitic alphaviruses (EEEV, VEEV, and WEEV) was not observed (Zhang et al., 2018), which suggests recognition of a different receptor that may contribute to the different pathogenesis and tissue tropisms observed for these viruses. Mxra8 binds domains A and B of the E2 glycoprotein, domain II of the E1 glycoprotein, and binds three E2/E1 heterodimers through intra-spike and inter-spike interactions. The E3 protein may obscure the binding site for Mxra8 (Schnierle, 2019).

LDLRAD3 is a member of the scavenger receptor superfamily and is expressed on the surface of neurons, epithelial cells, myeloid cells, and muscle tissues (Ma et al., 2020). This receptor was found to be important in VEEV infection *in vitro* of neuronal

cells and pathogenesis *in vivo.* Interaction with LDLRAD3 was not observed for EEEV or WEEV, indicating a different receptor may be utilized for these viruses (Ma et al., 2020). SINV and MAYV also did not interact with LDLRAD3, which may be due to preferential interaction with Mxra8 as a receptor for these viruses (Zhang et al., 2018).

NRAMP2 is expressed on the surface of macrophages and neuronal cells and results in SINV infection *in vitro*. This is supported by observation of direct binding of SINV to NRAMP2 and reduced infection in cells with deleted or downregulated expression of NRAMP2 (Rose et al., 2011).

Two additional receptors, laminin receptor and prohibitin 1 (PHB1), have also been implicated as receptors for SINV and CHIKV, respectively. Ab blockage was shown to reduce virus infection. However, further assessment for the role of these receptors in alphavirus entry is needed (Holmes et al., 2020).

For many alphaviruses, an entry receptor remains unknown. Since alphaviruses infect many different hosts and tissue tropisms, it is thought that different mechanisms may occur depending on the host cell (*i.e.*, mosquito versus mammalian), require multiple receptors for infection, or attach to highly conserved cellular factors (Ludwig et al., 1996; Schnierle, 2019; Griffin, 2016). In addition, residual infection is observed in several models lacking the corresponding receptor or attachment factor (*i.e.*, Mxra8, LDLRAD3, HS), which suggests involvement of other uncharacterized receptors or factors during virus entry. Mosquito orthologs do not exist for the Mxra8 and LDLRAD3 receptors, further supporting different mechanisms of virus entry (Holmes et al., 2020; Schnierle, 2019; Zhang et al., 2018; Ma et al., 2020).

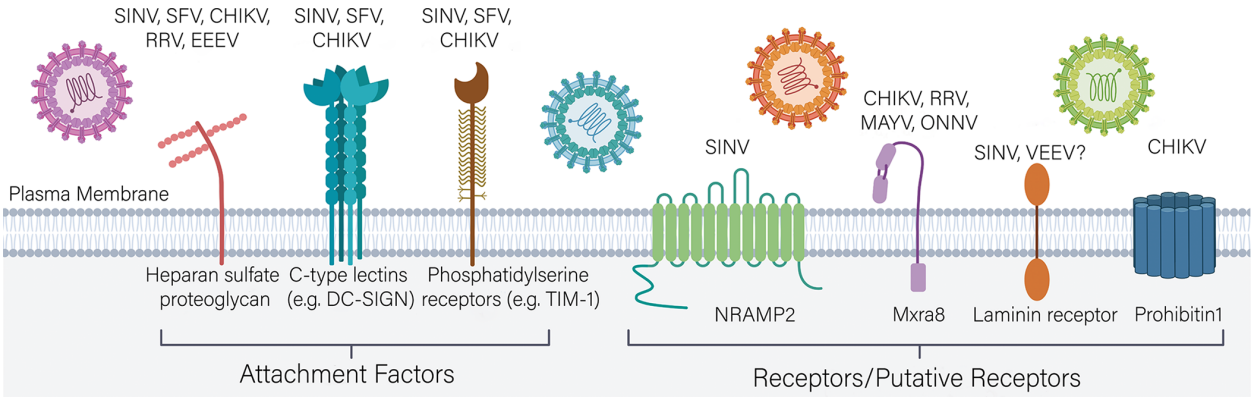

Figure 8. Alphavirus attachment factors and entry receptors. Alphaviruses infect a variety of hosts, which suggests interaction with multiple cellular factors is required for virus entry into host cells. Several attachment factors, such as HS, C-type lectins, and PS receptors have been implicated as factors that aid in alphavirus infection efficacy. Virus entry receptors (Mxra8, LDLRAD3, NRAMP2) have also been identified for several alphaviruses as an important role for alphavirus infection. However, for many alphaviruses the entry receptor still remains unknown and it may be that several entry factors to be involved during this process. (Open access: Holmes et al., 2020).

Alphavirus entry

Upon binding to entry receptors, alphaviruses enter cells predominantly by clathrin-mediated endocytosis (Holmes et al., 2020; Bernard et al., 2010; DeTulleo and Kirchhausen, 1998; Flynn et al., 1990; Meyer and Johnston, 1993). Evidence to support this mechanism of virus entry has been described through observation of co-localization of virus with clathrin (CHIKV) and reduction in virus infectivity (CHIKV) by clathrin inhibitors, such as anti-clathrin Abs (Doxsey et al., 1987). Other entry mechanisms may also occur depending on route of infection. Studies for encephalitic alphaviruses

crossing the blood-brain barrier (BBB) have shown that transcytosis across brain microvascular endothelial cells appears dependent on caveolin-1 (Salimi et al., 2020). Additional entry mechanisms have also been purposed, such as micropinocytosis-mediated uptake, micropinocytosis, and use of a pore at the plasma membrane (Schnierle, 2019). This may occur in a cell-type specific manner (Holmes et al., 2020).

Alphavirus fusion

Following virus entry, a drop in pH within early endosomes leads to movement of domain B of the E2 glycoprotein and destabilization of the E2 acid-sensitive connector region (Fields and Kielian, 2013; Li et al., 2010; Voss et al., 2010). Weak bases, such as ammonium chloride and chloroquine, block release of virus nucleocapsid into the cytosol of the cell (Helenius et al., 1982), which suggests the acidic pH environment of the endosome aids in virus fusion. The movement and destabilization induced by acidic pH exposes the fusion loop at the distal tip of the E1 glycoprotein, which enables insertion of the hydrophobic loop into cholesterol and sphingolipid-rich host cell membranes (Ahn et al., 2002; Chatterjee et al., 2002; Kielian et al., 2010). Further dissociation of the E2 glycoprotein from the E1 glycoprotein occurs following fusion loop insertion (Sánchez-San et al., 2008), which may result from disruption of a hydrophobic pocket between the E2 D-loop and transmembrane helices of E2/E1. Additionally, the low pH conditions can protonate conserved histidine residues at the E2/E1 heterodimer interface for further disruption (Chen et al., 2018; Zeng et al., 2015; Qin et al., 2009).

Three individual monomers inserted in the host cell membrane form E1 homotrimers following E2 dissociation (Wahlberg and Garoff, 1992; Justman et al., 1993; Wahlberg et al., 1992; Gibbons et al., 2000; Gibbons et al., 2004; Roussel et al., 2006). Substantial movement of the E1 hinge region and domain I/III linker helps to stabilize the E1 homotrimer during formation and enable domain III and stem region of the E1 glycoprotein to “fold-back” against the core trimer (Kielian, 2014; Gibbons et al., 2004; Mukhopadhyay et al., 2006; Zheng et al., 2011). This movement brings the cell and viral membranes together, resulting in fusion and release of the nucleocapsid into the cytosol (Gibbons et al., 2004; Mukhopadhyay et al., 2006) (**Figure 9**).

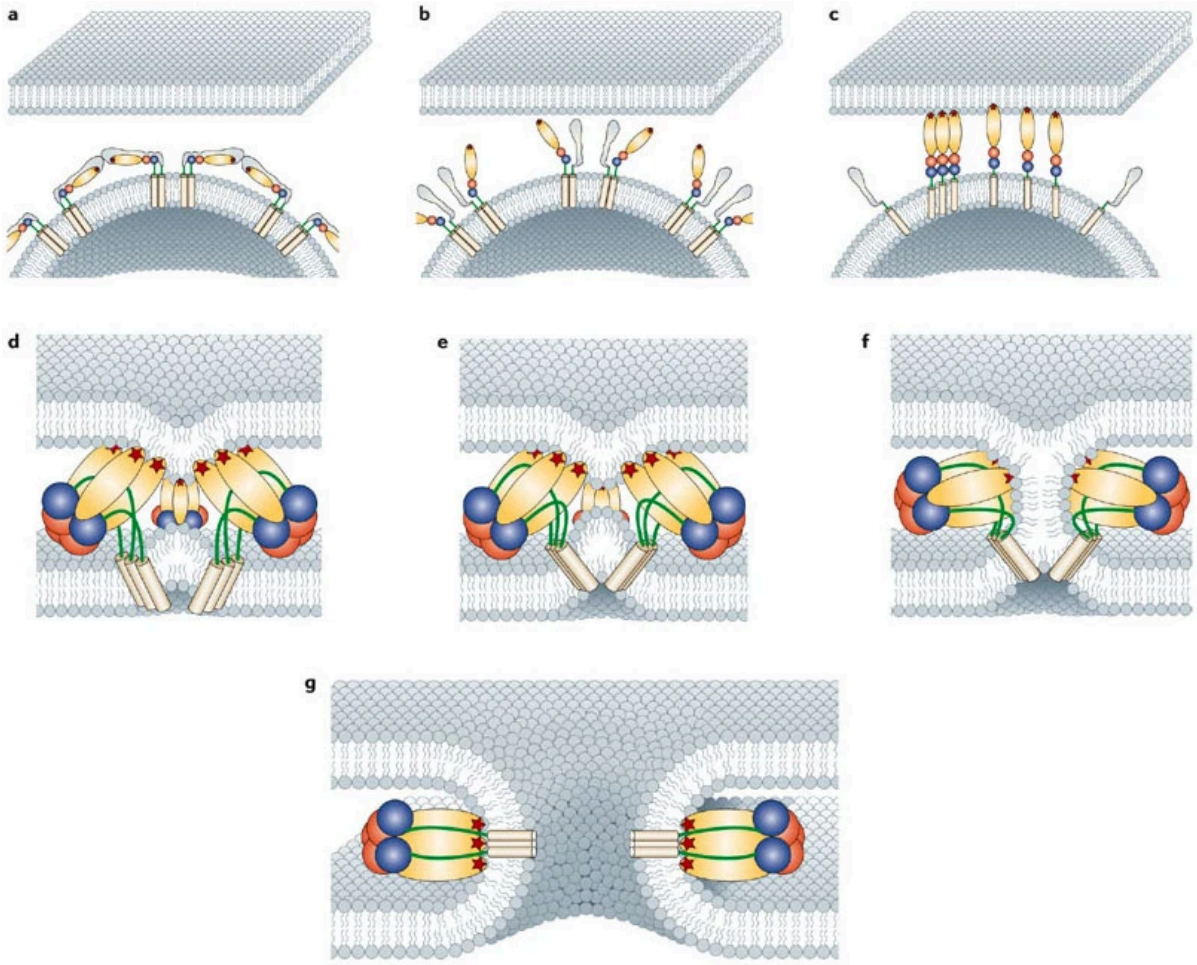

Figure 9. Cartoon diagram of the alphavirus fusion mechanism. Prior to virus entry into the endosome, the E2 (grey) and E1 (domain I: red, domain II: yellow, fusion loop: star, domain IIII: blue) glycoproteins are present on the virus surface as trimeric spikes of E2/E1 heterodimers (**A)**. Upon virus entry, the low pH environment leads to E2 dissociation from the heterodimer complex (**B**). This enables the fusion loop of the E1 glycoprotein to insert into the endosomal membrane and form E1 homotrimers (**C**). E1 homotrimer formation and movement of the E1 hinge and linker regions results in a "fold-back" mechanism, bringing domain III (blue) against the trimer (**D** and **E**). The viral and endosomal membrane then form a hemifusion intermediate (**F**) followed by complete fusion of the two membranes and release of the nucleocapsid into the cytosol (**G**). Copyright permission obtained from publisher: Springer Nature (Kielian and Rey, 2006).

Alphavirus RNA replication

Uncoating of the nucleocapsid occurs through cleavage of the capsid protein from the positive-sense single-stranded RNA genome by ribosomes within the cytosol (Singh and Helenius, 1992; Wengler et al., 1992). The released RNA genome serves as a template for translation of the nonstructural proteins (nsP1-4) as P123 and P1234 polyproteins. The P123 and P1234 polyproteins are proteolytically processed by the C-terminus of nsP2 during different stages in the replication cycle (Hardy and Strauss, 1989). Minus-sense strand RNA transcription occurs following nsP2 cleavage of P1234 to P123 and nsP4, RNA-dependent RNA polymerase (Shirako and Strauss, 1994; Lemm et al., 1994; Rupp et al., 2015). The minus-sense strand RNA serves as a template for replication of the positive-sense RNA genome following further nsP2 cleavage of P123 to nsP1, nsP2, and nsP3. Replication complexes form at the plasma membrane and within cytopathic vacuoles (Jose et al., 2017) (**Figure 11**). Transcription of the 26S subgenomic mRNA from the minus-sense strand RNA occurs after cleavage of the polyproteins to individual nsPs (Shriako and Strauss, 1994; Lemm et al., 1994; Rupp et al., 2015).

Alphavirus structural protein translation and processing

The structural proteins (capsid, E3, E2, 6K, E1, and TF) are translated from the subgenomic 26S mRNA. The capsid protein proteolytically cleaves itself from the

structural polyprotein for association with the positive-sense single-stranded RNA genome and assembly of the nucleocapsid core (Mendes and Kuhn, 2018; Choi et al., 1991). In the ER, a precursor protein (p62 = E3 + E2) is translated in association with the 6K protein and the E1 glycoprotein (**Figure 10**). The 6K protein is a small ~60 aa protein that has ion-channel activity and serves as a signal sequence for the E1 glycoprotein (Snyder et al., 2013; Griffin, 2016). Signal peptidases cleave the structural polyprotein to yield individual proteins (p62, 6K, and E1) (Brown et al., 2018). Processing of p62 by furin cleavage in the late secretory pathway (trans-Golgi network) yields the E2 glycoprotein in complex with the peripheral E3 protein (Uchime et al., 2013; Zhang et al., 2003; Brown et al., 2018). Prior to furin cleavage, the E3 protein protects the E2/E1 heterodimer from spontaneous fusion in the low pH environment of the Golgi apparatus and usually is released in the extracellular, neutral pH environment during final maturation of the virus to prime (Kielian, 2014; Sjöberg et al., 2011; Gibbons et al., 2004; Voss et al., 2010; Holmes et al., 2020). VEEV occasionally retains the E3 protein with the E2/E1 heterodimer in some mature virus particles (Zhang et al., 2011). The TF protein is produced when a ribosomal frameshift occurs during translation and can be incorporated in small amounts with the virus (Snyder et al., 2013; Firth et al., 2008). The structural proteins form a lattice of trimers of E2/E1 heterodimers within the ER membrane and traffic through the late secretory pathway to accumulate at the plasma membrane (Brown et al., 2018; Uchime et al., 2013; Jin and Simmons, 2019; Soonsawad et al., 2010).

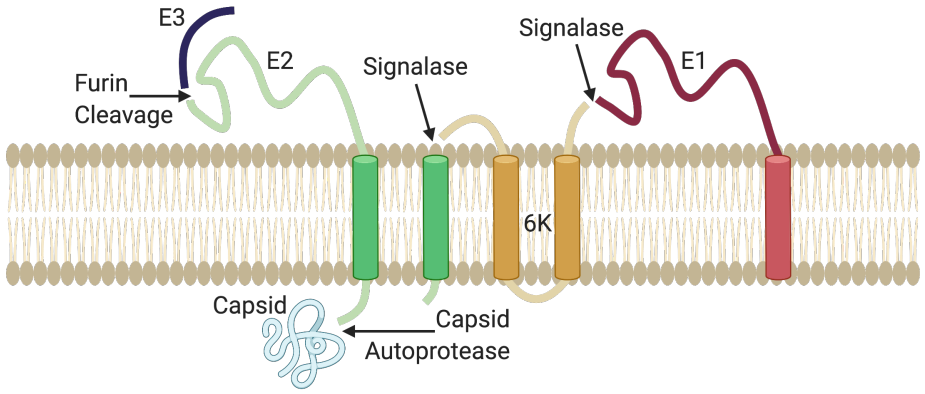

Figure 10. Organization of the alphavirus structural proteins during polyprotein processing. The alphavirus structural proteins are translocated across the ER membrane during translation and polyprotein processing. The capsid protein cleaves itself from the polyprotein and associates with the cytoplasmic tail of the E2 glycoprotein during virus maturation and budding at the plasma membrane. The two structural proteins are translocated across the ER membrane to incorporate the transmembrane domains of each and form heterodimer complexes. 6K serves as a signal sequence for the E1 glycoprotein. The E3 protein protects the heterodimer (p62E1) from inappropriate exposure of the E1 fusion loop in the low pH environment of the Golgi apparatus during the late secretory pathway. Furin cleaves the E3 protein late in this pathway to prime the virus for entry. Created with BioRender.com. Based on (Open Access: Brown et al., 2018).

Alphavirus egress

Nucleocapsid cores are icosahedral in symmetry and are formed through capsid protein dimerization and binding of the positively charged N-terminus of the capsid protein with the viral RNA genome (Zhang et al., 2011; Hong et al., 2006; Owen and Kuhn, 1996; Mendes and Kuhn, 2018). Virus budding is dependent on factors including physiological temperature, neutral pH, cholesterol, capsid protein and E2 interactions, and E2/E1 heterodimer interactions (Marquardt et al., 1993; Lu and Kielian, 2000;

Brown et al., 2018). The C-terminus of the capsid protein interacts with the cytoplasmic tail of the E2 glycoprotein with 1:1 stoichiometry at the plasma membrane, which induces virus budding (Brown et al., 2018; Zhang et al., 2011; Jose et al., 2009; Suomalainen et al., 1992; Zhao et al., 1994). Interactions between the E2/E1 proteins of a heterodimer also appear to induce virus budding. One region that takes part in this interaction occurs between the E2 D-loop and the E1 glycoprotein stem region since mutations in the E2 D-loop reduce virus budding (Byrd and Kielian, 2017). In addition, the 6K and TF proteins may aid in release of virus particles from infected cells through packaging with virus particles and ion channel activity (Liljeström et al., 1991; Loewy et al., 1995).

Virus budding takes place at the plasma membrane in mammalian cells (**Figure 11**). Clusters of E2/E1 heterodimers within the plasma membrane aid in formation of the icosahedral lattice (Forsell et al., 2000; Byrd and Kielian, 2017). Nucleocapsid cores may also contribute to virus symmetry. However, budding can occur in the absence of nucleocapsid cores, suggesting this is not necessary (Forsell et al., 1996).

Alphaviruses can also spread to cells via cell-to-cell transmission (Martinez and Kielian, 2016; Lee et al., 2011). Intercellular extensions have been observed during alphavirus infections and appear to aid in transmission of virus between infected and noninfected cells. Cell cytoskeleton remodeling by alphaviruses leads to formation of these extensions to bring the cellular membranes within proximity. The cells do not appear to connect such that virus budding still occurs at the plasma membrane.

However, the membrane proximity increases transmission between cells (Martinez and Kielian, 2016).

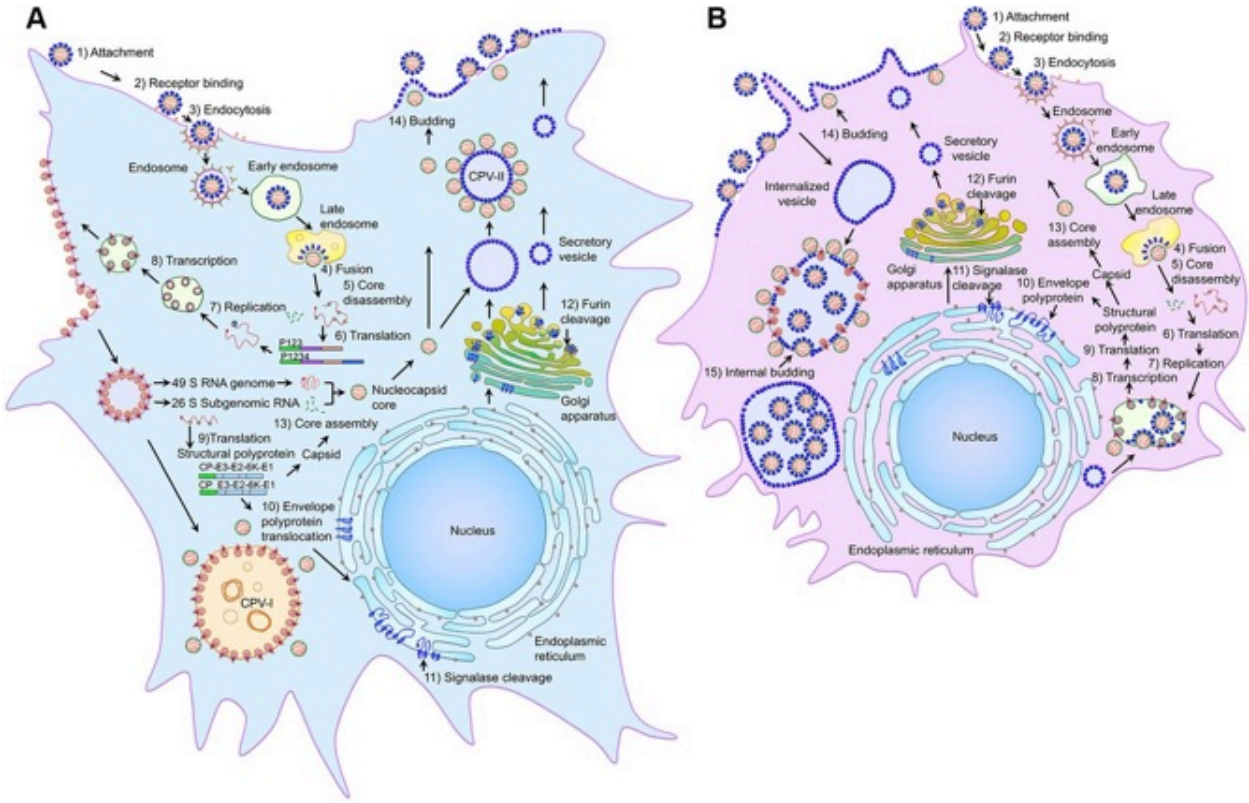

Figure 11. Overview of alphavirus replication cycle. Alphavirus replication cycle in mammalian (**A**) or insect (**B**) cells. The two cycles are very similar in the replication cycle for alphaviruses with attachment, entry, fusion, translation of nsPs, RNA replication, RNA transcription, structural polyprotein translation and processing, assembly of virus particles, and virus budding. However, several key differences exist between the two species. One difference includes the glycosylation patterns, which involve high mannose glycans in insect cells compared to the complex N-linked glycans for mammalian cells. Additionally, internal budding of virus particles can occur in insect cells, whereas virus budding in mammalian cells occurs only at the plasma membrane. (Open access: Jose et al., 2017).

Anti-alphavirus Abs

Importance of Abs during alphavirus infection

An Ab response against alphaviruses is important in the protection, treatment, and clearance of virus. In the following sections and chapters, I will focus more specifically on previously characterized alphavirus mAb-mediated mechanisms of action to supply sufficient background on the current knowledge in the field. Here I will provide a broader analysis on the importance of Abs against alphaviruses.

Studies involving passive transfer of immune animal serum or purified IgG from plasma samples of immune individuals have protected mice against alphavirus infection (Rabinowitz and Adler, 1973; Couderc et al., 2009; Ko et al., 2019). Potent neutralizing anti-CHIKV E2-specific and non-neutralizing anti-CHIKV E1 mAbs protect and treat in nonlethal and lethal CHIKV-induced joint swelling disease models (Selvarajah et al. 2013; Pal et al., 2013; Jin and Simmons, 2019; Broeckel et al., 2017). On the other hand, if the threshold for neutralization is not obtained, immune CHIKV plasma can lead to ADE through engagement of FcγRII on macrophages. An increase in virus replication within these cells can lead to greater disease severity in CHIKV joint swelling mouse models (Lum et al., 2018).

Neuroadapted SINV is used to study lethal alphavirus induced encephalitis (Schmaljohn et al., 1983; Griffin et al., 1997). Protection against neuroadapted SINV intracerebral (i.c.) challenge was observed for neutralizing anti-SINV E2-specific and

non-neutralizing anti-SINV E1-specific murine mAbs. The protective capability of murine anti-SINV E2-specific mAbs depended on potency of neutralizing activity against SINV. In contrast, the murine anti-SINV E1-specific mAbs primarily bound virus infected cells and not intact virions, which suggests differential exposure of protective E1 epitopes during the virus maturation processes (Schmaljohn et al., 1983). Additionally, complement-dependent lysis of infected cells was observed for the protective IgG2a and IgG2b murine anti-SINV E1-specific mAbs (Schmaljohn et al., 1983). This suggests a potential non-neutralizing mechanism of protection against alphaviruses through Fc-mediated effector functions. Together these studies show that neutralizing and non-neutralizing Ab-mediated mechanisms of action lead to protection against alphavirus infection.

SINV inoculation of SCID mice leads to a persistent encephalomyelitis, characterized by persistent virus replication of neurons in the brain and spinal cord (Levine et al., 1991; Griffin et al., 1997). Adoptive transfer of hyperimmune serum to SINV i.c. inoculated SCID mice resulted in clearance of SINV replication (**Figure 12**). Immune T cells can aid in control of persistent SINV but do not appear able to clear infectious virus as observed by the presence of virus in μMT mice (Binder and Griffin, 2001). Virus clearance was also shown to reduce viral RNA through inhibition of intracellular replication by bivalent murine anti-SINV E2-specific mAbs and did not depend on induction of complement-induced cytolysis or cell-mediated immune responses (Ubol et al., 1994; Levine et al., 1991; Griffin et al., 1997). Reactivation of persistent viral RNA corresponded with a reduction in Ab presence, which suggests the

need for continual presence of Ab pressure (Griffin et al., 1997). This is supported by the observation of infiltration of B cells into the brain parenchyma 3 to 4 days following infection and the enrichment of SINV Ab secreting B cells in immune mice for recurrent clearance of virus replication (Metcalf and Griffin, 2011; Griffin et al., 1997; Tyor and Griffin, 1993). All together, these studies highlighted the importance of Abs in non-cytolytic SINV clearance from infected neurons.

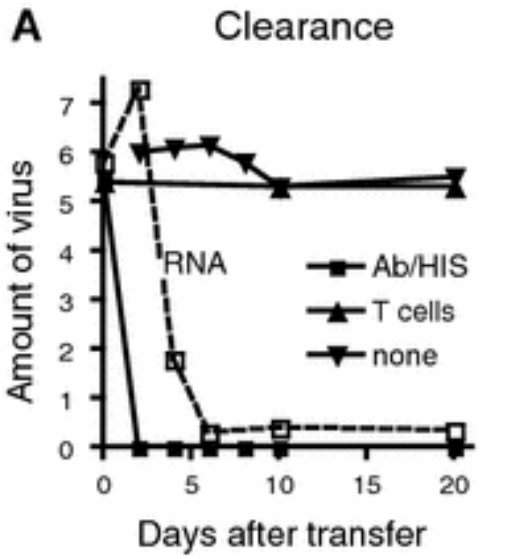

Figure 12. Importance in Ab response for the clearance and control of SINV infection. SCID mice were inoculated with neuroadapted SINV to establish persistent infection within the CNS. Passive transfer of either immune serum or T cells was administered to the mice. Reduction in the amount of infectious virus (y-axis) and viral RNA (open squares) was observed in mice treated with immune serum but not T cells. Copyright permission from publisher Springer Nature (Griffin, 2010).

E2-specific Abs

The E2 glycoprotein is a target for many neutralizing anti-alphavirus mAbs (Roehrig et al., 1982). In this section, I will discuss what is known about virus-specific E2-specific mAbs for the viruses, CHIKV, MAYV, EEEV, VEEV, or WEEV. Chapters III, V, VI will discuss human E2-specific mAbs against EEEV (chapters III and V) and VEEV (chapter VI).

Chikungunya virus (CHIKV)

The murine and human humoral responses against CHIKV have extensively been studied. A multitude of CHIKV E2-specific mAbs generated through phage display, immunizations of mice with recombinant proteins or virus particles, and from B cells of CHIKV immune donors, have described neutralization mechanisms from prevention of virus entry (*i.e.*, virus attachment and fusion processes) to inhibition of virus egress through recognition of the CHIKV E2 glycoprotein (Jin and Simmons, 2019).

Blockade of receptor attachment (Mxra8) occurs through binding to domain A of the E2 glycoprotein, which contains part of the receptor binding site (RBS). In addition, steric hindrance may account for blockade if a binding angle enables the Fc domain to prevent receptor binding. It is thought that anti-CHIKV E2-specific mAbs recognizing the RBS (*i.e.*, 8B10, 4J21 and 5M16) can block virus attachment (Porta et al., 2015; Jin and Simmons, 2019; Sun et al., 2013b; Long et al., 2015; Zhou et al., 2020).

Multiple mAbs targeting the CHIKV E2 glycoprotein inhibit fusion through blockade of exposure of the fusion loop on the E1 glycoprotein (Smith et al., 2015; Jin et

al., 2015; Porta et al., 2015; Quiroz et al., 2019). Stabilization of the E2 glycoprotein through mAb binding to domains A, B, and the β-connector region may prevent movement of the flexible domain B and dissociation of E2 from the heterodimer during the virus fusion process. In addition, mAbs (*i.e.*, 4J21, C9, IM-CKV063 [Smith et al., 2015; Selvarajah et al., 2013; Fong et al., 2014]) targeting domain A and the β-connector region of one E2/E1 heterodimer can also make contacts with a domains A and B in a neighboring E2/E1 heterodimer within the same spike (intra-spike) as shown through cryo-EM reconstructions of Fab complexes (Jin et al., 2015; Long et al., 2015). Binding to two E2/E1 heterodimers may further aid in stabilization.

Ab (*i.e.*, C9, IM-CKV063, CHK-152) inhibition of virus egress appears independent of inhibition of virus entry (attachment and fusion). Analysis of neutralization activity through standard focus forming neutralization assays of mAbs does not always appear to capture mAbs that inhibit egress regardless of previously defined neutralization activity (Jin et al., 2015; Jin and Simmons, 2019). Thus, separate analyses of mAb neutralization following virus infection showed that inhibition of virus egress appears to occur through mAb binding in a bivalent-dependent manner to the cell surface. This binding can cross-link and aggregate E2 glycoproteins on the surface of infected cells for inhibition (Jin et al., 2015; Jin et al., 2018). Additionally, presence of mAb at the surface of infected cells can cross-link and activate Fc receptors on immune effector cells for induction of Fc-mediated effector functions, such as ADCC or ADCP (Jin et al., 2018). Involvement of Fc-mediated effector functions has been shown to be optimal for neutralizing anti-CHIKV mAbs since a reduction in protection of CHIKV-

induced joint swelling in mice is observed through monocyte depletion studies (Fox et al., 2019).

Mayaro virus (MAYV)

A panel of murine anti-MAYV E2-specific mAbs that potently neutralize MAYV have elucidated some of the Ab-mediated mechanism(s) of action against MAYV (Earnest et al., 2019). Neutralizing mAbs appear to inhibit post-attachment, including fusion inhibition and viral egress. Even though some neutralizing mAbs were protective *in vivo*, Fc mediated effector functions were important for protection against lethal and musculoskeletal MAYV-induced disease in mouse models. This was observed as protection depended on mAb isotype, glycosylation of Fc domain (N297Q), and reduced efficacy was observed in $FcyR^{-/-}$ mice (Earnest et al., 2019).

Eastern equine encephalitis virus (EEEV)

The human humoral response against EEEV has yet to be described. Previous studies on the murine and avian humoral response towards EEEV began to elucidate the mechanisms of this response. Murine anti-EEEV sera and mAbs induced by immunization with recombinant E2 glycoprotein identified linear epitopes on the E2 glycoprotein through peptide scanning or phage display peptide library analyses (Zhao et al., 2012; EnCheng et al., 2013). Several of these linear epitopes were specific to

formally classified lineages of EEEV (I-IV-specific, I-specific, I/IV-specific, and I-III-specific) (EnCheng et al., 2013). More recently, characterization of neutralizing murine anti-EEEV E2-specific mAbs induced by inoculation with the chimeric virus, SINV/EEEV, identified domains A (residues 51-81) and B (residues 180-182; 213-215) as conformational epitopes on the E2 glycoprotein. These murine mAbs neutralized SINV/EEEV at a post-attachment step, several of which inhibited virus fusion, and protected against EEEV s.c. and aerosol challenge (Kim et al., 2019). Cryo-EM reconstructions described a model for murine anti-EEEV mAb binding to SINV/EEEV particles (**Figure 13**). In this model, it is suggested that Fabs to domain A of the E2 glycoprotein can bind with high or low occupancy in the tangential or radial orientation due to absence or presence of intra-spike (within the same trimeric spike) steric clashes, respectively. In contrast, Fabs that bind domain B of the E2 glycoprotein may exhibit binding in the opposite manner due to inter-spike (neighboring trimeric spikes) steric clashes (Hasan et al. 2018).

For EEEV, sentinel chickens are monitored for virus presence in several states in the United States (Olson et al., 1991) since birds are the primary reservoir hosts (Weaver et al., 2012). To study the avian humoral response, chicken and duck antisera following immunization with recombinant E2 glycoprotein identified linear epitopes on the E2 glycoprotein through peptide scanning (Sun et al., 2013a). The linear epitopes were reactive to the formally classified lineages of EEEV (I-IV-specific or I-specific) and were primarily distinct from the murine linear epitopes previously identified (Sun et al., 2013a).

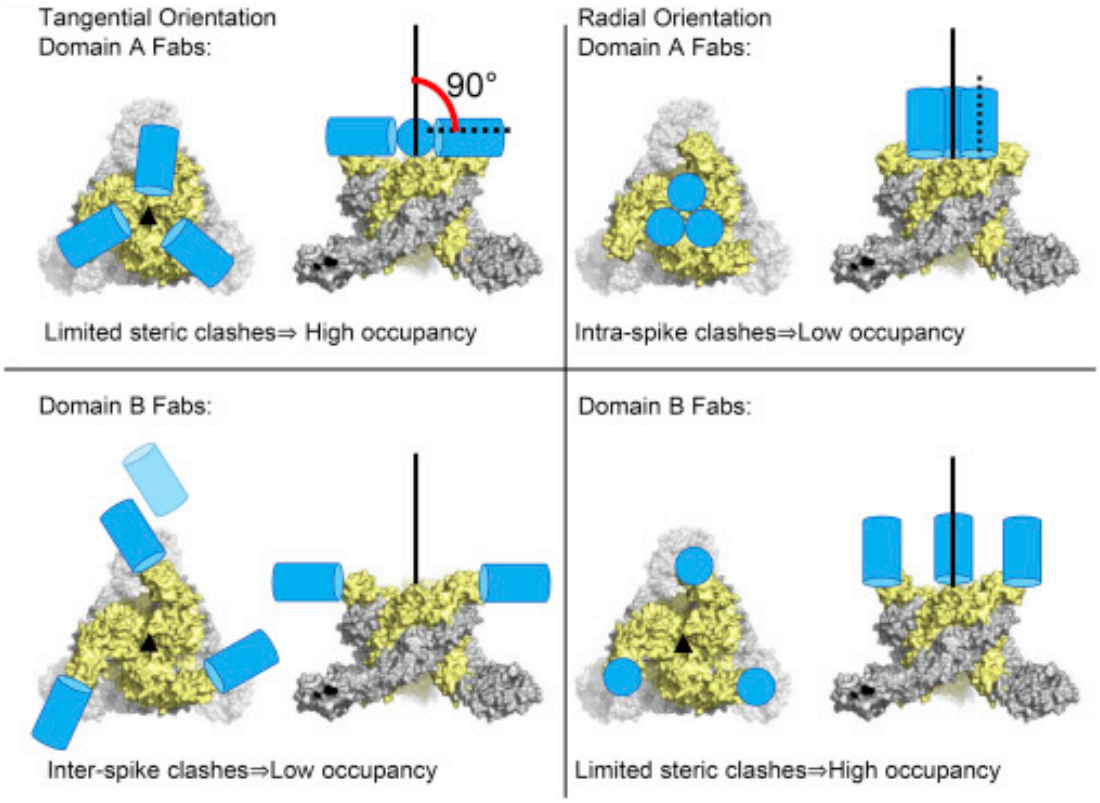

Figure 13. Model for murine anti-EEEV Fab binding to the E2 glycoprotein of SINV/EEEV surface exposed trimeric spikes. Cryo-EM reconstructions of murine Fabs in complex with SINV/EEEV particles elucidated potential binding mechanisms for neutralization due to correspondence between the epitope targeted and occupancy. It is suggested from these studies that E2 domain A targeting Fabs can bind with high occupancy if bound in a tangential orientation (upper left quadrant) but not in the radial orientation (upper right quadrant) due to steric clashes between Fab molecules. Furthermore, for E2 domain B targeting Fabs, binding may occur in the opposing manner, in which high occupancy would occur when Fab binds in the radial orientation (lower right quadrant) but not in the tangential orientation (lower left quadrant). (Open Access: Hasan et al., 2018).

Venezuelan equine encephalitis virus (VEEV)

Previous studies on the murine and human humoral response towards VEEV begin to elucidate the critical protective and neutralizing epitopes recognized by this response. Rabbit anti-VEEV E2-specific antisera and murine anti-VEEV E2-specific mAbs induced by immunization with VEE subtypes (IAB-IE and II) or recombinant E2 glycoprotein identified a conformationally stable and critical neutralization epitope (domain B: 182-210) on the E2 glycoprotein (Rico-Hesse et al., 1988; Roehrig et al., 1982; Roehrig and Mathews, 1985). Abs to this epitope protected mice from lethal VEEV intraperitoneal (i.p.) and aerosol challenge (Phillpotts, 2006; Mathews and Roehrig, 1982; Roehrig and Mathews, 1985). Cryo-EM reconstruction of VEEV (vaccine strain, TC-83) in complex with a Fab molecule (3B4C-4) that recognizes this epitope, appears to stabilize domain B of the E2 glycoprotein through inter-spike cross-linking, which likely prevents exposure of the fusion loop (Porta et al., 2014). Another murine (or humanized) mAb, 1A3B-7, that recognizes this epitope broadly binds to all VEE subtypes and neutralizes within the VEE antigenic complex (Phillpotts, 2006; Goodchild et al., 2011). Protection was observed in 1A3B-7 treated mice 24 hours prior to VEEV (subtypes IAB-IE, II, and IIIA) s.c. or aerosol challenge (Phillpotts, 2006). Intravenously (i.v.) administered humanized 1A3B-7 was also shown to reduce VEEV disease of NHPs up to 48 hours post-exposure (Burke et al., 2019).

A neutralizing human anti-VEEV E2-specific mAb, F5, was isolated using a phage display library from B cells of VEEV-immune donors and screened for reactivity to the VEEV vaccine strain, TC-83 (Hunt et al., 2010). Cryo-EM reconstructions of F5 Fab in complex with VEEV (vaccine strain, TC-83) displayed that F5 Fab binds in a

radial orientation to occupy one E2 glycoprotein per trimeric spike and recognize a distinct neutralization epitope (domain A: 115-119) on the E2 glycoprotein (Hunt et al., 2010; Porta et al., 2014). Additionally, F5 Fab binding brings the trimeric spikes closer together, which suggests that F5 may stabilize the trimer through intra-spike cross-linking for neutralization of VEEV (Porta et al., 2014). Prophylactic (24 hours prior inoculation) and therapeutic (24 hours post inoculation) administration of F5 was up to 90-100% effective against VEEV (Trinidad Donkey strain; subtype IAB) s.c. or aerosol challenge (Hunt et al., 2011). Little to no virus was detected in peripheral tissues except for neurons of the CNS when F5 was administered therapeutically, which suggests effective clearance of virus replication in this model (Hunt et al., 2011).

Western equine encephalitis virus (WEEV)

Anti-WEEV Abs have been isolated from llamas E2-specific single-domain Abs (sdAbs) following immunization with inactivated WEEV (Liu et al., 2018). However, assessment of neutralization activity or *in vivo* efficacy has not be performed. Human-like neutralizing anti-WEEV mAbs have been identified that are protective against aerosol challenge in mice (Hülseweh et al., 2014; Burke et al., 2018).

E1-specific Abs

The E1 glycoprotein is another target for anti-alphavirus mAbs (Roehrig et al., 1982). In contrast to E2-specific mAbs, E1-specific mAbs are generally non-neutralizing

or weakly neutralize virus (Roehrig et al., 1982; Roehrig et al., 1990). This may be due to obstruction by the E2 glycoprotein as exposure of some E1 epitopes requires treatment with different conditions, such as acidic pH, elevated temperature, and presence of detergent or reducing agents (Hunt and Roehrig, 1985; Ahn et al., 1999). In this section, I will discuss virus-specific E1-specific mAbs for the viruses, CHIKV, MAYV, EEEV, VEEV, or WEEV. Chapter IV will discuss human E1-specific mAbs against these viruses.

Chikungunya virus (CHIKV)

Human anti-CHIKV E1-specific mAbs isolated through phage display from the B cells of CHIKV immune donors were found to target the fusion loop on the E1 glycoprotein (Fong et al., 2014). Recognition of the fusion loop relied on exposure of E1 epitopes through fixation and elevated temperature, which supports occlusion of the fusion loop by the E2 glycoprotein on mature virions. These mAbs were non-neutralizing and did not protect against lethal CHIKV infection in mice. Similarly, human anti-CHIKV E1-specific mAbs were isolated through B cell sorting with a p62E1 antigen (Quiroz et al., 2019). In contrast to the fusion loop mAbs (Fong et al., 2014), these mAbs recognized a surface exposed epitope within domain III of the E1 glycoprotein for weak neutralization activity. However, these mAbs were not protective against lethal CHIKV infection. Another domain III anti-CHIKV mAb was found to inhibit virus egress (Masrinoul et al., 2014).

Mayaro virus (MAYV)

Serum analysis of immune individuals from South America, displayed anti-MAYV E1-specific reactivity, in contrast, to other alphaviruses, which showed cross-reactivity to the E1 glycoprotein (Smith et al., 2018). Characterization of murine anti-MAYV E1-specific mAbs with neutralizing and protective activity against MAYV musculoskeletal disease (Earnest et al., 2019) suggests that E1 mAbs may exhibit different Ab-mediated mechanism(s) compared to other alphaviruses.

Venezuelan equine encephalitis virus (VEEV)

Rabbit anti-VEEV E1-specific antisera and murine anti-VEEV E1-specific mAbs induced by immunization with the VEEV TC-83 vaccine strain protected mice from VEEV Trinidad Donkey strain (VEEV IAB subtype) intraperitoneal (i.p.) challenge (Mathews and Roehrig, 1982). Additionally, a human E1 specific Fab (L1A7) was isolated through a phage display library generated from B cells of VEEV-immune donors and screened for reactivity to the vaccine strain, VEEV TC-83 (Hunt et al., 2010). These Abs demonstrated little to no neutralizing activity against VEEV, which supports the role of non-neutralizing Abs in immunity against alphaviruses.

Western equine encephalitis virus (WEEV)

Similar to anti-VEEV E1-specific mAbs, murine anti-WEEV E1-specific mAbs induced by immunization with WEEV did not exhibit neutralization activity. Different patterns of binding reactivity (WEEV-specific, WEE-complex reactive, alphavirus reactive) and hemagglutinin inhibition activity were observed and depended on accessibility of the epitope, from surface exposed to cryptic epitopes (Hunt and Roehrig, 1985). Protection against WEEV i.p. challenge was only observed by mAbs that recognized cryptic epitopes, which suggests a protective mechanism utilized by E1-specific mAbs through recognition of epitopes not present on mature and intact virions (Hunt and Roehrig, 1985).

CHAPTER II

METHODOLOGY DEVELOPMENT FOR CHARACTERIZATION OF HUMAN MONOCLONAL ANTIBODIES AS POTENTIAL THERAPEUTIC CANDIDATES

The information contained in this chapter is adapted with permission from the following references:

Sangha AK, Dong J, **Williamson L**, Hashiguchi T, Saphire EO, Crowe JE Jr, Meiler J. Role of non-local interactions between CDR Loops in binding affinity of MR78 antibody to Marburg virus glycoprotein. *Structure*. 2017. 25(12): 1820-1828.e2. doi: 10.1016/j.str.2017.10.005. PMID: 29153506; PMCID: PMC5718948.

Williamson LE, Flyak AL, Kose N, Bombardi R, Branchizio A, Reddy S, Davidson E, Doranz BJ, Fusco ML, Saphire EO, Halfmann PJ, Kawaoka Y, Piper AE, Glass PJ, Crowe JE, Jr.. Early human B cell response to Ebola virus in four U.S. survivors of infection. *Journal of Virology*. 2019. 93(8): e01439-18. doi: 10.1128/JVI.01439-18. PMID: 30728263. PMCID: PMC6450119.

Vogt MR, Fu J, Kose N, **Williamson LE**, Bombardi R, Setliff I, Georgiev IS, Klose T, Rossmann MG, Bochkov YA, Gern JE, Kuhn RJ, Crowe JE Jr.. Human antibodies neutralize enterovirus D68 and protect against infection and paralytic disease. *Science Immunology*. 2020. 5(49): eaba4902. doi:10.1126/sciimmunol.aba4902. PMID: 32620559; PMCID: PMC7418079.

Zost SJ, Gilchuk P, Case JB, Binshtein E, Chen RE, Nkolola JP, Schäfer A, Reidy JX, Trivette A, Nargi RS, Sutton RE, Suryadevara N, Martinez DR, **Williamson LE**, Chen EC, Jones T, Day S, Myers L, Hassan AO, Kafai NM, Winkler ES, Fox JM, Shrihari S, Mueller BK, Meiler J, Chandrashekar A, Mercado NB, Steinhardt JJ, Ren K, Loo YM, Kallewaard NL, McCune BT, Keeler SP, Holtzman MJ, Barouch DH, Gralinski LE, Baric RS, Thackray LB, Diamond MS, Carnahan RH, Crowe JE Jr. Potently neutralizing and protective human antibodies against SARS-CoV-2. *Nature*. 2020. 584(7821): 443-449. doi: 10.1038/s41586-020-2548-6. PMID: 32668443; PMCID: PMC7584396.

Chapter Overview

Human monoclonal antibodies have therapeutic potential as antiviral candidates against different viruses, including HIV, influenza, Ebola, SARS-CoV-2, etc. (Zost et al., 2020; Flyak et al., 2015; Gilchuk et al., 2018; Krammer, 2019; Sok and Burton, 2018; Marston et al., 2018; Crowe, 2017; Forthal, 2014). During my initial studies in Dr. Crowe's laboratory, I performed enzyme-linked immunosorbent assay (ELISA)-based and epitope mapping techniques to gain experience in these technical skills and apply them to many different viruses, including filoviruses (Ebola virus [EBOV] and Marburg virus [MARV]), enterovirus D68 (EV-D68), and severe acute respiratory syndrome coronavirus 2 (SARS-CoV-2). In this chapter, I will focus on the studies I performed for EBOV, MARV, EV-D68, and SARS-CoV-2. In the following chapters III-VI, I will focus on my main thesis work pertaining to alphaviruses.

The studies described in this chapter would not have been possible without many members of Dr. Crowe's laboratory and their contribution to the isolation and initial characterization of the human mAbs. I would like to acknowledge Dr. Andrew Flyak and Nurgun Kose for isolation of the human anti-EBOV mAbs from Ebola virus disease (EVD) survivors. I would also like to thank Dr. Andrew Flyak for his mentorship on this project during my rotation in Dr. Crowe's laboratory. I would also like to acknowledge Drs. Pamela Glass, Peter Halfmann, Edgar Davidson, and Benjamin Doranz's

laboratories for *in vivo* studies, neutralization assays, and epitope mapping, respectively, of a neutralizing human anti-EBOV mAb, EBOV237. I would like to acknowledge Dr. Amandeep Sangha for analyzing MR78 through computational analysis with Rosetta. I would also like to acknowledge Dr. Matthew Vogt and Nurgun Kose for isolation and characterization of the human anti-EV-D68 mAbs. Lastly, I would like to acknowledge Drs. Seth Zost, Pavlo Gilchuk, Naveenchandra Suryadevara, Elad Binshtein, Robert Carnahan and Rachel Nargi, Rachel Sutton, Andrew Trivette, Joesph Reidy, and many other members of the DARPA team that isolated and characterized the human anti-SARS-CoV2 mAbs during the COVID-19 pandemic.

Introduction to Ebola virus

Ebola virus is a member of the *Filoviridae* family and causes intermittent outbreaks of severe human Ebola virus disease (EVD). The last outbreak occurred from June to November 2020 in the Democratic Republic of the Congo with 130 cases and 55 reported deaths (https://www.cdc.gov/vhf/ebola/outbreaks/drc/2020-june.html; accessed January 31st, 2021). In 2014, a large outbreak occurred in West Africa, with a total of 28,616 cases of EVD and 11,310 deaths that were reported in Guinea, Liberia, and Sierra Leone, and an additional 36 cases and 15 deaths that occurred when the outbreak spread outside these three countries (https://www.cdc.gov/vhf/ebola/history/2014-2016-outbreak/index.html; accessed

January 31st, 2021). Experimental vaccines, Abs, small molecules, and RNA treatments for Ebola virus infection are in development, which are intended to prevent or treat infection using immunologic principles. Indeed, Dr. Crowe's laboratory and others have shown that at late time points after recovery, survivors possess memory B cells in circulation specifying broad and potent protective Abs (Flyak et al., 2016; Bornholdt et al., 2016; Wec et al., 2017; Flyak et al., 2018; Saphire et al., 2018; Gilchuk et al., 2018). Monoclonal Abs (mAbs) isolated from human B cells of survivors can exert potent therapeutic effects in experimental infection models in nonhuman primates using cocktails of mAbs or even monotherapy (Qiu et al., 2014; Corti et al., 2016; Gilchuk et al., 2018).

Ebola virus is an enveloped, nonsegmented, negative-sense strand RNA virus (http://www.who.int/en/news-room/fact-sheets/detail/ebola-virus-disease). Together with the Marburg and Cuevaviruses, these members constitute the *Filoviridae* family. There are six species of Ebola virus: *Zaire ebolavirus* (EBOV), *Bundibugyo ebolavirus* (BDBV), *Sudan ebolavirus* (SUDV), *Taï Forest ebolavirus*, *Reston ebolavirus*, and *Bombali ebolavirus*. Of these species, EBOV, BDBV, and SUDV are the primary species associated with lethal disease in humans (Flyak et al., 2016). The surface glycoprotein (GP) of Ebola virus is the major target of neutralizing Abs. The envelope glycoprotein gene of Ebola virus encodes two GPs through transcriptional editing. The major product of the gene is a 364-residue soluble dimeric form of the GP (sGP). The precise role of sGP is not clear, however, it is thought that sGP may serve as a decoy to distract the immune response for virus evasion or contribute to pathogenesis (Pallesen et al., 2016).

The minor product of the gene is a 676-residue viral surface GP that is anchored to the viral envelope. The GP consists of two subunits, GP1 and GP2, which form a trimeric structure on the virus surface. The GP1 subunit contains the heavily glycosylated mucin-like domain and a glycan cap, which are cleaved proteolytically by cathepsins within the endosome during virus entry into the host cell (Pallesen et al., 2016; Lee et al., 2008). This exposes the receptor-binding site on the GP1 subunit that interacts with the endosomal receptor, domain C of the Niemann-Pick C1 protein (NPC1) (Bornholdt et al., 2016). Upon receptor binding, the fusion loop of the GP2 subunit becomes exposed, enabling fusion of the virus with the endosomal membrane (Pallesen et al., 2016; Lee et al., 2008). The involvement of GP in virus attachment and entry into host cells, receptor binding within the endosome, and membrane fusion with the endosomal membrane result in the GP being the major target of neutralizing mAbs (Saphire et al., 2018).

Cocktails of murine-human chimeric (ZMapp, ZMab, and MB-003) and human mAbs administered as a monotherapy have shown potent neutralizing and non-neutralizing activities for the prevention and treatment of EBOV in experimental infection animal models, including ZMapp protection of nonhuman primates (Qiu et al., 2014; Corti et al., 2016; Gilchuk et al., 2018). The mAbs characterized target diverse antigenic sites on GP, including the glycan cap, GP1 receptor-binding site, GP1 head, GP1/GP2 interface, GP2 fusion loop, GP2 stalk, and HR2/MPER region (Flyak et al., 2016; Bornholdt et al., 2016; Wec eet al., 2017; Flyak et al., 2018; Saphire et al., 2018; Gilchuk et al., 2018; Bornholdt et al., 2016; Hashiguchi et al., 2015; Misasi et al., 2016;

Wec et al., 2016; Audet et al., 2014; Murin et al., 2014; Davidson et al., 2015). Several mAbs that recognize antigenic sites present on the glycan cap and GP1 head are cross-reactive with sGP (Flyak et al., 2016; Saphire et al., 2018; Pallesen et al., 2016; Hashiguchi et al., 2015; Davidson et al., 2015) The ZMapp cocktail (2G4, 4G7, and 13C6) consists of three murine-human chimeric mAbs that recognize EBOV GP. 2G4 and 4G7 recognize the base of the GP at the GP1/GP2 interface and exhibit potent neutralization activity *in vitro* (Audet et al., 2014; Murin et al., 2014; Davidson et al., 2015). The other component of ZMapp is a weakly neutralizing mAb, 13C6, which recognizes the glycan cap and cross-reacts with EBOV sGP.

Characterization of human anti-EBOV mAbs

During my rotation project in Dr. Crowe's laboratory, I worked with Dr. Andrew Flyak to characterize human anti-EBOV mAbs he previously isolated from four survivors of EVD (designated subjects EVD2, EVD5, EVD9, and EVD15) that received treatment at Emory University Hospital in 2014. Peripheral blood mononuclear cells (PBMCs) were isolated from peripheral blood of these survivors collected one- and three-months post-discharge from the hospital. The human B cell response to natural filovirus infections early after recovery is poorly understood. Previous serologic studies suggest that some EBOV survivors exhibit delayed Ab responses with low magnitude and

quality. In this study, we sought to investigate the population of individual memory B cells induced early in convalescence.

Isolation of human GP-reactive mAbs from Ebola survivors

Prior to my rotation in Dr. Crowe's laboratory, Dr. Andrew Flyak and Nurgun Kose isolated a panel of 25 human mAbs from the EVD survivors. PBMCs were transformed with EBV, and after expansion, cell supernatants were screened to determine the relative magnitude of B cell responses to soluble forms of the EBOV, BDBV, SUDV, and MARV GP ectodomains. From the corresponding ELISA data, Circos plots were generated to illustrate the cross-reactivity of the B cell responses for each donor to the various GPs (**Figures 14A and 14B**). The relative height of each bar indicates the optical density (OD) values at 405 nm as determined by ELISA. Subjects EVD2 and EVD5 had a greater and broader B cell response to these GPs one-month after hospital discharge than subjects EVD9 and EVD15. However, an increase in B cell response to these GPs was observed for subject EVD15 at three-months after hospital discharge compared to one-month. The reactivities of EBOV GP and secreted GP (sGP)-specific B cell lines were primarily EBOV GP/sGP cross-reactive (**Figure 14C**) for all subjects at both time points, except for EVD15 at the one-month time point (EVD15_1). Additionally, a majority of the B cell reactivity was toward EBOV GP and sGP. There was an increase in cross-reactivity to BDBV GP of subject samples at

three-months compared to one-month post-discharge, indicating that development of these Abs occurred over the period of recovery. A minor percentage of reactive B cells were cross-reactive to EBOV, BDBV, and SUDV GP and again increased at the three-months compared to the one-month post-discharge time point.

During my rotation project, I determined the half-maximal effective concentration (EC_{50}) of binding values for the EBOV GP-reactive human mAbs via ELISA (**Figure 15A**). The mAbs exhibited values for EC_{50} in diverse ranges, including 0 to 100 ng/mL, 100 to 1,000 ng/mL, 1,000 to 10,000 ng/mL, or greater than 10,000 ng/mL, as indicated in the heat map by dark red, orange, or yellow color, or a greater than sign (>), respectively. The EBOV GP-reactive human mAbs are separated into four groups, with two subgroups (A and B) for groups 1 and 2 designated based on pattern of reactivity to the various GPs. The A subgroup indicates mAbs that bound GP and EBOV sGP, suggesting the GP1 glycan cap as the GP binding site for these mAbs, whereas mAbs from the B subgroup bound GP only. Increasing in cross-reactivity, group 1 bound EBOV, group 2 bound EBOV and BDBV or SUDV, and group 3 bound EBOV, BDBV, and SUDV. Group sGP mAbs bound to EBOV sGP only. None of these mAbs bound to MARV GP. The isolation of mAbs, primarily from subjects EVD2 and EVD5 at one- and three-months post-discharge, reflects the intensity and broad B cell response measured initially with EBV-transformed B cell line supernatants, as indicated by the Circos plots (**Figures 14A and 14B**).

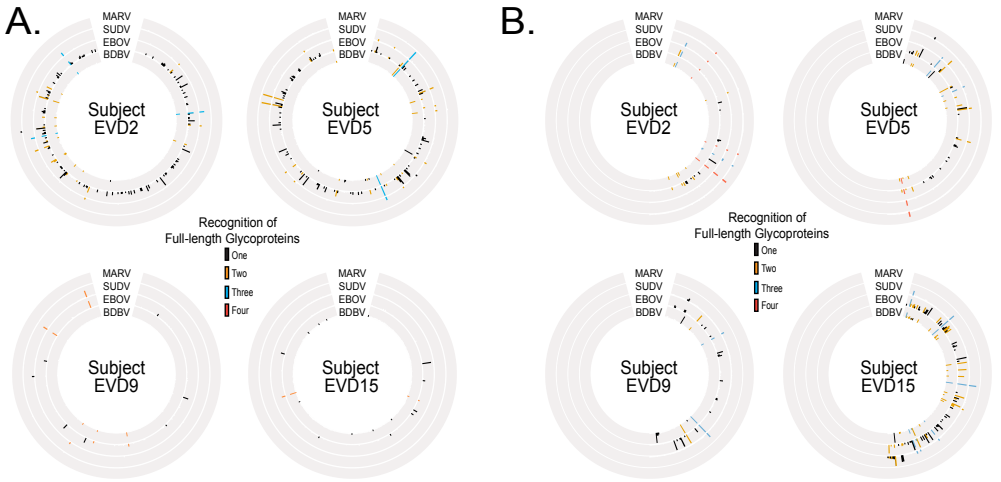

C.

		Reactivity of GP or sGP-specific B cell lines with diverse GPs (%)								
Subject	Total number of GP or sGP-specific lines	EBOV GP-specific	EBOV sGP-specific	EBOV GP/sGP cross-reactive	EBOV/BDBV GP cross-reactive	EBOV GP/sGP and BDBV cross-reactive	EBOV/SUDV GP cross-reactive	EBOV GP/sGP and SUDV cross-reactive	EBOV/BDBV/ SUDV GP cross-reactive	EBOV GP/sGP and BDBV/SUDV cross-reactive
EVD2_1	47	13	0	64	4	11	0	2	0	6
EVD5_1	24	8	0	63	0	4	4	13	4	4
EVD9_1	13	0	31	46	0	8	0	15	0	0
EVD15_1	10	30	50	10	10	0	0	0	0	0
EVD2_3	16	0	19	50	0	25	0	0	0	6
EVD5_3	28	14	18	25	4	25	0	11	0	4
EVD9_3	12	33	0	33	0	17	0	0	8	8
EVD15_3	36	6	0	56	8	19	0	0	3	8

% Reactivity
60-100
30-59
0-29

Figure 14. Circos plot representation of the four EVD survivors' cross-reactive B cell responses. A and B. PBMC samples isolated from donors EVD2, EVD5, EVD9, and EVD15 one-month (**A**) or three-months (**B**) post-discharge were transformed with EBV and subsequently expanded. The supernatants from the transformed B cell lines were screened initially for binding to the soluble form of full-length extracellular domain of MARV, SUDV, EBOV, or BDBV GP. The height of the lines indicates the relative intensity of the optical density (OD) values at 405 nm as determined by ELISA using the indicated GP. Black lines indicated the antibody bound only to GP from one species. Orange, blue, and red lines represent cross-reactive B cell responses to GP from two, three, or four virus species, respectively. For PBMC samples isolated from donors EVD9 and EVD15 at three-months post-discharge, supernatant reactivity from transformed B cell lines was not tested against MARV GP. **C.** The reactivity of EBOV, BDBV, SUDV GP and EBOV B cell lines are represented as the percentage of total GP and/or sGP-specific B cell lines. Positive reactivity was determined by >0.8 optical density values at 405 nm. The values are heat mapped according to percent reactivity with >60% in dark green, 30 to 60% in lighter green, and <30% in light green. Williamson et al., 2019.

EBOV237, a neutralizing mAb

To determine the antiviral activity of the EBOV GP-reactive human mAbs, we collaborated with Dr. Pamela J. Glass's laboratory to perform neutralization assays

against Ebola Zaire virus (EBOV/Kik-9510621, CDC no. 807224). Plaque reduction neutralization test (PRNT) assays were performed to determine the endpoint titer for 50% ($PRNT_{50}$) or 80% ($PRNT_{80}$) reduction in plaques compared to a virus-only control. From the panel of 25 human anti-EBOV mAbs, one mAb (designated EBOV237) was neutralizing with a $PRNT_{50}$ of 0.78 μg/ml and a $PRNT_{80}$ of 1.56 μg/ml (**Figure 15C**).

A representative curve for binding of EBOV237 to full-length EBOV, BDBV, SUDV, or MARV GP, or EBOV sGP (**Figure 15B**). EBOV237 bound to EBOV GP, BDBV GP, and EBOV sGP with EC_{50} values of 25, 3,367, and 9 ng/ml, respectively. EBOV237 did not bind SUDV and MARV GPs. Thus, EBOV237 primarily binds to EBOV GP, EBOV sGP, and BDBV GP, albeit with lower affinity. Stronger binding of EBOV237 to EBOV GP in comparison to the other human anti-EBOV mAbs correlated with its neutralization activity toward EBOV.

A. Binding and neutralizing activity of 25 human mAbs

EBOV mAb	Donor Sample	Binding Group	EC50 values for mAb binding to glycoprotein (ng/mL)				Neutralization Screen
			EBOV	BDBV	SUDV	EBOV sGP	
27	EVD2_1	1A	3,505	>	>	47	Negative
102	EVD5_1		180	>	>	32	Negative
106	EVD5_1		2,902	>	>	211	Negative
236	EVD5_3		964	>	>	32	Negative
229-2	EVD5_3	1B	690	>	>	>	Negative
9	EVD2_1	2A	559	219	>	251	Negative
29	EVD2_1		124	118	>	47	Negative
119	EVD5_1		1,108	314	>	294	Negative
173	EVD9_1		2,707	1,843	>	231	ND
196	EVD2_3		719	4,207	>	56	ND
202	EVD2_3		934	1,833	>	1,421	Negative
210	EVD2_3		576	176	>	196	Negative
211	EVD2_3		289	230	>	126	Negative
216	EVD5_3		1,284	4,912	>	269	ND
218	EVD5_3		2,110	2,898	>	440	ND
226	EVD5_3		1,315	2,633	>	245	Negative
237	EVD5_3		25	3,367	>	9	Positive
109	EVD5_1	2B	731	948	>	>	Negative
184	EVD15_1		230	413	>	>	Negative
214	EVD5_3		199	>	182	>	Negative
194	EVD2_3	3A	160	199	435	46	ND
220	EVD5_3		262	549	1,541	66	ND
229-1	EVD5_3		1,485	2,899	7,193	400	Negative
188	EVD15_1	"sGP"	>	>	>	87	Negative
208	EVD2_3		>	>	>	312	Negative

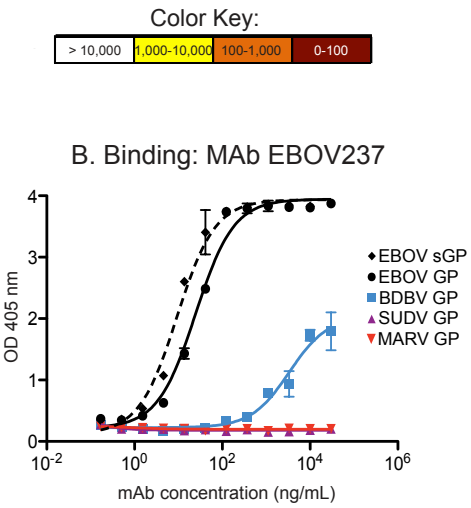

C. Neutralization: MAb EBOV237

Sample	$PRNT_{50}$ (µg/mL)	$PRNT_{80}$ (µg/mL)
EBOV237	0.78	1.56

Figure 15. Binding and neutralization characterization of mAb EBOV237. A. Twenty-five human mAbs were isolated from the four EVD survivors, with respective subject number and month of PBMC isolation post-discharge indicated. These mAbs are organized into groups and subgroups based on their breadth of binding for diverse GPs. Of the 25 mAbs, all but two bound to EBOV GP. These mAbs bound only to full-length EBOV sGP and are referred to as "sGP". Subgroup A includes mAbs able to bind to full-length EBOV GP and EBOV sGP. Subgroup B includes the mAbs that bound only to full-length EBOV GP. Group 1, 2, and 3 indicate the breadth of the mAb to EBOV, EBOV and BDBV, and EBOV, BDBV, and SUDV GP, respectively. The EC_{50} values (ng/mL) <100 ng/mL are in red, < 1,000 ng/mL in orange, and < 10,000 ng/mL in yellow. EC_{50} values (ng/mL) > 10,000 ng/mL are in white and indicated with the symbol >. The EC_{50} values shown are an average of technical triplicates, and are representative of two duplicate ELISAs, with similar results. Neutralization data for each mAb is shown as either positive or negative, with EBOV237 shown in red. **B.** Binding curve for EBOV237 to full-length EBOV, BDBV, SUDV, MARV GP, or EBOV sGP, as measured by OD at 405 nm with increasing mAb concentration. **C.** Neutralization data of EBOV237 as determined by plaque reduction neutralization tests (PRNTs) at 50% ($PRNT_{50}$) or 80% ($PRNT_{80}$) reduction, corresponding with the indicated IC_{50} values of 0.75 µg/mL and 1.56 µg/mL, respectively. ND, not tested. Williamson et al., 2019.

Epitope mapping of EBOV237 to the glycan cap region of EBOV GP1

To determine the epitopes recognized by the panel of human anti-EBOV mAbs, I performed competition-binding assays with mAbs that bound to EBOV GP or sGP as determined by a >0.19 nm shift in the interference pattern of light through biolayer interferometry. Four epitope groups were identified on EBOV GP from the panel of human anti-EBOV mAbs. Recombinant forms of two mAbs that are components of the ZMapp therapeutic cocktail (2G4 and 13C6) were used as controls for binding to EBOV GP. The epitopes for 2G4 and 13C6 are known, as they bind to the base of the GP or to the GP1 glycan cap, respectively (Murin et al., 2014; Davidson et al., 2015). None of the mAbs tested competed with 2G4, indicating that these mAbs do not bind to the base of EBOV GP. EBOV237 did not compete for binding with either 2G4 or 13C6 (**Figure 16A**), indicating that EBOV237 binds to a distinct site on EBOV GP. EBOV237 competed for binding with EBOV173 and EBOV236, suggesting that these human anti-EBOV mAbs bind similar sites on EBOV GP. Several unidirectional pairs were identified as well, such as EBOV173 and 13C6. This may be due to difference in angle of binding of the first mAb relative to the second mAb. This could allow for binding of the mAb in one direction but not in the other. Additionally, the relative kinetics of binding for the first mAb may also account for the unidirectional competition of mAb binding. EBOV237 and a previously isolated neutralizing BDBV mAb, BDBV43 (Flyak et al., 2016), were competed with the human anti-EBOV mAbs on EBOV sGP (**Figure 16B**). In addition to competition with BDBV43, EBOV237 competed partially with EBOV29 or EBOV102 on EBOV sGP. EBOV237 did not compete for binding with the previously isolated non-

neutralizing mAb BDBV91, which is known to bind to the hydrophobic pocket at the EBOV sGP dimer interface (Pallesen et al., 2016).

In collaboration with Drs. Edgar Davidson and Benjamin Doranz at Integral Molecular, mutations were introduced into GP through alanine-scanning shotgun mutagenesis of EBOV GPΔmucin (Ebola virus H.sapiens-tc/COD/1976/Yambuku-Mayinga [23], Δ311–461) to identify key residues recognized by EBOV237. Identification of the residues N278 and P279 as critical residues for binding confirmed that the EBOV237 epitope lies within the glycan cap region of GP1 (**Figures 16C** to **16E**). The critical residues for EBOV237 are conserved in BDBV, supporting the cross-reactivity profile of EBOV237 to BDBV GP. However, the reduction in binding of EBOV237 to BDBV GP (EC_{50} value, 3,367 ng/ml) suggests that other factors may be involved. This is also consistent with the cross-reactivity profile of EBOV237 in SUDV (not recognized by EBOV237) residues 278 and 279 are D278 and A279, respectively. The glycan cap region of GP1 also is bound by the ZMapp cocktail mAb 13C6. Residues G264 to W275, identified for binding of this mAb to EBOV GP, lie at the tip of the glycan cap (Pallesen et al., 2016; Davidson et al., 2015). The difference in residues bound by EBOV237 and 13C6 is consistent with the differences observed in the competition-binding assays done with EBOV GP (**Figure 16A**). Thus, even though these two mAbs bind to the glycan cap of GP1, EBOV237 and 13C6 recognize distinct residues or epitopes in this domain.

To identify key residues selectively pressured to mutate in the presence of EBOV237, we collaborated with Dr. Peter Halfmann's laboratory to isolate EbolaΔVP30-

GFP neutralization escape mutant viruses. Sequence analysis of EBOV GP for the mutant viruses identified the mutated residues I260R and S322G. These two mutations were identified in four different independently selected neutralization escape mutant viruses (**Figure 16F**). PRNTs confirmed the ablation of neutralization for escape mutant 4 in the presence of different concentrations of EBOV237 (**Figure 16F**). Plaque titers for escape mutant 4 were similar to those of the control MAb VP35 for wild-type or mutant viruses. Thus, EBOV237 selectively pressures the virus to mutate at these key residues as it binds the glycan cap of GP1, leading to escape of the virus from the neutralization capabilities of EBOV237. The escape mutation at I260 is consistent with glycan cap location and EBOV237 epitope (critical residues N278 and P279). However, the escape mutation S322G presumably exerts an allosteric effect, since it is not located within the glycan cap but instead within the mucin-like domain. The EBOV237 cross-reactivity with sGP, which lacks residue S322, is also inconsistent with inclusion of S322 as part of the epitope.

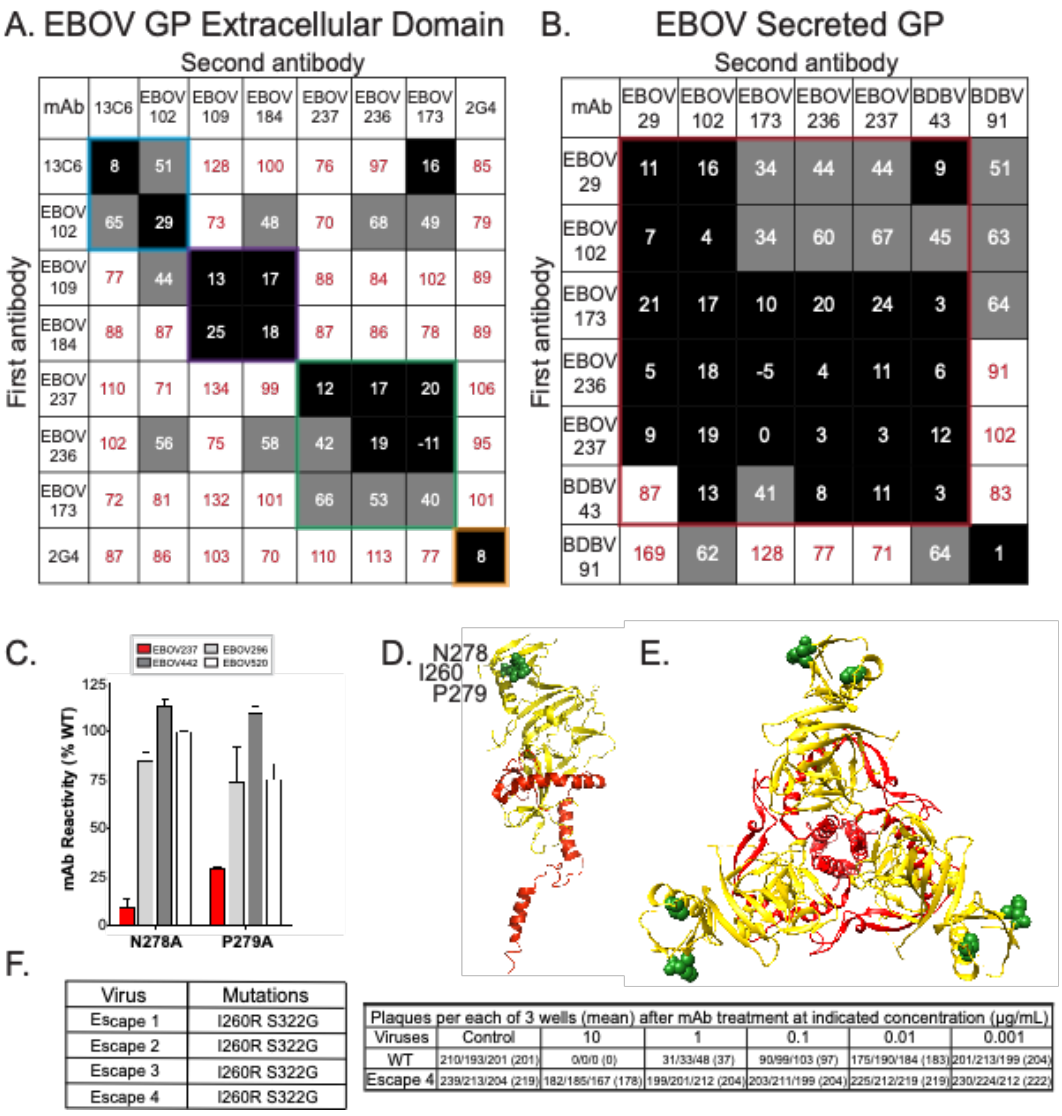

Figure 16. Epitope mapping of EBOV237 indicates binding to the glycan cap. A and B. Competition-binding analysis of mAbs to full-length EBOV GP (**A**) and EBOV sGP (**B**) are indicated. The numbers indicate residual percent binding of the second Ab in the presence of the first Ab, in comparison to the absence of the first Ab. A reduction in percent binding of the second Ab to <30% due to the presence of the first Ab (black boxes with white numbers), indicates full competition for binding. A reduction in percent binding of the second Ab to 30 to 70% due to the presence of the first Ab (grey boxes with black numbers), indicates intermediate competition. A reduction in percent binding of the second Ab >70% due to the presence of the first Ab (white boxes with red numbers), indicates a lack of competition. **C to E.** EBOV237 was epitope mapped by screening on an EBOV Δmucin GP alanine scan mutation library expressed in HEK-293T cells, with binding by EBOV237 assayed by flow cytometry. This identified N278A and P279A as a critical clones that showed specifically reduced binding for EBOV237 Fab (<20% and <30% of binding to WT EBOV GP, respectively; red bar), but a high level of binding to control mAbs EBOV296, EBOV442, or EBOV520 (gray/white bars) **C**. Error bars represent the mean and range (half of the maximum minus minimum values) of at least two replicate data points. The monomer (**D**; side view) or

trimer (**E**; top view) form of EBOV ∆mucin GP, with GP1 in yellow and GP2 in red (PDB: 5JQ3) is shown (Zhao et al., 2016). The critical binding residues for EBOV237 (N278, P279, and I260) to EBOV ∆mucin GP are indicated by the green spheres on either structure. S322 is not shown, as this residue corresponds to the mucin-like domain of EBOV GP. **F**. Four Ab neutralization escape mutant viruses were isolated, each with the mutations I260R and S322G. A PRNT assay was done using 10, 1, 0.1, 0.01, or 0.001 µg of EBOV237 incubated with either wild-type (WT) virus or escape mutant 4. The numbers for the assays, performed in triplicate, indicate plaque-forming units per well. Williamson et al., 2019.

In vivo studies revealed a correlate of protection

In collaboration with Dr. Pamela Glass's laboratory, mouse challenge studies were performed to determine the prophylactic efficacy of EBOV237. Initially, groups of 10 female BALB/c mice, age 6 to 8 weeks, were treated intraperitoneally (i.p.) 24 h prior to virus inoculation (day −1) with a single dose of 100 µg of EBOV237. For the positive-control group, mice were treated i.p. with 100 µg of mAb 13C6. For the negative-control group, mice were treated i.p. with an irrelevant IgG antibody. On day 0 (d0), mice were inoculated i.p. with 100 PFU of mouse-adapted Ebola Zaire virus (Mayinga) (ma-ZEBOV). Mice were monitored daily for 28 days after virus inoculation. EBOV237 provided a similar level of protection against ma-ZEBOV infection as the positive-control MAb 13C6 (**Figure 17A**). An irrelevant negative-control IgG Ab did not protect mice from lethal infection. To observe clinical signs of disease, mice were monitored twice daily for 28 days after virus inoculation (**Figure 17B**). Individual disease score parameters included normal (0), reduced grooming/ruffled fur (1), subdued but normal when stimulated (2), lethargic, hunched posture, subdued even when stimulated (3), and nasal discharge/bleeding/unresponsive when stimulated/weak/paralysis (4).

Animals treated with the irrelevant negative-control IgG Ab exhibited several signs of disease. Animals treated with mAb 13C6 or EBOV237 also showed some signs of disease. However, there was a reduction in signs of clinical disease for both of these groups, with a slight improvement shown for EBOV237. Group body weights were taken daily for 28 days after virus inoculation (**Figure 17C**). Groups treated with EBOV237 or 13C6 showed little variation in average weight of mice over the 28 days. The group treated with irrelevant negative-control IgG Ab showed variation in average weight, corresponding with survival of the mice (**Figure 17A**). These data confirm the prophylactic efficacy of EBOV237 against ma-ZEBOV infection.

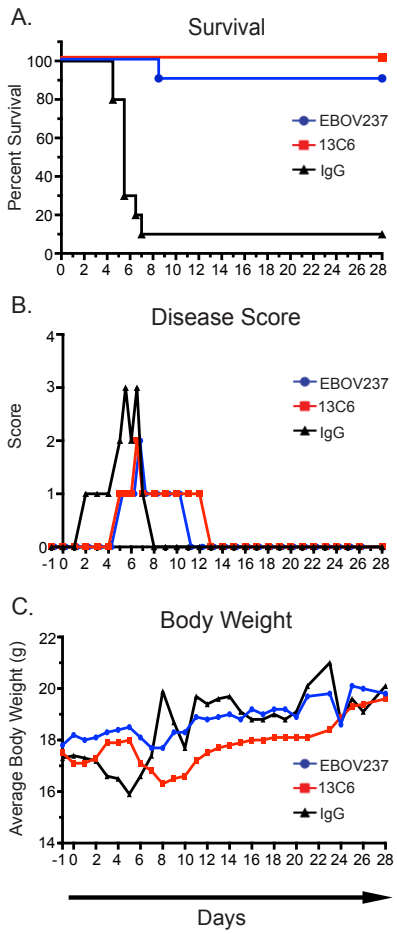

Figure 17. EBOV237 provided prophylactic protection from mouse-adapted Ebola Zaire (Mayinga) infection. BALB/c mice in groups of 10 were each given 100 µg of EBOV237 intraperitoneally 24 hours prior to challenge with 100 PFU of Mayinga virus i.p.. **A.** Kaplan-Meier survival curve indicates that EBOV237 provides similar protection against lethal disease as mAb 13C6, in comparison to the irrelevant negative control IgG. **B.** Disease scores were recorded based on the sickest animal in each treatment group over the course of 28 days (normal (0), reduced grooming/ruffled fur (1), subdued, but normal when stimulated (2), lethargic: hunched posture; subdued even when stimulated (3), nasal discharge/bleeding/unresponsive when stimulated/weak/paralysis (4)). Animals treated with mAb 13C6 or the irrelevant negative-control IgG exhibited several signs of disease, with an improvement shown for EBOV237. **C.** Average weight of mice (calculated from group weight divided by number of mice weighed) taken over a course of 28 days. Mice treated with EBOV237 or 13C6 showed little variation in average weight of mice over the course of study. Mice treated with the irrelevant negative-control IgG showed variation in average weight. Williamson et al., 2019.

A dose-response curve also was performed to determine the efficacy of protection for EBOV237 against mouse-adapted Ebola Zaire virus (Mayinga) (ma-ZEBOV) infection. At 24 h prior to virus inoculation, groups of 10 female BALB/c mice, age 6 to 8 weeks, were treated i.p. with a single dose of 200, 100, 50, or 25 μg of EBOV237. The positive- and negative-control groups were the same as described for the initial study. On day 0, mice were inoculated i.p. with 100 PFU of ma-ZEBOV. Mice were monitored daily for 21 days after virus inoculation. Survival depended on the dose of EBOV237 administered, with a dose of 200 μg providing similar protection against ma-ZEBOV infection to the positive-control mAb 13C6 administered at 100 μg (**Figure 18A**). Animals treated with EBOV237 showed a reduction in signs of disease in a dose-dependent manner. Similar improvement of disease was observed for mice treated with 200 μg of EBOV237 and with the positive-control mAb 13C6 (**Figure 18B**). Little variation in the average weight of mice over the course of 21 days was observed for animals treated with any dose of EBOV237 compared to animals treated with the irrelevant negative-control Ab.

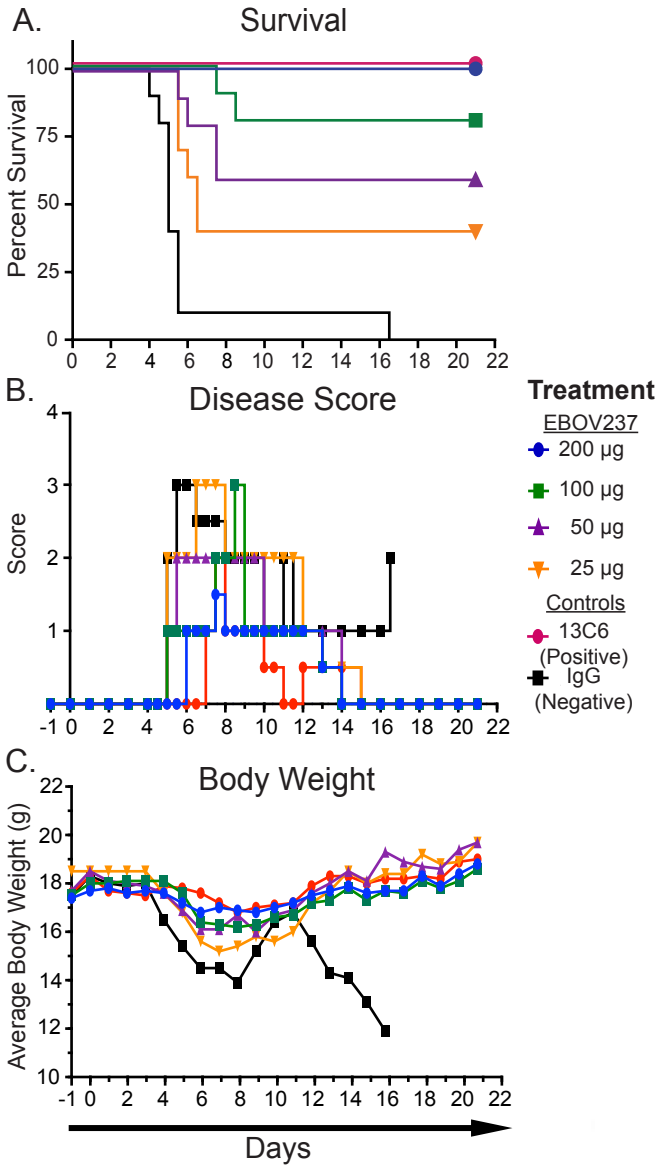

Figure 18. EBOV237 provides dose-dependent efficacy. Groups of ten mice were given either 200, 100, 50, or 25 μg EBOV-237, or 100 μg of a positive-control mAb 13C6, or 100 μg of an irrelevant negative-control IgG i.p. 24 hours prior to challenge with 100 PFU of Mayinga virus i.p. **A.** Kaplan-Meier survival curve over the course of 21 days demonstrates the extent of survival depended on the dose of mAb. EBOV237 given at 200 μg provided a similar level of protection against lethal disease caused by Mayinga virus as mAb 13C6, in comparison to the irrelevant negative-control IgG. **B.** Individual disease scores were determined over the course of 21 days (normal (0), reduced grooming/ruffled fur (1), subdued but normal when stimulated (2), lethargic, hunched posture, subdued even when stimulated (3), nasal discharge/bleeding/unresponsive when stimulated/weak/paralysis (4)). Reduction of disease score was observed in a dose-dependent manner for animals treated with EBOV237. **C.** Average weight of mice (calculated from group weight divided by number of mice weighed) taken over a course of 21 days. Mice treated with any dose of EBOV237 or 13C6 showed little variation in average weight of mice over

the course of the study compared to mice treated with the irrelevant negative-control IgG. Williamson et al., 2019.

Non-canonical inter-CDR loop interaction of MR78

In addition to the studies on EBOV237, I performed ELISA binding assays of the human anti-MARV mAb, MR78, previously described and isolated by Dr. Andrew Flyak (Flyak et al., 2015). MR78 is potent neutralizing human mAb that targets the NPC1 receptor binding site of GP1 (Hashiguchi et al., 2015). Dr. Amandeep Sangha modeled MR78 in complex with MARV GP using Phenix.Rosetta refinement and identified a critical interaction between the HCDR3 and HCDR1 loop for binding to MARV GP (Sangha et al., 2017). To confirm this interaction, I tested binding of wild-type (WT) MR78 IgG and the MR78 Tyr37Phe mutant to MARV GP. A ten-fold reduction in binding was observed for the Tyr37Phe mutant, which highlighted the importance of this residue for inter-CDR loop interactions (**Figure 19**).

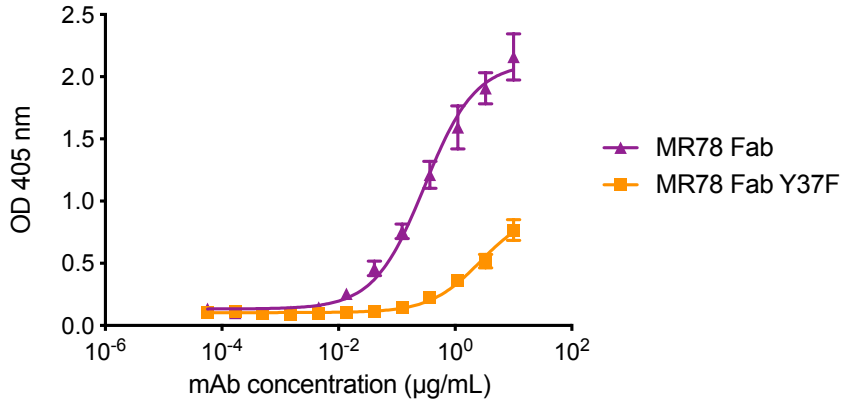

Figure 19. Binding of MR78 Fab and MR78 Tyr37Phe Fab to MARV GP. MR78 binds MARV GP with an EC_{50} value of 0.30 µg/mL (95% confidence interval: 0.22-0.42 µg/mL) and MR78 Tyr37Phe Fab binds MARV GP with an EC_{50} value of 2.71 µg/mL (95% confidence interval: 1.77-4.15 µg/mL), resulting in a ten-fold reduction in binding to MARV GP. EC_{50} values of MR78 and MR78 Tyr37Phe Fab to MARV GP were obtained via ELISA. Technical triplicates of each were performed. Plates were coated with 1 µg/mL MARV GP. MR78 and MR78 Tyr37Phe Fab molecules were serially diluted three-fold from 10 µg/mL to 56.5 ng/mL. EC_{50} values and 95% confidence intervals were calculated using a non-linear regression analysis of the curves generated in Prism v.5 (GraphPad Software). GraphPad Prism software was used to determine average values, standard errors, and standard deviations. Copyright permission from publisher Elsevier (Sangha et al., 2017).

ELISA optimization for isolation of human anti-EV-D68 mAbs

My initial project in Dr. Crowe's laboratory involved the isolation of human anti-picornavirus mAbs, such as rhinoviruses (RV). RVs are the etiological agents of the common cold and consists of three species groups, A, B, and C. RVs are highly morbid and can result in severe respiratory illnesses in children (RV-C) (Jacobs et al., 2013). In the lab, the goal of my project was to isolate human anti-RV mAbs and study their mechanism(s) of neutralization. However, initial ELISA studies with RV immune guinea pig serum showed high levels of background due to non-specific binding to negative

controls, such as cell culture media and blocking buffer. Following many iterations of ELISA optimization, involving different blocking buffers, secondary Ab detection methods, and ELISA plates, I was able to have an ELISA based assay with some specificity to highly purified RVs (**Figure 20**).

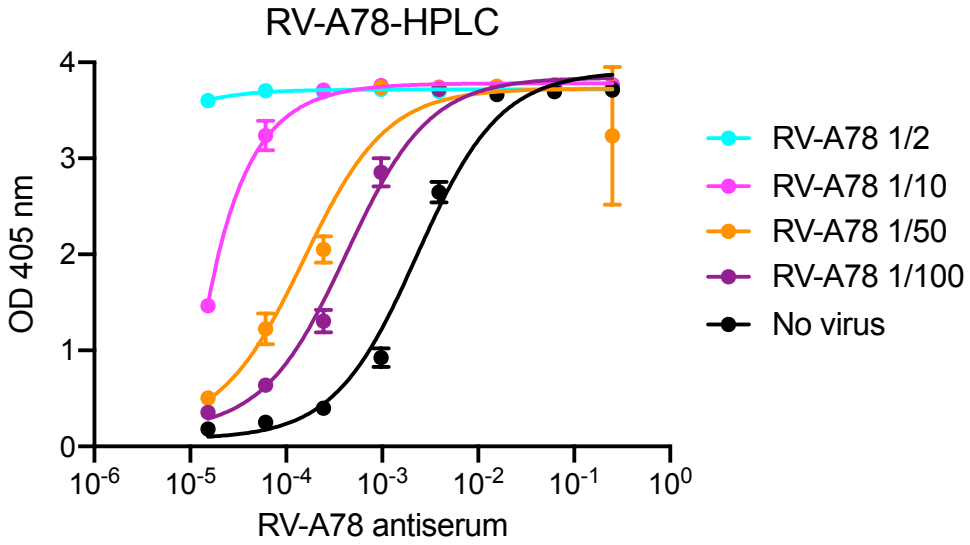

Figure 20. Optimized RV ELISA assay. Purified RV-A78 was directly coated on ELISA plates at the indicated dilutions. RV-A78 was detected with RV-A78 immune guinea pig serum. A negative control was included, which contained only blocking buffer, and has a high background due to non-specific binding. Data represent mean ± SD of technical triplicates.

A high signal is still observed in the no-virus control with highly purified RV, which is suboptimal for hybridoma screening and selection of human anti-RV mAbs. As I transitioned to studying the human humoral response against alphaviruses, Dr. Matthew Vogt continued on with the project to overcome this high non-specificity and isolated potently neutralizing and protective human anti-EV-D68 mAbs (Vogt et al., 2020).

Competition-binding studies and human ACE2 blocking by human anti-SARS-CoV-2 mAbs

During the COVID-19 pandemic, I contributed to epitope mapping studies of a panel of neutralizing human anti-COV2 mAbs to the receptor binding domain (RBD) of the SARS-CoV-2 spike protein through biolayer interferometry (**Figure 21**). I tested the panel against two mAbs, COV2-2196 and CR3022, as reference mAbs. CR3022 is a previously described SARS-CoV neutralizing and RBD binding mAb isolated from a SARS-CoV immune individual that recognizes a conserved epitope of SARS-CoV and SARS-CoV-2. However, CR3022 does not neutralize SARS-CoV-2 at the concentrations tested (Yuan et al., 2020; Zost et al., 2020). COV2-2196 was identified in this panel of mAbs from individuals with documented SARS-CoV-2 infection and potently neutralizes SARS-CoV-2 (Zost et al., 2020). Through competition-binding studies, I identified three antigenic sites targeted by the panel of neutralizing mAbs. A majority of the mAbs competed with COV2-2196, which suggests a critical neutralization site. A few mAbs competed with CR3022. Two mAbs, COV2-2130 and COV2-2096, did not compete with either reference mAb, which indicates recognition of a distinct antigenic site. Furthermore, all of the mAbs tested, excepted for CR3022, blocked ACE2 binding, which suggests the antigenic sites are within or close in proximity to the ACE2 RBD on the spike protein.

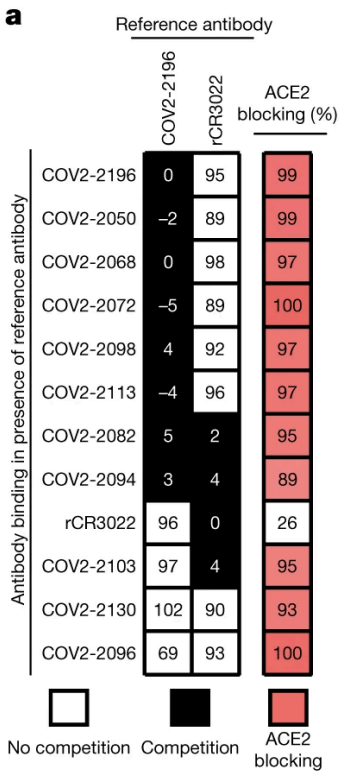

Figure 21. Competition-binding analysis of neutralizing human anti-SARS-CoV-2 mAbs to the RBD of the spike protein. Ab (left-hand column) binding was assessed as percent binding in the presence of reference Ab (top) to the spike protein RBD. Black boxes indicate competition between the mAbs (<33% relative binding compared to maximal binding). White boxes indicate the mAbs do not compete (>67% relative binding compared to maximal binding). Abs were also incubated with ACE2 to measure relative blocking of ACE2 binding to the RBD of the spike protein. Red boxes indicate % blocking of ACE2 binding. Copyright permission from publisher Springer Nature (Zost et al., 2020).

Discussion

During my initial studies in Dr. Crowe's laboratory, I learned ELISA-based and epitope mapping techniques that I was able to apply to the main part of my thesis work on characterization of human anti-alphavirus mAbs. I learned the importance of

validated reagents and assays. Additionally, I learned the importance of proper positive and negative controls.

In addition to gaining technical expertise in these methods, I was fortunate to have the opportunity to apply these skills to study RBD-blocking, neutralizing epitopes targeted by human anti-COV2 mAbs on the SARS-CoV-2 S protein during the COVID-19 pandemic. I also studied the quality of human anti-EBOV mAbs isolated from early convalescent EVD survivors during my rotation project in Dr. Crowe's laboratory. The pathogenesis of Ebola virus disease (EVD) in humans is complex, and the mechanisms contributing to immunity are poorly understood. At the beginning of this chapter, I investigated the B cell response in survivors one- and three-months post-discharge from the hospital, at a time when immune activation persisted, and virus may have persisted in immune-privileged sites. The results show that soon after the resolution of viremia, the memory B cell response in blood is characterized by a low frequency of EBOV-specific B cells, with the Abs encoded by those cells displaying low neutralizing activity. Of twenty-five mAbs isolated from four donors, only one exhibited neutralization activity. This neutralizing mAb, designated mAb EBOV237, recognizes an epitope in the glycan cap of the surface GP. *In vivo* murine lethal challenge studies showed that EBOV237 conferred protection when given prophylactically at a level similar to that of the ZMapp component mAb, 13C6. The results suggest that the human B cell response to EVD one- to three- months post-discharge is characterized by a paucity of broad or potent neutralizing clones. However, the neutralizing epitope in the glycan cap recognized by EBOV237 may play a role in the early human Ab response to EVD. Further

characterization of this site in rational design strategies for Ebola virus vaccine candidates should be considered.

Materials and Methods

Research subjects

The subjects, designated EVD2, EVD5, EVD9, and EVD15, were patients who survived EVD and received treatment at Emory University Hospital in 2014. The clinical course and immune activation profiles for these patients were previously described (McElroy et al., 2015; Lyon et al.; 2014). Peripheral blood from the subjects was collected one- month and three-months post-discharge from the hospital. The sample that yielded the mAb EBOV237 is designated EVD5_3, indicating the subject sample identification (EVD5) and time point of peripheral blood collection (three-months post-discharge). Multiple PCR tests were performed to detect the presence of virus, which were negative, indicating the absence of virus at these time points. The institutional review boards (IRBs) at Emory University and Vanderbilt University Medical Center approved the protocol for the recruitment and collection of blood samples used in this study. Specifically, the subjects were enrolled under an Emory protocol, IRB00076700, The Longitudinal Characterization of Immune Responses to Ebola Virus Infections. The

samples were obtained after the subjects gave written informed consent. PBMCs were isolated and cryopreserved in liquid nitrogen until use.

Generation of human hybridomas

Previously cryopreserved PBMCs were thawed rapidly in a 37°C water bath. The cells were washed and resuspended in prewarmed medium A (catalog no. 03801; ClonaCell-HY) prior to EBV transformation. In 16 mL of B cell growth medium (medium A, 50 µL CpG [2.5 mg/mL; Invitrogen oligonucleotide ZOEZOEZZZZZOEEZOEZZZT], 15 µL Chk2 inhibitor [10 mM in dimethyl sulfoxide {DMSO}; catalog no. C3742; Sigma], and 20 µL cyclosporine [1 mg/mL in ethanol; catalog no. C1832; Sigma]), 4.5 mL of filtrate containing EBV from the B95.8 cell line (ATCC CRL-1612) was added. The PBMCs then were added and plated at 50 µL/well for 8 to 10 million cells per 384-well plate (catalog no. 164688; Thermo Scientific). After 7 to 10 days at 37°C, cells were expanded into four 96-well plates (catalog no. 353072; Falcon) at 200 µL/well in 20 mL of B cell expansion medium (medium A, 50 µL CpG, 15 µL Chk2 inhibitor, and irradiated [9,000 rads] heterologous human PBMCs [Nashville Red Cross] at 10 million cells/mL) per 96-well plate. The plates were incubated for an additional 4 days at 37°C, prior to screening by ELISA with purified GPs (described below and as previously described (Flyak et al., 2016)). Cells from positive wells containing supernatant reactive for an EBOV-specific ELISA were added to 1 mL of prewarmed BTX cytofusion medium (300 mM sorbitol [catalog no. 36021; Sigma], 0.1 mM calcium acetate [catalog no. AC21105-2500; Fisher], 0.5 mM magnesium acetate [catalog no. AC42387-0050;

Fisher], and 1 mg/mL bovine serum albumin [BSA; catalog no. A9418; Sigma]) in microcentrifuge tubes. The microcentrifuge tubes were centrifuged at 3,000 rpm for 4 min, and the supernatant was decanted. This procedure was repeated for a total of three times. HMMA 2.5 cells were washed 3× in BTX cytofusion medium and resuspended in BTX cytofusion medium for a total of 10 million cells/mL. HMMA 2.5 nonsecreting myeloma cells then were added to the microcentrifuge tubes containing the positive EBV-transformed B cell pellet, for a total of 1.15 million cells per fusion. These cells were resuspended and transferred to a cytofusion cuvette (catalog no. 450125; BTX). Electrofusion of the cells was performed as described previously (Yu et al., 2008). The cuvettes were incubated at 37°C for 30 min. The cells then were added to 21 mL of HAT medium (400 mL of medium A, 100 mL of medium E [catalog no. 03805; ClonaCell-HY], 50× HAT medium supplement [100 µM hypoxanthine, 0.4 µM aminopterin, 16 µM thymidine; catalog no. H0262; Sigma], 150 µL ouabain octahydrate [1 mg/mL; catalog no. O3125; Sigma]) and plated at 50 µL/well in 384-well plates. The plates were incubated for a total of 18 days at 37°C in 7% CO_2 prior to screening by ELISA.

Human MAb production and purification

Positive wells from hybridoma fusions containing supernatant reactive for an EBOV-specific ELISA were cloned biologically by single-cell fluorescence-activated cell sorting. These clones then were expanded serially in 1, 2, and then 30 mL of medium E

into 48-well plates (catalog no. 3548; Corning), 12-well plates (catalog no. 3513; Corning), and T-75-cm^2 flasks (catalog no. 430641; Corning), respectively. For each T-75-cm^2 flask, the cells were scraped and expanded further into four T-225-cm^2 flasks (catalog no. 431082; Corning) in 250 mL of serum-free medium (Hybridoma-SFM, catalog no. 12045-076; Gibco). After 21 days at 37°C, the supernatants were filtered using a 0.2-μm-pore-size filter. Abs were purified from the filtrate using HiTrap protein G or HiTrap MabSelectSure columns (catalog no. 17040501 and 11003494, respectively; GE Healthcare Life Sciences).

Screening ELISA

Soluble forms of the full-length extracellular domain of EBOV, BDBV, SUDV, and MARV GPs (1 μg/mL) or EBOV secreted GP (sGP) (1 μg/mL) were diluted in 1× Dulbecco's phosphate-buffered saline without calcium and magnesium (D-PBS) to coat 384-well ELISA plates (catalog no. 265203; Thermo Scientific) at 25 μL/well and incubated at 4°C overnight. The plates were washed 3× with D-PBS-T (1× D-PBS plus 0.05% Tween 20) and blocked for 1 h at room temperature with blocking solution (1% nonfat dry milk [blotting-grade blocker, catalog no. 170-6404; Bio-Rad], 1% goat serum [catalog no. 16210-072; Gibco] in D-PBS-T). After blocking, the plates then were washed 3× with D-PBS-T, and 10 μL/well of supernatant from wells containing EBV-transformed B cells was added. Plates were incubated for 2 h at room temperature and then washed 3× with D-PBS-T. A solution of secondary Abs (goat anti-human IgG Fc

gamma fragment-specific alkaline phosphatase [AP] conjugated, catalog no. W99008A; Meridian Life Science) at a 1:4,000 dilution in blocking solution was then added at 25 µL/well for 1 h at room temperature. Alkaline phosphatase substrate solution (phosphatase substrate tablets [catalog no. S0942; Sigma] in AP substrate buffer (1 M Tris aminomethane [catalog no. BP152-5; Fisher], 30 mM MgCl2 [catalog no. M1028; Sigma]) was added at 25 µL/well following plate washing 6× with 1× D-PBS-T. Plates were incubated at room temperature in the dark for 2 h then read at an optical density of 405 nm with a Biotek plate reader. Reactive wells were chosen based of an optical density of >0.5 nm. For data visualization, the Circos software package was used (Krzywinski et al., 2009).

Recombinant GP

To produce recombinant EBOV, BDBV, SUDV, and MARV GP ectodomains (amino acids 1 to 636) and EBOV sGP (amino acids 1 to 316), stable *Drosophila* S2 cell lines were generated. Briefly, Effectene transfection reagent (Qiagen) was used to transfect S2 cells with modified pMTpuro vector plasmids containing the GP gene of interest, followed by stable selection of transfected cells with 6 µg/mL puromycin in complete Schneider's medium. Stable cells were transitioned to Insect Xpress medium (Lonza) in shaker culture, and GP ectodomain expression was induced with 0.5 mM $CuSO_4$. Supernatants were harvested after 4 days. All proteins were engineered with a double strep tag at the C terminus to facilitate purification using Strep-Tactin resin

(Qiagen), and the GPs were further purified by Superdex 200 size-exclusion chromatography in Tris-buffered saline or PBS buffer.

Viruses and cells

Neutralization assays were performed using a virus stock containing Ebola virus Zaire (EBOV/Kik-9510621, CDC no. 807224, Vero E6p2), which was passed additionally in Vero cell monolayer cultures once and Vero E6 cell monolayer cultures twice (Vero E6p2, Vero p1, E6p2). Mouse-adapted Ebola Zaire (ma-ZEBOV) was prepared from the original Bray stock (1976 strain, Mayinga) (Bray et al., 1999) with an additional passage on Vero E6 cell monolayer cultures (Mp3, Vp2, Mp9, ppGH, Vp1). For plaque reduction neutralization tests (PRNTs), a biologically contained Ebola virus, EbolaΔVP30 virus, was generated as previously described possessing the green fluorescent protein (GFP) reporter gene instead of the VP30 open reading frame in the viral genome (Halfmann et al., 2008). VeroVP30 cells were maintained in complete growth medium (10% fetal bovine serum, 1× minimal essential medium with antibiotics and supplements), and EbolaΔVP30-GFP virus was propagated in a reduced medium (2% fetal bovine serum, 1× minimal essential medium with antibiotics and supplements) as previously described (Halfmann et al., 2008). EbolaΔVP30 viruses were approved for use under biosafety level 2 containment at the University of Wisconsin—Madison by the NIH and CDC in February 2016.

Half-maximal effective concentration (EC_{50}) binding ELISA analysis

EBOV, BDBV, SUDV, or MARV GP, or EBOV sGP (1 µg/mL) was prepared in 1× D-PBS to coat 384-well ELISA plates at 25 µl/well and incubated at 4°C overnight. The plates were washed 3× with D-PBS-T and blocked for 1 h at room temperature with blocking solution (1% nonfat dry milk, 1% goat serum, D-PBS-T). After blocking, the plates were washed 3× with D-PBS-T, and 25 µL/well of 3-fold serially diluted purified EBOV human mAb (30 µg/mL to 170 ng/mL) in blocking solution was added. A solution of secondary Abs (goat anti-human IgG Fc gamma fragment-specific alkaline phosphatase conjugated, catalog no. W99008A; Meridian Life Science) at a 1:4,000 dilution in blocking solution was added at 25 µL/well for 1 h at room temperature. Alkaline phosphatase substrate solution was added at 25 µL/well following plate washing 6× with D-PBS-T. Plates were incubated at room temperature in the dark for 2 h and then read at an optical density of 405 nm with a Biotek plate reader. EC_{50} values were calculated using a nonlinear regression analysis of the curves generated in Prism version 5 (GraphPad Software).

Neutralization assay

Virus-specific neutralizing Ab responses were titrated in a plaque reduction neutralization test (PRNT), as previously described (Bornholdt et al., 2016). Abs were diluted serially in minimal essential medium (Corning Cellgro, Manassas, VA) containing

5% heat-inactivated fetal bovine serum (Gibco-Invitrogen, Gaithersburg, MD), 1× antibiotic-antimycotic (Gibco-Invitrogen) (MEM complete) and incubated 1 h at 37°C with virus. After incubation, the Ab-virus mixture was added in duplicate to 6-well plates containing 90 to 95% confluent monolayers of Vero E6 cells. Plates were incubated for 1 h at 37°C with gentle rocking every 15 min. Following the incubation, wells were overlaid with 0.5% agarose in supplemented Eagle's basal minimum essential medium, 10% heat-inactivated fetal bovine serum (Gibco-Invitrogen), and 2× antibiotic-antimycotic (Gibco-Invitrogen), and plates were incubated at 37°C in 5% CO_2 for 7 days. On day 7, cells were stained by the addition of a second overlay prepared as described above containing 4 to 5% neutral red. Plates were incubated for 18 to 24 h at 37°C in 5% CO_2. The endpoint titer was determined to be the highest dilution with ≥50% or ≥80% reduction ($PRNT_{50}$ or $PRNT_{80}$, respectively) in the number of plaques observed to virus-only control wells.

Plaque reduction neutralization test (PRNT)

To determine the neutralizing activity of EBOV237, a standard PRNT was performed with EbolaΔVP30-GFP virus (Halfmann et al., 2008). Approximately 200 PFU of virus was incubated with EBOV237 (serial 10-fold dilutions of Ab in reduced medium) or a VP35 MAb as a control for 60 min at 37°C. After incubation, standard plaque assays were performed (in triplicate) in which the virus-Ab mixture was inoculated on VeroVP30 cell monolayers for 60 min. After washing off unbound virus, cells were

overlaid with 1.25% methylcellulose medium and incubated for 7 days. Cells were fixed, an immunostaining assay using an Ab against VP40 was performed as previously described (Halfmann et al., 2008), and the number of plaques was counted in each well.

Generation of Ab escape mutant viruses

To generate mutant viruses that no longer were neutralized, approximately 10,000 PFU of EbolaΔVP30-GFP virus was incubated with 5 μg/mL of EBOV237 at 37°C for 60 min. After incubation, the virus-antibody mixture was inoculated onto VeroVP30 cells and incubated for 60 min at 37°C, and after incubation, cells were washed three times with reduced medium. Any escape mutant viruses were propagated for 9 days in reduced medium containing 5 μg/mL of mAb EBOV237. Four individual escape mutant viruses were isolated by selection of resistant plaques (Halfmann et al., 2008), and virus stocks were generated for each escape mutant virus in reduced medium in the presence of EBOV237 (5 μg/mL). The sequence of the virus GP was determined using viral RNA isolated from the cell culture supernatant of the stock virus (RNeasy minikit; Qiagen). A reverse transcription-PCR (RT-PCR; Verso 1-Step RT-PCR kit; Thermo Fisher Scientific) was performed to amplify the viral GP gene using forward and reverse primers at positions 6000 and 8110 of the Zaire Ebola virus (strain Mayinga 1976) genome that flank the 5′ and 3′ open reading frames of the GP gene, respectively. The resulting RT-PCR product was blunt end cloned into the TOPO pCR-XL vector (Thermo Fisher Scientific), and the sequence of the GP was determined by

Sanger DNA sequencing method for plasmid DNA from 10 to 20 bacterial clones for each virus escape mutant.

Competition-binding analysis using biolayer interferometry

For competition-binding experiments, EBOV GP or EBOV sGP was biotinylated using an EZ-link Micro NHS-PEG_4-biotinylation kit (catalog no. 21955; Thermo Scientific). The biosensors were soaked for 10 min in 200 µL of 1× kinetics buffer (catalog no. 18-1092; ForteBio), followed by a baseline signal measurement for 60 s. The biotinylated proteins (5 µg/mL) then were immobilized onto streptavidin-coated biosensor tips (catalog no. 18-5019; ForteBio) for 120 s. After washing the biosensor tips by immersion into 1× kinetics buffer for 60 s, the biosensors were immersed into 1× kinetics buffer containing the first Ab (100 µg/mL) for 600 s. The tips then were immersed into kinetics buffer containing the second Ab (100 µg/ml) for 300 s. Comparison between the maximal signal of the second Ab in the absence or presence of the first Ab was used to determine the percent binding of the second Ab. If the percent binding of the second Ab was reduced to <30% of the maximal signal that occurred in the absence the first Ab, the Abs were considered to display full competition for binding. If the percent binding was reduced from 30% to 70% of the maximal signal that occurred in the absence of the first Ab, the Abs were considered to display intermediate competition for binding. If the percent binding was >70% of the maximal

signal that occurred in the absence of the first Ab, the Abs were considered noncompeting.

Fab production

To generate the Fab fragment of EBOV237, purified mAb IgG protein was digested with papain (0.1 mg/mL stock solution, catalog no. P3125; Sigma) at a ratio of 20:1 (wt:wt) mAb-papain. Digestion was performed at 37°C for 1 h before termination by the addition of a 1/10 volume of 0.3 M iodoacetamide in PBS, followed by immediate 10-fold dilution in 10% normal goat serum and storage at 4°C.

Alanine-scanning shotgun mutagenesis for epitope mapping

We created an alanine-scanning mutagenesis library for EBOV GP (Davidson et al., 2015) using an expression construct of EBOV GPΔmucin (Ebola virus H.sapiens-tc/COD/1976/Yambuku-Mayinga (Kuhn et al., 2014), Δ311–461). Each of the amino acid residues 33 to 310 and 462 to 676 of EBOV GPΔmucin were substituted in individual GP constructs one at a time to alanine (or alanine residues to serine). The signal peptide sequence, residues 1 to 32, was not altered. The alanine-scanning mutagenesis library clones constituted 99.9% of the target residues (492 of 493), and the presence of the mutations was confirmed by DNA sequencing. Clones were arrayed at one mutant per well per into 384-well plates. HEK-293T cells were transfected with the mutant library. After 22 h of incubation to allow for expression of the mutant GPs,

the cells were either fixed with 4% paraformaldehyde in PBS with calcium and magnesium or unfixed. The cells then were incubated with the Fab fragment of EBOV237 in 10% normal goat serum (Sigma-Aldrich, St. Louis, MO) for 1 h at room temperature. An Alexa Fluor 488-conjugated secondary Ab (Jackson ImmunoResearch Laboratories, West Grove, PA) in 10% normal goat serum was added, and the cells were incubated for 30 min at room temperature. The cells then were washed twice in PBS without calcium and magnesium and resuspended in Cellstripper (Cellgro, Manassas, VA) with 0.1% BSA (Sigma-Aldrich). A multiwell automated flow cytometer (HTFC; Intellicyt, Albuquerque, NM) then was used to detect cellular fluorescence. The relative EBOV237 Fab fragment reactivity to the mutants in comparison to the wild-type EBOV GPΔmucin was determined by subtracting the background signal given by mock vector-transfected control cells and normalizing the signal to the wild-type EBOV GPΔmucin-transfected control. Critical clones were determined if they did not bind the EBOV237 Fab fragment but bound other control EBOV mAbs (EBOV296, EBOV442, and EBOV520). This approach excludes mutants with misfolding or expression defects (Paes et al., 2009). The mutagenesis data were analyzed by detailed algorithms, as described previously (Davidson and Doranz, 2014).

In vivo protection studies

All animal research was conducted under an IACUC-approved protocol in compliance with the Animal Welfare Act, PHS Policy, and other federal statutes and regulations relating to animals and experiments involving animals. The facility where

this research was conducted is accredited by the Association for Assessment and Accreditation of Laboratory Animal Care, International and adheres to principles stated in the Guide for the Care and Use of Laboratory Animals, National Research Council, 2011. Female BALB/c mice, age 6 to 8 weeks, were purchased from Charles River Laboratories. Upon arrival, mice were housed in microisolator cages in an animal biosafety level 4 containment area and provided chow and water *ad libitum*. An initial study evaluated the efficacy of EBOV237 at a single concentration. Twenty-four hours before infection (day −1), groups of mice (10 mice per group) were treated intraperitoneally (i.p.) with a single dose (100 μg) of Ab. Negative-control mice received an irrelevant, IgG Ab. Positive-control mice received 100 μg of the previously described mAb 13C6. On day 0, mice were inoculated by the i.p. route with 100 PFU of ma-ZEBOV. Mice were monitored daily (twice daily if clinical signs of disease were noted) for 28 days after virus inoculation. Group weights were recorded daily after virus inoculation. Body weights were calculated by dividing the group weight by the number of mice weighed. In a second study, efficacy was evaluated at various decreasing doses. For this study, mice (n = 10/group) were administered a single dose of 200, 100, 50, or 25 μg of EBOV237 at 24 h before virus exposure. Negative-control mice received an irrelevant, IgG Ab. Positive-control mice received a single dose of 100 μg of mAb 13C6. On d0, mice were inoculated by the i.p. route with 100 PFU of ma-ZEBOV. Mice were monitored daily (twice daily if there were clinical signs of disease) for 21 days after virus inoculation. Group weights were recorded daily after virus inoculation. Body weights were calculated by dividing the group weight by the number of mice weighed.

MR78 EC_{50} binding ELISA analysis

The soluble form of the full-length extracellular domain of MARV GP (1 μg/mL) was diluted in 1x D-PBS to coat 384-well ELISA plates (Thermo Scientifi) at 25 μL/well and incubated at 4°C overnight. The plates were washed 3x with D-PBS-T (1× DPBS + 0.05% Tween 20) and blocked for 1 hour at room temperature with blocking solution (1% non-fat dry milk (Blotting Grade Blocker Bio-rad), 1% goat serum (Gibco) in D-PBS-T). After blocking, the plates were then washed 3× with D-PBS-T and 25 μL/well of 3-fold serially diluted purified Fab MR78 or Fab MR78 Try37Phe (10 μg/mL – 56.5 ng/mL) in blocking solution was added. Plates were incubated for 2 hours at room temperature and then washed 3× with D-PBS-T. Secondary Ab (goat anti-human kappa-alkaline phosphatase conjugated; Southern Biotech) at a 1:4,000 dilution in blocking solution was added at 25 μL/well for 1 hour at room temperature. Alkaline phosphatase substrate solution (phosphatase substrate tablets (Sigma) in AP substrate buffer (1M Tris aminomethane (Fisher), 30 mM $MgCl_2$ (Sigma)) was added at 25 μL/well following plate washing 4× with D-PBS-T. Plates were incubated at room temperature in the dark for 2 hours then read at an optical density of 405 nm with a Biotek plate reader. EC_{50} and 95% confidence interval values were calculated using a non-linear regression analysis of the curves generated in Prism v.5. (GraphPad Software).

RV-A78 ELISA binding assay

Purified RV-A78 was diluted (1/2, 1/10, 1/50, or 1/100) in 1x D-PBS to coat 384-well MaxiSorp ELISA plates (Thermo Fisher Scientific 464718). The plates were washed 3× with D-PBS-T (1× DPBS + 0.05% Tween 20) in a biosafety laminar flow cabinet and incubated for 1 hour at room temperature in blocking solution (0.5% D-PBS-T). After blocking, the plates were then washed 3× with D-PBS-T and 4-fold serial dilutions of RV-A78 immune guinea pig serum in 0.1% D-PBS-T was added. Plates were incubated for 2 hours at room temperature and then washed 3× with D-PBS-T. Secondary Ab (goat anti-guinea pig IgG alkaline phosphatase conjugated; US Biological Life Sciences I1903-04) at a 1:4,000 dilution in blocking solution was added at 25 µL/well for 1 hour at room temperature. Alkaline phosphatase substrate solution (phosphatase substrate tablets (Sigma) in AP substrate buffer (1M Tris aminomethane (Fisher), 30 mM $MgCl_2$ (Sigma)) was added at 25 µL/well following plate washing 4× with D-PBS-T. Plates were incubated at room temperature in the dark for 2 hours then read at an optical density of 405 nm with a Biotek plate reader. Binding curves were generated using a non-linear regression analysis in Prism v.5. (GraphPad Software).

Competition-binding analysis of human anti-COV2 mAbs through biolayer interferometry

Anti-mouse IgG Fc capture biosensors (FortéBio 18-5089) on an Octet HTX biolayer interferometry instrument (FortéBio) were soaked for 10 minutes in 1× kinetics

buffer (Molecular Devices 18-1105), followed by a baseline signal measurement for 60 seconds. Recombinant SARS-CoV-2 RBD fused to mouse IgG1 (RBD-mFc, Sino Biological 40592-V05H) was immobilized onto the biosensor tips for 180 seconds. After a wash step in 1× kinetics buffer for 30 seconds, the reference Ab (5 μg/mL) was incubated with the antigen-containing biosensor for 600 seconds. Reference Abs included the SARS-CoV human mAbs CR3022 and COV2-2196. After a wash step in 1× kinetics buffer for 30 seconds, the biosensor tips then were immersed into the second Ab (5 μg/mL) for 300 seconds. The maximum binding of each Ab was normalized to a buffer-only control. Self-to-self blocking was subtracted. A comparison between the maximal signal of each Ab was used to determine the percent binding of each Ab. A reduction in maximum signal to <33% of the un-competed signal was considered full competition of binding for the second Ab in the presence of the reference Ab. A reduction in maximum signal to between 33 to 67% of the un-competed signal was considered intermediate competition of binding for the second Ab in the presence of the reference Ab. A percent binding of the maximum signal >67% was considered absence of competition of binding for the second Ab in the presence of the reference Ab.

Human ACE2 blocking assay using biolayer interferometry

Anti-mouse IgG biosensors on an Octet HTX biolayer interferometry instrument (FortéBio) were soaked for 10 minutes in 1× kinetics buffer,

followed by a baseline signal measurement for 60 seconds. Recombinant SARS-CoV-2 RBD fused to mouse IgG1 (RBD-mFc, Sino Biological 40592-V05H) was immobilized onto the biosensor tips for 180 seconds. After a wash step in 1× kinetics buffer for 30 seconds, the Ab (5 μg/mL) was incubated with the antigen-coated biosensor for 600 seconds. After a wash step in 1× kinetics buffer for 30 seconds, the biosensor tips then were immersed into human ACE2 (20 μg/mL) (Sigma-Aldrich SAE0064) for 300 seconds. The maximum binding of human ACE2 was normalized to a buffer-only control. Percent binding of human ACE2 in the presence of Ab was compared to human ACE2 maximal binding. A reduction in maximal signal to <30% was considered human ACE2 blocking.

CHAPTER III

HUMAN ANTIBODIES PROTECT AGAINST AEROSOLIZED EASTERN EQUINE ENCEPHALITIS VIRUS INFECTION

The information contained in this chapter is adapted with permission from the following reference:

Williamson LE, Gilliland T Jr., Yadav PK, Binshtein E, Bombardi R, Kose N, Nargi RS, Sutton RE, Durine CL, Armstrong E, Carnahan RH, Walker LM, Kim AS, Fox JM, Diamond MS, Ohi MD, Klimstra WB, Crowe JE Jr. Human antibodies protect against aerosolized Eastern equine encephalitis virus infection. *Cell*. 2020. 183(7): 1884-1990.e23. doi: 10.1016/j.cell.2020.11.011. PMID: 33301709; PMCID: PMC7806206.

Introduction

Ab responses to alphaviruses contribute to prevention of new infection, treatment, clearance, and maintenance of an established infection (Baxter and Griffin, 2016; Griffin, 1995; Griffin et al., 1997; Levine et al., 1991; Metcalf et al., 2013; Metcalf and Griffin, 2011). Previous studies of Abs to CHIKV, MAYV, RRV (Powell et al., 2020), VEEV, EEEV, and WEEV helped elucidate the mechanisms of neutralization and protection mediated by Abs to alphaviruses as described in chapter I. Potently

neutralizing Abs primarily target the E2 glycoprotein and interfere with different steps in the virus replication cycle from receptor attachment to viral egress (Fox et al., 2015; Jin et al., 2015; Kim et al., 2019; Powell et al., 2020; Jin and Simmons, 2019).

The conformational epitopes recognized by human Abs in the context of natural infection of EEEV and mechanism(s) of neutralization used are unknown. Previous studies of EEEV focused on identification of linear epitopes recognized by murine or avian Abs induced by immunization with recombinant E2 glycoprotein (EnCheng et al., 2013; Zhao et al., 2012; Sun et al., 2013). More recently, studies of EEEV E2 glycoprotein-specific murine mAbs elicited through inoculation with the chimeric virus SINV/EEEV, defined conformational epitopes within domains A and B of the E2 glycoprotein and elucidated a molecular mechanism of neutralization through fusion inhibition (Hasan et al., 2018; Kim et al., 2019).

In this chapter, I studied the molecular basis for human Ab recognition and neutralization of EEEV through characterization of human mAbs from the memory B cells of two survivors of natural EEEV infection. I identified a number of potently neutralizing human mAbs that recognized several epitopes on the E2 glycoprotein of EEEV, revealing multiple antigenic sites of vulnerability to neutralization. EEEV mAbs inhibit following virus attachment to cells and appear to inhibit virus entry or prevent conformational changes necessary for the fusion process. Two extremely potent neutralizing mAbs, EEEV-33 and EEEV-143, were characterized structurally to determine the molecular basis of neutralization. EEEV-33 identifies a conformational epitope on virus particles that enable for potent neutralization, and EEEV-143 uses

avidity effects to enhance interactions for cross-linking of E2 protomers as IgG or IgA molecules to neutralize virus. In a stringent small animal aerosol challenge model of EEEV infection, EEEV-33 and EEEV-143 exhibited efficacy when given before or after infection. The studies described in this chapter help elucidate the neutralization mechanism(s) of action for human anti-EEEV mAbs, which may help identify lead therapeutic candidate(s) and inform rationale vaccine design for EEEV.

I would like to acknowledge Dr. William B. Klimstra's laboratory (including Theron Gilliland, Jr.) at the University of Pittsburgh for performing BSL-3 wild-type EEEV neutralization assays and mice aerosol challenge prophylactic and therapeutic studies. I would also like to acknowledge Dr. Melanie D. Ohi's laboratory (including Drs. Pramod Yadav and Clarissa Durie) at the University of Michigan and Dr. Elad Binshtein at Vanderbilt University for performing cryo-EM studies of SINV/EEEV in complex with either EEEV-33 or EEEV-143 Fab molecules or EEEV VLPs in complex with EEEV-143 Fab molecules, respectively. I would like to acknowledge Dr. Michael S. Diamond's laboratory (including Drs. Arthur S. Kim and Julie M. Fox) for supplying murine anti-EEEV mAbs as key reagents. Lastly, I would also like to thank members of the iCore and TechCore teams in Dr. Crowe's laboratory for assistance with mAb expression and purification, and mAb or antigen sequencing, respectively.

Isolation of human anti-EEEV mAbs

To understand the human humoral response against EEEV, I isolated a panel of fifty-seven and twenty-one human anti-EEEV mAbs (**Figure 22**) from the B cells of peripheral blood samples of two individuals, respectively, who had prior documented, naturally acquired EEEV infections. The first research subject was a 38-year-old otherwise healthy female subject who contracted EEEV infection naturally in September 2015 in New York state. The disease course was marked by systemic illness including acute meningoencephalitis and resolved with supportive therapy delivered in hospital. The New York State Department of Health (NYSDOH) Wadsworth Laboratory reported this was a laboratory-confirmed infection with EEEV. Peripheral blood from the subject was collected 13 months after infection. The second research subject was a 60-year-old female subject who succumbed to infection ~4-5 days following mosquito bite(s) at the end of July 2014. The subject was hospitalized for ~1 month. Peripheral blood was collected 17 months after infection. PBMCs were isolated from the peripheral blood by density gradient purification and cryopreserved until use. Following EBV transformation, antigen-reactive B cells were fused with the HMMA 2.5 myeloma cell line to generate hybridomas. Hybridomas were single cell sorted to produce human mAbs. Human mAbs were purified through affinity chromatography.

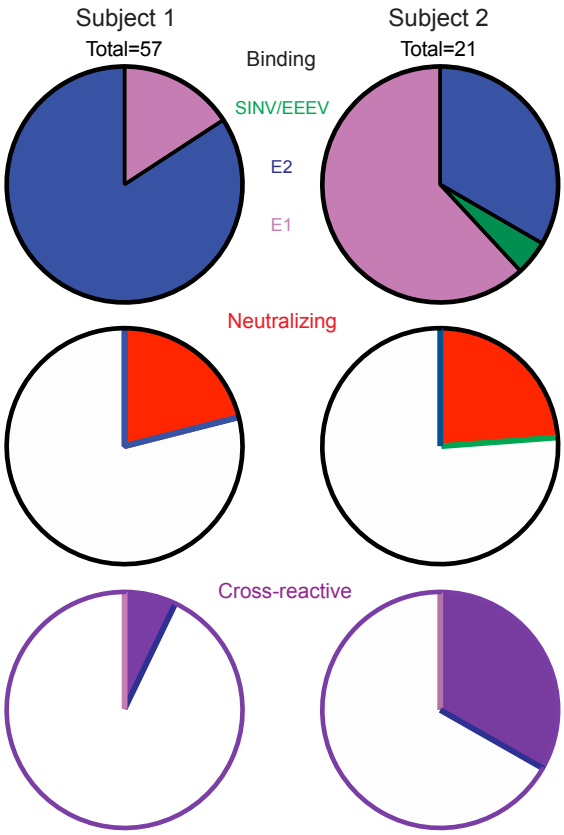

Figure 22. Binding reactivity of human anti-EEEV mAbs isolated from two survivors of natural EEEV infection. Pie chart summary of human anti-EEEV mAbs isolated from subject 1 (left; total: 57) and subject 2 (right; total: 21). Binding reactivity (top), neutralizing activity (middle; red), and cross-reactivity (bottom; purple) are shown for the panel of human anti-EEEV mAbs isolated (SINV/EEEV-specific [green; chapter III], E2-specific [blue; chapters III and V], E1-specific [purple; chapter IV]).

Human anti-EEEV mAbs isolated from naturally infected EEEV survivors potently neutralize EEEV

To down-select from the panel of human anti-EEEV mAbs isolated, I focused on the mAbs that could efficiently neutralize Sindbis virus (SINV)/EEEV, a chimeric virus for use in BSL2 conditions containing the nonstructural proteins (nsp1-4) of SINV and the structural proteins (capsid-E3-E2-6K-E1) of EEEV strain FL93-939 (Kim et al.,

2019). Seventeen mAbs exhibited neutralizing activity against SINV/EEEV (**Figures 23A and 23D**). All mAbs isolated were of the IgG1 subclass except for EEEV-143, which was an IgA1 (**Figure 23D**). Of these, nine exhibited *potent* neutralization activity (here defined as half-maximal inhibitory concentration (IC_{50}) <20 pM; <6 ng/mL) and eight exhibited *moderate* neutralization activity (here defined as mAbs with 20 pM – 5 nM [6 ng/mL – 1.5 µg/mL] IC_{50} values) against SINV/EEEV.

To confirm neutralization activity of the human anti-EEEV mAbs, we collaborated with Dr. William B. Klimstra's laboratory to test neutralization potency against the pathogenic EEEV strain FL93-939 under BSL-3 conditions. Overall, the neutralization potency with EEEV was consistent with results obtained with SINV/EEEV, validating the use of chimeric virus for isolation and functional analysis of neutralizing human anti-EEEV mAbs (**Figure 23C**). Eleven mAbs neutralized EEEV completely at 75 nM (22.5 µg/mL), such that a residual fraction of infectious virus was not observed (**Figure 23C**). Several mAbs exhibited extremely potent neutralization activity against EEEV; four mAbs (EEEV-27, -33, -106, and -352) achieved nearly 100% neutralization of EEEV even at the lowest concentration tested, 37 pM (11 ng/mL) (**Figures 23C and 23D**). Twelve mAbs exhibited neutralization activity of <400 pM (120 ng/mL) IC_{50} values against EEEV. Additionally, two mAbs exhibited weak neutralization activity with IC_{50} values in a range of 400 pM – 5 nM (120 ng/mL – 1.5 µg/mL) against EEEV (**Figure 23D**). EEEV-97, EEEV-319, and EEEV-397 did not inhibit EEEV by 50% at <10 nM mAb concentration, which corresponded with the weak activity against SINV/EEEV observed for these mAbs.

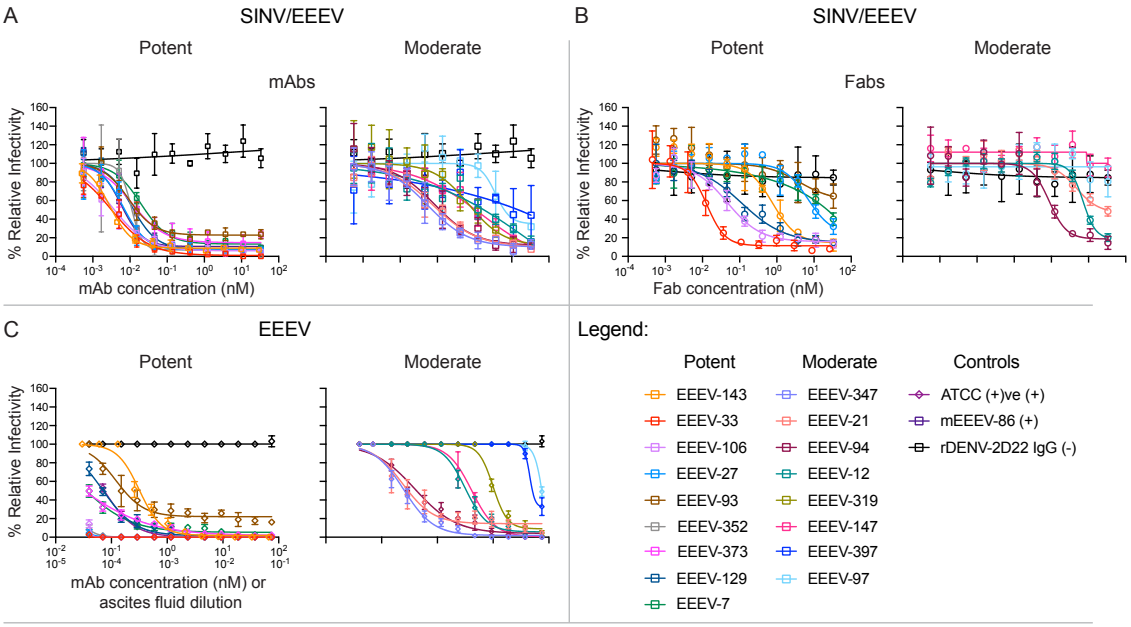

D

Potent Abs

IC_{50} (pM)	Isotype	SINV/EEEV		EEEV
		mAb	Fab	mAb
EEEV-143	IgA1, κ	2.8	772.0	315.5
EEEV-33	IgG1, λ	3.1	13.0	<37
EEEV-106	IgG1, κ	3.3	46.5	<37
mEEEV-86	IgG2c	5.8	NT	NT
EEEV-27	IgG1, λ	6.5	6,835	<37
EEEV-93	IgG1, λ	9.3	>	120.5
EEEV-352	IgG1, κ	10.7	NT	<37
EEEV-373	IgG1, κ	11.1	NT	<37
EEEV-129	IgG1, λ	11.2	112.5	69.6
EEEV-7	IgG1, κ	19.7	>	<37

Moderate Abs and Controls

IC_{50} (pM)	Isotype	SINV/EEEV		EEEV
		mAb	Fab	mAb
EEEV-347	IgG1, λ	54.8	NT	251.0
EEEV-21	IgG1, λ	76.3	>	239.9
EEEV-94	IgG1, κ	84.1	876.0	393.6
EEEV-12	IgG1, λ	381.3	7,110	3,144
EEEV-319	IgG1, ND	703.2	NT	>
EEEV-147	IgG1, κ	1,574	>	4,128
EEEV-397	IgG1, κ	2,398	NT	>
EEEV-97	IgG1, λ	3,653	>	>
ATCC (+)ve	NA	NT	NT	1/10,240
rDENV-2D22	IgG1, κ	>	IgG (>)	>

Figure 23. Human anti-EEEV mAbs isolated from EEEV survivors potently neutralize Sindbis (SINV)/EEEV and WT EEEV. A to **B.** Representative neutralization curves of potent (left) or moderate (right) neutralizing human anti-EEEV mAbs (open squares; **A**) or Fab molecules (open circles; **B**) against SINV/EEEV with mAb (**A**) or Fab (**B**) concentration (nM) on the x-axis and % relative infectivity on the y-axis. A positive control mouse mAb, EEEV-86 (dark purple) (Kim et al., 2019), and a negative control mAb, rDENV-2D22 (black), were included. **C.** Neutralization curves of potent (left) or moderate (right) neutralizing human anti-EEEV mAbs (open diamonds) against EEEV with mAb concentration (nM) on the x-axis and % relative infectivity on the y-axis. A positive control mouse anti-EEEV ascites fluid, ATCC (+)ve, and a negative control mAb, rDENV-2D22 (black), were included. **D.** Half-maximal inhibitory concentration (IC_{50}) values (pM) for human anti-EEEV mAbs or Fabs against SINV/EEEV and mAbs against EEEV strain FL93-939 are indicated in the table. Neutralizing human anti-EEEV mAbs are listed in order of increasing IC_{50} value against SINV/EEEV. IC_{50} value in pM is indicated by the orange heat map (<33 [dark orange], 33.01 to 333 [medium orange], 333.01 to 3,333 [light orange], <10,000 [lightest orange]). Isotype is indicated as heavy chain (IgG1 or IgA1) and light chain (κ or λ) as determined by antibody gene sequencing. Data in **A** and **B** represent mean ± SD of technical triplicates and are representative of at least two independent focus reduction neutralization test (FRNT) experiments. Data

in **C** represent mean ± SD of technical triplicates of a plaque reduction neutralization test (PRNT) experiment. Modified from Williamson et al., 2020.

Neutralizing human anti-EEEV mAbs bind to SINV/EEEV particles and/or recombinant EEEV E2 glycoprotein

To identify the antigen specificity of the neutralizing human anti-EEEV mAbs, I assessed binding to SINV/EEEV particles and EEEV E2 or E1 glycoproteins (**Figures 24 and 25**). The ratio of virus/protein half-maximal effective binding concentration (EC_{50}) values for binding was determined (**Figure 24B**) to identify differences in reactivity of mAbs recognizing virion particle-specific epitopes versus those more accessible in recombinant glycoprotein. Preferential binding to virion-specific epitopes suggests that some mAbs recognize quaternary epitopes on the virion or require bivalent binding with specific geometric orientation. A majority of the mAbs bound strongly to either E2 antigen (isolated protein or SINV/EEEV particles) by ELISA (<100 pM [<30 ng/mL] EC_{50} values), with a virus/protein EC_{50} ratio of ~1. EEEV-33 bound weakly to recombinant E2 glycoprotein compared to SINV/EEEV particles (EEEV-33: <4 nM vs 11 pM [<1.2 µg/mL vs 3.3 ng/mL] EC_{50} values), indicated by a virus/protein EC_{50} ratio of 0.003 (**Figure 24B**). EEEV-373 bound preferentially to SINV/EEEV particles as no detectable binding was observed to recombinant E2 glycoprotein (> vs 34 pM [> vs 10.2 ng/mL] EC_{50} values). A few mAbs bound E2 protein better than SINV/EEEV particles, such as EEEV-147 (virus/protein EC_{50} ratio = 4.4), indicating that these mAbs

may recognize an epitope that is less accessible on the virion surface under the conditions tested. Binding to EEEV or CHIKV E1 glycoproteins was not detected.

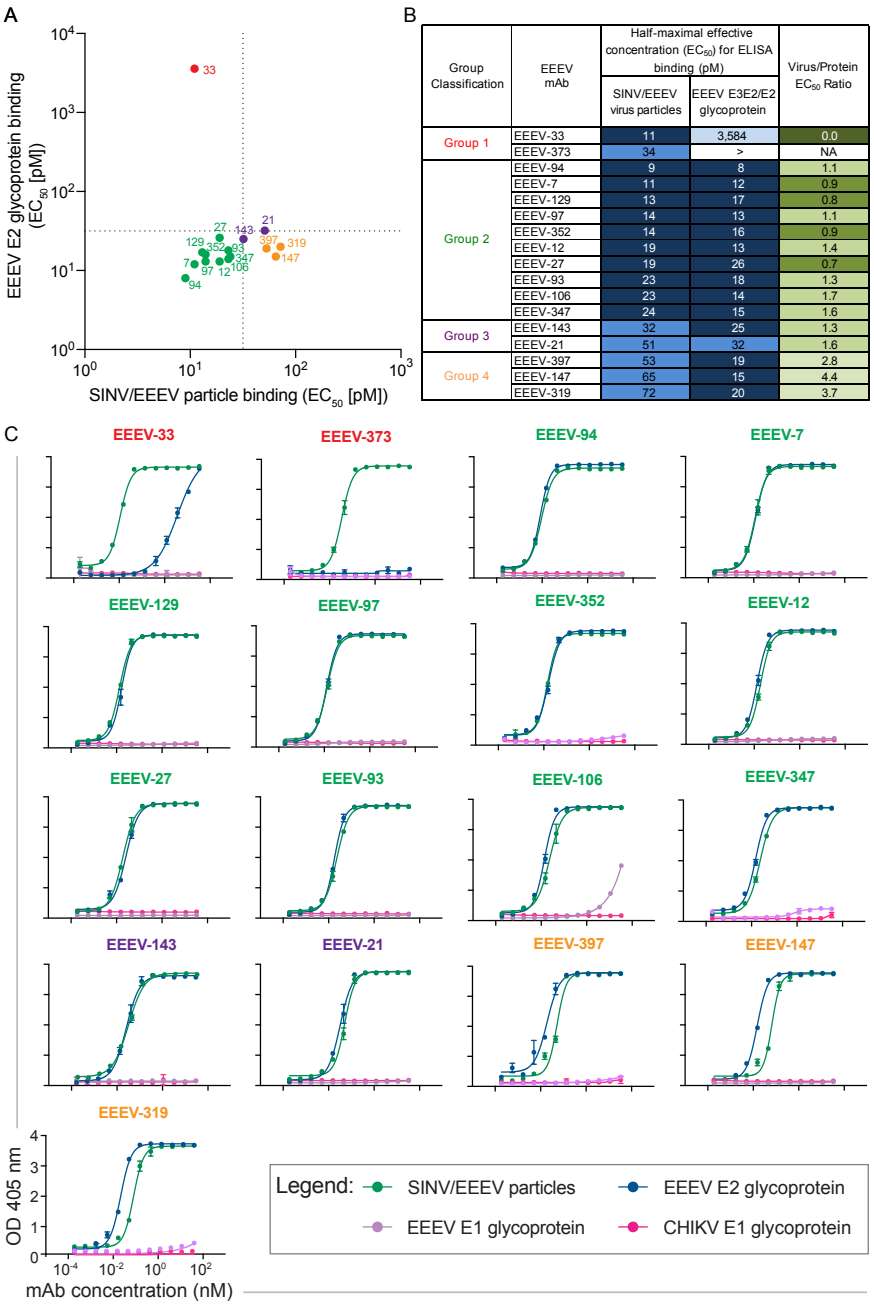

Figure 24. Neutralizing human anti-EEEV mAbs bind to SINV/EEEV particles and/or recombinant EEEV E2 glycoprotein. A. Binding ratio of neutralizing human anti-EEEV mAbs to SINV/EEEV particles versus recombinant monomeric EEEV E2 glycoprotein. A dotted line indicates 32 pM EC_{50} values for binding, revealing distinct binding patterns of human anti-EEEV mAbs to SINV/EEEV particles and EEEV E2 glycoprotein. Neutralizing human anti-EEEV mAbs are labeled with the anti-EEEV mAb name and are colored according to binding group (group 1 [red] = virus > protein binding; group 2 [green] = strong (SINV/EEEV EC_{50} = <32 pM) virus » protein binding; group 3 [purple] = weak (SINV/EEEV EC_{50} = >32 pM) virus » protein binding; and group 4 [orange] = protein > virus binding). **B.** EC_{50} values (pM) for binding of neutralizing human anti-EEEV mAbs to SINV/EEEV particles or EEEV E2 glycoprotein. Neutralizing human anti-EEEV mAbs are listed in order of binding group and increasing EC_{50} value for

binding to SINV/EEEV particles. EC_{50} value in pM is indicated by the blue heat map (<32 [dark blue], 32.01 to 100 [medium blue], 100.01 to 320 [light blue], and <10,000 [lightest blue]). Ratio of binding to SINV/EEEV particles versus EEEV E2 glycoprotein is indicated as the ratio of EC_{50} values, corresponding to **A**. Increasing depth of green color indicates lower ratios (<0.1 [dark green], 0.1 to 1.0 [medium green], 1.01 to 2.0 [light green], and >2.0 [lightest green]), suggesting recognition of a quaternary epitope on virion particles. **C.** Representative binding curves of neutralizing human anti-EEEV mAbs to four different antigens. Binding curves of neutralizing human anti-EEEV mAbs to SINV/EEEV particles (green) and EEEV E2 glycoprotein (blue), with mAb concentration (nM) on the x-axis and optical density at 405 nm on the y-axis. Binding to EEEV E1 (purple) or CHIKV E1 (pink) glycoproteins was not detected.
Data in **A** to **C** represent mean ± SD of technical triplicates and are representative of at least one independent experiment. Modified from Williamson et al., 2020.

Optimal neutralization of SINV/EEEV requires bivalent interactions

The neutralization potency of Fab and IgG molecules has been compared previously for several alphaviruses (Hasan et al., 2018; Long et al., 2015). In some cases, the neutralizing activity of the Fab form of the mAb is substantially lower than the intact IgG (Hasan et al., 2018). However, I found that the Fab forms for some neutralizing human anti-EEEV mAbs (EEEV-33, -94, -106, -129, -143) still neutralized SINV/EEEV efficiently with <1 nM (<300 ng/mL) IC_{50} values (**Figures 23B and 23D**), indicating that the monovalent Fab molecules may achieve sufficient occupancy of binding for neutralization of EEEV. This finding of similar neutralization potency was consistent with the similar binding strength to SINV/EEEV particles (**Figure 25**). The neutralization potency of EEEV-94, -106, -129, and -143 as Fab molecules was still reduced (~10 [EEEV-94] to 276 [EEEV-143]-fold change in IC_{50} values), suggesting bivalent or tetravalent interactions as an IgG (EEEV-94, -106, and -129) or IgA (EEEV-

143), respectively, may contribute to optimal neutralization of SINV/EEEV. EEEV-33 had comparable neutralization potency as a Fab or IgG molecule (~4-fold change).

In contrast, EEEV-27 and EEEV-93 exhibited greatly reduced neutralization potency when expressed as Fab molecules, compared to IgG, and showed a corresponding reduction in binding to SINV/EEEV particles (>1,000-fold reduction in IC_{50} and EC_{50} values) (**Figure 25**). These findings suggest that for EEEV-27 and EEEV-93, the monovalent interaction of Fab with SINV/EEEV particles likely is of low affinity and the avidity benefits of interactions achieved though bivalent binding facilitate optimal binding and neutralization of SINV/EEEV. The IC_{50} values of neutralization and EC_{50} values for binding to SINV/EEEV did not correspond for all of the inhibitory human anti-EEEV mAbs or Fabs. EEEV-7, -12, -21, -97, and -147 bound SINV/EEEV particles with similar strength as Fab molecules, compared to IgG. However, a reduction in neutralization potency was observed for Fab molecules.

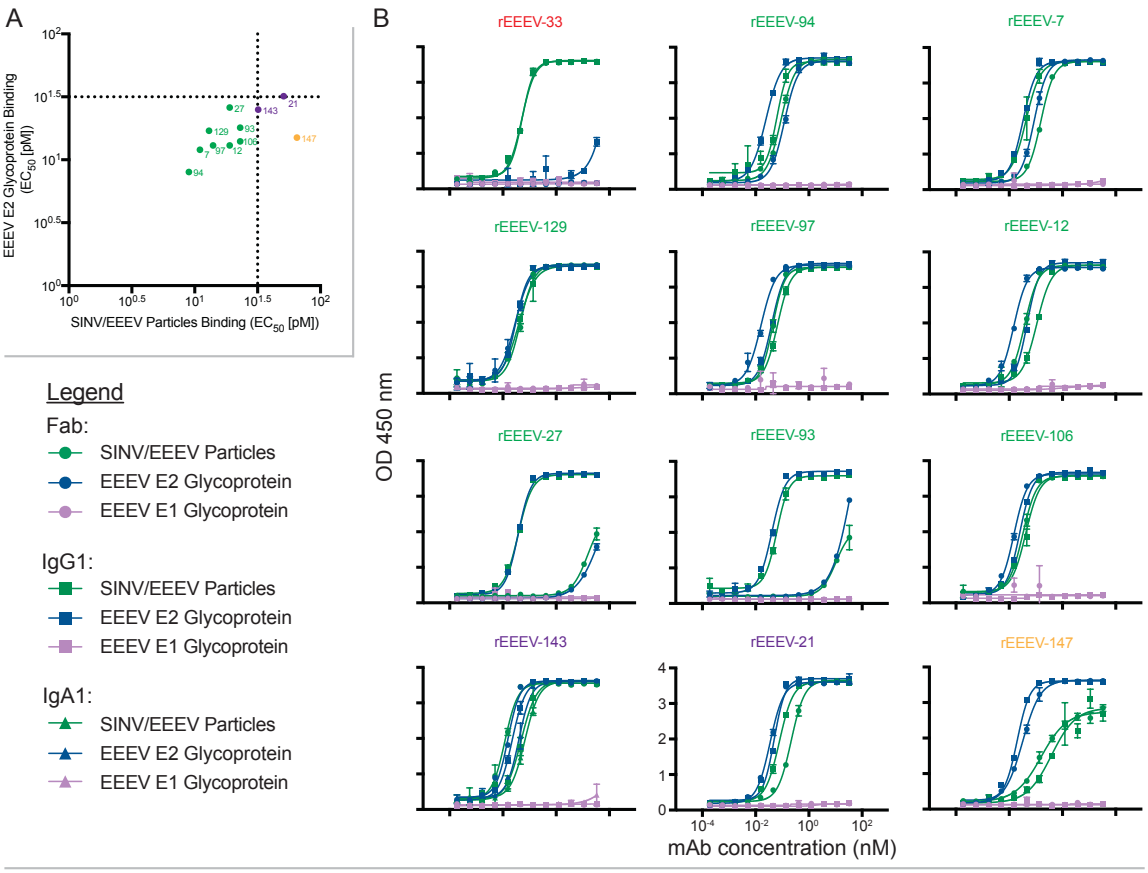

C

EEEV mAb	Antibody Isotype (Heavy Chain, Light Chain)	IgG1 (IgA1)	Fab	IgG1 (IgA1)	Fab	IgG1	Fab	SINV/EEEV particles	EEEV E2 glycoprotein
		SINV/EEEV particles		EEEV E2 glycoprotein		Virus/Protein EC_{50} Ratio		IgG/Fab EC_{50} Ratio	
EEEV-33	IgG1,λ	51.1	52.5	>	>	0.0	0.0	1.0	NA
EEEV-94	IgG1,κ	63.1	89.4	24.3	119.9	2.6	0.7	0.7	0.2
EEEV-7	IgG1,κ	42.7	154.1	32.8	85.5	1.3	1.8	0.3	0.4
EEEV-129	IgG1,λ	39.9	45.0	30.2	29.0	1.3	1.6	0.9	1.0
EEEV-97	IgG1,λ	65.9	43.8	39.9	16.0	1.7	2.7	1.5	2.5
EEEV-12	IgG1,λ	108.1	38.0	46.7	14.7	2.3	2.6	2.8	3.2
EEEV-27	IgG1,λ	37.6	>	37.6	>	1.0	>	NA	NA
EEEV-93	IgG1,λ	62.1	>	40.8	>	1.5	>	NA	NA
EEEV-106	IgG1,κ	41.7	32.3	24.6	15.1	1.7	2.1	1.3	1.6
EEEV-143	IgA1,κ	48.3 (67.5)	11.9	22.3 (39.6)	15.4	2.2	0.8	4.1	1.4
EEEV-21	IgG1,λ	78.2	216.2	49.8	34.9	1.6	6.2	0.4	1.4
EEEV-147	IgG1,κ	385.0	158.5	19.9	32.0	19.3	5.0	2.4	0.6

Figure 25. Binding reactivity of neutralizing human anti-EEEV mAbs to SINV/EEEV particles or EEEV E2 glycoprotein. A. Binding ratio of neutralizing human anti-EEEV mAbs to SINV/EEEV particles vs. recombinant monomeric EEEV E2 glycoprotein. EEEV-33 is removed to display the binding reactivity groups for the rest of the panel of neutralizing human anti-EEEV mAbs at higher resolution. A dotted line indicates 32 pM half-maximal effective concentration (EC_{50}) values for binding, revealing distinct binding patterns of human anti-EEEV mAbs to SINV/EEEV particles and EEEV E2 glycoprotein. Neutralizing human anti-EEEV mAbs are labeled with the anti-EEEV mAb name and colored according to binding group (Group 2 [green] = strong (SINV/EEEV EC_{50} = <32 pM) virus » protein binding; Group 3 [purple] = weak (SINV/EEEV EC_{50} = >32 pM) virus»protein binding; Group 4 [orange] = protein>virus binding). **B.** Representative binding curves of recombinant neutralizing human anti-EEEV IgG1, IgA1, or Fab molecules to three different antigens. Binding curves of recombinant neutralizing human anti-EEEV IgG1

(square), IgA1 (triangle), or Fab (circle) molecules to SINV/EEEV particles (green) or EEEV E2 glycoprotein (blue), with mAb concentration (nM) on the x-axis and optical density at 405 nm on the y-axis. Binding to EEEV E1 glycoprotein (purple) was not detected. **C.** EC_{50} values (pM) for binding of recombinant neutralizing human anti-EEEV IgG1, IgA1, or Fab molecules to SINV/EEEV particles or EEEV E2 glycoprotein. EC_{50} value in pM is indicated by blue fill color (<32 [dark blue], 32.01 to 100 [medium blue], 100.01 to 320 [light blue], <10,000 [lightest blue]). Ratio of binding to SINV/EEEV particles versus EEEV E2 glycoprotein is indicated as the ratio of EC_{50} values. Increasing depth of green color indicates lower ratios (<0.1 [dark green], 0.1 to 1.0 [medium green], 1.01 to 2.0 [light green], >2.0 [lightest green]), suggesting recognition of a quaternary epitope on virion particles. Ratio of binding of recombinant IgG1 versus Fab molecules to SINV/EEEV particles or EEEV E2 glycoprotein is indicated as the ratio of EC_{50} values. Increasing depth of purple color indicates lower ratios (<0.1 [dark purple], 0.1 to 1.0 [medium purple], 1.01 to 2.0 [light purple], >2.0 [lightest purple]), suggesting dependence on valency for binding. Antibody isotype is indicated as IgG1 or IgA1 for the heavy chain or k or l for the light chain. NA = not applicable. Data in **A** to **C** represent mean ± SD of technical triplicates and are representative of two independent ELISA experiments. Each mAb is colored based on the binding group defined in **Figure 24**. Williamson et al., 2020.

Neutralizing human anti-EEEV mAbs recognize three antigenic determinants on the EEEV E2 glycoprotein

The E2 glycoprotein consists of three structural domains: 1) a flexible domain B at the apical surface that shields the fusion loop at the distal tip of the E1 glycoprotein, 2) domain A, which is suspected to contain the putative receptor binding site, and 3) domain C that lies proximal to the viral membrane and contains the transmembrane domain (Voss et al., 2010; Chen et al., 2020; Gardner et al., 2013; Gardner et al., 2011; Hasan et al., 2018; Zhang et al., 2011). To determine the number of major antigenic sites recognized by neutralizing human anti-EEEV mAbs, I performed competition-binding studies utilizing biolayer interferometry and previously described domain B-specific murine anti-EEEV mAbs, including mEEEV-69 and mEEEV-86 (Kim et al., 2019). From this analysis, I identified at least three competition-binding groups on the EEEV E2 glycoprotein (**Figure 26A**). Partial overlap for some of these competition

groups was observed, suggesting proximity of the epitopes to each other. A majority of the mAbs competed with murine anti-EEEV mAbs that recognize domain B on the E2 glycoprotein (mEEEV-69 or mEEEV-86), showing that this antigenic determinant was most immunogenic in this individual.

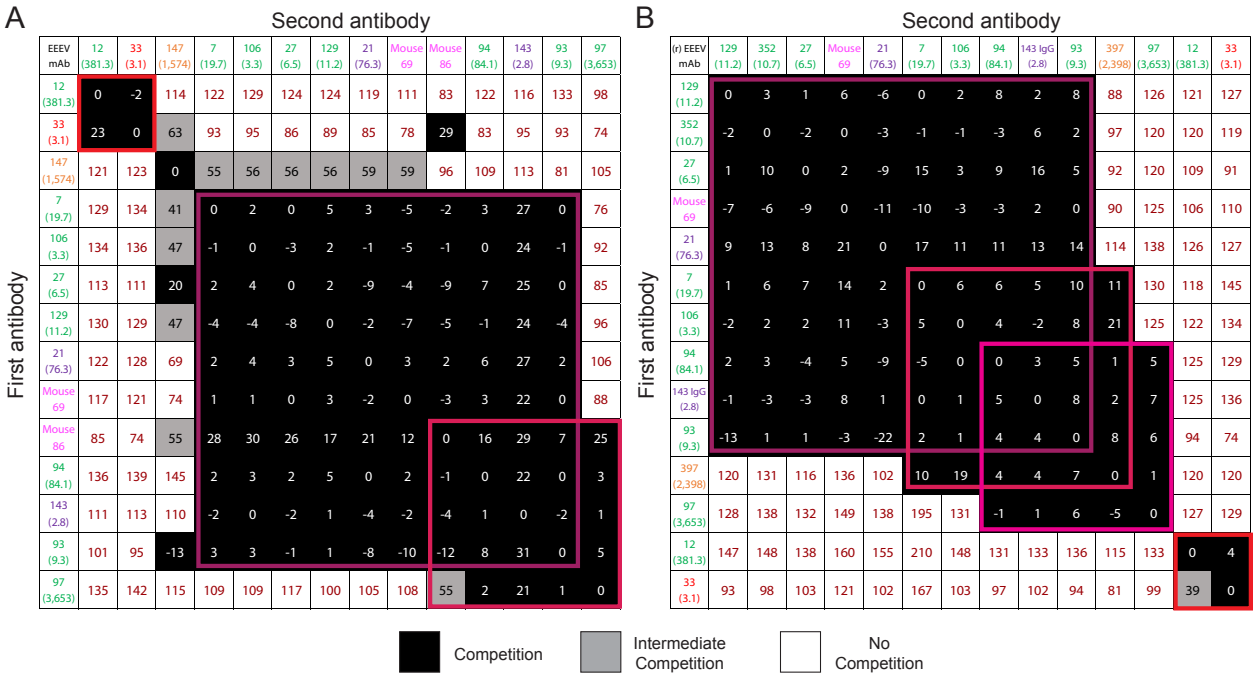

Figure 26. Human anti-EEEV mAbs recognize three neutralizing antigenic determinants on the EEEV E2 glycoprotein. A. Competition-binding groups of neutralizing human anti-EEEV mAbs to recombinant EEEV E2 monomeric glycoprotein as determined through biolayer interferometry. Mouse domain B (magenta) and human mAbs were incubated with EEEV E2 glycoprotein to identify the number of antigenic determinants recognized by these mAbs. The first mAb incubated with E2 is shown in the left-hand column and the second mAb is shown in the top column. Black boxes indicate competition, or reduction in maximum signal for binding of the second mAb to <33%. Grey boxes indicate intermediate competition, or reduction in maximum signal for binding of the second mAb to between 33 to 67%. White boxes indicate no competition, or little to no reduction in maximum signal for binding of the second mAb to >67%. Competition-binding groups are highlighted by a pink or red colored box. Each mAb is colored based on binding group as defined in **Figure 24**. IC_{50} (pM) values for neutralization activity against SINV/EEEV are indicated in parentheses (**Figure 23D**). **B.** Competition-binding groups of neutralizing human anti-EEEV mAbs as described in **A**. However, additional neutralizing human anti-EEEV mAbs (unpublished) are included in the matrix. Modified from Williamson et al., 2020.

To identify critical interaction residues for neutralizing human anti-EEEV mAbs, Twist Bioscience Inc. generated an alanine-scanning mutagenesis library for the EEEV E2 glycoprotein and I used this library to map residues for which a loss-of-binding phenotype of the Ab occurred. Similar to the competition-binding analysis, three groups emerged. Critical alanine residues identified in this analysis were mapped to the 4.2 Å cryo-EM 3D model of EEEV virus-like particle (VLP) (EMD-22276; PDB ID: 6XO4; **Figure 33**). The antigenic sites correspond to epitopes on domains A (EEEV-33), B (EEEV-7, -21, -97, -106, -129, -143), or A/B (EEEV-27, -93, -94) of the E2 glycoprotein (**Figure 27D and Table 1**). Variable gene sequence analysis revealed EEEV-7 and -106 belong to a common lineage, which is supported by their recognition of similar residues for binding. Several mAbs (EEEV-27, -33, -93, -94, and -147) also recognized critical residues in the arch 1 or 2 regions, an acid-sensitive β-connecter region that connects domain A to domain B. Some E2 residues mutated to alanine were identified as critical that are not surface exposed, which may reflect allosteric effects on the epitope that impact Ab binding (**Table 1**). Critical residues in the EEEV E2 domains were identified previously for murine anti-EEEV mAbs (Kim et al., 2019) (**Figures 27C and 38**). However, some of the residues identified here are distinct (**Table 1**), indicating that there are differences in recognition by human and mouse Abs.

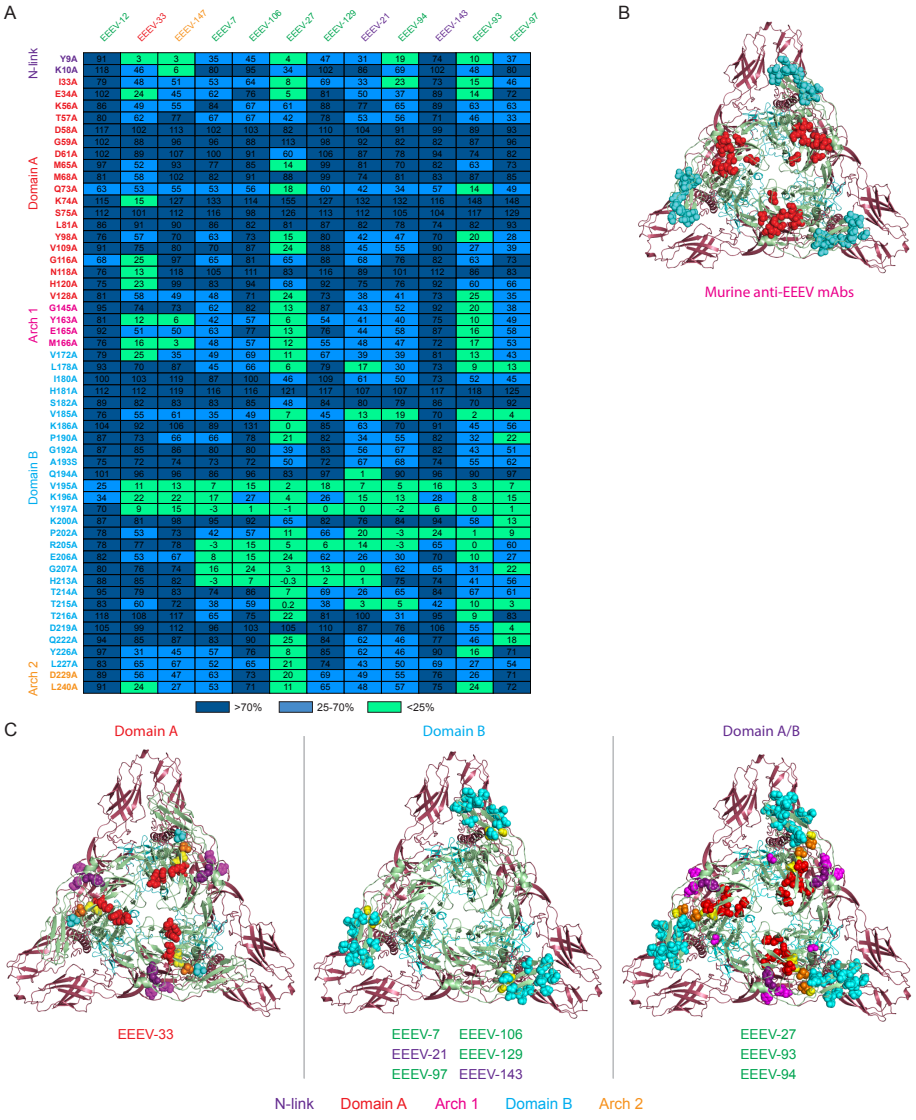

Figure 27. Human anti-EEEV mAbs recognize three neutralizing antigenic determinants on the EEEV E2 glycoprotein. A. Heat map of critical residues for neutralizing human anti-EEEV mAbs as determined through alanine-scanning mutagenesis library analysis. The average percent binding of each neutralizing human anti-EEEV mAbs is indicated for the critical residues identified (<25% binding of mAb in which at least two mAbs exhibited >70% binding to control for expression; D1-L267) and for the previously characterized murine anti-EEEV mAbs (Kim et al., 2019) and the VEEV-specific human mAb, F5 (Hunt et al., 2010; Porta et al., 2014). The heat map displays average % binding relative to WT EEEV E2 glycoprotein with dark blue (>70%), light blue (25-70%), and light green (<25%). Residues are colored based on E2 domain (N-link – purple, Domain A – red, Arch 1 – magenta, Domain B – cyan, and Arch 2 – orange). Each mAb is colored based on binding group as defined in **Figure 24** and ordered to correspond with the competition-binding groups as defined in **Figure 26**. Data represents mean of at least two independent experiments. **B.** Epitope mapping of critical alanine and arginine residues previously identified for neutralizing murine anti-EEEV mAbs binding to the E2 glycoprotein. Critical residues for binding of murine anti-EEEV mAbs as previously determined through alanine and arginine mutagenesis analyses were mapped onto the 4.2 Å cryo-EM reconstruction of EEEV VLP (EMD-22276; PBD ID:

6XO4) for comparison to the critical alanine residues identified for human anti-EEEV mAbs (see **Figure 27C**). A trimeric top view of the E2 (green) and E1 (red) glycoproteins is shown with critical residues (spheres) for murine anti-EEEV mAbs that recognize the E2 domains A, B, and A/B. Residues are colored based on E2 domain (Domain A – red and Domain B – cyan). **C.** Epitope mapping of critical alanine residues identified for neutralizing human anti-EEEV mAbs binding to the E2 glycoprotein. Critical residues for binding of human anti-EEEV mAbs as identified through alanine-scanning mutagenesis library analyses (**Figure 27A**) were mapped as described in **Figure 27B**. Residues are colored based on E2 domain (N-link – purple, Domain A – red, Arch 1 – magenta, Domain B – cyan, and Arch 2 – orange). Yellow spheres indicate the previously identified SINV/EEEV neutralization escape mutants (M68T, G192R, and L227R) (Kim et al., 2019). Each mAb is presented with its respective E2 domain and is colored based on binding group as defined in **Figure 24**. Modified from Williamson et al., 2020.

SINV/EEEV neutralization escape mutant viruses with the mutations M68T, G192R, or L227R of the E2 glycoprotein were identified previously using domain A/B murine anti-EEEV mAbs. The mutated residues affected the neutralization potency of domain A and A/B specific murine mAbs to SINV/EEEV. Domain B-specific murine mAbs inhibited the escaped viruses as efficiently as WT SINV/EEEV (Kim et al., 2019). To assess whether viral escape also occurred for the neutralizing human anti-EEEV mAbs, I tested activity of the mAbs against these viruses (**Figure 28**). Similar to the murine mAbs, mAbs that recognized domain B of the EEEV E2 glycoprotein still neutralized the G192R and L227R escaped viruses with comparable potency to WT SINV/EEEV. The domain B-specific mAb EEEV-97, however, displayed reduced neutralization potency against all three escape mutant viruses. This finding may be due to the weak neutralization potency of EEEV-97 against SINV/EEEV. A number of domain B-specific mAbs (EEEV-7, -106, -129) displayed a >10-fold reduction in neutralization potency to SINV/EEEV (M68T). M68T may lead to an allosteric effect on the epitope for these mAbs, which all depend on the critical alanine residues R205, G207, and H213 for binding. Two other domain B-specific mAbs, EEEV-21 and EEEV-

143, also displayed a >5-fold reduction in neutralization potency to SINV/EEEV (M68T), possibly due to an allosteric effect. However, M68T does not affect neutralization potency for EEEV-21 and EEEV-143 to the same extent, which may be due to different critical alanine residues for binding. The domain A-specific EEEV-33 efficiently neutralized the G192R and L227R mutant viruses. However, a >5-fold reduction in neutralization potency was observed for SINV/EEEV (M68T). A loss-of-binding phenotype for clones in the EEEV E2 alanine mutant library was not observed for EEEV-12. However, EEEV-12 displayed a >10-fold or >5-fold reduction in neutralization potency to SINV/EEEV (M68T) or SINV/EEEV (L227R), respectively. Thus, EEEV-12 likely recognizes domain A on the E2 glycoprotein due to reduction of neutralization potency at these mutated residues and observed competition with EEEV-33 for binding to the E2 glycoprotein. Two mAbs, EEEV-94 (domain A/B) and EEEV-147 (N-link/arch 1), displayed comparable neutralization potency of the escaped viruses and WT SINV/EEEV, which correspond with the critical alanine residues identified for these mAbs. EEEV-27 and -93 (domain A/B) displayed reduced neutralization potency for M68T and L227R or comparable potency for the G192R escaped mutant viruses. The observed mutated residues correspond with the epitope identified through alanine-scanning mutagenesis library analysis for EEEV-27 and -93. Thus, through complementary epitope mapping techniques, we defined three major neutralizing E2 antigenic determinants for human mAbs (domain A, B, and A/B).

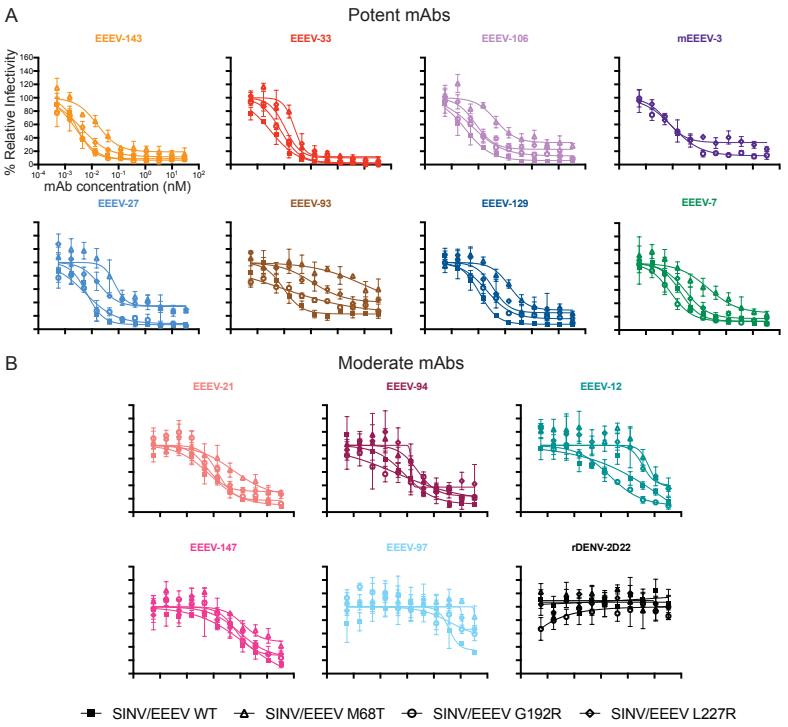

C

EEEV mAb	SINV/EEEV IC_{50} (pM)				Fold Difference in IC_{50} ratio to SINV/EEEV WT		
	WT	M68T	G192R	L227R	M68T	G192R	L227R
EEEV-143	2.8	16.3	2.6	3.8	6	1	1
EEEV-33	3.1	23.7	7.3	10.7	8	2	3
EEEV-106	3.3	44.7	6.0	7.7	14	2	2
mEEEV-3	NT	NT	9.9	5.8	NT	NT	NT
EEEV-27	6.5	72.8	5.6	19.1	11	1	3
EEEV-93	9.3	>	7.7	114.5	>	1	12
EEEV-129	11.2	145.8	20.6	34.9	13	2	3
EEEV-7	19.7	212.4	8.4	29.7	11	0	2
EEEV-21	76.3	567.3	143.9	58.2	7	2	1
EEEV-94	84.1	244.9	41.3	142.6	3	0	2
EEEV-12	381.3	6,057	204.9	3,607	16	1	9
EEEV-147	1,574	1,273	705.0	928.0	1	0	1
EEEV-97	3,653	>	>	>	>	>	>
rDENV-2D22	>	>	>	>	>	>	>

Figure 28. Neutralization activity of human anti-EEEV mAbs to SINV/EEEV escape mutant viruses. **A.** Representative neutralization curves of potent neutralizing human anti-EEEV mAbs against SINV/EEEV WT, and escape mutant viruses M68T, G192R, and L227R. Neutralization curves of potent human anti-EEEV mAbs against SINV/EEEV WT (closed square), M68T (open triangle), G192R (open circle), and L227R (open diamond), with mAb concentration (nM) on the x-axis and % relative infectivity on the y-axis. mAbs are ordered based on IC_{50} values against SINV/EEEV WT. A positive control mouse mAb, mEEEV-3 (dark purple) (Kim et al., 2019), and a negative control mAb, rDENV-2D22 (black; B), were included. **B.** Representative neutralization curves of moderate neutralizing human anti-EEEV mAbs against SINV/EEEV WT and escape mutant viruses M68T, G192R, and L227R. Neutralization curves of moderate human anti-EEEV mAbs against SINV/EEEV WT (closed square), M68T (open triangle), G192R (open circle), and L227R (open diamond), with mAb concentration (nM) on the x-axis and % relative infectivity on the y-axis. A positive control mouse mAb, mEEEV-3 (dark purple; A) (Kim et al., 2019), and a negative control mAb, rDENV-2D22 (black), were included. **C.** Half-maximal inhibitory concentration (IC_{50}) values (pM) for human anti-EEEV mAbs against SINV/EEEV WT and escape mutant viruses M68T, G192R, and L227R. IC_{50} values (pM) for neutralizing human anti-EEEV mAbs against SINV/EEEV WT, M68T, G192R, and L227R are indicated in the table. Neutralizing human anti-EEEV mAbs are listed in order of increasing IC_{50} value against SINV/EEEV WT. IC_{50} value in pM is indicated by

the orange heat map (<33 [dark orange], 33 to 333 [medium orange], 333.01 to 3,333 [light orange], <10,000 [lightest orange]). Fold difference in IC_{50} value ratio of SINV/EEEV WT versus each escape mutant virus (M68T, G192R, or L227R) are indicated. Ratio of neutralization activity against SINV/EEEV WT versus each escape mutant virus (M68T, G192R, or L227R) is indicated as the fold difference of IC_{50} values. Increasing depth of maroon color indicates greater fold differences (>15 or > [dark maroon], 10-15 [medium maroon], 5-10 [light maroon], <5 [white]), suggesting reduction in neutralization activity of the mAb. Data in **A** to **C** represent mean ± SD of technical triplicates and are representative of two independent focus reduction neutralization test (FRNT) experiments. mAbs are colored based on mAb legend in **Figure 23**. Williamson et al., 2020.

EEEV mAb	E2 Domain	Critical EEEV E2 alanine residues[a]	Allosteric EEEV E2 alanine residues[b]	Reduction in neutralization potency for SINV/EEEV escape mutant viruses[c]
EEEV-12	A	No reduction	N/A	M68T (L227R)
EEEV-33	A (N-link/A/Arch 1/B/Arch 2)	**9**, 74, **116, 118, 120**	**34**, **163, 166, 172, 240**	(M68T)
EEEV-147	N-link/Arch 1	**9, 10**	**163, 166**	Minimal reduction
EEEV-7	B	**205, 206, 207**, 213	N/A	M68T
EEEV-106	B	**205, 206, 207**, 213	N/A	M68T
EEEV-27	A/B (N-link/A/Arch 1/B/Arch 2)	**9**, 73, **178, 186, 190, 202, 205-207**, 213-**216, 222, 229**	**33-34, 65, 98, 109, 128, 145 163, 165-166, 172, 185, 226**-227, **240**	M68T
EEEV-129	B	**205, 207**, 213	N/A	M68T
EEEV-21	B	**178,** 194, **202, 205, 207**, 213, 215	**185**	(M68T)
EEEV-94	A/B (N-link/A/B)	**9, 202, 205**, 215	**33, 185**	Minimal reduction
EEEV-143	B	**202**	N/A	(M68T)
EEEV-93	A/B (N-link/A/Arch 1/B/Arch 2)	**9**, 73, **178, 202, 205-206**, 215-**216**	**33-34, 98, 128, 145, 163, 165-166, 172, 185, 226, 240**	M68T, L227R
EEEV-97	B	**178, 190, 200, 202, 207**, 215, **219, 222**	**185**	M68T, G192R, L227R

Table 1. Summary table of EEEV E2 neutralizing antigenic determinants recognized by human anti-EEEV mAbs.

[a] Surface-exposed critical alanine residues (<25% binding relative to WT) are identified as determined through alanine-scanning mutagenesis library analyses for each mAb.

[b] Critical alanine residues (<25% binding relative to WT) that are not surface exposed, as determined through alanine-scanning mutagenesis library analyses for each mAb are identified. The identified residues may result in a loss of binding phenotype due to allosteric effects on the epitope. N/A = not applicable

[c] Neutralization potency of human anti-EEEV mAbs for the SINV/EEEV escape mutant viruses (M68T, G192R, and L227R). Minimal reduction indicates that neutralization potency of respective human anti-EEEV mAb is similar to neutralization activity against WT SINV/EEEV. Escape mutants with a >10-fold reduction in neutralization potency are indicated for each mAb. Parentheses include escape mutants with > 5-fold reduction in neutralization potency. **Bold** indicates residues distinct from those previously identified with a loss-of-binding phenotype for the murine anti-EEEV mAbs (Kim et al., 2019). Williamson et al., 2020.

Neutralizing human anti-EEEV mAbs inhibit SINV/EEEV entry into cells

To elucidate the mechanism of neutralization for human anti-EEEV mAbs, I assessed entry blockade by incubating mAbs with SINV/EEEV, allowing the virus to bind and internalize into cells at 37°C, and followed by extensive washing to remove unbound virus and mAb (**Figure 29**). This approach limits exposure of virus to mAb at the attachment, entry and fusion steps of the infection cycle (Fox et al., 2015; Jin et al., 2015). A similar neutralization potency was observed compared to experiments in which the mAb was present at all stages, including egress, suggesting these mAbs act at one of the early entry stages of virus infection.

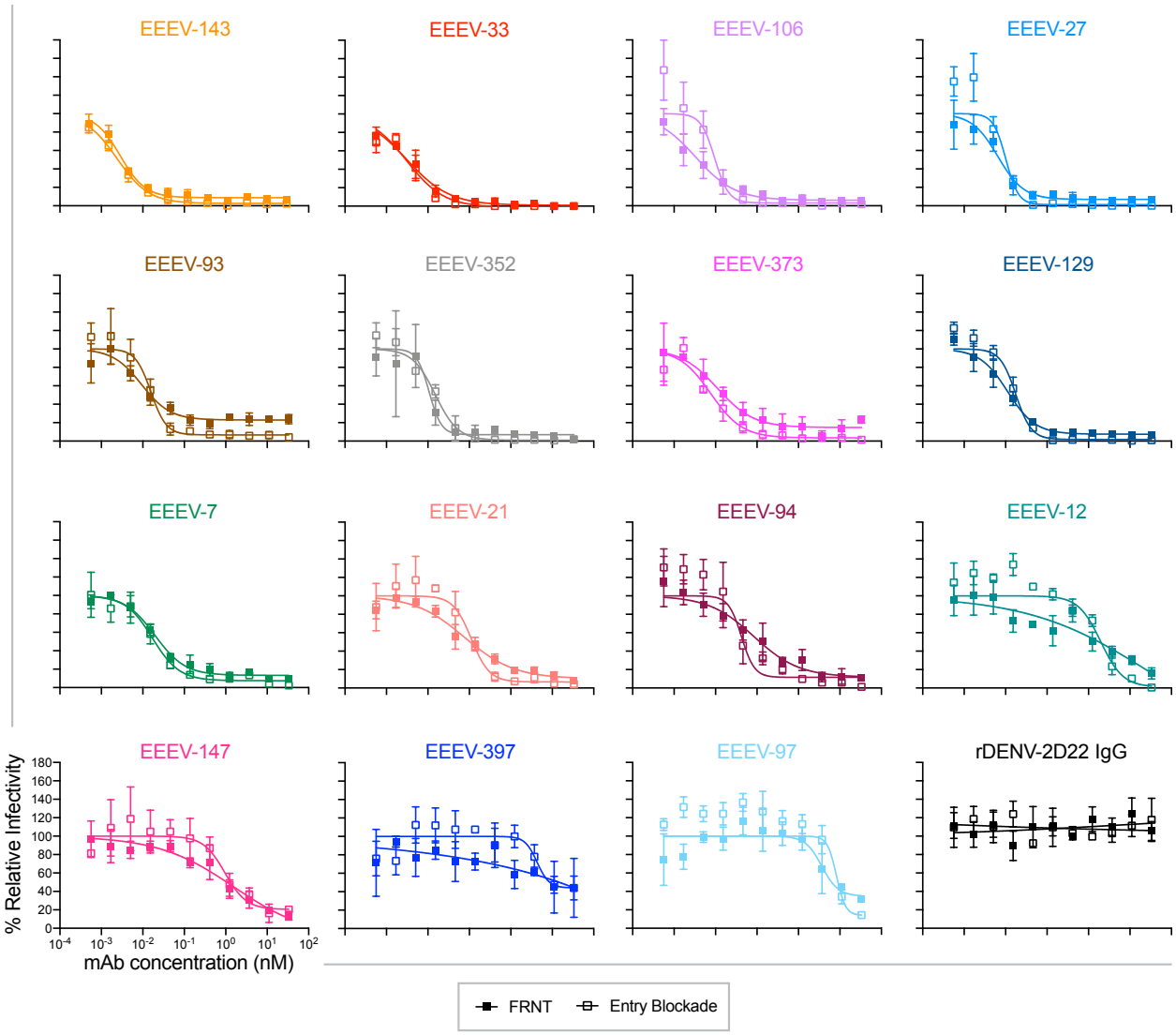

Figure 29. Entry blockade of SINV/EEEV by human neutralizing anti-EEEV mAbs. An entry blockade assay (open squares) was performed by extensive washing of mAb from the medium following internalization of SINV/EEEV into Vero cells. Representative neutralization curves are shown for each mAb as determined through FRNT (closed squares; see **Figure 23A**) or the entry blockade assay with mAb concentration (nM) on the x-axis and percent relative infectivity on the y-axis. mAbs are colored based on mAb legend in **Figure 23**. Data represent mean ± SD of technical triplicates and are representative of at least one independent experiment. Modified from Williamson et al., 2020.

Next, to assess whether human anti-EEEV mAbs block virus attachment to cells, I performed a post-attachment neutralization assay (**Figure 30**). In this assay, virus was incubated with cells at 4°C followed by addition of the mAb at 4°C after attachment and

removal of free virus. A reduction in neutralization potency for most mAbs was observed, which could indicate the mAbs block virus attachment to cells to some degree or cannot reach full occupancy of virion binding sites for optimal neutralization due to epitopes blocked by the initial virus attachment to host cells. However, substantial inhibition still occurred post-attachment, indicating that inhibition of virus entry into cells occurs after adsorption to the cell surface.

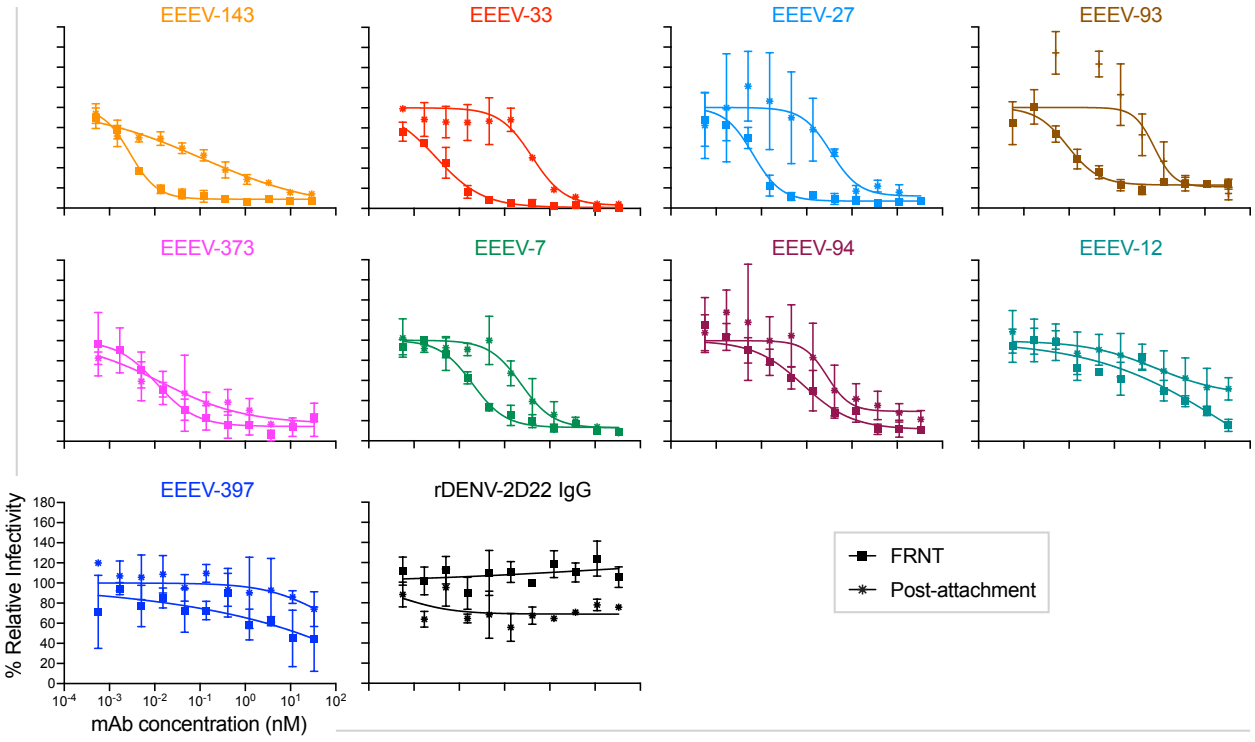

Figure 30. Post-attachment neutralization of SINV/EEEV. A post-attachment neutralization assay (starred circles) was performed by incubation of Vero cells with SINV/EEEV at 4°C for 1 hour followed by addition of indicated mAb at 4°C for 1 hour. Cells were incubated at 37°C for 15 min prior to addition of an overlay and incubation at 37°C for 18 h. Representative neutralization curves are shownas determined through FRNT (closed squares; see **Figure 23A**) or the post-attachment neutralization assay with mAb concentration (nM) on the x-axis and percent relative infectivity on the y-axis. mAbs are colored based on mAb legend in **Figure 23**. Data in represent mean ± SD of technical triplicates and are representative of at least independent experiment. Modified from Williamson et al., 2020.

EEEV-33 binds to a critical epitope within domain A of the E2 trimer of SINV/EEEV particles

In collaboration with Dr. Melanie D. Ohi's laboratory, we characterized the structural basis for an extremely potent mAb, EEEV-33, recognition of SINV/EEEV using single particle cryo-electron microscopy (cryo-EM) and determined a 3D structure of the complex at ~7.2 Å resolution (**Figures 31, 34, and 39**). Analyses above showed that EEEV-33 recognizes domain A of the EEEV E2 glycoprotein (**Figure 27**). Additionally, the observation that EEEV-33 preferentially recognizes virion particles over E2 glycoprotein suggests that a quaternary interaction between the variable domain of the Fab and E2 protomers in the trimer facilitates binding (**Figures 24 and 25**). Thus, EEEV-33 may recognize a critical epitope within domain A of the E2 trimer for neutralization of SINV/EEEV. The structural analysis showed that three Fab molecules bound per E2 trimer in a radial orientation. Each E2 protomer was bound to one Fab molecule. The constant domains of each Fab within the trimer appear to clash sterically with one another, such that occupancy might be reduced for the bulkier IgG form of EEEV-33 (**Figure 31E and 31F**). Additionally, the protomers within the E2 trimer do not move upon EEEV-33 Fab binding, when compared to the apo form of E2 (**Figure 34**).

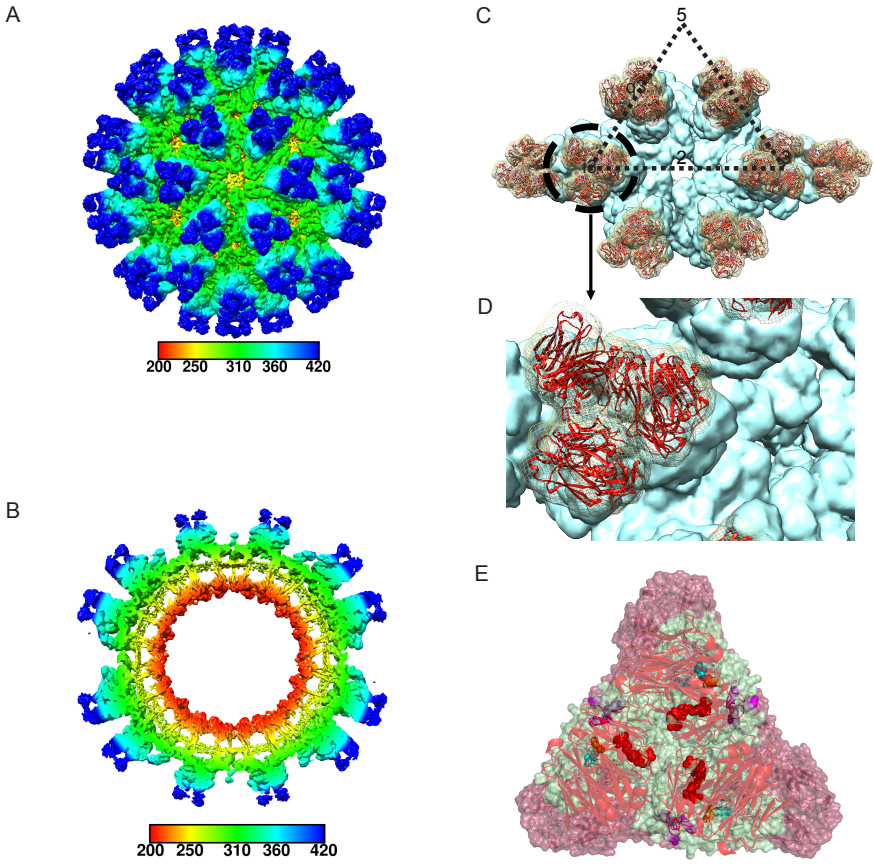

Figure 31. EEEV-33 recognizes a critical domain A epitope on SINV/EEEV particles for inhibition of viral entry or fusion. A and **B.** Cryo-EM reconstruction of SINV/EEEV in complex with EEEV-33 Fab. Cryo-EM structure of EEEV-33 Fab complex (~7.2 Å) showing radially colored surface representation of full **(A)** and cross section **(B)** of the map. **C.** EEEV-33 Fab binding footprint to E2 trimeric spikes on SINV/EEEV particles. View of map surface to illustrate binding of EEEV-33 Fab (red) to the q3 and i3 spikes along the icosahedral 2-fold axis. **D.** EEEV-33 Fab constant domain contact interactions. Close-up view of EEEV-33 Fab binding to the i3 spike (black circle in **C**), in which overlapping Fab constant domain density is observed. **E.** Cryo-EM E2 trimeric view of EEEV-33 Fab binding with critical alanine residues. Critical alanine residues identified for EEEV-33 are indicated with spheres to illustrate the epitope of EEEV-33 corresponds with the SINV/EEEV (PDB ID: 6MX4) and EEEV-143 Fab (mutated sequence of PDB: 6MWX) docked and rigid body refined cryo-EM model of rEEEV-33 Fab in complex with SINV/EEEV. Sphere color corresponds to E2 domain (N-link – purple, Domain A – red, Arch 1 – magenta, Domain B – cyan, and Arch 2 – orange) as described in **Figure 27D**. Modified from Williamson et al., 2020.

EEEV-143 binds to a critical epitope within domain B of the E2 trimer of SINV/EEEV particles and EEEV virus-like particles (VLPs)

In collaboration with Dr. Melanie D. Ohi's laboratory, we also characterized the structural basis of neutralization of the potent neutralizing mAb, EEEV-143, by studying the Fab in complex with SINV/EEEV particles using single particle cryo-EM to determine a 3D structure at ~8.3 Å resolution (**Figures 32, 34, and 39**). EEEV-143 in complex with EEEV VLPs (Ko et al., 2019) was also determined to ~8.5 Å resolution. Similar results to the SINV/EEEV complex reconstruction above were obtained, indicating the structural conformation of VLPs in development as a candidate vaccine is similar to that of SINV/EEEV (**Figure 33**). Previous analyses indicated that EEEV-143 recognizes an epitope in domain B of EEEV E2 glycoprotein. The structure shows that three EEEV-143 Fab molecules associate with each E2 trimer with each E2 protomer bound to one Fab molecule in a tangential orientation. The constant domains of Fabs bound between neighboring trimeric spikes across the 2-fold axis appear to make contacts. In addition, Fabs bound to one q3 spike were ~11 Å apart from the constant domain of another Fab bound to the i3 spike across the 3-fold axis (**Figure 32E and 32F**). Occupancy might be reduced for the IgG form of EEEV-143, due to steric clashes of the Fc regions, and even more so with a polymeric IgA molecule, a model which is supported by the greater binding strength of EEEV-143 IgG1 and Fab molecules to SINV/EEEV (**Figure 25**). As observed for EEEV-33, alignment of the structural protein asymmetric unit of the solved EEEV VLP (**Figures 33A** to **C**; ~4.2 Å) with the EEEV-Fab complex did not show movement of the E2 glycoprotein (**Figures 33I** and **34**).

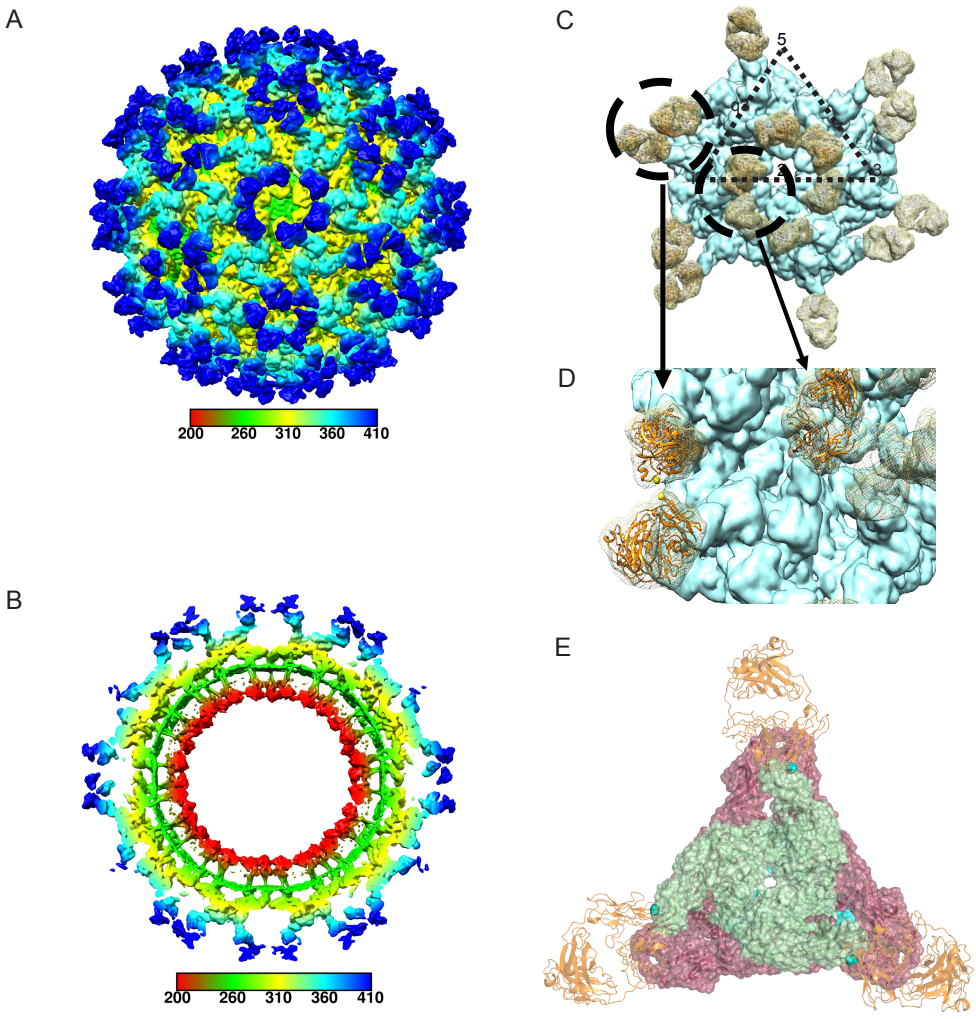

Figure 32. EEEV-143 recognizes a critical domain B epitope on SINV/EEEV particles for inhibition of viral entry or fusion into cells. A and **B.** Cryo-EM reconstruction of SINV/EEEV in complex with EEEV-143 Fab. Cryo-EM structure of EEEV-143 Fab complex (~8.3 Å) showing radially colored surface representation of full (**A**) and cross section (**B**) of the map. **C.** EEEV-143 Fab binding footprint to E2 trimeric spikes on EEEV virus-like particles (VLPs). View of map surface to illustrate binding of EEEV-143 Fab (in orange) to the q3 and i3 spikes along the icosahedral 2-fold axis. **D.** EEEV-143 Fab constant domain contact interactions. Close-up view of EEEV-143 Fab binding to the q3 and i3 spikes (black circles in **C**), in which overlapping Fab constant domain density is observed around the 2-fold axis. Fabs bound to the q3 and i3 spikes across the 3-fold axis are ~11 Å apart, in which the flexibility of the Fab may allow for contacts to occur. **E.** Cryo-EM E2 trimeric view of EEEV-143 Fab binding with critical alanine residues. Critical alanine residues identified for EEEV-143 are indicated with spheres to illustrate the epitope of EEEV-143 corresponds with the EEEV VLP (EMD-22276; PDB ID: 6XO4) and EEEV-143 Fab (mutated sequence of PDB: 6MWX) docked and rigid body refined cryo-EM model. Sphere color

corresponds to E2 domain (N-link – purple, Domain A – red, Arch 1 – magenta, Domain B – cyan, and Arch 2 – orange) as described in **Figure 27D**. Modified from Williamson et al., 2020.

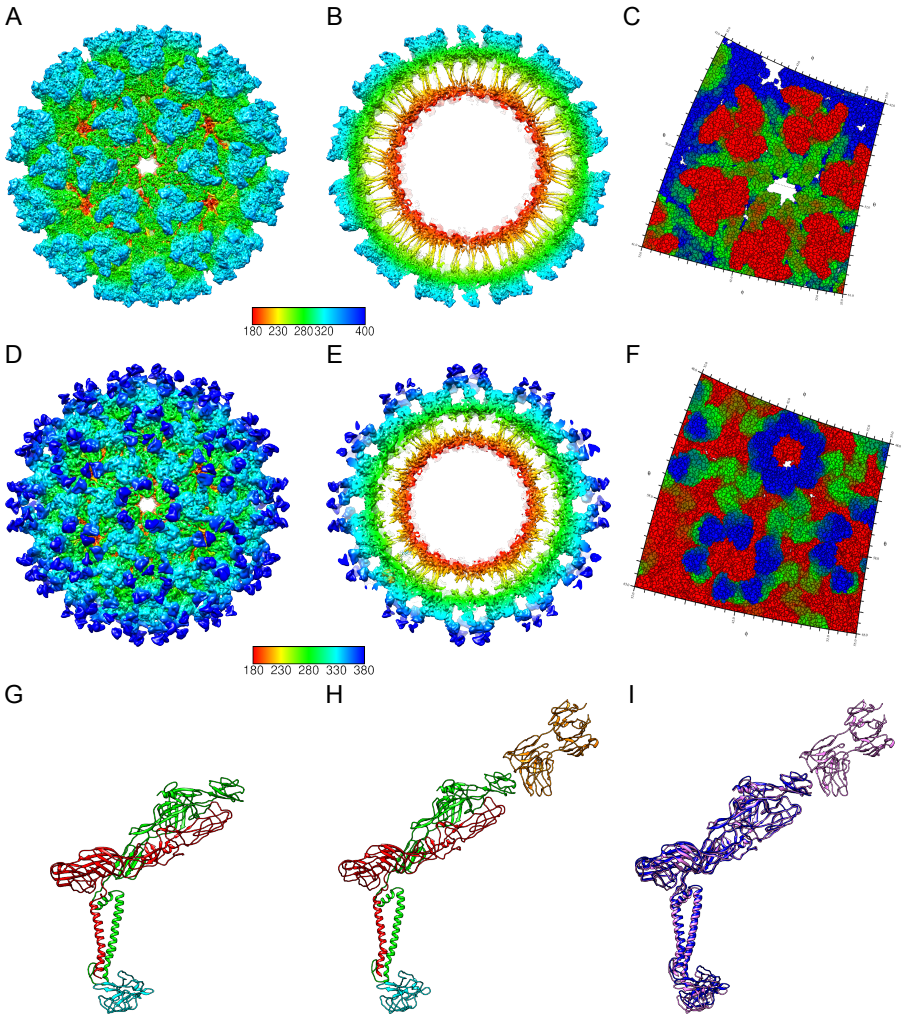

Figure 33. Cryo-EM reconstruction of EEEV VLP in complex with EEEV-143 Fab molecules. Cryo-EM structure of the apo form of EEEV VLP (**A** to **C**) and of EEEV VLP:EEEV-143 Fab complex (**D** to **F**) showing radially colored surface representation of full (**A, D**) and cross-section (**B, E**) of the map. **C, F.** Roadmaps of the apo form of EEEV VLP and EEEV VLP:EEEV-143 Fab complex reconstructions to illustrate EEEV-143 Fab binding sites (in dark blue). EEEV-143 binds in a tangential orientation and makes contacts with neighboring spikes for inter-spike cross-linking of SINV/EEEV particles. **G to H.** Asymmetric unit view of EEEV structural proteins (E2 = green, E1 = red, capsid protein = cyan) of the apo form of EEEV VLP (**G**) or in complex with EEEV-143 Fab molecules (**H**; orange) bound in a tangential orientation. **I.** Alignment of EEEV structural proteins of the EEEV VLP apo form (dark blue) to the EEEV VLP:EEEV-143 Fab complex (pink) to show stabilization of the E2 glycoprotein upon EEEV-143 Fab binding. Williamson et al., 2020.

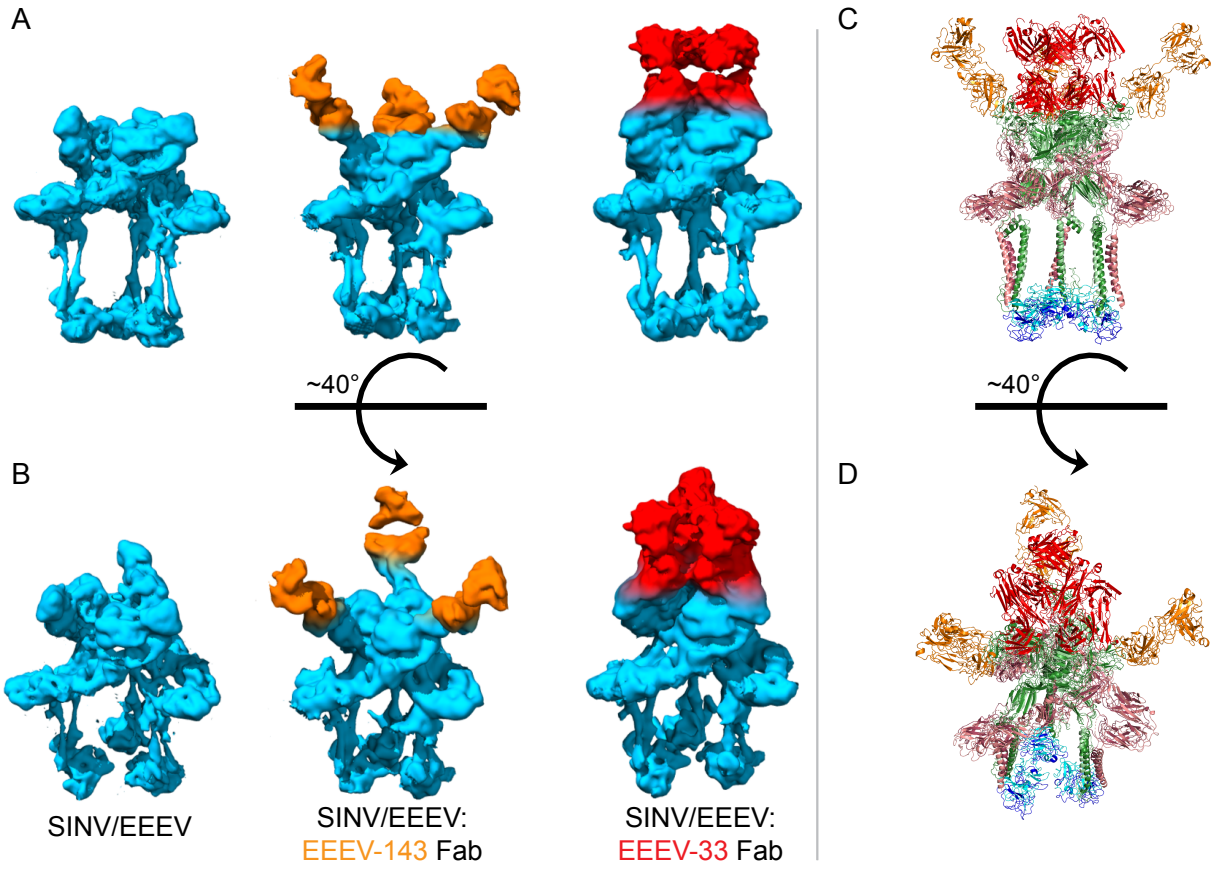

Figure 34. EEEV-33 or EEEV-143 Fab binding to the E2 trimeric spike of SINV/EEEV particles. Side view (**A**) or 40° top-view (**B**) of EEEV E2 trimeric spikes (in light blue) for side-by-side comparisons of native SINV/EEEV (left), SINV/EEEV:EEEV-33 Fab complex (right) and SINV/EEEV:EEEV-143 Fab complex (middle) showing binding of one Fab (EEEV-33 – red; EEEV-143 - orange) per E2 protomer within the trimeric spike. Low pass map of published native SINV/EEEV structure (EMD-9280) used for the comparison. Side view (**C**) or 40° top-view (**D**) of EEEV-33 Fab (red) and EEEV-143 Fab (orange) bound to SINV/EEEV or EEEV VLP, respectively. For the SINV/EEEV (PDB ID: 6MX4) and EEEV-143 Fab (mutated sequence of PDB ID: 6MWX) docked and rigid body refined model of SINV/EEEV:EEEV-33 Fab complex, the structural proteins are colored with E2 = dark green, E1 = salmon, and capsid = blue. For the EEEV VLP:EEEV-143 Fab complex (EMD-22277; PDB ID: 6XOB), the structural proteins are colored with E2 = light green, E1 = raspberry, and capsid = cyan. Williamson et al., 2020.

EEEV-33 protects against WT EEEV aerosol challenge in mice

EEEV is classified as a USDA/CDC Select Agent due to potential for aerosolization and use as a bioterrorism agent. To mimic potential exposure of EEEV as a bioterrorism agent, aerosol challenge has been studied in mice and NHPs (Phelps et al., 2019; Trobaugh et al., 2019; Ko et al., 2019). In collaboration with Dr. William B. Klimstra's laboratory, we assessed the efficacy for EEEV-33 *in vivo* using an aerosol-challenge mouse model and a nanoLuciferase-expressing strain of EEEV FL93-939 (Sun et al., 2014). In this model, prophylaxis with a 100-μg dose of EEEV-33 resulted in 91% survival, when administered by the i.p. route 24 hours prior to virus exposure (**Figure 35A**). Representative *in vivo* imaging (days 4 or 5 after virus inoculation) is shown in which EEEV replication was not observed in the brain, which differed from animals treated with the control antibody rDENV-2D22 (**Figure 35C**). Survival was consistent with the body weight patterns of the mice over the course of 14 days (**Figure 35E**). Additionally, clinical signs of disease (defined as ruffled fur, hunched back/behavioral, seizures/ataxia, moribund, or death) were not observed for the mice that survived. One mouse appeared moribund on day 4 and subsequently died by day 5 (**Figure 35G**). Survival was reduced (27%) when the same dose of Ab was given 24 hours after exposure compared to rDENV-2D22 (**Figure 36A**). Representative *in vivo* imaging (days 4 or 5) is shown for mice that survived infection and reveal EEEV replication was not observed in the brain (**Figure 36D**). Survival was consistent with the body weight patterns of the mice over the course of 14 days. A reduction in body weight

was observed for the mice that died (**Figure 36F**). Clinical signs of disease were observed for the mice that died (**Figure 36H**).

EEEV-143 protects and treats against WT EEEV aerosol challenge in mice

The mucosal IgA response is suspected to play a role in protection because mice with low IgG serum titers following vaccination with EEEV live attenuated virus candidates still were protected against lethal EEEV aerosol challenge (Trobaugh et al., 2019). To assess this possibility, in collaboration with Dr. William B. Klimstra's group, we studied the treatment efficacy of the IgA isotype form of the neutralizing mAb EEEV-143. EEEV-143 mediated 100% survival when a 100-μg dose was administered i.p. route 24 hours prior to virus exposure compared to rDENV-2D22 (**Figure 35A**). Remarkably, in one study (**Figure 36A**), 4 of 5 (80%) mice inoculated survived when EEEV-143 was administered 24 hours after exposure (1,825 PFU/mouse) compared to rDENV-2D22. In a replicate study, EEEV-143 also mediated 100% survival when a 100-μg dose was administered i.p. route 24 hours prior to virus exposure (2,379 PFU/mouse) compared to rDENV-2D22 (**Figure 35B**). However, in this cohort, only 20% of the EEEV-143-treated mice survived when mAbs were administered 24 hours after exposure (2,379 PFU/mouse) compared to rDENV-2D22 (**Figure 36B**). The difference in therapeutic efficacy between these two studies may be due to the variability of infection efficiency in the aerosol model, as slightly different virus titers were administered according to results from back-titration of the inocula on the days of

challenge. To corroborate our findings, an additional study was performed. Here, 20% of the EEEV-143-treated mice survived when mAbs were administered a 200-µg dose 24 hours after exposure (1,897 PFU/mouse) (**Figure 36C**). Representative *in vivo* imaging (days 4 or 5) is shown for mice that survived infection in which EEEV replication was not observed in the brain as compared to rDENV-2D22 (**Figures 35C** and **36D**). Survival was consistent with body weight of the mice over the course of 14 days. A reduction in body weight was observed for the mice that died (**Figures 35E** to **35F** and **36F, 36G,** and **36J**). For the mice that died, all clinical signs of disease were observed (**Figures 35G** to **35H** and **36H, I,** and **K**).

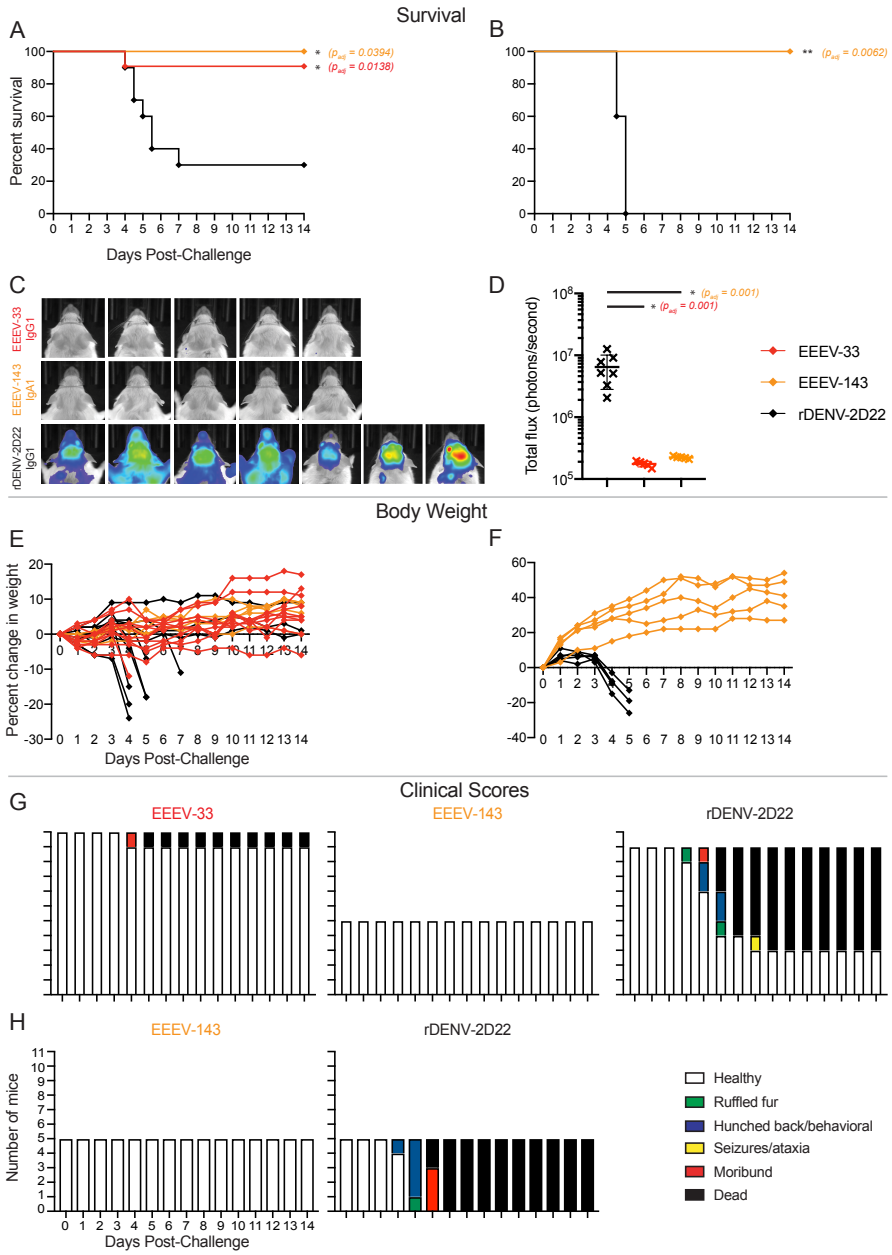

Figure 35. EEEV-33 and EEEV-143 protect in an aerosol challenge model. A. Anti-EEEV mAbs protect against EEEV lethality. EEEV-33 (red; n=11) and EEEV-143 (orange; n=5) were administered prophylactically (24 h prior to virus challenge) at 100 µg via the IP route to CD-1 female mice (4-6-weeks old). EEEV-33 or EEEV-143 protected mice with 91 or 100% survival, respectively, against EEEV (FL93-939) aerosol challenge (1,631 to 1,825 PFU/mouse) compared to the control mAb rDENV-2D22 (black; n=10) (Fibriansah et al., 2015). **B.** EEEV-143 protects against a higher inoculation dose of EEEV. EEEV-143 (orange; n=5) was administered as described in **A**. EEEV-143 exhibited 100% prophylactic survival against EEEV (FL93-939) aerosol challenge (2,739 PFU/mouse). rDENV-2D22 (black; n=5) served as a negative control. **C.** *In vivo* imaging system (IVIS) images of CD-1 mice for EEEV-33, EEEV-143, and rDENV-2D22 prophylactically treated groups at days 4-5 after EEEV aerosol challenge. IVIS images for EEEV-33 (red), EEEV-143 (orange), and rDENV-2D22 (black). One of the mice in the EEEV-33 group

and three of the mice in the rDENV-2D22 negative control group died prior to IVIS imaging on day 5 after virus challenge. **D.** Luminescence intensity of IVIS images. Total flux (photons/second) for the corresponding IVIS images in **C** of the EEEV-33, EEEV-143, and rDENV-2D22 groups is indicated. ~1 x 10^5 total flux is the background for uninfected mice. One-way ANOVA with Dunnett's multiple comparisons correction was used to compare luminescence of the images to the rDENV-2D22 control group. *$p < 0.01$. **E.** Percent body weight change of EEEV-33, EEEV-143, and rDENV-2D22 prophylactically treated CD-1 mice over the course of 14 days. Percent change in weight (y-axis) for EEEV-33 (red; n=11), EEEV-143 (orange; n=5), and rDENV-2D22 (black; n=10) are indicated over the course of 14 days after EEEV challenge (1,631 to 1,825 PFU/mouse; x-axis). **F.** Percent body weight change of EEEV-143 and rDENV-2D22 prophylactically treated CD-1 mice over the course of 14 days. Percent change in weight (y-axis) for EEEV-143 (orange; n=5) and rDENV-2D22 (black; n=5) are indicated over the course of 14 days after EEEV challenge (2,739 PFU/mouse; x-axis). **G.** Clinical scores of EEEV-33, EEEV-143, and rDENV-2D22 prophylactically treated CD-1 mice over the course of 14 days. The number of mice (y-axis) for EEEV-33 (red; n=11), EEEV-143 (orange; n=5), and rDENV-2D22 (black; n=10) with defined clinical scores (dead (black), moribund (red), seizures/ataxia (yellow), hunched back/behavioral (blue), ruffled fur (green), healthy (white)) are indicated over the course of 14 days post EEEV challenge (1,631 to 1,825 PFU/mouse; x-axis). **H.** Clinical scores of EEEV-143 and rDENV-2D22 prophylactically treated CD-1 mice over the course of 14 days. The number of mice (y-axis) for EEEV-143 (orange; n=5) and rDENV-2D22 (black; n=5) with defined clinical scores (dead (black), moribund (red), seizures/ataxia (yellow), hunched back/behavioral (blue), ruffled fur (green), healthy (white)) are indicated over the course of 14 days after EEEV challenge (2,739 PFU/mouse; x-axis). Data **A, C** to **E,** and **G** represent combined *in vivo* data for EEEV-33 (n=6, n=5) or rDENV-2D22 (n=5, n=5) in two independent experiments (1,631 to 1,825 PFU/mouse). Data in **A** represent *in vivo* data for EEEV-143 (n=5) in one independent experiment (1,631 to 1,825 PFU/mouse). Data in **B** to **D, F,** and **H** represent *in vivo* data for EEEV-143 (n=5) in one independent experiment (2,739 PFU/mouse). Data in **A** and **B**, the survival curves were compared using the log-rank test with Bonferroni multiple comparison correction. *$p < 0.05$, **$p < 0.01$, ns = not significant. Modified from Williamson et al., 2020.

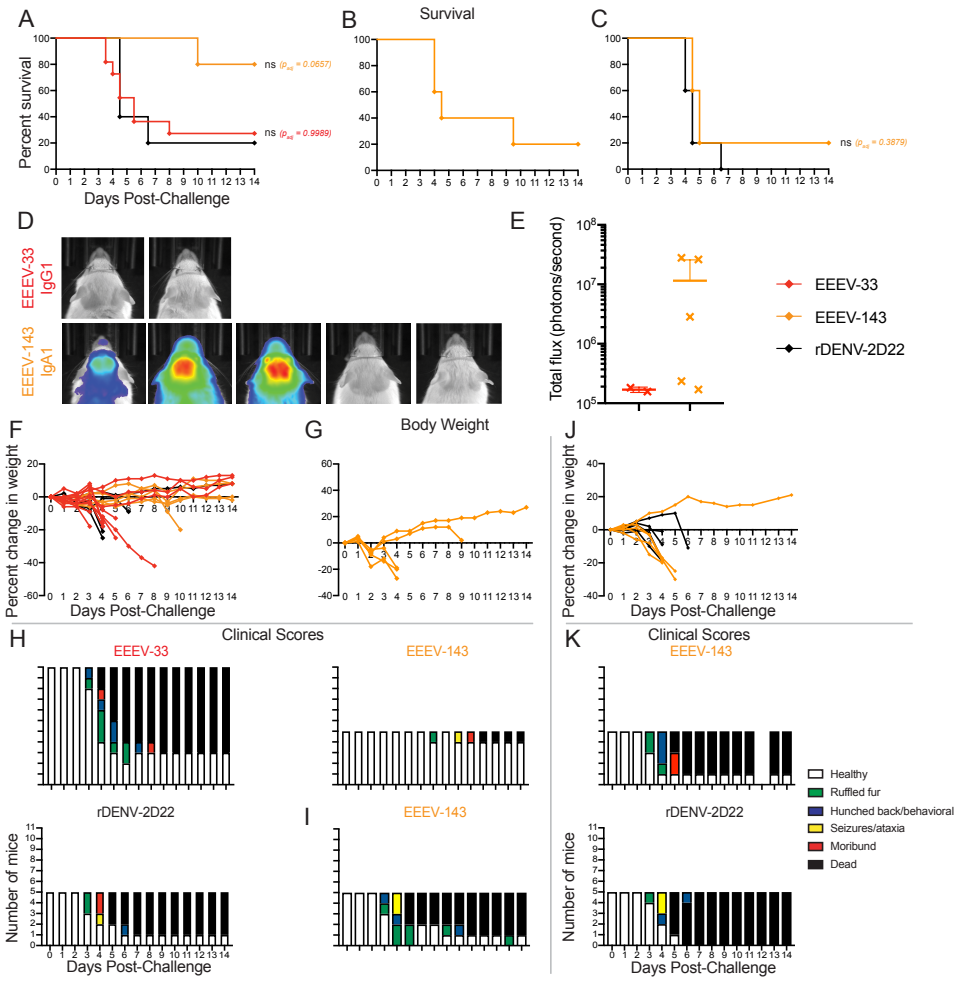

Figure 36. Post-exposure therapy with EEEV-33 and EEEV-143 partially protects mice in an aerosol challenge model. A. Anti-EEEV mAbs protect against EEEV lethality as post-exposure therapy. EEEV-33 (red; n=11) and EEEV-143 (orange; n=5) were administered therapeutically (24 h post virus challenge) at 100 µg via the IP route to CD-1 female mice (4-6-weeks old). EEEV-33 or EEEV-143 exhibited 27% or 80% therapeutic survival, respectively, against EEEV (FL93-939) aerosol challenge (1,631-1,825 PFU/mouse) compared to the control mAb (black; n=5). **B.** EEEV-143 administration at a higher inoculation dose of EEEV. EEEV-143 (orange; n=5) was administered as described in **A**. EEEV-143 exhibited 20% therapeutic survival against EEEV (FL93-939) aerosol challenge (2,739 PFU/mouse). **C.** EEEV-143 administration at 200-µg dose after EEEV exposure. EEEV-143 (orange; n=5) was administered as described in **A** except at a 200 µg dose. EEEV-143 conferred 20% therapeutic survival against EEEV (strain FL93-939) aerosol challenge (1,897 PFU/mouse) compared to the control mAb (black; n=5; 200 µg). **D.** In vivo imaging system (IVIS) images of CD-1 mice for EEEV-33 and EEEV-143 therapeutically treated group at days 4-5 after EEEV aerosol challenge. IVIS images for EEEV-33 (red) or EEEV-143 (orange). Four of the mice in the EEEV-33 group died prior to IVIS imaging on day 5 after virus challenge. **E.** Luminescence intensity of IVIS images. Total flux (photons/second) for the corresponding IVIS images in **D** of the EEEV-33 and EEEV-143 groups are indicated. ~1 x 10^5 total flux is the background for uninfected mice. **F.** Percent body weight change of EEEV-33, EEEV-143, and rDENV-2D22 therapeutically treated CD-1 mice over the course of 14 days. Percent change in weight (y-axis) for EEEV-33 (red; n=11), EEEV-143 (orange; n=5), and rDENV-2D22 (black; n=5) are indicated over the course of 14 days after EEEV challenge (1,631 to 1,825 PFU/mouse; x-axis). **G.** Percent body weight

change of EEEV-143 therapeutically treated CD-1 and BALB/c mice, respectively, over the course of 14 days. Percent change in weight (y-axis) for EEEV-143 (orange; n=5) is indicated over the course of 14 days after EEEV challenge (2,739 PFU/mouse; x-axis). **H.** Clinical scores of EEEV-33, EEEV-143, and rDENV-2D22 therapeutically treated CD-1 mice over the course of 14 days. The number of mice (y-axis) for EEEV-33 (red; n=11), EEEV-143 (orange; n=5), and rDENV-2D22 (black; n=5) with defined clinical scores (dead (black), moribund (red), seizures/ataxia (yellow), hunched back/behavioral (blue), ruffled fur (green), healthy (white)) are indicated over the course of 14 days after EEEV challenge (1,631 to 1,825 PFU/mouse; x-axis). **I.** Clinical scores of EEEV-143 therapeutically treated CD-1 and BALB/c mice, respectively, over the course of 14 days. The number of mice (y-axis) for EEEV-143 (orange; n=5) with defined clinical scores (dead (black), moribund (red), seizures/ataxia (yellow), hunched back/behavioral (blue), ruffled fur (green), healthy (white)) are indicated over the course of 14 days after EEEV challenge (2,739 PFU/mouse; x-axis). **J.** Percent body weight change of CD-1 mice treated therapeutically with EEEV-143 or rDENV-2D22. Percent change in weight (y-axis) for EEEV-143 (orange; n=5) or rDENV-2D22 (black; n=5) treated animals is indicated over the course of 14 days after EEEV challenge (1,897 PFU/mouse; x-axis). **K.** Clinical scores of CD-1 mice treated therapeutically with EEEV-143 or rDENV-2D22. The number of mice (y-axis) treated with EEEV-143 (orange; n=5) or rDENV-2D22 (black; n=5) with defined clinical scores (dead (black), moribund (red), seizures/ataxia (yellow), hunched back/behavioral (blue), ruffled fur (green), or healthy (white)) are indicated over the course of 14 days after EEEV challenge (1,897 PFU/mouse; x-axis). Data **A, D** to **F,** and **H** represent combined *in vivo* data for EEEV-33 (n=6, n=5) in two independent experiments (1,631 to 1,825 PFU/mouse). Data in **A** represent *in vivo* data for EEEV-143 (n=5) and rDENV-2D22 (n=5) in one independent experiment (1,631 to 1,825 PFU/mouse). Data in **B, D, E, G,** and **I** represent in vivo data for EEEV-143 (n=5) in one independent experiment (2,739 PFU/mouse). Data in **C, J,** and **K** represent in vivo data for EEEV-143 (n=5) and rDENV-2D22 (n=5) in one independent experiment (1,897 PFU/mouse). Data in **A** to **C**, the survival curves were compared using the log-rank test with Bonferroni multiple comparison correction. *p < 0.05, **p < 0.01, ns = not significant. Modified from Williamson et al., 2020.

Neutralizing human anti-EEEV mAbs treat against EEEV-induced disease after subcutaneous challenge

Natural transmission of EEEV occurs through the bite of an infected mosquito. To mimic this route of inoculation, we collaborated with Dr. Justin G. Julander's laboratory to assess the therapeutic *in vivo* efficacy of neutralizing human anti-EEEV mAbs against s.c. inoculation of EEEV in mice. EEEV was inoculated s.c. into C57BL/6 mice at a dose of $10^{3.3}$ $CCID_{50}$, which normally results in mice succumbing to neurological disease by about nine days post-inoculation. Twenty-four hours later, neutralizing human anti-EEEV mAbs (EEEV-21, -27, -33, -106, -143 (IgG), -352, or -373) were administered by

i.p. injection at a dose of 200 µg mAb/mouse (10 mg/kg), and mice were monitored for 21 days. 90% (EEEV-33) to 100% (EEEV-21, -27, -106, -143, -352, and -373) of the mice treated with the neutralizing human anti-EEEV mAbs survived infection, whereas only 10% of the animals given rDENV-2D22 (negative isotype control) mAb survived (**Figure 37A**). Body weight measurements corresponded with the survival data (**Figure 37B**). The neutralizing human anti-EEEV mAbs also reduced viremia to the limit of detection, whereas the majority of rDENV-2D22-treated animals had virus in the serum (**Figure 37C**).

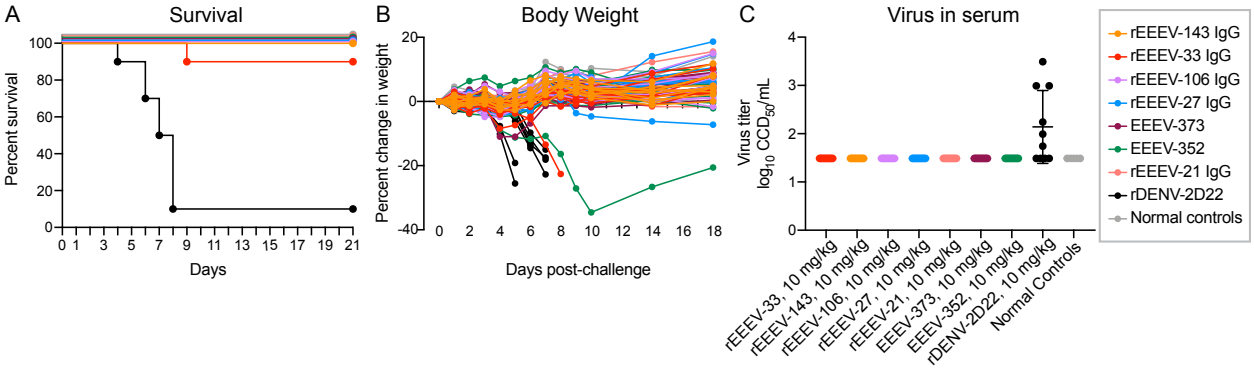

Figure 37. Neutralizing human anti-EEEV E2-specific mAbs treat against EEEV disease after s.c. challenge. A. C57BL/6 mice were inoculated s.c. with $10^{3.3}$ $CCID_{50}$ of EEEV (strain FL93-939) twenty-four hours prior to mAb administration i.p. at 200 µg/mouse. A mock control was included (n=5; grey). Neutralizing human anti-EEEV mAbs (10 mg/kg; n=10; blue) mediated 90% (EEEV-33) to 100% therapeutic survival against EEEV compared to the negative control mAb rDENV-2D22 (10 mg/kg; n=10; black). **B.** Percent body weight change of anti-EEEV mAb, rDENV-2D22, and mock-treated C57BL/6 mice over the course of 18 days after EEEV inoculation. **C.** Virus titer ($log_{10}CCID_{50}$/mL; y-axis) in serum collected three days post-inoculation was determined by an infectious cell culture assay. Anti-EEEV mAbs, rDENV-2D22, or mock controls are indicated on the x-axis.

Discussion

In this chapter, I describe human mAbs isolated against EEEV from the B cells of EEEV-immune individuals with prior natural infection. Isolation of human anti-EEEV mAbs with moderate or potent neutralization activity against the chimeric virus SINV/EEEV allowed for the characterization of the molecular and structural basis of neutralization against EEEV and addressed important questions relating to the human anti-EEEV Ab response. I observed diverse patterns of mAb reactivity and dependence on valency for binding and/or neutralization of SINV/EEEV. Potent mAbs neutralized SINV/EEEV as Fab molecules, suggesting bivalency or tetravalency is not necessary but may be required for optimal neutralization of SINV/EEEV. Two mAbs, EEEV-27 and EEEV-93, displayed reduced binding and neutralization potency as Fab molecules, indicating the requirement for bivalent interactions. Additionally, EEEV-7, -12, -21, -97, and -147 displayed reduced neutralization potency but not reduced binding as Fab molecules, indicating the neutralization mechanism for these mAbs may involve cross-linking of two E2 protomers as IgG molecules. Recognition of three antigenic determinants (domains A, B, and A/B) was observed, with a majority of neutralizing mAbs isolated from this individual recognizing the E2 structural domain B. Further characterization of EEEV-33 and EEEV-143 identified the molecular and structural basis of neutralization, which enabled these mAbs to exhibit *in vivo* efficacy against highly pathogenic EEEV in an aerosol challenge model.

EEEV-33 is a potently neutralizing human anti-EEEV mAb, with 3.1 pM or <37 pM IC_{50} values for neutralization against SINV/EEEV or EEEV, respectively. EEEV-33 preferentially binds SINV/EEEV particles compared to recombinant EEEV E2 glycoprotein, suggesting recognition of a quaternary epitope on the viral surface. A ~7.2 Å 3D image of SINV/EEEV bound to EEEV-33 Fab molecules elucidated the structural basis of neutralization by this Ab. The high neutralization potency of EEEV-33, which has similar potency as a Fab molecule, was consistent with the ability of three Fabs to bind each domain A binding site in the E2 trimer. The ability of three EEEV-33 Fabs to bind to each E2 trimer in the virus is unusual, compared to previous structural analyses of murine anti-EEEV mAbs in complex with SINV/EEEV particles (Hasan et al., 2018; **Figure 13**). From the murine Ab structural analysis, it was observed that steric clashes between Fab molecules, which target domain A of the E2 glycoprotein in a radial orientation, would limit the capacity for complete occupancy of the E2 trimer. However, EEEV-33 binds a unique epitope compared to the murine anti-EEEV mAbs, and the neutralization potency of EEEV-33 even as a Fab molecule is consistent with the occupancy observed in the cryo-EM model. Fab constant domain contacts were observed between Fabs bound within the trimeric spike, indicating that as an IgG molecule steric hindrance may limit occupancy. However, this feature may allow for intra-spike cross-linking to occur for neutralization. We also observed that the protomers of the E2 trimer do not change conformation upon EEEV-33 Fab binding. Together, these data suggest that EEEV-33 recognizes a conformational epitope present on

domain A of the E2 trimer of SINV/EEEV particles. Binding to this epitope, EEEV-33 may stabilize or sterically hinder the E2 trimer, inhibiting viral entry or fusion.

A neutralizing VEEV-specific human mAb similar to EEEV-33, designated F5, was characterized previously (Hunt et al., 2010; Porta et al., 2014). Ab F5 was isolated using phage display from B cells of VEEV TC-83 immune donors. This Ab binds to residues 115-119 in domain A of the E2 glycoprotein, analogous to those recognized by EEEV-33. In contrast to EEEV-33, F5 Fab molecules bind this region of VEEV in a radial orientation and occupy one third of the binding sites. F5 stabilized the E2 trimer via intra-spike cross-linking (Porta et al., 2014). The similarity in binding and neutralization activity for two human mAbs (EEEV or VEEV) suggests a conserved antigenic site (residues 115-120).

EEEV-143 is another potently neutralizing human anti-EEEV mAb with 2.8 pM or 315 pM IC_{50} values against SINV/EEEV or EEEV, respectively. The ~100-fold difference in IC_{50} values against SINV/EEEV and EEEV may be due to physical differences in the various virus preparations used, such as particle/PFU ratio or post-translational modifications of the structural proteins (Jose et al., 2009). EEEV-143 was isolated from a human B cell as an IgA1 antibody. In mice vaccinated with live-attenuated EEEV vaccine candidates, protection against aerosol challenge was observed even in some mice with low serum $PRNT_{80}$ values, suggesting other immune responses may contribute to protection (Trobaugh et al., 2019). Strategies to prevent and/or treat EEEV through Ab-based methods that specifically target mucosal sites could be an important approach. Naturally occurring polymeric IgA (pIgA) molecules are transported actively

across mucosal surfaces via the polymeric immunoglobulin receptor (pIgR) (Turula and Wobus, 2018). Transcytosis of neutralizing Abs across the mucosa may block EEEV infection at or near the site of inoculation to prevent dissemination to the brain.

The structural basis of neutralization for EEEV-143 was determined using single particle cryo-EM of SINV/EEEV bound to EEEV-143 Fab molecules. The resulting ~8.3 Å structure showed that three Fabs also bound to each protomer in the E2 trimer. Fab constant domain contacts were observed around the 2-fold axis and ~11 Å distance between Fabs bound to the q3 and i3 spikes across the 3-fold axis. These contacts suggest that EEEV-143 forms inter-spike cross-links between adjacent E2 trimers as an IgG or IgA. This inter-E2 trimer cross-linking could stabilize or sterically hinder the trimer to inhibit viral entry or fusion. Again, the binding of three EEEV-143 Fab molecules to each E2 trimer is unusual when compared to studies of neutralizing Abs generated in mice, where steric clashes between Fab molecules that target domain B of the E2 glycoprotein in a tangential orientation limited the capacity for complete occupancy of the E2 trimer (**Figure 13**). However, the neutralization potency of EEEV-143 as Fab molecules is consistent with our structural analysis. Steric clashes may still occur in the context of EEEV-143 expressed as a polymeric IgA molecule (dimeric IgA complex with joining [J] chain) as suggested by the reduction in the detected binding strength of this molecule compared to recombinant IgG1 or Fab molecules. Optimal *in vitro* neutralization of SINV/EEEV occurs as a polymeric IgA compared to Fab molecule, as there is >200-fold reduction in neutralization potency. Thus, the inter-spike cross-linking

observed for EEEV-143 may require a bivalent (IgG) or tetravalent (IgA) Ab interaction for optimal neutralization of SINV/EEEV.

A neutralizing CHIKV mAb similar to EEEV-143, designated CHK-265, was characterized previously (Fox et al., 2015) CHK-265 is a broadly neutralizing and protective arthritogenic alphavirus mAb that inhibits viral entry and egress from cells. The ~16 Å cryo-EM reconstruction of CHIKV 181/25 particles in complex with CHKV-265 Fab molecules displays binding of three Fab molecules to each trimeric spike (q3 and i3). Inter-spike cross-linking was observed between two E2 protomers through recognition of domain B residues on one protomer and contacts domain A residues on an adjacent protomer. This binding leads to movement of domain B further over the E1 fusion loop and repositioning of domain A upon binding. CHK-265 Fab constant domain contacts were observed across the 2-fold axis further supporting the cross-liking mechanism of virus particles by CHK-265 as an IgG molecule. In contrast, EEEV-143 recognizes residues within domain B on one protomer and does not appear to induce conformational changes upon binding. Similarly, the constant domain Fab contacts observed for EEEV-143 around the 2-fold axis suggests that EEEV-143 may form inter-spike cross-links as an IgG or IgA molecule. The reduction in neutralization of EEEV-143 as a Fab molecule suggests that this mechanism is important for optimal neutralization of EEEV-143 at this site.

EEEV is classified as a USDA/CDC Select Agent due to potential for aerosolization and use as a bioterrorism agent. To mimic potential exposure of EEEV as a bioterrorism agent, aerosol challenge has been studied in mice and NHPs (Phelps et

al., 2019; Trobaugh et al., 2019; Ko et al., 2019). In our approach, mice were inoculated with EEEV via the aerosol route to assess the pre- or post-exposure treatment efficacy of EEEV-33 (IgG1) and EEEV-143 (IgA1). When given 24 hours before infection, EEEV-33 or EEEV-143 each protected mice with 91 or 100% survival compared to the control, respectively. When administered 24 hours after EEEV inoculation, EEEV-33 treated mice had a 27% survival rate whereas EEEV-143 treated mice showed 20 to 80% survival rates compared to the 0 to 20% for controls. This experimental animal aerosol challenge model is stringent, since the rapid kinetics of viral replication in the central nervous system quickly decreases the likelihood of Ab-mediated protection. There is need to study the *in vivo* efficacy in more detail, as multiple factors could affect effectiveness. Treatment of EEEV-induced disease following s.c. inoculation to mimic natural exposure of EEEV through a mosquito bite by EEEV-33 (90%) and EEEV-143 (100%), further supports the importance of mAb administration since virus replication in peripheral tissues may delay pathogenesis compared to aerosol inoculation. Additionally, since EEEV-33 and EEEV-143 recognize two different antigenic sites on the E2, a potential combination therapy with EEEV-33 and EEEV-143 might have greater efficacy and decrease the likelihood of viral escape mutant viruses generated *in vivo*.

In this chapter, I describe the isolation and characterization of neutralizing human antibodies against EEEV. These studies provide molecular and structural bases of neutralization of EEEV by human mAbs and suggest future research directions that could provide treatment options for patients. These include defining the importance of

mucosal IgA and avidity interactions for optimal neutralization of EEEV, the correlates of Ab-mediated protection, and mechanisms for enhancing Ab transport into the CNS. These studies focused on binding, neutralization, and *in vivo* efficacy against the 1993 Florida FL93-939 isolate of EEEV. Genomic analysis of North American EEEV strains from 1934 to 2014 revealed a high level of conservation, with 99.76% average amino acid similarity (Tan et al., 2018), which suggests the FL93-939 strain may be representative of a majority of the EEEV strains. However, *Madariaga virus* (MADV), formally known as South American EEEV, is genetically distinct from EEEV (Lednicky et al., 2019). Analysis of neutralization activity by the mAbs described here against other EEEV strains circulating in North America, such as the 2019 strain and MADV, warrants further investigation. Overall, the studies described may help inform rationale structure-guided vaccine design and identify possible correlates of protection for lead therapeutic candidates against EEEV, and possibly other encephalitic alphaviruses.

Materials and Methods

Human subject information

The subjects gave written informed consent prior to participation, and the Institutional Review Board (IRB) at Vanderbilt University Medical Center approved the protocols for the recruitment and collection of blood samples used in this study.

Mouse model

For the EEEV aerosol challenge studies in collaboration with Dr. William B. Klimstra's laboratory, mice were specific-pathogen-free CD-1 females of 4 to 6 weeks of age purchased from Charles River Laboratories. These studies were performed under University of Pittsburgh IACUC protocol #17121689 in accordance with the recommendations of the Association for Assessment and Accreditation of Laboratory Animal Care (AAALAC).

For the EEEV s.c. challenge studies in collaboration with Dr. Justin G. Julander's laboratory, C57BL/6 mice were purchased from Jackson Laboratories. All animal procedures were carried out in accordance with the recommendations in the Guide for the Care and Use of Laboratory Animals of the National Institutes of Health. The protocols were approved by the Institutional Animal Care and Use Committee at the Utah State University IACUC protocol #10025.

Cell lines

BHK-21 (hamster, male origin; ATCC) and Vero (monkey, female origin; ATCC) cells were maintained in DMEM (Gibco) and 10% heat-inactivated FBS (Thermo Fisher Scientific) at 37ºC in a humidified atmosphere of 5% CO_2. HMAA 2.5 cells (mouse-human, gender information not available; kindly provided by Lisa Cavacini) are a non-secreting myeloma cell line and were maintained in ClonaCell^{TM}-HY Medium A (Stem

Cell Technologies) at 37ºC in a humidified atmosphere of 7% CO_2 as previously described (Yu et al., 2008a; Yu et al., 2008b). B95.8 (monkey, gender information not available; ATCC) cells were cultured in Medium A for collection of supernatants containing Epstein-Barr virus (EBV). Expi293F (human, female origin; Thermo Fisher Scientific) cells were maintained in Expi293 expression medium (Gibco) or Freestyle F17 medium (Gibco) supplemented with 4 mM L-glutamine (Gibco) and 0.1% pluronic F-68 (Gibco) at 125 rpm 37ºC in a humidified atmosphere of 8% CO_2. Expi293F cells were authenticated by the ATCC cell line authentication service using Short Tandem Repeat (STR) analysis. Cells were checked routinely for mycoplasma detection using a universal mycoplasma detection kit (ATCC).

Viruses

The chimeric virus, Sindbis virus (SINV; TR339)/Eastern equine encephalitis virus (EEEV; FL93-939), and SINV/EEEV escape mutant viruses (M68T, G192R, and L227R) were described previously (Kim et al., 2019). EEEV FL93-939 was derived from the cDNA clone, as previously described (Gardner et al., 2011).

Plasmids

Recombinant EEEV E1 ectodomain (strain FL93-939; amino acids Y1-S409) with the osteonectin leader sequence and a C-terminal 6x his-tag was codon-optimized,

synthesized and cloned into the mammalian expression vector pcDNA3.1(+). Recombinant EEEV (strain FL93-939) structural protein genes (capsid-E3-E2-6K-1) were codon-optimized, synthesized and cloned into the mammalian expression vector pcDNA3.1(+) for expression of the WT EEEV structural proteins. Using the WT EEEV structural protein vector, residues D1-L267 of EEEV E2 structural protein were mutated to alanine or alanine residues to serine for expression of the EEEV E2 mutants for alanine-scanning mutagenesis library analyses. Recombinant human anti-EEEV variable genes were synthesized and cloned into a pTwist CMV Betaglobin WPRE Neo mammalian expression vector that was customized to contain isotype-specific constant regions (IgG1, IgA1, or Fab) (Twist Bioscience Inc.). Additionally, for expression of polymeric IgA1, the mouse J chain sequence (Uniprot: P01592) was synthesized a pTwist CMV Betaglobin WPRE Neo mammalian expression vector (Twist).

Recombinant proteins

Recombinant EEEV E2 glycoprotein (strain v105) was purchased from IBT BioServices and contains a mixture of the p62 (E3E2) and E2 glycoproteins. Recombinant CHIKV E1 was purchased from Meridian Life Science. EEEV virus-like particles (VLPs) were kindly provided by Dr. John Mascola at the NIH/NIAID Vaccine Research Center (Ko et al., 2019).

SINV/EEEV production

BHK-21 cells were plated the day before using 3 x 10^7 cells per T-225 cm^2 flask (Corning). The following day, cells were inoculated with SINV/EEEV at a MOI of 0.2 in DMEM/2% FBS. After incubation at 37°C in 5% CO_2 for 48 hours, SINV/EEEV was harvested by clarification of infected BHK-21 cell supernatants through a 0.2-µm pore size filter (Nalgene). Virus then was used fresh or stored at -80°C until use. For cryo-EM studies, BHK-21 cells were inoculated with SINV/EEEV at a MOI of 5 in DMEM/2% FBS. After incubation at 37°C in 5% CO_2 for 16 hours, SINV/EEEV was harvested by centrifugation at 2,000 x *g* at 4°C for 10 minutes. Virus supernatant was precipitated in 14% (w/v) PEG 6000 (Sigma-Aldrich) and 4.6% (w/v) NaCl (Corning) overnight at 4°C, followed by centrifugation at 2,500 x *g* at 4°C for 30 minutes. A linear, continuous 10 to 50% OptiPrep (Sigma-Aldrich) gradient was used to purify the SINV/EEEV particles further at 136,873 x *g* (r_{max}) for 1.5 hours at 4°C using an AH-650 swinging bucket rotor (Sorvall). SINV/EEEV particles were collected and buffer exchanged into TNE buffer (50 mM Tris-HCl pH 7.5 (Sigma), 100 mM NaCl, 0.1 mM EDTA (Corning)) to a concentration of ~0.1 mg/mL total protein content, as determined by a Bradford assay or BCA assay (Thermo Fisher Scientific). Virus then was used fresh or stored at 4°C until use.

Recombinant EEEV E1 ectodomain expression

E1 was produced in Expi293F cells using the ExpiFectamine 293 transfection kit (Gibco). Briefly, 1 µg/mL of pcDNA3.1(+)-EEEV E1 ectodomain was diluted in Opti-MEM medium (Gibco) with ExpiFectamine 293 reagent for 15 to 20 minutes at room temperature before addition to Expi293F cells. Cells were incubated at 37°C in 8% CO_2 and supernatant was harvested by centrifugation and subsequent filtering through a 0.45-µm pore size filter (Nalgene) 2 to 6 days after transfection. Cell supernatant was purified through a HisTrap excel column (GE Healthcare) according to the manufacturer's protocol on an ÄKTA pure 25M chromatography system.

Human hybridoma generation

Cryopreserved PBMCs were thawed and transformed with Epstein-Barr virus (EBV), as described (Yu et al., 2008a; Yu et al., 2008b). Briefly, in B cell growth medium (ClonaCell-HY Medium A [Stem Cell Technologies]), CpG (Invitrogen), Chk2 inhibitor (Sigma-Aldrich), cyclosporin A (Sigma-Aldrich), and EBV filtrate from the B95.8 cell line), 5 to 7 million PBMCs were added at 50 µL/well to 384-well plates (Thermo Fisher Scientific) and incubated at 37°C in 7% CO_2. After 7-10 days, cells were expanded to 96-well plates in B cell expansion medium (Medium A, CpG, Chk2 inhibitor, and irradiated heterologous human PBMCs (Nashville Red Cross) at a density of 10 million cells/mL. The plates were incubated at 37°C in 7% CO_2 for an additional 4-5 days prior to screening by ELISA, as below. Cells from wells containing reactive supernatants were fused with the myeloma cell line HMMA2.5 using an electrofusion protocol as

described (Yu et al., 2008a). Fused hybridomas were selected by plating in HAT medium (Medium A, ClonaCell™-HY Medium E (Stem Cell Technologies), 50x HAT medium supplement (Sigma-Aldrich), ouabain octahydrate [Sigma-Aldrich]) at 50 µL/well in 384-well plates. The plates were incubated for 14 to 21 days at 37°C in a humidified atmosphere of 7% CO_2 prior to screening by ELISA.

mAb generation

Wells containing reactive hybridomas were cloned by single-cell fluorescence-activated cell sorting. These hybridoma clones were expanded in Medium E serially into 48-well plates, 12-well plates, and T-75 cm^2 flasks, respectively. Hybridoma clones were expanded further into T-225 cm^2 flasks or G-Rex® devices (Wilson Wolf) in serum-free medium (Hybridoma SFM [Gibco]). Supernatants were harvested after approximately 21 days, or in sets of 3 to 5 days, respectively, through a 0.2-µm pore size filter. Abs were purified from the filtrate using HiTrap Protein G (GE Healthcare Life Sciences), HiTrap MabSelect SuRe (GE Healthcare Life Sciences), HiTrap KappaSelect (GE Healthcare Life Sciences), HiTrap LambdaFabSelect (GE Healthcare Life Sciences), or CaptureSelect™ IgA affinity matrix (Thermo Fisher Scientific) columns on an ÄKTA pure 25M chromatography system. Abs were concentrated using 50K MWCO Amicon® Ultra centrifugal filter units (Millipore) followed by desalting and buffer exchange with 7K MWCO Zeba desalting columns (Thermo Fisher Scientific).

Hybridoma supernatant protein ELISA

For screening of subjects 1 and 2, recombinant EEEV E2 glycoprotein (E3E2) (strain V105; IBT Bioservices) was diluted to 0.5 µg/mL in 1x D-PBS to coat 384-well ELISA plates (Thermo Fisher Scientific) at 25 µL/well and incubated at 4°C overnight. For screening of subject 2 recombinant EEEV E1 ectodomain (2 µg/mL; strain FL93-939), EEEV p62E1 (2 µg/mL; strain FL93-939), CHIKV E1 protein (2 µg/mL; Meridian Life Science), or EEEV, VEEV, WEEV virus-like particles (VLPs; 2 µg/mL) were diluted in 1× D-PBS to coat 384-well ELISA plates (Thermo Fisher Scientific) and incubated at 4°C overnight. The plates were washed 3× with D-PBS-T (1× D-PBS + 0.05% Tween 20 [Cell Signaling Technology]) and blocked for 1 hour at room temperature with 25 µL/well blocking solution (2% non-fat dry milk (Bio-Rad), 2% goat serum (Gibco) in D-PBS-T). After blocking, the plates then were washed 3× with D-PBS-T and cell supernatant from each well containing EBV-transformed B cells or hybridoma cell lines was added. Plates were incubated for 2 hours at room temperature or overnight at 4°C. Plates then were washed 3× with D-PBS-T and a suspension of secondary Abs (goat anti-human IgG-AP (Meridian Life Science) and goat anti-human IgA-AP [Southern Biotech]) at a 1:4,000 dilution in 1% blocking solution (1% non-fat dry milk, 1% goat serum) was added at 25 µL/well for 1 hour at room temperature. Alkaline phosphatase substrate solution (phosphatase substrate tablets (Sigma-Aldrich) in AP substrate buffer (1M Tris aminomethane and 30 mM $MgCl_2$) was added at 25 µL/well following plate washing 4x

with D-PBS-T. Plates were incubated at room temperature in the dark for 1-2 hours and then read at an optical density of 405 nm with a plate reader.

Hybridoma supernatant SINV/EEEV ELISA

For SINV/EEEV screening for subjects 1 and 2, a murine mAb (EEEV-66; MSD and ASK (Kim et al., 2019)) was diluted to 0.5 µg/mL in 1x D-PBS to coat 384-well ELISA plates at 25 µL/well and incubated at 4°C overnight. The remainder of the ELISA protocol follows as described above for the protein ELISA. However, after blocking, clarified SINV/EEEV supernatant diluted 1:10 in 1x D-PBS (approximately 1 x 10^6 to 1 x 10^7 FFU/mL as determined through focus forming assay (FFA) with BHK-21 cells) at 25 µL/well was added. After incubation for 1-2 hours at room temperature, the plates were washed 6x with D-PBS-T (the first 2-3 washes were conducted under BSL-2 conditions).

5′ RACE nucleotide sequence analysis

Ab heavy and light-chain variable region genes were sequenced from antigen-specific hybridoma lines that had been cloned biologically using single-cell flow cytometric sorting. Total RNA was extracted using the RNeasy Mini kit (Qiagen). A modified 5′ RACE (Rapid Amplification of cDNA Ends) approach was similar to that previously reported (Turchaninova et al., 2016). Briefly, 5 µL of total RNA was mixed

with cDNA synthesis primer mix (10 μM each) and incubated for 2 min at 70°C and then the incubation temperature was decrease to 42°C to anneal the synthesis primers (1 to 3 min). After incubation, a mix containing 5× first-strand buffer (Clontech), 20 mM DTT, 5′ template switch oligo (10 μM), dNTP solution (10 mM each) and 10× SMARTScribe Reverse Transcriptase (Clontech) was added to the primer-annealed total RNA reaction and incubated for 60 min at 42°C. The first-strand synthesis reaction was purified using the AMPure Size Select Magnetic Bead Kit at a ratio of 0.6× (Beckman Coulter). Following, a single PCR amplification reaction containing 5 μL first-strand cDNA, 2x Q5 High Fidelity Mastermix (NEB), dNTP (10 mM each), forward universal primer (10 μM) and reverse primer mix (0.2 μM each in heavy-chain mix, 0.2 μM each in light-chain mix) were subjected to thermal cycling with the following conditions: initial denaturation for 1 min 30 s followed by 30 cycles of denaturation at 98°C for 10 s, annealing at 60°C for 20 s, and extension at 72°C for 40 s, followed by a final extension step at 72°C for 4 min. The first PCR reaction was purified using the AMPure Size Select Magnetic Bead Kit at a ratio of 0.6× (Beckman Coulter). Amplicon libraries then were prepared according to the Pacific Biosciences Multiplex SMRT Sequencing protocol and sequenced on a Pacific Biosciences Sequel system platform. Raw sequencing data was demultiplexed and circular consensus sequences (CCS) were determined using the Pacific Biosciences SMRT Analysis tool suite. The identities of gene segments and mutations from germlines were determined by alignment using the ImMunoGenetics database (Brochet et al., 2008; Giudicelli and Lefranc, 2011).

Recombinant human Fab, IgG1, and IgA1 production

Recombinant human anti-EEEV mAb or Fab molecules were produced in Expi293F cells using the ExpiFectamine 293 transfection kit according to the manufacturer's protocol. Briefly, 1 µg/mL of DNA was diluted in Opti-MEM I medium with ExpiFectamine 293 reagent for 15 to 20 minutes at room temperature before addition to the Expi293F cells. Cells were incubated at 37°C in a humidified atmosphere of 8% CO_2 and supernatant was harvested by centrifugation and subsequent filtering through a 0.45-µm pore size filter 6 to 7 days after transfection. For IgG1, IgA1, Fab molecules, cell supernatant was purified through a HiTrap MabSelect SuRe, CaptureSelect™ IgA affinity matrix, or CaptureSelect™ CH1-XL affinity column, respectively, according to the manufacturer's protocol on an ÄKTA pure 25M chromatography system. Abs were concentrated using 30K or 50K MWCO Amicon® Ultra Centrifugal Filter Units followed by desalting and buffer exchange with 7K MWCO Zeba desalting columns.

Protein EC_{50} ELISA

Recombinant EEEV E2 glycoprotein (E3E2) (strain V105; IBT BioServices), EEEV E1 ectodomain (strain FL93-939), or CHIKV E1 protein (Meridian Life Science) was diluted to 0.5, 2, or 2 µg/mL, respectively, in 1× D-PBS to coat 384-well ELISA plates at 25 µL/well and incubated at 4°C overnight. A protein screening ELISA was

performed as previously described above. However, instead of hybridoma supernatant, purified mAb was diluted to 10 µg/mL in blocking solution (1% non-fat dry milk, 1% goat serum) and added at 25 µL/well for 2 hours at room temperature. Additionally, plates were incubated at room temperature in the dark for 2 hours and then read at an optical density of 405 nm with a BioTek™ plate reader. For recombinant anti-EEEV mAbs and Fab molecules, a suspension of secondary Abs (goat anti-human kappa-HRP (Southern Biotech) and goat anti-human lambda-HRP (Southern Biotech)) at a 1:4,000 dilution in 1% blocking solution (1% non-fat dry milk, 1% goat serum) was added at 25 µL/well for 1 hour at room temperature. 1-Step Ultra TMB-ELISA substrate solution (Thermo Fisher Scientific) was added at 25 µL/well following plate washing 4× with D-PBS-T. The reaction was stopped after 10 minutes at room temperature by addition of 25 µL/well of 1N HCl (Fisher Scientific). The plates then were read at an optical density of 450 nm with a BioTek™ plate reader. EC_{50} values were determined after log transformation of concentration values and non-linear regression analysis using sigmoidal dose-response (variable slope) using GraphPad Prism software version 8.

SINV/EEEV EC_{50} ELISA

A mouse anti-EEEV mAb (EEEV-66; MSD and ASK (Kim et al., 2019)) was coated onto 384-well plates and incubated at 4°C overnight, as previously described above. After the blocking step, SINV/EEEV was diluted in 1× D-PBS to a titer of approximately 2.2 x 10^7 FFU/mL as determined through FFA with BHK-21 cells. After

incubation for 2 hours at room temperature, the plates then were washed 6× with D-PBS-T (the first 2-3 washes were conducted under BSL-2 conditions in a laminar flow biosafety cabinet).

Focus forming assay (FFA)

BHK-21 or Vero cells were plated at 2.5 x 10^6 cells/96-well plate in DMEM/5% FBS/10 mM HEPES (Corning) at 150 µL/well. Cells were incubated at 37°C in 5% CO_2 overnight. Cells plated approximately 24 hours prior were washed 2× with 1x D-PBS. Serial ten-fold dilutions of SINV/EEEV were diluted in DMEM/2% FBS/10 mM HEPES and added at 100 µL/well to the cells. The virus and cells were incubated at 37°C in 5% CO_2 for 1.5 hours. A 2% methylcellulose (Sigma-Aldrich):2× DMEM (Millipore):4% FBS:20 mM HEPES overlay then was added to the cells at 100 µL/well. Cells then were incubated at 37°C in 5% CO_2 for 18 hours. Plates were fixed with 1% PFA (diluted in 1x D-PBS; Alfa Aesar) at 100 µL/well for 1 hour at room temperature. Plates then were washed 3x with 1x D-PBS followed by 1× Perm Wash (1× D-PBS, 0.1% saponin (Sigma-Aldrich), 0.1% BSA (Sigma-Aldrich)) at 200 µL/well. Immune EEEV ascites fluid (ATCC) at 1:6,000 dilution in 1x Perm Wash was then added at 50 µL/well. The plates were incubated either at room temperature for 2 hours with rocking or overnight at 4°C. Plates were washed 3× with 1× D-PBS-T followed by the addition of a suspension of secondary Abs (goat anti-mouse IgG-Fc-specific-HRP (Jackson ImmunoResearch)) at 1:2,000 dilution in 1× Perm Wash. Plates were incubated for 1 hour at room

temperature with rocking. Plates were washed 3× with 1x D-PBS-T followed by addition of TrueBlue™ peroxidase substrate solution (SeraCare) at 40 µL/well. Plates were incubated for ~15 minutes at room temperature followed by a rinse with MilliQ water. The plates then were air dried and imaged on an ImmunoSpot S6 Universal machine (CTL).

Focus reduction neutralization test (FRNT)

Vero cells were plated at 2.5 x 10^6 cells/96-well plate in DMEM/5% FBS/10 mM HEPES at 150 µL/well. Cells were incubated at 37°C in 5% CO_2 overnight. Purified mAb was diluted to 20 µg/mL (final concentration 10 µg/mL) in DMEM/2% FBS/10 mM HEPES. Serial three-fold dilutions of the mAb were performed. MAb-only dilutions were separated to serve as a negative control. SINV/EEEV was diluted to ~100 focus-forming units (FFU)/well in DMEM/2% FBS/10 mM HEPES and added to the mAb serial dilutions. The mAb:virus mixture was incubated at 37°C in 5% CO_2 for 1 hour. Vero cells plated approximately 24 hours prior were washed 2× with 1x D-PBS. The mAb:virus mixture then was added at 100 µL/well to the cells and incubated at 37°C in 5% CO_2 for 1.5 hours. A 2% methylcellulose:2× DMEM/4% FBS/20 mM HEPES overlay then was added to the cells at 100 µL/well. Cells were incubated at 37°C in 5% CO_2 for 18 hours. Plates were fixed and immunostained as described for FFA.

Post-attachment neutralization assay

Vero cells were plated at 2.5 x 10^6 cells/96-well plate in DMEM/5% FBS/10 mM HEPES at 150 µL/well. Cells were incubated at 37°C in 5% CO_2 overnight. Vero cells plated approximately 24 hours prior the media was replaced with chilled DMEM/2% FBS/10 mM HEPES and cells were chilled at 4°C for 15 minutes. SINV/EEEV was diluted to ~100 FFU per well in chilled DMEM/2% FBS/10 mM HEPES and added to the cells at 4°C for 1 hour. Purified mAb was diluted to 10 µg/mL in chilled DMEM/2% FBS/10 mM HEPES. Serial three-fold dilutions of the mAb were performed. MAb-only dilutions were separated to serve as a negative control. Cells were washed 3× with chilled DMEM/2% FBS/10 mM HEPES. mAb then was added at 100 µL/well to the cells and incubated at 4°C for 1 hour. Cells were washed 3× with DMEM/2% FBS/10 mM HEPES and incubated at 37°C for 15 minutes. A 2% methylcellulose:2× DMEM/4% FBS/20 mM HEPES overlay then was added to the cells at 100 µL/well. Cells were incubated at 37°C in 5% CO_2 for 18 hours. Plates were fixed and immunostained as described for FFA.

Entry inhibition assay

A FRNT was performed as previously described. However, prior to addition of overlay, the cells were washed 4× with DMEM/2% FBS/10 mM HEPES and incubated at 37°C in 5% CO_2 for 15 minutes. A 2% methylcellulose:2× DMEM/4% FBS/20 mM

HEPES overlay then was added to the cells at 100 µL/well. Cells were incubated at 37°C in 5% CO_2 for 18 hours. Plates were fixed and immunostained as described for FFA.

EEEV plaque reduction neutralization test (PRNT)

Ab preparations were diluted serially (using 2-fold dilutions) and incubated with ~100 PFU of EEEV FL93-939 for 1 h at 37°C. Anti-EEEV ascites serum (ATCC) was used as a positive control. After incubation, Vero cell monolayer cultures in 6-well plates were inoculated and incubated for 1 h at 37°C. After overlay with agarose immunodiffusion grade (MP Biomedicals), plates were incubated for 2 days followed by overlay with neutral red for at least 6 h to count plaques. Percent neutralization was calculated based on the number of plaques in each mAb dilution compared to the number of plaques in untreated control wells inoculated with virus.

Competition-binding analysis using biolayer interferometry

Anti-penta his (HIS1K) biosensor tips (FortéBio) on an Octet Red96 or HTX biolayer interferometry instrument (FortéBio) were soaked for 10 minutes in 1× kinetics buffer (FortéBio), followed by a baseline signal measurement for 60 seconds. Recombinant EEEV E2 glycoprotein (5 µg/mL; IBT BioServices) was immobilized onto the biosensor tips for 60 seconds. After a wash step in 1× kinetics buffer for 30 to 60

seconds, the first Ab (50 μg/mL) was incubated with the antigen-containing biosensor for 600 seconds. After a wash step in 1× kinetics buffer for 30 to 60 seconds, the biosensor tips then were immersed into the second Ab (50 μg/mL) for 180 seconds. Comparison between the maximal signal of each Ab compared to a buffer-only control was used to determine the percent binding of each Ab. A reduction in maximum signal to <33% of un-competed signal was considered full competition of binding for the second Ab in the presence of the first Ab. A reduction in maximum signal to between 33 to 67% of un-competed was considered intermediate competition of binding for the second Ab in the presence of the first Ab. Percent binding of the maximum signal >67% was considered absence of competition of binding for the second Ab in the presence of the first Ab.

Alanine-scanning mutagenesis analysis

WT EEEV (strain FL93-939) structural proteins (capsid-E3-E2-6K-E1) and E2 mutants were expressed on the surface of Expi293F cells using the ExpiFectamine 293 transfection kit according to the manufacturer's protocol as previously described. Cells were incubated at 37°C in a humidified atmosphere of 8% CO_2, were harvested 24 hours after transfection, and fixed with 1% PFA/PBS. Cells were washed twice with 1x DPBS and stored at 4°C in FACS buffer (1× DPBS, 2% FBS, 2 mM EDTA) until use or used immediately. Cells were plated at 40,000-50,000 cells/well in 96-well V-bottom plates (Corning). Anti-EEEV mAbs or the irrelevant mAb negative control, rDENV-2D22,

were diluted to 1 µg/mL in FACS buffer and incubated with the cells for 1 hour at 4°C. Cells were washed with FACS buffer and then incubated with secondary Abs (anti-human IgG-PE (Southern Biotech) and anti-human IgA-PE (Southern Biotech) or anti-mouse IgG-PE (Southern Biotech)) diluted 1:1,000 in FACS buffer for 1 hour at 4°C. Cells were washed with FACS buffer and resuspended in 25 µL/well of FACS buffer. Number of events were collected on an IntelliCyt® iQue Screener PLUS flow cytometer (Sartorius). For analysis, mock transfected Expi293F cells were included as a negative control and subtracted as background. The percent binding of each mAb to the alanine mutants was compared to the WT EEEV structural protein control. An initial screen of residues D1-L267 was performed to identify residues with <25% binding and at least two mAbs with >70% binding to control for expression. These residues were further assessed for loss-of-binding phenotype for at least two additional biological replicates. Critical residues were defined as at least two mAbs with >70% binding to control for expression and <25% binding relative to WT protein.

Cryo-EM sample preparation and data acquisition

Purified SINV/EEEV particles and recombinant anti-EEEV Fab (EEEV-33 or EEEV-143) (1:10 molar ratio) were incubated on ice for 30 minutes. 3 µL of mixture was applied on Lacy 400 mesh copper grids (TED PELLA) or carbon coated R2/2 copper Quantifoil holey grids (Electron Microscopy Sciences). The samples were vitrified in liquid ethane using a Vitrobot (Thermo Fisher Scientific) set at 4°C and 100% relative

humidity under BSL-2 containment conditions. Images for SINV/EEEV:EEEV-33 Fab were collected on a Titan Krios electron microscope (Thermo Fisher Scientific) equipped with a K2 Summit Direct Electron Detector (Gatan) operated at 300 kV and having a nominal pixel size of 1.64 Å per pixel. Images for SINV/EEEV:EEEV-143 Fab were collected on a Glacios electron microscope (Thermo Fisher Scientific) equipped with a K2 Summit Direct Electron Detector operated at 200 kV and having a nominal pixel size of 2.0 Å per pixel. Micrographs were acquired automatically using Leginon software (Carragher et al., 2000). The total exposure time for both samples was 10 sec and frames were recorded every 0.2 sec. Defocus values ranged from 1.0 to 2.5 µm. The total accumulated does was ~50 $e^{-}/Å^2$ for SINV/EEEV:EEEV-33 Fab and ~25 $e^{-}/Å^2$ for and SINV/EEEV: EEEV-143 Fab samples.

Cryo-EM data processing

Cryo-EM movies (50 frames, 200 msec exposure per frame) were corrected for beam-induced motion and dose-weighted using MotionCor2 (Zheng et al., 2017) resulting in global motion-corrected frame stacks and summed micrographs. Contrast transfer function (CTF) parameters was estimated using Gctf (Zhang, 2016). EEEV particles manually picked from selected micrographs in RELION 3.0 (Zivanov et al., 2018) using a box size of 800 pixels (1.64 Å) or 700 pixels (2.0 Å). Approximately 18,000 particles were picked from 2,111 micrographs of SINV/EEEV:EEEV-33 Fab and 10,000 particles were picked from 2,501 micrographs of SINV/EEEV:EEEV-143 Fab.

The particles were subjected to reference-free 2D classification in RELION 3.0 and selected particles associated with good classes were exported to cisTEM (Grant et al., 2018). The *de-novo* initial model was generated without imposing any symmetry (C1 symmetry) which was subjected for 3D auto refinement (I1 symmetry) without mask in cisTEM. Further, the 3D model and associated particles obtained from cisTEM were exported to RELION 3.0 and used for the final masked 3D refinement (I1 symmetry) and postprocessing (**Figure 39A**). The resolution of the maps was evaluated using the ‘‘gold standard’’ Fourier shell correlation (FSC) at 0.143 criterion (Henderson et al., 2012; Scheres and Chen, 2012) (**Figure 39B**).

EEEV VLP negative stain grid preparation and imaging

For screening and imaging of negatively stained (NS) EEEV VLP (Ko et al., 2019) or EEEV VLP:EEEV-143 Fab samples, ~3 µL of the sample at concentrations of 10-15 µg/mL was applied to glow discharged grid with continuous carbon film on 400 square mesh copper EM grids (Electron Microscopy Sciences). The grids were stained with 0.75% uranyl formate (Ohi et al., 2004). Images were recorded on a 4k × 4k CCD camera using an FEI TF20 transmission electron microscope (Thermo Fisher Scientific) operated at 200 keV and control with SerialEM (Mastronarde, 2005). All images were taken at 50,000x magnification with a pixel size of 2.18 A/pix in low-dose mode at a defocus of 1.5 to 1.8 µm. Image processing was performed using the Scipion software package (de la Rosa-Trevin et al., 2016). Images were import and particles were CTF

estimated (Rohou and Grigorieff, 2015), then picked (Sorzano et al., 2013) . 2D class averages were performed using Xmipp3.0 cl2d (de la Rosa-Trevin et al., 2013; Sorzano et al., 2013) .

EEEV VLP cryo-EM sample preparation and data collection

For the EEEV VLP:EEEV-143 Fab complex, EEEV VLP at concentration of 0.2 mg/mL was mixed with EEEV-143 Fab in a molar ratio of 720:1 (Fab:VLP) and incubated on ice for 1 hour. Then, 2.2 µL of either EEEV VLP or EEEV VLP/EEEV-143 Fab was applied 2x to a 300 mesh Lacey grid that was glow discharged for 25 s at 25 milliamperes. The grid was blotted for 2 s before being plunged into liquid ethane using a FEI Vitrobot Mark4 (Thermo Fisher Scientific) at 8° C and 100% humidity. The grids were imaged in Titan Krios (Thermo Fisher Scientific) operated at 300 keV equipped with Falcon 3EC Direct Electron Detector (Thermo Fisher Scientific) using counting mode. Movies collected at a nominal magnification of 96,000x, pixel size of 0.8608 A/pix for the EEEV VLP and at 75,000x, pixel size of 1.11 A/pix for the EEEV VLP:EEEV-143 Fab complex. Both data set were in a defocus range of 0.8 to 2.8 µm. Grids were exposed at 1e−/Å^2/frame over 30 frames resulting in a total dose of ~30 e−/Å^2 (see also **Table 2**).

EEEV VLP cryo-EM data processing

Movies were pre-processed on-the fly (MotionCor2 (Zheng et al., 2017), Gctf (Zhang, 2016), using RELION (Scheres, 2012; Zivanov et al., 2018). Micrographs with low resolution, high astigmatism and defocus were removed from the data set. Further processing was done using RELION 3.1 beta. A small subset of micrographs were autopicked first by RELION LoG (Fernandez-Leiro and Scheres, 2017) and 2D class averages were determined. Representative classes were selected and used as templates for another round of autopicking. The particles were then subjected to multiple rounds of 2D class averages and 3D classification (with and without symmetry). The particles from the selected classes were re-extracted, 3D classified and subjected to 3D auto refinement. The data was processed further with Ctfrefine, polished and postprocessing was done (detailed statistics are provided in **Table 2 and Figure 39**).

EEEV VLP model building

For the EEEV VLP, a homology model of SINV/EEEV (PDB: 6MX4) was used for docking to the cryoEM map with PHENIX (Adams et al., 2010). To improve coordinate fitting, the model was subjected to iterative refinement of manual building in Coot (Emsley and Cowtan, 2004) and PHENIX real-space refine (Adams et al., 2010). The model was validated with Molprobity (Chen et al., 2010). For the EEEV VLP:EEEV-143 Fab complex, the refined model of the VLP was used as starting model and was docked

to the EM map with UCSF Chimera (Pettersen et al., 2004). The model was then refined in PHENIX (phenix real-space refine) by rigid body and a homology model of EEEV-143 Fab (PDB: 6MWX) was mutated to the EEEV-143 Fab sequence, docked, and rigid body refined to the EM map.

Mouse aerosol challenge with EEEV

Mice were inoculated with EEEV strain FL93-939 by aerosol, as previously described (Trobaugh et al., 2019). Briefly, mice were challenged with ~10 LD_{50} (~2,500 PFU) of 20% sucrose-purified WT EEEV FL93-nLuc TaV using the AeroMP exposure system (Biaera Technologies, Hagerstown, MD) inside a class III biological safety cabinet and either an Aeroneb nebulizer (Aerogen) or 3-jet Collison nebulizer (CH Technologies). All mice were monitored twice daily for morbidity and mortality.

In vivo imaging

At different times after challenge, mice were injected with 10 µg of Nano-Glo substrate (Promega) subcutaneously in 500 µL PBS, as previously described (Gardner et al., 2017). Four minutes after substrate injection, the mice were imaged using the IVIS Spectrum CT Instrument (PerkinElmer) using the autoexposure setting. The total

flux (photons per second) in the head region was calculated for each animal using Living Image Software 4.5.1, with all images set to the same scale.

Mouse s.c. challenge with EEEV

Mice were challenged with EEEV via bilateral s.c. injections. Animals were treated with Abs at doses of 10 mg/kg or 100 μg/kg via a single i.p. injection 24 hours post-virus challenge. Animals were monitored until 21 days post-virus inoculation (dpi) for disease signs and survival. Individual weights were recorded daily 0-10 dpi and on 14 and 18 dpi. Serum was collected from all mice 3 dpi for assessment of serum viremia.

EEEV infectious cell culture assay

Virus titer was quantified using an infectious cell culture assay where a specific volume of either tissue homogenate or serum was added to the first tube of a series of dilution tubes. Serial dilutions were made and added to Vero cells. Three days later cytopathic effect (CPE) was used to identify the endpoint of infection. Four replicates were used to calculate the 50% cell culture infectious doses ($CCID_{50}$) per mL of plasma or gram of tissues.

Quantification and Statistical Analysis

Statistical details can be found in the figure legends. EC_{50} values for binding and IC_{50} values for neutralization were determined after log transformation of concentration values and non-linear regression analysis using sigmoidal dose-response (variable slope). Direct comparison of differences in mAb binding to virion particle-specific epitopes versus sites in recombinant E2 glycoprotein cannot be performed on a molar basis. The precise total number of epitopes present on SINV/EEEV particles is unknown in an Ab-based capture ELISA format and may be greater than that on the recombinant EEEV E2 glycoprotein. To describe the differences in mAb binding, a virus/protein EC_{50} ratio was used. Survival curves were generated using the Kaplan-Meier method and curves compared the log-rank test with Bonferroni multiple comparison correction (n = number of mice, * = $p<0.05$, ** = $p<0.01$, ns = not statistically significant). A one-way ANOVA with Dunnett's multiple comparison correction was used to compare luminescence intensity of IVIS images (* = $p<0.01$). All statistical analyses were performed using Prism software version 8 (GraphPad).

Supplemental Information

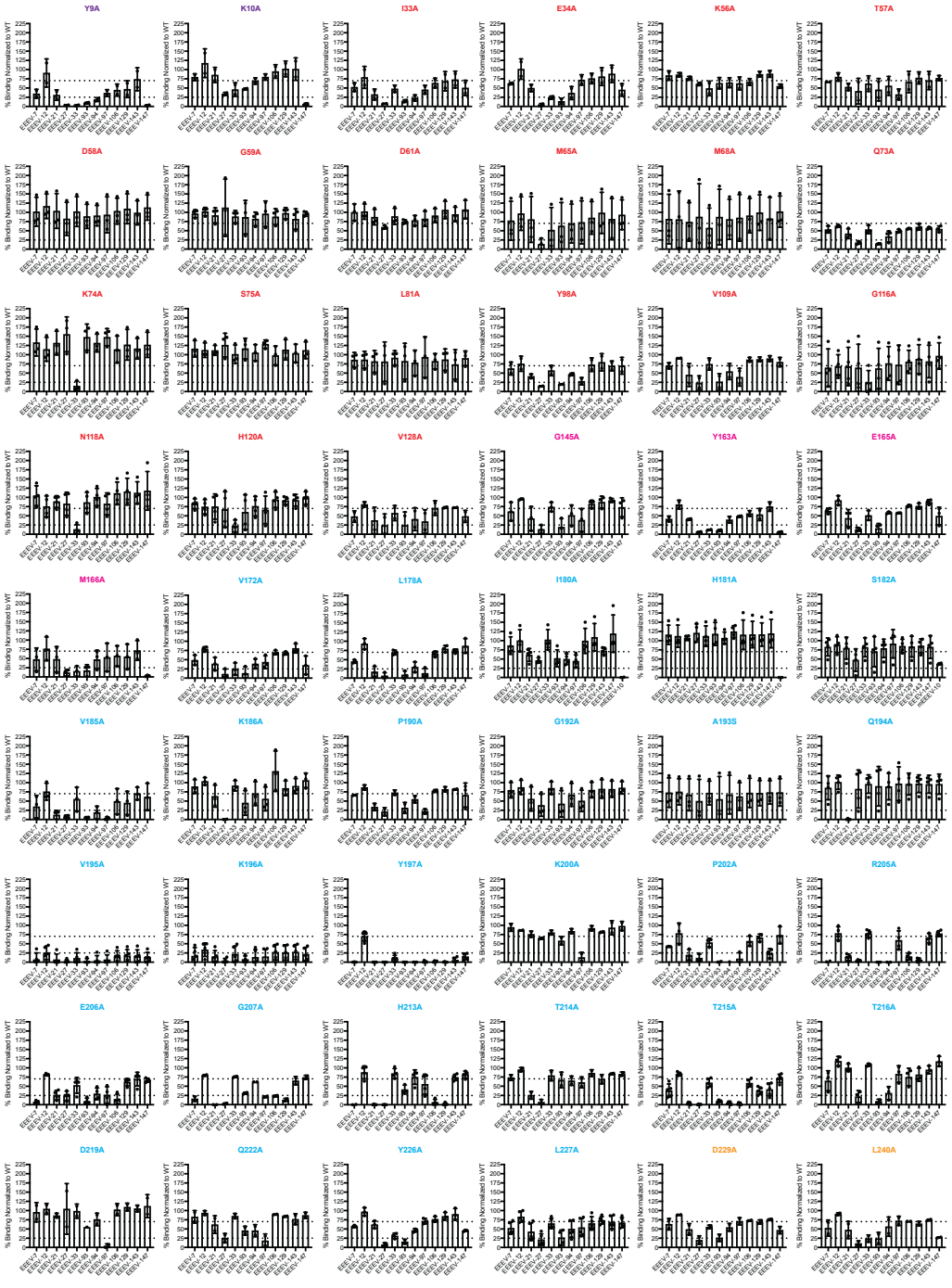

Figure 38. Alanine-scanning mutagenesis library analysis. Bar graphs of neutralizing human anti-EEEV mAb binding to critical residues (<25% mAb binding with at least two other mAbs >70% to control for expression) or critical residues previously characterized for murine anti-EEEV mAbs (Kim et al., 2019) and the VEE-specific human mAb, F5 (Hunt et al., 2010; Porta et al., 2014). Each mAb is listed on the x-axis and percent binding relative to wildtype is on the y-axis. Residues are colored based on E2 domain (N-link – purple, Domain A – red, Arch 1 – magenta, Domain B – cyan, and Arch 2 – orange). Data represent mean ± SD of at least two independent experiments. Williamson et al., 2020.

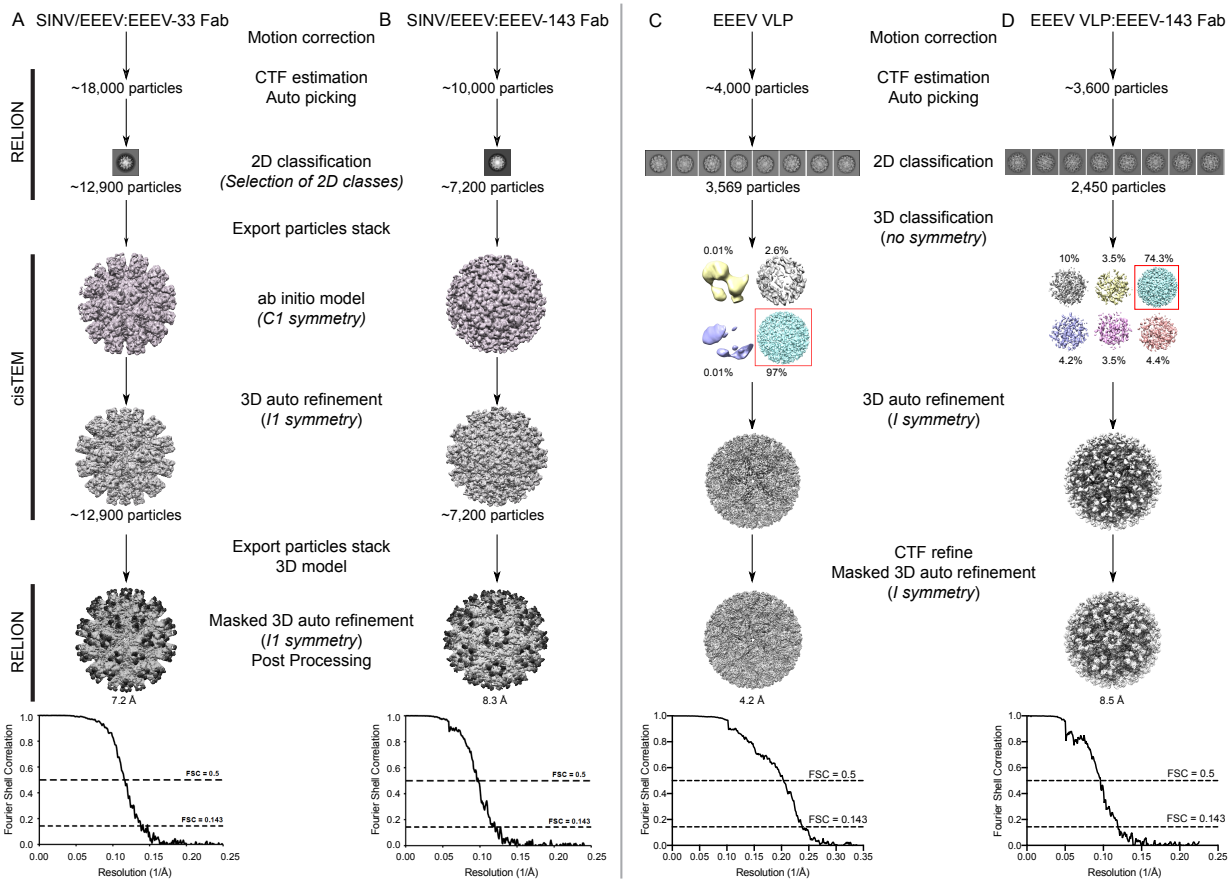

Figure 39. Cryo-EM processing of SINV/EEEV complexes with either EEEV-33 or EEEV-143 Fabs. Flow chart of cryo-EM processing steps and Fourier shell correlation (FSCs) of the maps of SINV/EEEV:rEEEV-33 Fab complex (**A**), SINV/EEEV:rEEEV-143 Fab complex (**B**), EEEV VLP (**C**), and EEEV VLP:rEEEV-143 Fab complex (**D**). The FSCs of the refined models agree with each other, suggesting that the models are not over-refined. Williamson et al., 2020.

	Parameters	SINV/EEEV:rEEEV-33 Fab	SINV/EEEV:rEEEV-143 Fab	EEEV VLP	EEEV VLP:rEEEV-143 Fab
Data Deposition	EMDB	22223	22188	22276	22277
	PDB			6XO4	6XOB
Microscope setting	Microscope	Titan-Krios	Glacios	Titan Krios	Titan Krios
	Acceleration voltage (kV)	300	200	300	300
	Detector			Falcon 3EC	Falcon 3EC
	Magnification (x)	18,000	22,000	96,000	75,000
	Pixel size (Å)	1.64	2	0.8608	1.11
	Dose Exposure (e^- /Å2)	50	25	30	30
	Defocus range (μm)	1.0 – 2.5	1.0 – 2.5	0.8-2	1-2.5
Data	# Micrographs			1,745	~4,800
	# particles	~18,000	~10,000	3,935	3,600
	# particle after 2D	~12,900	~7,200	3,569	2,471
	Final particles #	~12,900	~7,200	3,469	1,300
	Symmetry	icosahedral	icosahedral	icosahedral	icosahedral
	Resolution FSC=0.143 (Å)	7.2	8.3	4.2	8.5
Model refinement and validation	Protein residues	-	-	3,992	5,700
	Map CC	-	-	0.79	0.69
	RMSD	-	-		
	Bond lengths (Å)	-	-	0.006	0.004
	Bond angles	-	-	0.671	0.816
	Ramachandran	-	-		
	Outliers (%)	-	-	0	0
	Allowed (%)	-	-	10.93	21.64
	Favored (%)	-	-	89.07	78.36
	Poor rotamers (%)	-	-	5.41	21.99
	MolProbity score	-	-	2.9	3.98
	Clash score	-	-	18.8	53.27
	CaBLAM score	-	-	6.42	7.28

Table 2. Parameters used for high-resolution data collection of SINV/EEEV:rEEEV-33 Fab, SINV/EEEV:rEEEV-143 Fab, EEEV VLP, and EEEV VLP:rEEEV-143 Fab. Williamson et al., 2020.

CHAPTER IV

PROTECTIVE E1-SPECIFIC HUMAN ALPHAVIRUS ANTIBODIES RECOGNIZE CRYPTIC VIRAL EPITOPES

The information contained in this chapter is adapted from the following reference:

Williamson LE, Reeder KM, Bailey K, Roy V, Fouch ME, Kose N, Trivette A, Nargi RS, Winkler ES, Kim AS, Gainza C, Rodriguez J, Armstrong E, Sutton RE, Reidy J, Carnahan R, Klimstra WB, Diamond MS, Davidson E, Doranz BJ, Alter G, Julander JG, Crowe JE Jr. Protective E1-specific human alphavirus antibodies recognize cryptic viral epitopes. *Cell*. 2020. **In review.**

Introduction

During the alphavirus entry, fusion, and egress processes, large rearrangements and presentation of different conformational states of the surface proteins occur (Fuller et al., 1995; Li et al., 2010; Mukhopadhyay et al., 2006; Sahoo et al., 2020; Voss et al., 2010), likely exposing cryptic epitopes on the virion surface (Fong et al., 2014; Gibbons et al., 2004; Schmaljohn et al., 1983). Murine WEEV and SINV, and human CHIKV E1-specific mAbs previously identified some of these cryptic and/or transitional epitopes at various stages of virus maturation. Treatment with detergent, elevated temperature,

acidic pH, reducing agents, or fixation strategies could induce exposure for some of these epitopes (Fong et al., 2014; Gibbons et al., 2004; Hunt and Roehrig, 1985; Meyer et al., 1992; Schmaljohn et al., 1983). In addition, murine SINV anti-E1 mAbs recognized cryptic epitopes on the surface of infected cells, suggesting a difference in E1 presentation (Meyer et al., 1992; Schmaljohn et al., 1983). Neutralizing and non-neutralizing epitopes have been identified for murine anti-E1 mAbs that protect against CHIKV, WEEV, SINV, or SFV infection (Boere et al., 1984; Hunt and Roehrig, 1985; Mendoza et al., 1988; Pal et al., 2013; Schmaljohn et al., 1983). However, moderately neutralizing and non-neutralizing cross-reactive human anti-E1 mAbs did not protect against infection (Fong et al., 2014; Quiroz et al., 2019).

Several murine and human E2-specific mAbs have been identified with cross-neutralizing activity against the arthritogenic alphaviruses. These include murine anti-MAYV mAbs, which exhibited cross-reactivity and cross-neutralization for different arthritogenic alphaviruses (*i.e*., MAYV, RRV, ONNV, CHIKV, or UNAV) (Earnest et al., 2019). RRV-12, a human mAb, blocked Mxra8 receptor attachment by recognizing a conserved region of E2 domain B and cross-neutralized infection of multiple arthritogenic alphaviruses (*i.e*., RRV, GETV, SAGV, MAYV, ONNV, and CHIKV) (Powell et al., 2020). CHK-265, a murine anti-CHIKV mAb, cross-neutralized (*i.e*., CHIKV, RRV, MAYV, SFV, and ONYV) and cross-protected (*i.e*., CHIKV, ONNV, and MAYV) against multiple arthritogenic alphaviruses by blocking viral entry and egress through recognition of a conserved region of E2 domain B, with additional contacts in E2 domain A of a neighboring spike (Fox et al., 2015).

For the encephalitic alphaviruses, a cross-protective murine mAb was identified that reacts to EEEV and VEEV. However, cross-neutralization was not observed for this mAb (Pereboev et al., 1996). In addition, analysis of serum samples from immune individuals in South America, displayed a low frequency of cross-reactivity to the encephalitic alphaviruses (Smith et al., 2018). A cross-neutralizing mAb against the encephalitic alphaviruses contrary to the arthritogenic alphaviruses has yet to be identified.

Human cross-reactive, cross-neutralizing, and cross-protective E1-specific mAbs that react with both the arthritogenic (CHIKV and MAYV) and encephalitic (EEEV, VEEV, and WEEV) alphaviruses have yet to be defined. Additionally, identification of human anti-EEEV E1-specific mAbs have not been described. In this chapter, I outline the molecular basis for human Ab interaction with the alphavirus E1 glycoprotein through isolation and characterization of naturally occurring human E1-specific mAbs from survivors of natural EEEV infection. From this collection of isolated human EEEV mAbs, I identified human mAbs specific to the E1 glycoprotein of EEEV, the encephalitic alphaviruses (EEEV and VEEV), and broadly-reactive (EEEV, VEEV, and WEEV) mAbs that also recognize an arthritogenic alphavirus (CHIKV). Through epitope mapping, I determined the distinct antigenic determinants and epitopes recognized by human EEEV-specific and cross-reactive mAbs on the EEEV E1 glycoprotein, some of which became exposed under acidic-pH conditions for mAb recognition. In addition, I found that mAb binding to EEEV-infected cells facilitated Ab-mediated inhibition of virus egress from infected cells. The studies described here can aid in rational pan-alphavirus

vaccine design and identification of combinatorial therapies for EEEV-specific or pan-alphavirus Ab cocktails.

I would like to acknowledge studies done in collaboration to further characterize human anti-EEEV mAbs. I would like to acknowledge Dr. Galit Alter's laboratory (including Vicky Roy) for performing functional assays to probe for Fc-mediated effector functions. I would like to acknowledge Dr. Edgar Davidson and Benjamin Doranz at Intergral Molecule (including Mallorie Fouch) for identifying loss-of-binding phenotype residues for cross-reactive anti-EEEV mAbs with a CHIKV alanine scanning mutagenesis library. I would also like to acknowledge Dr. Justin G. Julander's laboratory (including Kevin Bailey), for performing therapeutic mAb administration studies against WT EEEV s.c. challenge and analysis of infectious virus from tissues. I would like to acknowledge Dr. Michael S. Diamond's laboratory (including Emma S. Winkler and Dr. Arthur S. Kim) for assessing the protective efficacy of EEEV-346 in a CHIKV joint swelling disease mouse model. I would like to acknowledge Dr. William B. Klimstra for providing SINV/VEEV and SINV/WEEV cDNA constructs that enabled production of SINV/VEEV and SINV/WEEV. Lastly, I would like to thank members of the iCore and TechCore teams in Dr. Crowe's laboratory for assistance with mAb expression and purification, and mAb or antigen sequencing, respectively.

Isolation of human E1-specific mAbs against EEEV

From the panel of human anti-EEEV mAbs isolated from B cells in peripheral blood samples from donors who had been naturally infected with EEEV as described in chapter III, I identified mAbs with binding reactivity to the E1 protein. Twenty-two human mAbs isolated were identified and selected based on reactivity in ELISA to EEEV E1 glycoprotein, EEEV p62E1 glycoprotein, EEEV virus-like particles (VLPs), or Sindbis/EEEV (SINV/EEEV) virions (Kim et al., 2019).

Binding characterization of human E1-specific mAbs

To characterize the panel of E1 mAbs, I assessed binding to EEEV, VEEV, or WEEV VLPs, recombinant E1 glycoproteins (EEEV, CHIKV, or MAYV), and recombinant EEEV E2 glycoprotein in ELISA. The nonionic detergent Tween®20 was included in buffers during the incubation and wash steps to enhance exposure of epitopes that might otherwise be occluded in the native virus structure. Increased exposure of epitopes for E1-specific mAbs can be induced by several treatment conditions, such as elevated temperature, acidic pH, addition of reducing agents or detergent (Gibbons et al., 2004; Meyer et al., 1992; Schmaljohn et al., 1983; Wengler et al., 1999).

Using different ELISA formats with purified proteins or intact virions, I defined antigen binding groups within the panel of mAbs. Two classes of E1-reactive mAbs emerged, defined by mAb antigen specificity of either EEEV-specific (anti-EEEV) or cross-reactive (anti-alphavirus – EEEV, VEEV, WEEV, and/or CHIKV) mAbs (**Figure**

40). In one class of mAb, human anti-EEEV mAbs bound avidly (exhibiting <100 ng/mL half-maximal effective binding concentration [EC_{50}] values) to EEEV VLPs or recombinant EEEV E1 glycoprotein (**Figure 40B**), but these mAbs did not bind to VEEV or WEEV VLPs, recombinant CHIKV or MAYV E1 glycoproteins, or recombinant EEEV E2 glycoprotein in ELISA (**Figure 40C**).

A second class of mAbs, involving the human anti-alphavirus mAbs, exhibited cross-reactivity with some variation in the number of alphaviruses bound. The broadest cross-reactive subgroup of mAbs (designated here as 'pan-alphavirus'), comprised mAbs EEEV-138, -342, -346, -368, and -387, which recognized EEEV, VEEV, WEEV VLPs and recombinant EEEV, CHIKV, and MAYV E1 glycoproteins (**Figure 40G**). Another cross-reactive subgroup of mAbs (designated here as 'broadly-reactive'), comprised mAbs EEEV-307 and -354, recognized EEEV and VEEV VLPs and recombinant EEEV, CHIKV, and MAYV E1 glycoproteins (**Figure 40F**), but did not bind WEEV VLPs under the conditions tested. A third subgroup (designated here as 'New World' reactive) formed by the single mAb, EEEV-179, recognized EEEV, VEEV, WEEV VLPs and recombinant EEEV E1 glycoprotein (**Figure 40E**), but not CHIKV or MAYV E1 glycoproteins under the conditions tested. Lastly, the mAb EEEV-157 exhibited a 'EEEV-VEEV' pattern, recognizing EEEV and VEEV VLPs and recombinant EEEV E1 glycoprotein (**Figure 40D**), but not WEEV VLPs or recombinant CHIKV or MAYV E1 glycoproteins. None of the human E1 mAbs isolated bound to the EEEV E2 glycoprotein. The human anti-alphavirus mAbs also bound avidly (possessing EC_{50} values <100 ng/mL) to their respective antigens (**Table 3**; 'pan-alphavirus' = EEEV,

VEEV, WEEV, and CHIKV; ‘broadly-reactive’ = EEEV, VEEV, and CHIKV; ‘New World’ = EEEV, VEEV, and WEEV; ‘EEEV-VEEV’ = EEEV and VEEV). EEEV-157, however, bound weakly to VEEV VLPs with an EC_{50} value <2 µg/mL (**Table 3**).

For several mAbs, differences in binding strength to VLPs and recombinant EEEV E1 glycoprotein was observed. I calculated the ratio of VLP/protein EC_{50} values for binding (**Figure 40B**) to define groups of mAbs that preferentially bind to epitopes on virion particles, compared to exposed epitopes that are more accessible on recombinant E1 glycoprotein. As the E1 glycoprotein on the virion surface is obscured by the overlying the E2 glycoprotein (Voss et al., 2010), I expected most mAbs to recognize the recombinant E1 glycoprotein better than E1 displayed on the virion. Indeed, four mAbs (EEEV-98, -109, -312, and -379) bound to recombinant EEEV E1 glycoprotein more avidly than to EEEV VLPs, with a VLP/protein EC_{50} ratio >5 (**Figure 40B**). However, other mAbs (EEEV-126, -127, -320, -369, -377, -400) recognized the recombinant E1 glycoprotein and the VLPs equivalently, with a VLP/protein EC_{50} ratio ~1 (**Figure 40B**). Moreover, the human anti-alphavirus (‘EEEV-VEEV’, ‘New World’, ‘broadly-reactive’, and ‘pan-alphavirus) mAbs recognized VLPs more strongly than recombinant E1 glycoproteins, with VLP/protein EC_{50} ratios <1 (**Figure 40B**). The presence of Tween®20 detergent in the binding and wash buffers likely exposed cryptic epitopes of E1 on VLPs.

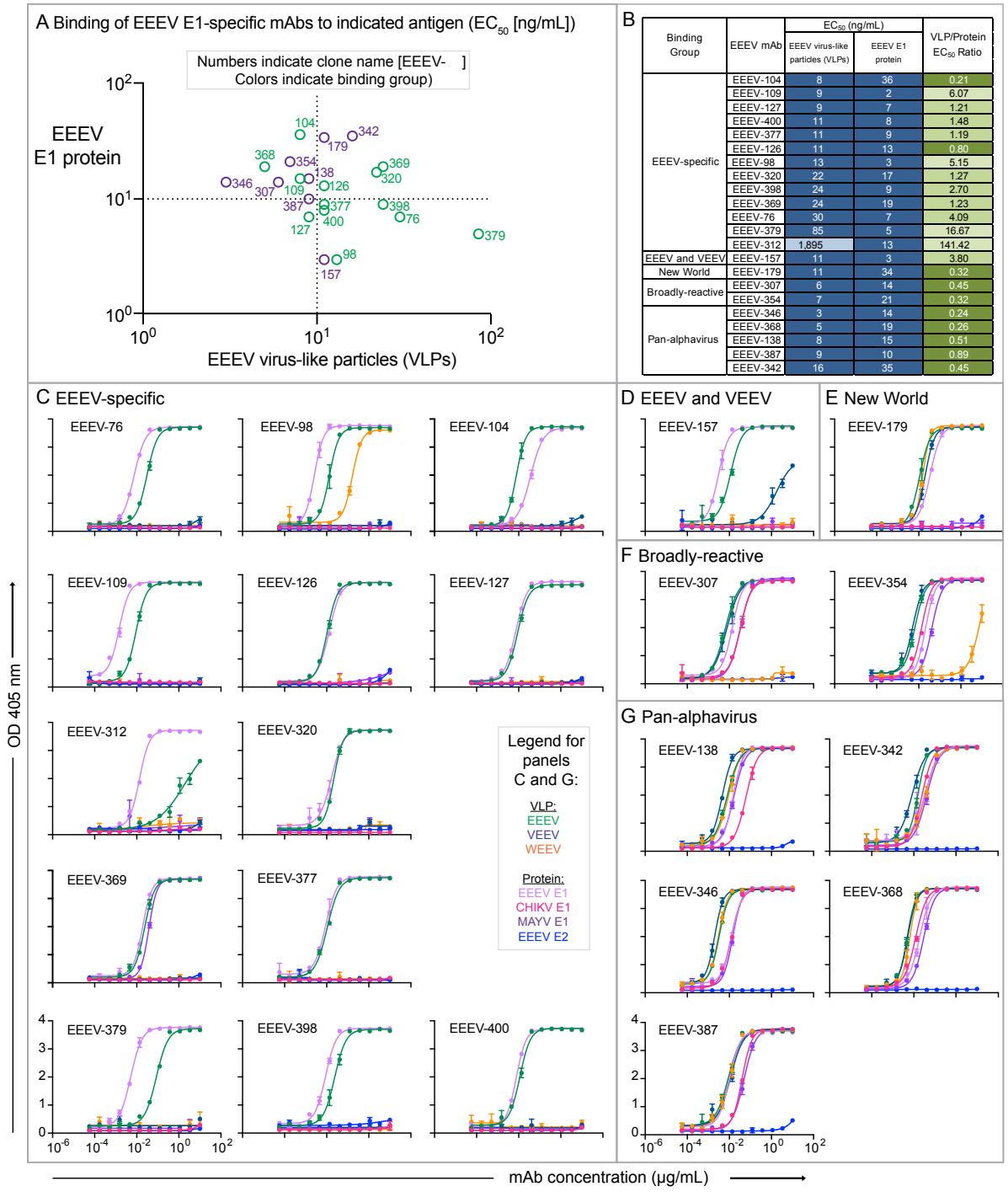

Binding Group	EEEV mAb	EC50 (ng/mL) EEEV virus-like particles (VLPs)	EC50 (ng/mL) EEEV E1 protein	VLP/Protein EC50 Ratio
EEEV-specific	EEEV-104	8	36	0.21
	EEEV-109	9	2	6.07
	EEEV-127	9	7	1.21
	EEEV-400	11	8	1.48
	EEEV-377	11	9	1.19
	EEEV-126	11	13	0.80
	EEEV-98	13	3	5.15
	EEEV-320	22	17	1.27
	EEEV-398	24	9	2.70
	EEEV-369	24	19	1.23
	EEEV-76	30	7	4.09
	EEEV-379	85	5	16.67
	EEEV-312	1,895	13	141.42
EEEV and VEEV	EEEV-157	11	3	3.80
New World	EEEV-179	11	34	0.32
Broadly-reactive	EEEV-307	6	14	0.45
	EEEV-354	7	21	0.32
Pan-alphavirus	EEEV-346	3	14	0.24
	EEEV-368	5	19	0.26
	EEEV-138	8	15	0.51
	EEEV-387	9	10	0.89
	EEEV-342	16	35	0.45

Figure 40. Binding of human anti-EEEV and anti-alphavirus E1-specific mAbs to virus-like particles (VLPs) or recombinant E1 glycoproteins. A. EC_{50} (ng/mL) binding ratio of human anti-EEEV (green) and anti-alphavirus (purple) E1-specific mAbs to EEEV VLPs (x-axis) versus recombinant EEEV E1 glycoprotein (y-axis). Distinct binding patterns were revealed for the human E1-specific mAbs to EEEV VLPs and EEEV E1 glycoprotein. The dotted line indicates 10 ng/mL EC_{50} values for binding, and circles are labeled with antibody clone name [EEEV-]. **B.** EC_{50} values (ng/mL) for binding of human anti-EEEV

E1-specific mAbs to EEEV VLPs or recombinant EEEV E1 glycoprotein in the presence of the nonionic detergent Tween®20. The human anti-EEEV and anti-alphavirus mAbs are listed in order of increasing EC_{50} value for binding to EEEV VLPs. The human anti-alphavirus mAbs also are grouped according to binding cross-reactivity ('EEEV and VEEV', 'New World', 'broadly-reactive, or 'pan-alphavirus'). EC_{50} value in ng/mL is indicated by the blue fill color (≤100.00 [dark blue], 100.01-500.00 [light blue], 500.01-4,999 [lightest blue]). Ratio of binding to EEEV VLPs compared to EEEV E1 glycoprotein is indicated as the ratio of EC_{50} values. Increasing depth of green color indicates lower ratios and suggests greater dependence on virion-specific epitopes. **C** to **G.** Representative binding curves for human anti-EEEV and anti-alphavirus E1-specific mAbs binding to VLPs for EEEV (green), VEEV (dark blue), or WEEV (orange) VLPs, or recombinant E1 glycoprotein for EEEV (light purple), CHIKV (magenta), or MAYV (purple), or recombinant EEEV E2 glycoprotein (blue) in the presence of Tween®20 on the x-axis and optical density at 405 nm on the y-axis. Binding curves are ordered numerically and grouped according to binding pattern (EEEV-specific [**C**], 'EEEV and VEEV'-reactive [**D**], 'New World' alphavirus-reactive [**E**], 'broadly-reactive' [**F**], or 'pan-alphavirus'-reactive [**G**]). Data in **A** to **G** represent mean ± SD of technical triplicates and are representative of two independent experiments.

Binding Group	EEEV mAb	EC_{50} (ng/mL; [Tween®20])						
		Virus-like particles (VLPs)			Protein			
		EEEV	VEEV	WEEV	EEEV E1	CHIKV E1	MAYV E1	EEEV E3E2/E2
EEEV-specific	EEEV-76	30	>	>	7	>	>	>
	EEEV-98	13	>	166	3	>	>	>
	EEEV-104	8	>	>	36	>	>	>
	EEEV-109	9	>	>	2	>	>	>
	EEEV-126	11	>	>	13	>	>	>
	EEEV-127	9	>	>	7	>	>	>
	EEEV-312	1,895	>	>	13	>	>	>
	EEEV-320	22	>	>	17	>	>	>
	EEEV-369	24	>	>	19	>	38	>
	EEEV-377	11	>	>	9	>	>	>
	EEEV-379	85	>	>	5	>	>	>
	EEEV-398	24	>	>	9	>	>	>
	EEEV-400	11	>	>	8	>	>	>
EEEV and VEEV	EEEV-157	11	1,731	>	3	>	>	>
New World	EEEV-179	11	20	16	34	>	>	>
Broadly-reactive	EEEV-307	6	8	>	14	33	33	>
	EEEV-354	7	5	>	21	14	41	>
Pan-alphavirus	EEEV-138	8	5	9	15	61	16	>
	EEEV-342	16	8	35	35	24	40	>
	EEEV-346	3.2	2	3	13.6	12	14.4	>
	EEEV-368	4.8	5.1	6.4	18.7	12.2	29.1	>
	EEEV-387	8.9	11.4	10	10	39.9	49.9	>

Table 3. Human E1-specific mAb VLP and recombinant protein binding in presence of the nonionic detergent Tween®20. EC_{50} value in ng/mL is indicated by the blue fill color (≤10.00 [dark blue], 10.01-100.00 [light blue], 100.01-4,999 [lightest blue]) for binding to respective antigen. > symbol indicates > 5 µg/mL EC_{50} value.

Anti-EEEV E1-specific mAbs recognize EEEV and MADV subtypes

To define binding breadth of the human anti-EEEV E1-specific mAbs, I assessed the binding to EEEV (formally known as the North American lineage of EEEV) and MADV (formally known as the South American lineage of EEEV) subtypes (≥89% amino acid identity in the E1 protein (**Figure 41**)) using an antigen display method in which we transfected Expi293F cells with a plasmid encoding the structural proteins (capsid-E3-E2-6K-E1) and assessed mAb binding to the cell surface (**Figure 42**). Binding to EEEV and MADV subtypes was observed for the anti-EEEV mAbs, EEEV-104, -109, -126, -127, and -312, as defined by a >two-fold change in mAb binding compared to the dengue virus (DENV)-specific negative control mAb, rDENV-2D22. EEEV-126 displayed reactivity to Pixuna virus (VEEV, subtype IV, strain BeAr 35645). Multiple sequence alignment of the E1 glycoprotein of different alphavirus subtypes (**Figure 41**) highlighted the residue Q79, which was a uniquely conserved residue among the EEEV, MADV, and Pixuna virus subtypes tested here. Thus, based on binding reactivity, EEEV-126 may recognize this residue, which lies proximal to the fusion loop on the E1 glycoprotein. However, several mAbs displayed little (<two-fold change) or no binding to the E1 protein of the EEEV or MADV subtypes on the cell surface, indicating that the epitope for these mAbs may not be exposed or displayed properly at the cell surface, or that the mAb did not recognize E1 of the particular EEEV or MADV strain tested.

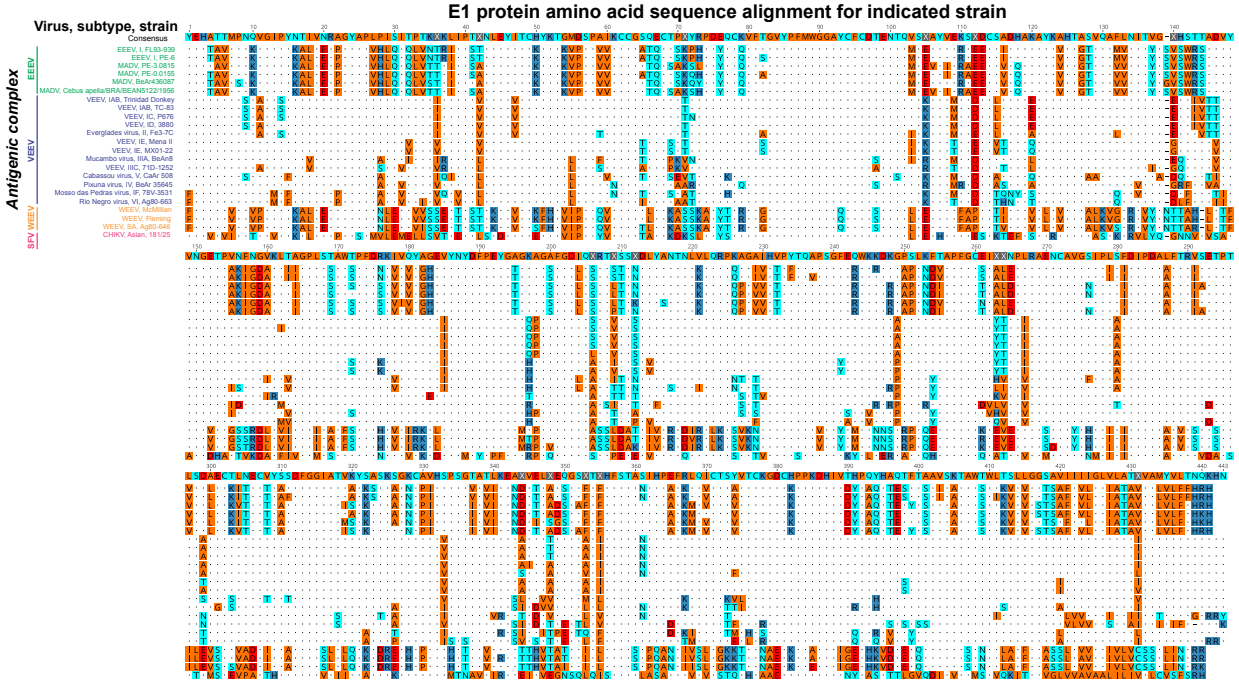

Figure 41. Sequence alignment of E1 protein for diverse alphavirus subtypes. Multiple amino acid sequence alignment of the E1 protein for alphavirus subtypes (virus, subtype, and strain) labeled in the left-hand column (made with Geneious software). Alphavirus subtypes are grouped by antigenic complex for EEEV (green), VEEV (blue), WEEV (orange), or Semliki Forest virus (magenta). Dots represent conserved amino acids. Amino acids that are not conserved are colored based on polarity (cyan [polar, uncharged], orange [non-polar], red [polar, acidic], or dark blue [polar, basic]). The consensus sequence is shown at the top of the sequence alignment.

Anti-alphavirus E1-specific mAbs exhibit broad binding breadth to alphavirus subtypes

Among the alphavirus structural proteins, the E1 protein has the greatest (≥44%) amino acid identity between encephalitic (EEEV, VEEV, WEEV) and arthritogenic (*e.g.*, CHIKV) alphaviruses (**Figure 41**). To further define the binding breadth of the human anti-alphavirus E1-specific mAbs, I tested binding to the structural proteins (capsid-E3-

E2-6K-E1) of different alphavirus subtypes using cell-surface antigen display (**Figure 42**). I observed several groups of binding breadth that were similar to the binding profiles identified by ELISA. The 'pan-alphavirus' mAbs (EEEV-138, -342, -346, -368, and -387) recognized EEEV, VEEV, WEEV, and CHIKV subtypes. The 'broadly-reactive' mAbs (EEEV-307 and -354) recognized EEEV, VEEV, and CHIKV but not WEEV subtypes. The 'New-World' mAb EEEV-179 also recognized EEEV, VEEV, WEEV, and CHIKV subtypes, which contrasted with the ELISA results showing no appreciable binding reactivity to recombinant CHIKV E1 or MAYV E1 glycoproteins. The increase in binding breadth of EEEV-179 to CHIKV in the cell-surface antigen display assay suggests either a difference in the conformational state of the epitope between intact virions and the surface of infected cells or a dependence on a quaternary epitope. Lastly, the 'EEEV-VEEV' mAb EEEV-157 recognized only the EEEV and VEEV subtypes.

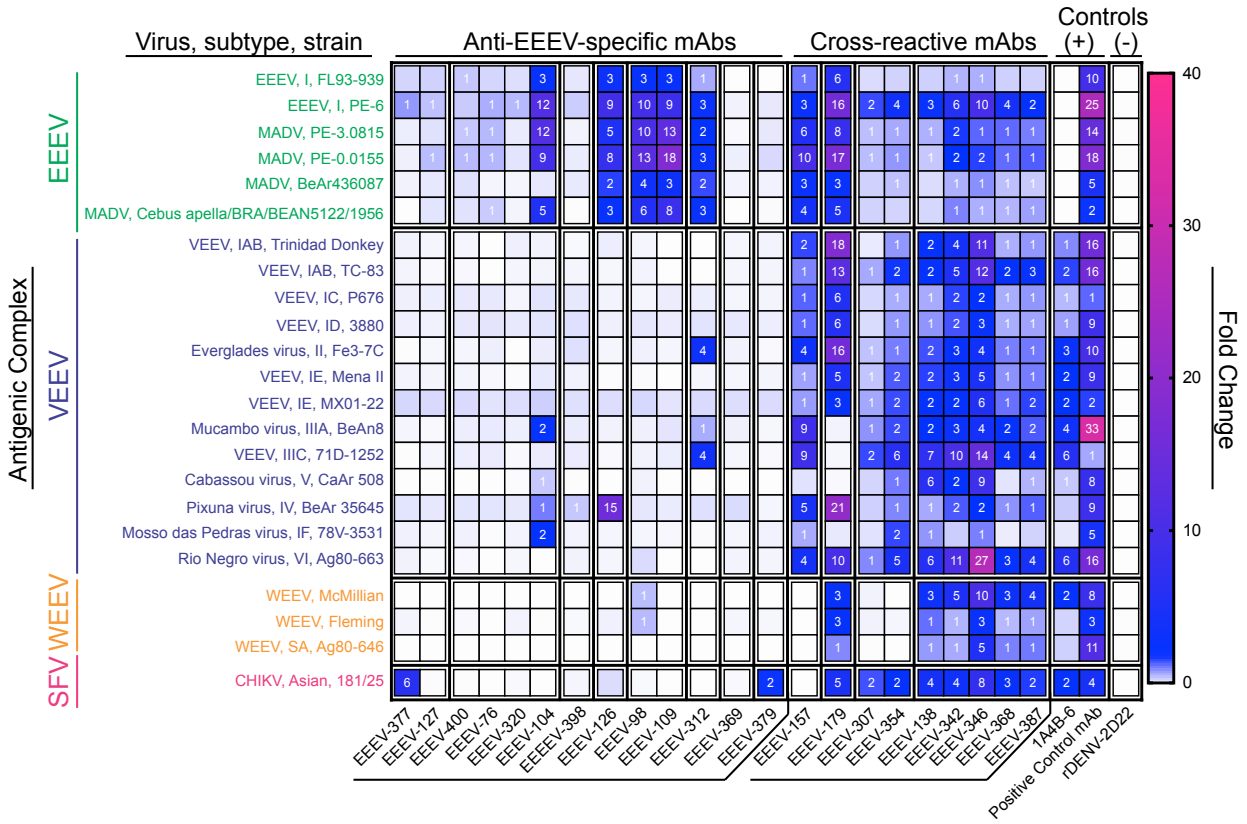

Figure 42. Breadth of binding of human E1-specific mAbs to antigens from diverse alphavirus subtypes. Heatmap of fold-change for human E1-specific mAb binding to antigens from particular alphavirus subtypes (virus, subtype, and strain) grouped by antigenic complex for either EEEV (green), VEEV (blue), WEEV (orange), or Semliki Forest virus (magenta). The relative fold-change for mAb binding to each subtype was calculated after subtraction of background median fluorescence to Expi293F cells and was normalized relative to the negative control mAb rDENV-2D22. The alphavirus group E1-reactive mouse mAb,1A4B-6 (Roehrig et al., 1990) served as a positive control. The following additional positive control mAbs were used: rEEEV-97 IgG (human mAb; EEEV E2-specific; Williamson et al., 2020), 1A3B-7 (mouse mAb; VEEV E2-specific; Rico-Hesse et al., 1988, Roehrig and Mathews, 1985, Roehrig and Bolin, 1997, Goodchild et al., 2011), 2A3D-5 (mouse mAb; WEEV E1-specific; Hunt and Roehrig, 1985), and mouse anti-CHIKV ascites fluid (CHIKV; ATCC). The mAbs are shown in order based on antigen-specificity (EEEV-specific or cross-reactive) and competition-binding group, as defined in **Figure 43**. Human anti-EEEV mAbs primarily recognized the EEEV antigenic complex. Human anti-alphavirus mAbs ('cross-reactive mAbs') recognized the EEEV, VEEV, WEEV, and/or CHIKV antigenic complexes. Data represents mean ± SD of technical triplicates and are representative values of two independent biological replicates.

Identification of antigenic determinants on the EEEV E1 glycoprotein

To begin to identify the number of major antigenic sites recognized by human E1-specific mAbs, I performed competition-binding studies with EEEV VLPs by ELISA. For the E1-specifc mAbs that recognized recombinant EEEV E1 glycoprotein via ELISA, I observed up to seven competition-binding groups (**Figure 43**). Some of these groups overlap with each other, suggesting proximity of the epitopes on the E1 glycoprotein. The ‘pan-alphavirus’ and ‘broadly-reactive’ mAbs grouped together, which suggests recognition of a common antigenic determinant for these mAbs. The ‘New World’ or ‘EEEV-VEEV’ mAbs, EEEV-179 or EEEV-157, respectively, did not compete with the ’pan-alphavirus’ or ‘broadly-reactive’ mAbs or with each other, indicating that these mAbs recognize distinct conserved determinants on the E1 glycoprotein. Thus, up to three antigenic determinants may be present on the E1 glycoprotein for recognition by cross-reactive mAbs. The human anti-EEEV E1-specific mAbs bound to different competition-binding groups, some of which competed with certain cross-reactive mAbs.

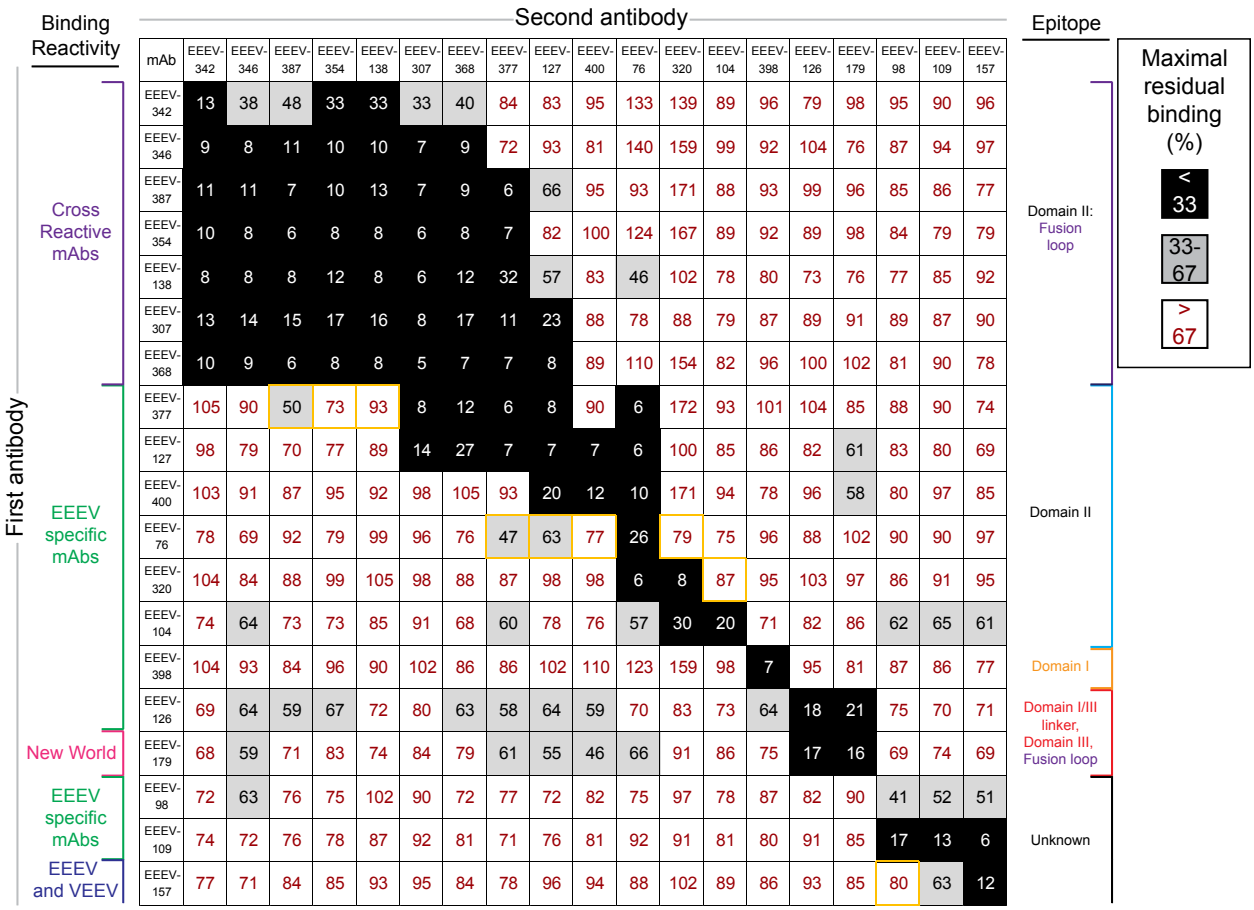

Figure 43. Human anti-EEEV E1-specific mAb recognize at least seven antigenic determinants on EEEV VLPs. Competition-binding groups of human anti-EEEV and anti-alphavirus E1- specific mAbs as determined through competition-binding ELISA using EEEV VLPs. Results for a total of 19 human anti-EEEV mAbs are shown. EEEV-312, -369, -379 are not shown due to minimal binding to EEEV VLP under the conditions tested. The first mAb (10 µg/mL) incubated with EEEV VLPs is shown in the left-hand column and the second mAb (biotinylated; 0.5 µg/mL) is shown in the top row. Black boxes indicate competition (reduction in maximal binding to <33%), grey boxes indicate intermediate competition (33 to 67% maximal residual binding), and white boxes indicate no competition (>67% maximal residual binding). The competition groups correspond with the binding reactivity and epitopes identified for each mAb. Data represent values of three independent experiments performed with technical duplicates.

Pan-alphavirus and broadly-reactive E1-specific mAbs recognize the highly conserved fusion loop

The fusion loop is highly conserved (≥83% amino acid identity) among alphaviruses. I hypothesized that the 'pan-alphavirus' and 'broadly-reactive' mAbs might recognize epitopes within the fusion loop. To assess this hypothesis, in collaboration with Integral Molecular, we examined loss-of-binding phenotype(s) to CHIKV E1 fusion loop single-residue alanine substitution mutants that were identified previously (W89A, F95A, and N100A; **Figure 44**) in the context of mAb mapping experiments (Fong et al., 2014). For the 'pan-alphavirus' and 'broadly-reactive' mAbs, these variant residues caused a loss-of-binding phenotype, supporting the hypothesis that these mAbs recognize a shared antigenic determinant within the highly conserved fusion loop. To test for additional critical interaction residues, Twist Bioscience Inc. generated an alanine-scanning mutagenesis library of residues within the EEEV E1 glycoprotein and I transfected Expi293F cells with cDNAs encoding the structural proteins (capsid-E3-E2-6K-E1), each containing a separate individual mutant (**Figures 45B, 45C, 46, and 55; Table 4**). The 'pan-alphavirus' and 'broadly-reactive' mAbs showed markedly reduced binding when mutations were introduced into residues within or at the base of the fusion loop (residues W89A, G91A, Y93A, F95A, and N100A [cd loop]). The residues identified were relatively consistent between the two library analyses (EEEV and CHIKV). One key difference for EEEV-307, -354, -368, and -387 was the lack of a loss-of-binding phenotype observed at F95A in the EEEV library. For the CHIKV alanine mutant library, more stringent conditions, such as binding of Fab molecules instead of bivalent IgG, were tested and showed the loss-of binding-phenotype at F95A (**Figure 44**).

A

mAb	% WT binding (mean (SD)) for CHIKV E2/E1 protein			
	WT	W89A	F95A	N100A
EEEV-342	100 (11.1)	9.1 (3.8)	6.9 (2.7)	4.1 (1.7)
EEEV-138	100 (6.5)	52.1 (21.9)	3.1 (1.3)	3.2 (1.9)
EEEV-346	100 (20.8)	12.2 (2.0)	6.6 (1.2)	9.1 (4.9)
EEEV-307	100 (9.9)	5.2 (2.1)	11.5 (4.0)	86.5 (9.6)
EEEV-354	100 (22.1)	21.5 (13.8)	20.1 (14.0)	57.8 (12.6)
EEEV-368	100 (13.1)	58.5 (27.1)	19.2 (9.6)	111.6 (17.9)
EEEV-387	100 (27.1)	64.2 (9.1)	21.1 (7.7)	124.2 (20.2)

B

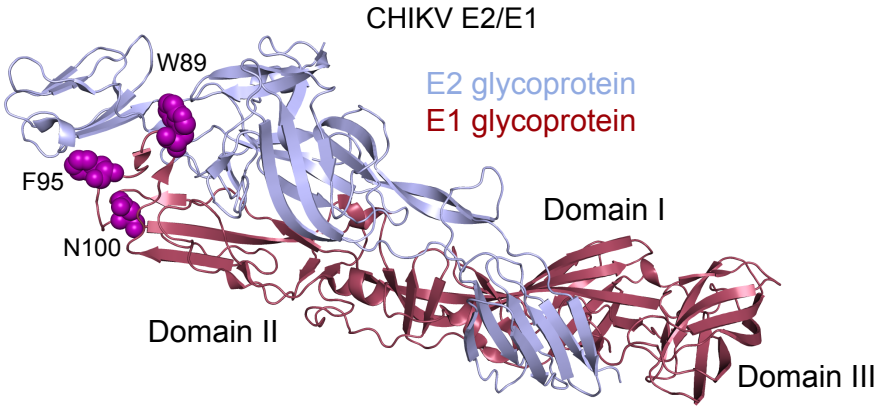

Figure 44. Human anti-alphavirus E1-specific mAbs recognize the CHIKV fusion loop. A. Binding of anti-alphavirus E1-specific mAbs to CHIKV E2/E1 clones. MAbs or Fabs were screened at a 1 µg/mL concentration for binding to CHIKV E2/E1 constructs expressed in HEK 293T cells. Binding was detected by flow cytometry (as described previously; Fong et al., 2014). Binding to each mutant protein clone was calculated relative to that for wild-type (WT) protein by subtracting the signal from mock-transfected controls and normalizing to the signal from WT-transfected controls. Data represent the mean (standard deviation) of four replicate data points. **B.** Epitope mapping of critical residues identified by alanine scanning (**A**) for human anti-alphavirus E1-specific mAbs binding to the CHIKV E1 glycoprotein. Critical residues were mapped onto the CHIKV E2/E1 heterodimer (PDB ID: 3N42). A side view of the CHIKV E2/E1 heterodimer (E2 – blue, E1 – red) is shown with critical residues indicated (purple spheres) for the anti-alphavirus E1-specific mAbs.

The ‘New World’ reactive mAb EEEV-179 binds to the encephalitic (EEEV, VEEV, and WEEV) alphaviruses in ELISA and also the arthritogenic (CHIKV) alphavirus in cell-surface antigen display (**Figures 42** and **47**). The critical interaction residues identified for EEEV-179 were within the domain I/III linker (A286S), domain III (N361A),

and proximal to the fusion loop (Y93A [cd loop]), which together are unique among mAbs and consistent with the distinct competition-binding group for this mAb. Binding residues were not identified for the 'EEEV-VEEV' reactive mAb EEEV-157, which may be due to multiple factors including a requirement for more stringent conditions or dependence on mutation of several residues together to observe a loss-of-binding phenotype.

Anti-EEEV E1-specific mAbs recognize epitopes in domain I, II, and III of the E1 glycoprotein

To further define the epitopes recognized by human anti-EEEV E1-specific mAbs, I assessed for a loss-of-binding phenotype with the EEEV alanine-scanning mutagenesis library (**Figures 45B, 45C, 46, and 55; Table 4**). These mAbs recognized epitopes consistent with the competition-binding groups. EEEV-312 recognized residues within and proximal to the fusion loop (V80A, F81A, Y85A, F87A, W89A, G90A, G91A, F95A, N100A [cd loop]; T218A [central b sheet] and L220A [ij loop]). While several residues were similar to those identified for the cross-reactive mAbs, additional residues were identified in this region that may account for EEEV specificity of EEEV-312. Several residues were identified at the interface of E2 and E1 or on the membrane proximal side of the heterodimer, which may become exposed during the fusion process as the E1 homotrimer complex forms. EEEV-377 and -127 lost binding with an L220A substitution in E1. These anti-EEEV mAbs compete with some of the fusion-loop cross-reactive mAbs, which is expected given their proximity of binding.

EEEV-76, -104, -320, and -400 partially compete with EEEV-377 and -127 but do not compete with the cross-reactive mAbs. These mAbs recognize additional critical residues within domain II (G182A [central b sheet; EEEV-320], Y193A [central b sheet – gh loop; EEEV-104], K197A [central b sheet – gh loop; EEEV-400], T218A [central b sheet; EEEV-76]), which suggests a distinct antigenic determinant on the E1 glycoprotein recognized by these mAbs that is EEEV-specific and does not hinder the fusion loop anti-alphavirus mAbs from binding. EEEV-398 recognizes a distinct antigenic determinant (G165A, S168A, S169A, and W171A) within domain I. However, binding residues were not identified for EEEV-98, -109, or -126 using this mutagenesis approach.

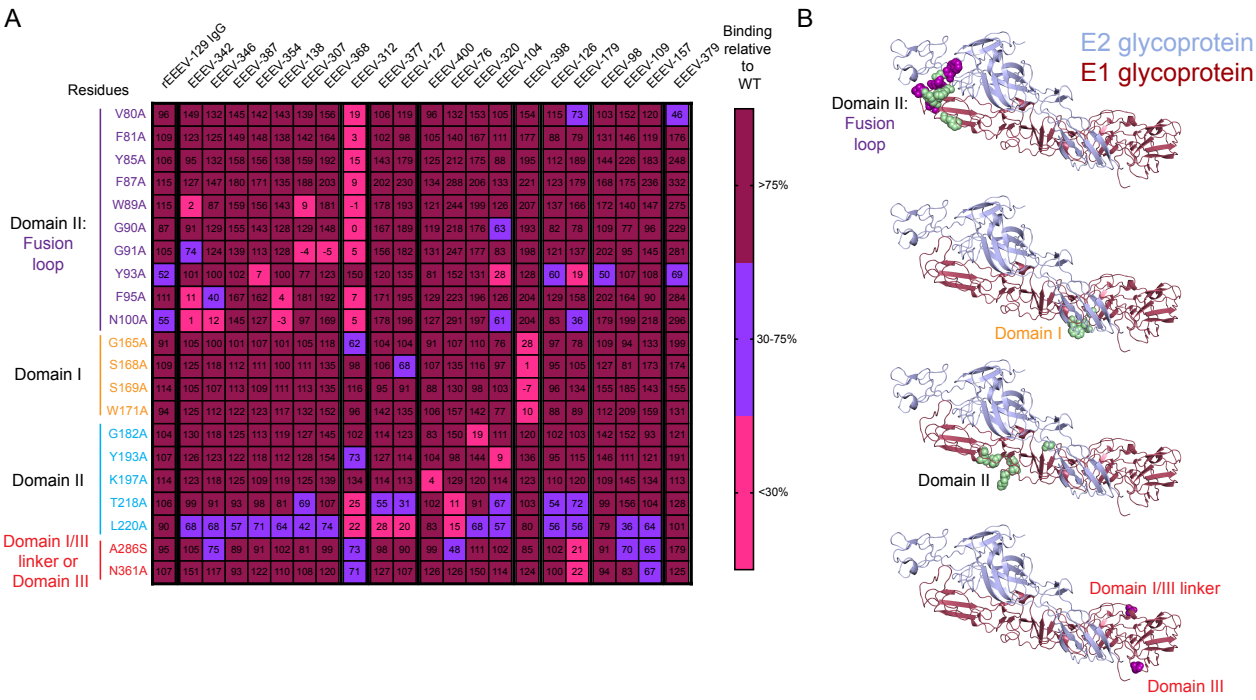

Figure 45. Human anti-alphavirus E1-specific mAbs recognize the conserved fusion loop on the EEEV E1 glycoprotein. A. Heatmap of critical residues identified for human E1-specific mAbs as determined through alanine-scanning mutagenesis library analysis of the EEEV E1 glycoprotein. The average percent binding for each mAb is indicated for the critical alanine residues (<30% binding of mAb in which the positive control mAb, rEEEV-129 IgG (Williamson et al., 2020), or at least five mAbs exhibited >75% binding to control for expression) identified relative to the percent binding to wild-type (WT). The average percent binding is displayed as a heatmap with maroon (>75%), light blue (30 to 75%), or magenta (<30%) binding relative to WT. Residues are colored based on E1 domain or region (purple [domain II, fusion loop]), cyan [domain II], orange [domain I], red [domain I/III linker or domain III]). Each mAb is ordered to correspond with the competition-binding groups as defined in **Figure 43** and residues identified for EEEV-312 and EEEV-379. **B.** Epitope mapping of critical residues identified by alanine scanning (**A**) for human E1-specific mAbs binding to the E1 glycoprotein. Critical residues were mapped onto the cryo-EM reconstruction of SINV/EEEV (PDB: 6MX4). A side view of the EEEV E2-E1 heterodimer (E2 – blue, E1 – red) is shown with critical residues (spheres) for the E1-specific mAbs. Residues are colored based on binding reactivity (purple, cross-reactive and green, EEEV-specific). Data in **A** represent mean of at least two independent experiments.

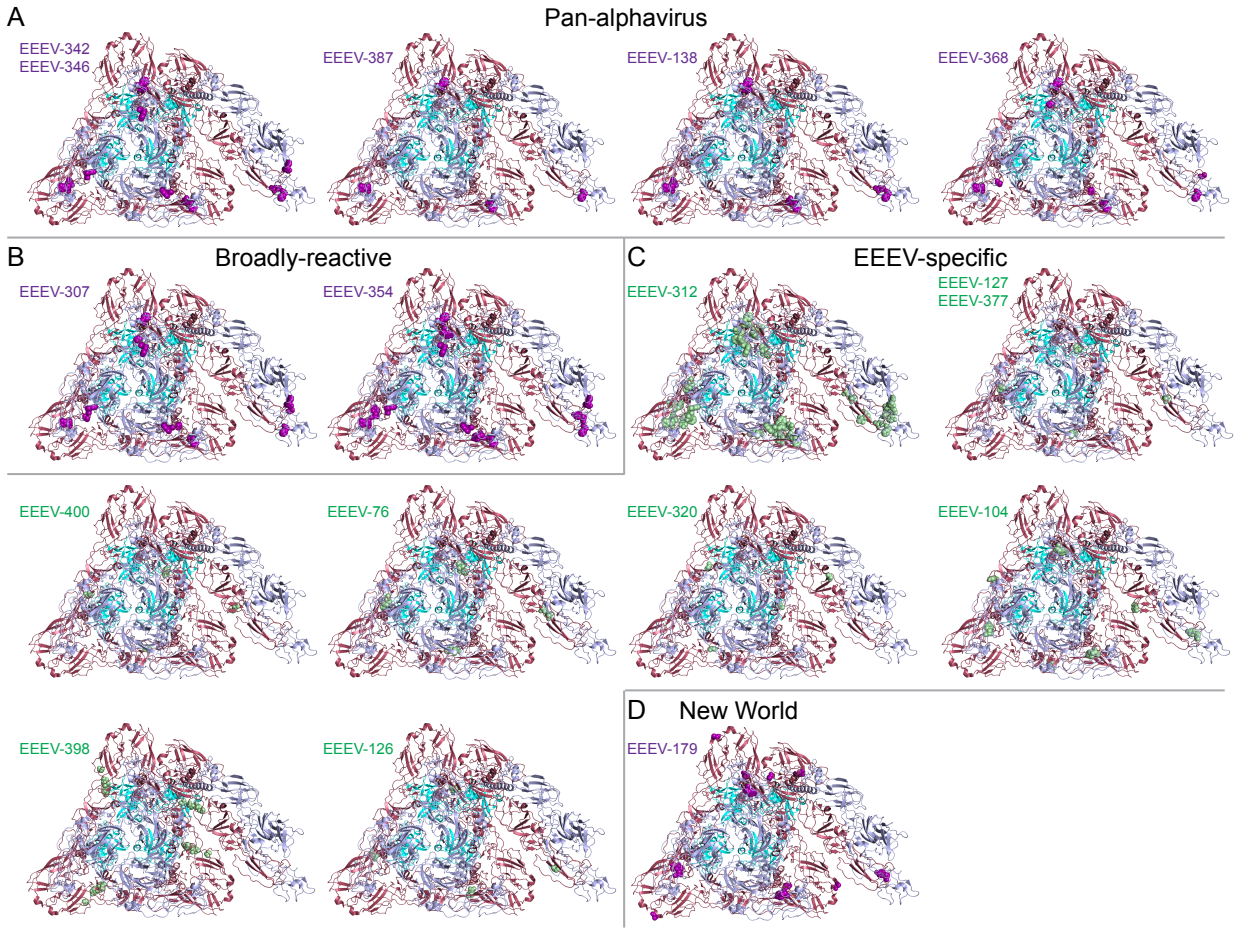

Figure 46. Epitope mapping of human anti-EEEV and anti-alphavirus E1-specific mAbs. Epitope mapping from cell-surface-display antigen and EEEV and CHIKV E1 alanine-scanning mutagenesis analyses of human E1-specific mAbs binding to the E1 glycoprotein. Critical residues were mapped onto the cryo-EM reconstruction of SINV/EEEV (PDB: 6MX4). A top trimeric view with an asymmetric unit of a neighboring spike (E2 – blue, E1 – red) is shown with critical residues (spheres) for the E1-specific mAbs. Residues are colored based on binding reactivity (purple, cross-reactive and green, EEEV-specific). Each mAb is grouped according to antigen binding reactivity and EEEV E1 alanine analysis as described in **Figures 43** and **44**.

Binding Group	EEEV mAb	Epitope	Critical Binding Residues[1]
EEEV-specific	EEEV-76	Domain II (central β sheet, ij loop)	T218, L220
	EEEV-98	Unknown	ND
	EEEV-104	Domain II (central β sheet, gh loop)	Y93, Y193
	EEEV-109	Unknown	ND
	EEEV-126	Domain II (cd loop)	Q79
	EEEV-127	Domain II (ij loop)	L220
	EEEV-312	Domain II (cd loop, central β sheet, ij loop)	V80, F81, Y85, F87, W89, G90, G91, F95, N100, T218, L220
	EEEV-320	Domain II (central β sheet)	G182
	EEEV-369	Unknown	ND
	EEEV-377	Domain II (ij loop)	L220
	EEEV-379	Unknown	ND
	EEEV-398	Domain I	G165, S168, S169, W171
	EEEV-400	Domain II central β sheet, gh loop	K197
EEEV and VEEV	EEEV-157	Unknown	ND
New World	EEEV-179	Domain I/III linker, Domain III, Fusion loop	Y93, A286, N361
Broadly-reactive	EEEV-307	Fusion loop	W89, G91, F95
	EEEV-354		W89, Y93, F95
Pan-alphavirus	EEEV-138		F95, N100
	EEEV-342		W89, F95, N100
	EEEV-346		W89, F95, N100
	EEEV-368		G91, F95
	EEEV-387		F95

Table 4. Human E1-specific mAb epitope mapping. [1]Critiical binding residues were determined through cell-surface-display antigen binding, EEEV and CHIKV E1 alanine-scanning mutagenesis library analyses. ND = not determined

Temperature does not affect binding of human E1-specific mAbs

Elevated temperature has been shown to increase binding of many E1-specific mAbs (Fong et al., 2014). In addition, I hypothesized that some cryptic E1 epitopes might become exposed at higher temperatures, such as at physiological temperature or during febrile illness, for recognition by E1-specific mAbs. To examine this condition for epitope exposure, I compared binding of E1-specific mAbs to VLPs or recombinant protein at room temperature, 37ºC, or 42ºC (**Figure 47**). Previous assessment of mAb binding to alphavirus VLPs and recombinant structural proteins in ELISA was performed in the presence of detergent as described above. To identify potential mechanisms of exposure for recognition of cryptic epitopes by these human E1-specific mAbs, binding was assessed in PBS without detergent to maintain a more native-like antigenic structure. Unexpectedly, I found that temperature did not affect binding of E1-specific mAbs, as shown by the similar EC_{50} values for binding at diverse temperatures (**Figures 47A** and **47B; Table 5**). However, binding of the human E1-specific mAbs in the absence of the nonionic detergent Tween 20 enabled further characterization of the binding profiles for the human anti-EEEV E1-specific mAbs. Three binding groups emerged for these mAbs based on differences in binding strength to VLPs versus recombinant EEEV E1 glycoprotein. The ratio of VLP/protein EC_{50} values for binding was calculated (**Figure 47A**) to identify dependence on virion-specific versus

recombinant E1 glycoprotein to elucidate exposure of the epitope. EEEV-98, -109, -126, -127, -377, and -398 had VLP/protein EC_{50} ratios for binding at room temperature of <1, indicating stronger binding to EEEV VLPs than recombinant EEEV E1 glycoprotein. EEEV-76, -104, -320, and -400 had minimal to no binding to recombinant EEEV E1 glycoprotein under the conditions tested. Thus, these mAbs likely engage a virion-specific or complex E2/E1 epitope for binding. The third group of mAbs, EEEV-312, -369, and -379, had VLP/protein EC_{50} ratios for binding at room temperature >1, indicating preferential binding strength to the recombinant EEEV E1 glycoprotein compared to EEEV VLPs.

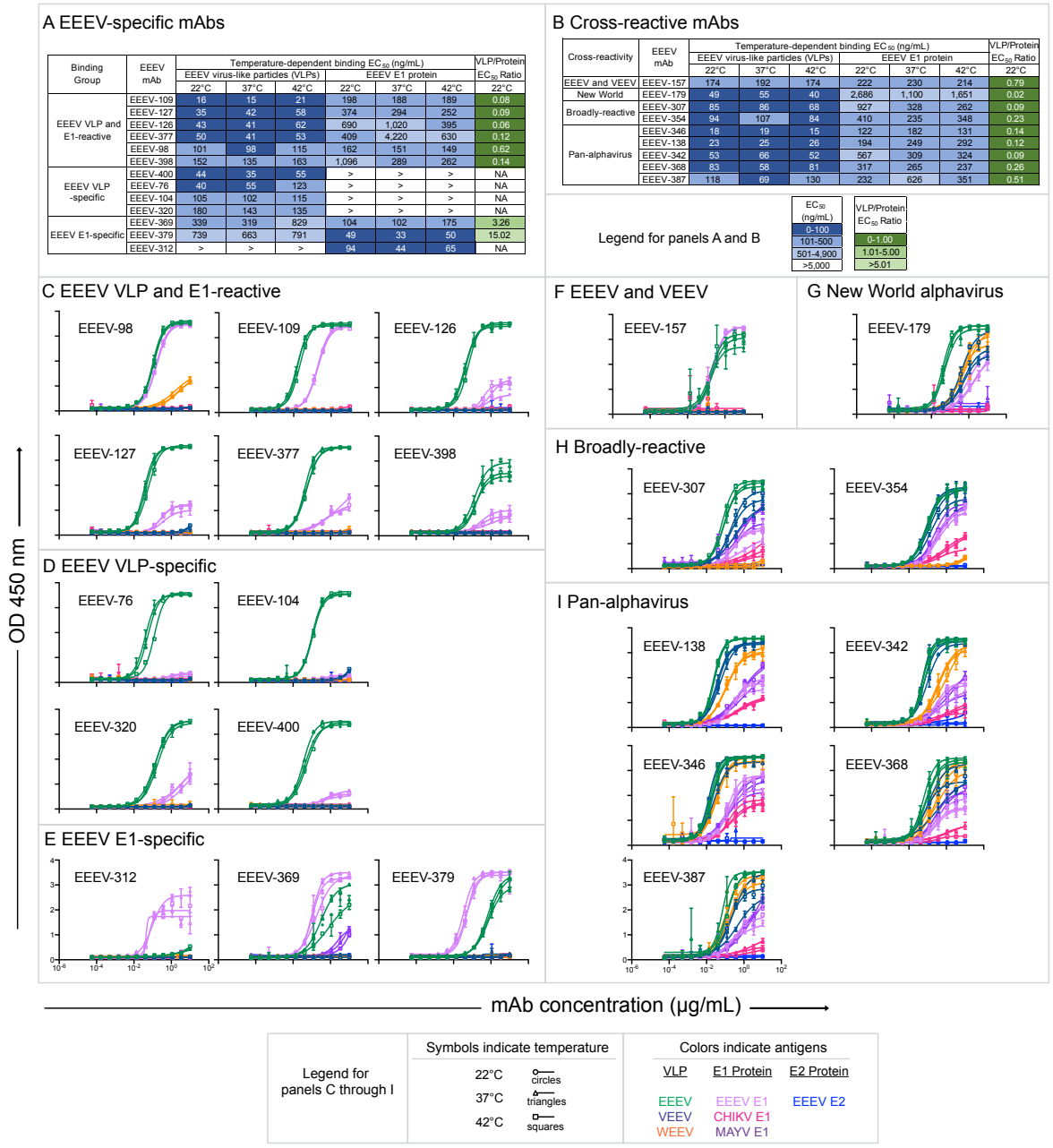

Binding Group	EEEV mAb	Temperature-dependent binding EC_{50} (ng/mL)						VLP/Protein EC_{50} Ratio
		EEEV virus-like particles (VLPs)			EEEV E1 protein			
		22°C	37°C	42°C	22°C	37°C	42°C	22°C
EEEV VLP and E1-reactive	EEEV-109	16	15	21	198	188	189	0.08
	EEEV-127	35	42	58	374	294	252	0.09
	EEEV-126	43	41	62	690	1,020	395	0.06
	EEEV-377	50	41	53	409	4,220	630	0.12
	EEEV-98	101	98	115	162	151	149	0.62
	EEEV-398	152	135	163	1,096	289	262	0.14
EEEV VLP -specific	EEEV-400	44	35	55	>	>	>	NA
	EEEV-76	40	55	123	>	>	>	NA
	EEEV-104	105	102	115	>	>	>	NA
	EEEV-320	180	143	135	>	>	>	NA
EEEV E1-specific	EEEV-369	339	319	829	104	102	175	3.26
	EEEV-379	739	663	791	49	33	50	15.02
	EEEV-312	>	>	>	94	44	65	NA

Cross-reactivity	EEEV mAb	Temperature-dependent binding EC_{50} (ng/mL)						VLP/Protein EC_{50} Ratio
		EEEV virus-like particles (VLPs)			EEEV E1 protein			
		22°C	37°C	42°C	22°C	37°C	42°C	22°C
EEEV and VEEV	EEEV-157	174	192	174	222	230	214	0.79
New World	EEEV-179	49	55	40	2,686	1,100	1,651	0.02
Broadly-reactive	EEEV-307	85	86	68	927	328	262	0.09
	EEEV-354	94	107	84	410	235	348	0.23
Pan-alphavirus	EEEV-346	18	19	15	122	182	131	0.14
	EEEV-138	23	25	26	194	249	292	0.12
	EEEV-342	53	66	52	567	309	324	0.09
	EEEV-368	83	58	81	317	265	237	0.26
	EEEV-387	118	69	130	232	626	351	0.51

EC_{50} (ng/mL)
0-100
101-500
501-4,900
>5,000

VLP/Protein EC_{50} Ratio
0-1.00
1.01-5.00
>5.01

Figure 47. Temperature-independent binding of human E1-specific mAbs to virus-like particles (VLPs) or recombinant E1 glycoproteins. A. EC_{50} values (ng/mL) for binding of human anti-EEEV E1-specific mAbs to EEEV VLPs or recombinant EEEV E1 glycoprotein at room temperature, 37°C, or 42°C. The human anti-EEEV mAbs are grouped according to binding reactivity (VLP or E1-specific, VLP- and E1-reactive) and listed in order of increasing EC_{50} value for binding to EEEV VLPs for each respective group. EC_{50} value in ng/mL is indicated by the blue fill color (≤100.00 [dark blue] 100.01-500.00 [light blue], 500.01-4,999 [lightest blue]). Ratio of binding to EEEV VLPs compared to EEEV E1 glycoprotein at room temperature is indicated as the ratio of EC_{50} values. Increasing depth of green color indicates lower ratios and thus more dependence on virion-specific epitopes. **B.** EC_{50} values (ng/mL) for binding of human anti-alphavirus E1-specific mAbs to EEEV VLPs or recombinant EEEV E1 glycoprotein at room

temperature, 37°C, or 42°C. The human anti-alphavirus mAbs are grouped according to binding cross-reactivity ('EEEV and VEEV', 'New World', 'broadly-reactive, and 'pan-alphavirus') and listed in order of increasing EC_{50} value for binding to EEEV VLPs for each respective group. EC_{50} value in ng/mL is indicated by blue fill color (≤100.00 [dark blue] 100.01-500.00 [light blue], 500.01-4,999 [lightest blue]). Ratio of binding to EEEV VLPs compared to EEEV E1 glycoprotein at room temperature is indicated as the ratio of EC_{50} values. A VLP/protein EC_{50} ratio of <1 suggests a greater dependence on virion-specific epitopes. **C** to **I.** Representative curves for human anti-EEEV E1-specific mAbs binding to EEEV (green), VEEV (dark blue), or WEEV (orange) VLPs, recombinant EEEV (light purple), CHIKV (magenta), or MAYV (purple) E1 glycoproteins, or recombinant EEEV E2 (blue) glycoprotein at room temperature (open circles), 37°C (open triangles), or 42°C (open squares) with mAb concentration (μg/mL) on the x-axis and optical density at 450 nm on the y-axis. Binding curves are ordered numerically and grouped according to binding reactivity (EEEV VLP and E1-reactive [**C**], EEEV VLP-specific [**D**], EEEV E1-specifc [**E**], 'EEEV and VEEV'-reactive [**F**], 'New World' alphavirus-reactive [**G**], 'broadly-reactive' [**H**], or 'pan-alphavirus'-reactive [**I**]). Data in **A** to **I** represent mean ± SD of technical triplicates and are representative of two independent experiments.

EEEV mAb	Temperature-dependent binding EC_{50} (ng/mL; [1× PBS])																	
	Virus-like particles (VLPs)									Protein								
	EEEV			VEEV			WEEV			EEEV E1			CHIKV E1			MAYV E1		
	22°C	37°C	42°C	22°C	37°C	42°C	22°C	37°C	42°C	22°C	37°C	42°C	22°C	37°C	42°C	22°C	37°C	42°C
76	40	55	123	>	>	>	>	>	>	>	>	>	>	>	>	>	>	>
98	101	98	115	>	>	>	>	>	>	162	151	149	>	>	>	>	>	>
104	105	102	115	>	>	>	>	>	>	>	>	>	>	>	>	>	>	>
109	16	15	21	>	>	>	>	>	>	198	188	189	>	>	>	>	>	>
126	43	41	62	>	>	>	>	>	>	690	1,020	395	>	>	>	>	>	>
127	35	42	58	>	>	>	>	>	>	374	294	252	>	>	>	>	>	>
312	>	>	>	>	>	>	>	>	>	94	44	65	>	>	>	>	>	>
320	180	143	135	>	>	>	>	>	>	>	>	>	>	>	>	>	>	>
369	339	319	829	>	>	>	>	>	>	104	102	175	>	>	>	>	>	>
377	50	41	53	>	>	>	>	>	>	409	4,220	630	>	>	>	>	>	>
379	739	663	791	>	>	>	>	>	>	49	33	50	>	>	>	>	>	>
398	152	135	163	>	>	>	>	>	>	1096	289	262	>	>	>	>	>	>
400	44	35	55	>	>	>	>	>	>	>	>	>	>	>	>	>	>	>
157	174	192	174	>	>	>	>	>	>	222	230	214	>	>	>	>	>	>
179	49	55	40	519	530	412	395	360	698	2,686	1,100	1,651	>	>	>	>	>	>
307	85	86	68	192	346	210	>	>	>	927	328	262	>	>	>	357	943	397
354	94	107	84	142	86	122	>	>	>	410	235	348	405	1,342	765	356	342	226
138	23	25	26	53	39	35	112	99	127	194	249	292	401	419	646	836	688	724
342	53	66	52	64	96	51	340	371	1,063	567	309	324	285	2,708	1,300	371	3,175	629
346	18	19	15	20	25	13	30	34	32	122	182	131	148	272	172	113	186	168
368	83	58	81	338	110	69	293	155	253	317	265	237	1,020	1,607	346	355	247	409
387	118	69	130	461	250	158	163	102	168	232	626	351	2,017	4,931	4,933	2,440	1,044	3,597

Table 5. Human E1-specific mAb temperature-independent binding. EC_{50} value in ng/mL is indicated by the blue fill color (≤10.00 [dark blue], 10.01-100.00 [light blue], 100.01-4,999 [lightest blue]) for binding to respective antigen. > symbol indicates > 5 μg/mL EC_{50} value.

Acidic pH exposes cryptic epitopes on virions for binding of human E1-specific mAbs

Exposure to acidic pH, which mimics the endosomal environment during the viral fusion process, can increase recognition of virus particles by some E1 mAbs (Gibbons

et al., 2004; Meyer et al., 1992; Schmaljohn et al., 1983). To assess exposure of epitopes recognized by human E1-specific mAbs, I tested binding to VLPs or recombinant proteins under neutral or acidic pH conditions (**Figure 48 and Table 6**). Binding was assessed in PBS without detergent to maintain a more native-like antigenic structure. Several binding phenotypes emerged, which corresponded with the different epitope mapping groups identified by competition-binding experiments and alanine-scanning mutagenesis library analyses. For most mAbs that recognize the domain II of the E1 glycoprotein involving the fusion loop, an acidic pH of 5.4 increases the binding strength of both human anti-EEEV and anti-alphavirus E1-specific mAbs compared to neutral pH 7.4 conditions. For the anti-EEEV mAbs, EEEV-104 and -400 bound to EEEV VLPs in a pH-independent manner. Binding to the EEEV E1 glycoprotein was not detected (**Figure 48C**). One group of mAbs, containing EEEV-76, -104, -126, -127, -320, -377, and -398, bound to EEEV VLPs but not to the EEEV E1 glycoprotein (**Figure 48A**). A second group of mAbs includes EEEV-312, which exhibited a similar binding profile to EEEV VLP but also recognized the EEEV E1 glycoprotein (**Figure 48B.1**). At neutral pH, EEEV-312 does not bind to EEEV VLPs and preferentially binds recombinant E1 glycoprotein (**Figure 40**). A third group of mAbs, EEEV-98, -109, -369, and -379, recognized EEEV VLPs and EEEV E1 glycoprotein with similar binding strength irrespective of pH (**Figure 48E.1**).

For the human anti-alphavirus E1-specific mAbs, EEEV-157 (‘EEEV-VEEV’) recognized EEEV VLPs and EEEV E1 glycoprotein in a pH-independent manner, with a slight increase in binding strength to the EEEV E1 glycoprotein compared to EEEV

VLPs (**Figure 48E.2**). EEEV-179 (‘New World’) preferentially recognized EEEV VLPs at either pH, with some binding reactivity to VEEV and WEEV VLPs. Binding to EEEV E1 glycoprotein was not observed (**Figure 48D.2**). The ‘broadly-reactive’ mAbs EEEV-307 and -354 bound to EEEV VLPs more avidly under acidic pH conditions. Some binding reactivity also was observed for VEEV VLPs and MAYV E1 glycoprotein. Binding reactivity was observed to WEEV VLPs at acidic but not neutral pH. These results suggest that the epitope for EEEV-307 and -354 is less exposed in WEEV virions than in EEEV or VEEV virions. Binding was not observed to EEEV or CHIKV E1 glycoproteins (**Figure 48B.2**). For the ‘pan-alphavirus’ mAbs (EEEV-138, -342, -346, -368, and -387), binding was stronger at acidic pH to EEEV, VEEV, and WEEV VLPs. Some binding reactivity also was observed to the EEEV, CHIKV, and MAYV E1 glycoproteins (**Figure 48B.3**). Binding of the human anti-alphavirus E1-specific mAbs to the EEEV E2 glycoprotein was not observed.

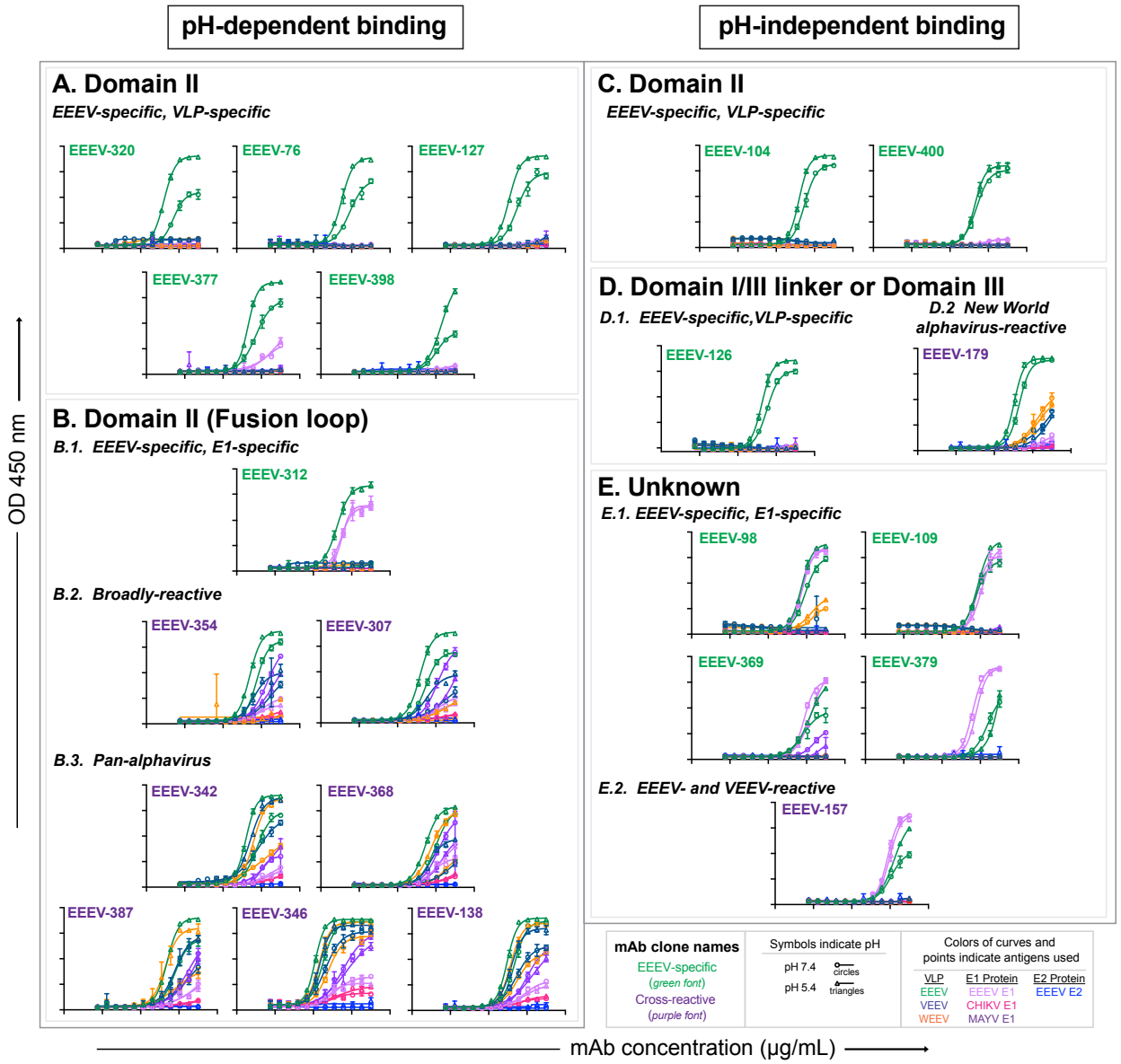

Figure 48. pH-dependent or -independent binding reactivity of human E1-specific mAbs to virus-like particles (VLPs) or recombinant E1 glycoproteins. A and **B.** Representative binding curves of pH-dependent human anti-EEEV (green font) and anti-alphavirus (purple font) E1-specific mAbs to EEEV (green), VEEV (dark blue), or WEEV (orange) VLPs, recombinant EEEV (light purple), CHIKV (magenta), or MAYV (purple) E1 glycoproteins, and recombinant EEEV E2 (blue) glycoprotein at 1x DPBS pH 5.4 (open circles) or 1x DPBS pH 7.4 (open triangles) with mAb concentration (µg/mL) on the x-axis and optical density at 450 nm on the y-axis. Binding curves are ordered by decreasing dependence on pH 5.4 for binding and grouped according to epitope and binding reactivity (domain II (**A**) [EEEV VLP-specific] and fusion loop (**B**) [EEEV E1-specifc (**B.1.**), 'broadly-reactive' (**B.2.**), and 'pan-alphavirus'-reactive (**B.3.**)]. **C** to **E.** Representative binding curves of pH-independent human anti-EEEV (green font) and anti-alphavirus (purple font) E1-specific mAbs to EEEV (green), VEEV (dark blue), or WEEV (orange) VLPs, recombinant EEEV (light purple), CHIKV (magenta), or MAYV (purple) E1 glycoproteins, and recombinant EEEV E2 (blue) glycoprotein at 1x D-PBS pH 5.4 (open circles) or 1x D-PBS pH 7.4 (open triangles) with

mAb concentration (μg/mL) on the x-axis and optical density at 450 nm on the y-axis. Binding curves are ordered numerically and grouped according to epitope and binding reactivity (domain II (**C**) [EEEV VLP-specific], the domain I/III linker or domain III (**D**) [EEEV VLP-specific (**D.1.**) and 'New World' alphavirus-reactive (**D.2.**)], or the unknown epitope (**E**) [EEEV E1-specific (**E.1.**) and 'EEEV-VEEV'-reactive (**E.2.**)]). Data in **A** through **D** represent mean ± SD of technical triplicates and are representative of two independent experiments.

EEEV mAb	Binding EC_{50} (ng/mL; [in 1× PBS]) for indicated antigen and pH (5.4 or 7.4)											
	Virus-like particles (VLPs)						Protein					
	EEEV		VEEV		WEEV		EEEV E1		CHIKV E1		MAYV E1	
	5.4	7.4	5.4	7.4	5.4	7.4	5.4	7.4	5.4	7.4	5.4	7.4
EEEV-76	292	790	>	>	>	>	>	>	>	>	>	>
EEEV-98	537	823	>	>	>	>	602	554	>	>	>	>
EEEV-104	154	300	>	>	>	>	>	>	>	>	>	>
EEEV-109	726	1,183	>	>	>	>	579	675	>	>	>	>
EEEV-126	174	330	>	>	>	>	>	>	>	>	>	>
EEEV-127	114	297	>	>	>	>	>	>	>	>	>	>
EEEV-312	172	>	>	>	>	>	318	285	>	>	>	>
EEEV-320	164	499	>	>	>	>	>	>	>	>	>	>
EEEV-369	1,409	679	>	>	>	>	1,755	754	>	>	>	>
EEEV-377	197	509	>	>	>	>	>	>	>	>	>	>
EEEV-379	>	>	>	>	>	>	615	396	>	>	>	>
EEEV-398	1,970	1,078	>	>	>	>	>	>	>	>	>	>
EEEV-400	198	246	>	>	>	>	>	>	>	>	>	>
EEEV-157	1,586	1,118	>	>	>	>	945	748	>	>	>	>
EEEV-179	108	202	>	>	1,790	1,760	>	>	>	>	610	>
EEEV-307	147	299	342	3,001	4,363	4,009	862	1,315	>	1,647	>	1,211
EEEV-354	245	562	412	3,053	>	>	692	978	4,696	2,889	4,028	2,020
EEEV-138	90	221	143	277	137	308	696	711	556	337	2,014	1,020
EEEV-342	154	578	267	664	394	2,912	3,451	2,998	2,750	>	2,795	965
EEEV-346	12	31	21	43	20	59	64	131	177	88	534	365
EEEV-368	282.7	979.2	503.8	>	587.3	3,400	1,883	722.4	>	>	2,134	1,350
EEEV-387	237	626	599	2,941	195	769	2,958	>	>	>	>	3,536

Table 6. Human E1-specific mAb acidic pH-dependent or pH-independent binding. EC_{50} value in ng/mL is indicated by the blue fill color (≤10.00 [dark blue], 10.01-100.00 [light blue], 100.01-4,999 [lightest blue]) for binding to respective antigen. > symbol indicates > 5 μg/mL EC_{50} value.

Differential exposure of the fusion loop leads to partial neutralization of SINV/VEEV by human anti-alphavirus E1-specific mAbs

I next assessed the functionality for the E1-specific mAbs. Initially, I tested neutralization activity against SINV/EEEV at an antibody concentration of 10 μg/mL. Most E1-specific mAbs did not show evidence of neutralization of SINV/EEEV (as defined by <30% reduction in relative infection) at the concentration tested (**Figure 49A**

and Table 7). Several mAbs (EEEV-98, -104, -109, and -126) that exhibited some modest reduction in SINV/EEEV infectivity were tested at higher assay temperatures (*i.e.*, 42ºC) but still showed little inhibitory activity (**Figure 49B**).

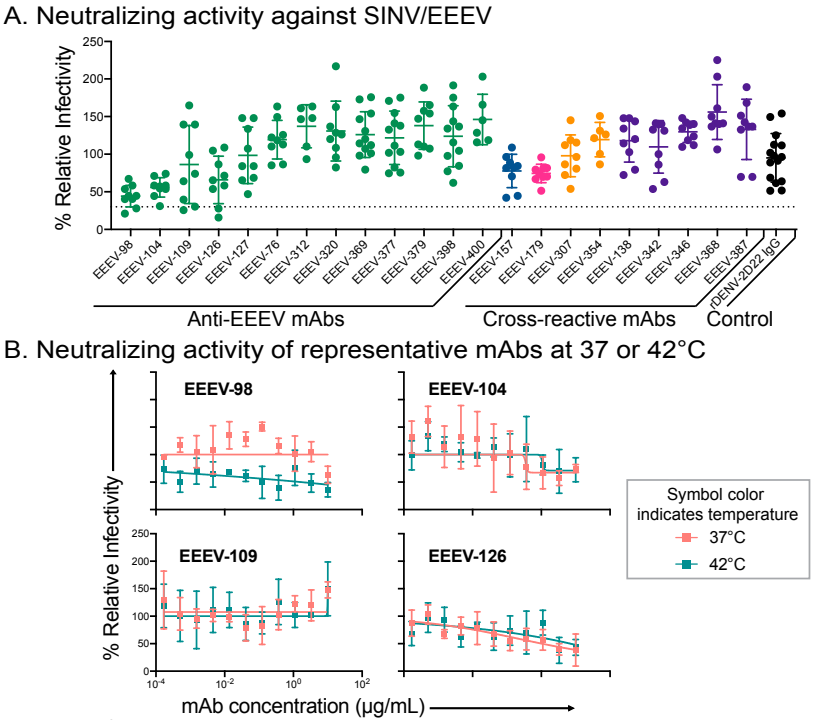

Figure 49. Human anti-EEEV E1-specific mAbs do not potently neutralize SINV/EEEV entry. A. Neutralization activity of human anti-EEEV and anti-alphavirus E1-specific mAbs (10 µg/mL) against SINV/EEEV with mAb name on the x-axis and % relative infectivity on the y-axis. The dotted line indicates 30% relative infectivity as an arbitrary cutoff for neutralization activity. Each mAb is colored based on binding reactivity (EEEV-specific [green], 'EEEV and VEEV'-reactive [blue], 'New World'-reactive [magenta], 'broadly-reactive' [orange], 'pan-alphavirus' [purple], or negative control [black]. **B.** Neutralization curves for the potential weakly neutralizing human anti-EEEV E1-specific mAbs, EEEV-98, -104, -109, and -126, identified in **A** against SINV/EEEV at 37ºC or 42ºC with mAb concentration (µg/mL) on the x-axis and % relative infectivity on the y-axis. Data in **A** represent mean ± SD of technical triplicates and of at least two independent experiments. Data in **B** represent mean ± SD of technical triplicates of a focus reduction neutralization test (FRNT) experiment.

I also assessed neutralization activity of the human anti-alphavirus E1-specific mAbs for SINV/EEEV, SINV/VEEV, SINV/WEEV, CHIKV, or MAYV at 37ºC or 42ºC (**Figure 50 and Table 7**). The cross-reactive E1 mAbs did not neutralize SINV/EEEV, SINV/WEEV, CHIKV, or MAYV at either temperature. However, EEEV-342, -346, -354, and -387 moderately neutralized SINV/VEEV (IC_{50}: 2,000 – 5,000 ng/mL). This finding suggests that there may be differential exposure of the fusion loop on native virion particles possibly during morphogenesis or in solution that enables these mAbs to neutralize SINV/VEEV.

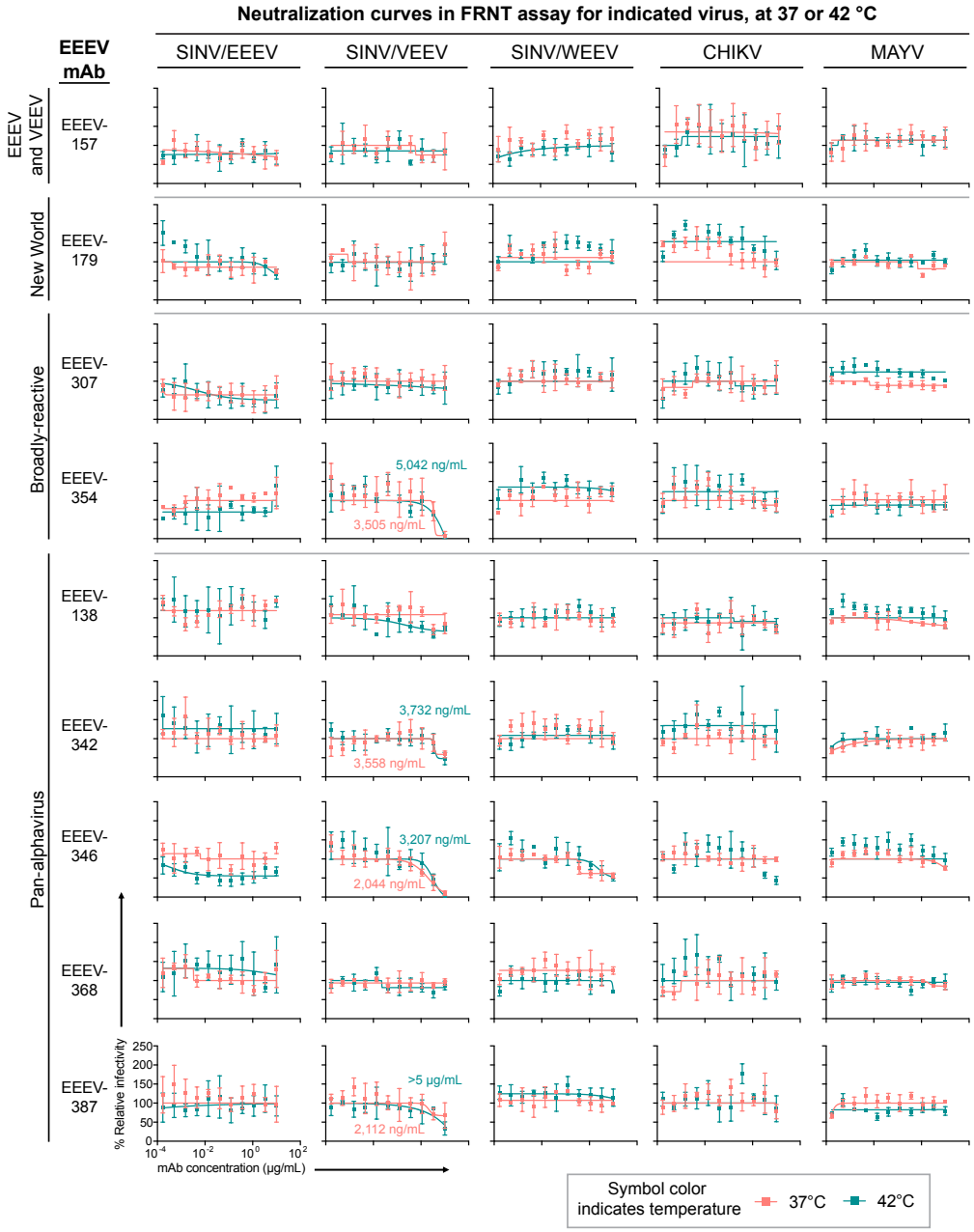

Figure 50. Human anti-alphavirus E1-specific mAbs moderately neutralize SINV/VEEV. Neutralization curves of human anti-alphavirus E1-specific mAbs against SINV/EEEV, SINV/VEEV, SINV/WEEV, CHIKV, or MAYV at 37°C (light pink squares) or 42°C (teal squares) with mAb concentration (µg/mL) on the x-axis and % relative infectivity on the y-axis. Each mAb is grouped according to cross-reactivity and ordered numerically within each group. Half-maximal inhibitory concentration (IC_{50}) values (ng/mL) for moderately neutralizing mAbs (EEEV-342, -346, -354, and -387) against SINV/VEEV are indicated at each temperature (light pink - 37°C, teal - 42°C). Data represent mean ± SD of technical triplicates of a focus reduction neutralization test (FRNT) experiment.

Binding group	EEEV mAb	IC_{50} (ng/mL [37°C; 42°C])					Egress inhibition (yes or no)
		SINV/EEEV	SINV/VEEV	SINV/WEEV	CHIKV	MAYV	SINV/EEEV
EEEV-specific	EEEV-76	>	NA				no
	EEEV-98	>					yes
	EEEV-104	>					yes
	EEEV-109	>					yes
	EEEV-126	>					yes
	EEEV-127	>					no
	EEEV-312	>					no
	EEEV-320	>					no
	EEEV-369	>					no
	EEEV-377	>					no
	EEEV-379	>					no
	EEEV-398	>					no
	EEEV-400	>					no
EEEV and VEEV	EEEV-157	>	>	>	>	>	no
New World	EEEV-179	>	>	>	>	>	yes
Broadly-reactive	EEEV-307	>	>	>	>	>	no
	EEEV-354	>	3,505; 5,042	>	>	>	no
Pan-alphavirus	EEEV-138	>	>	>	>	>	no
	EEEV-342	>	3,558; 3,732	>	>	>	no
	EEEV-346	>	2,044; 3,207	>	>	>	no
	EEEV-368	>	>	>	>	>	no
	EEEV-387	>	2,112; >	>	>	>	no

Table 7. Human E1-specific mAb neutralization activity. IC_{50} value in ng/mL is indicated by the orange fill color (<5 µg/mL [light blue]) for neutralization of respective virus. > symbol indicates > 5 µg/mL EC_{50} value.> symbol indicates > 5 µg/mL. NA = not applicable

Human anti-EEEV and 'New World' E1-specific mAbs inhibit SINV/EEEV egress

The presentation of the E2 and E1 glycoproteins prior to virus egress is not well understood. Some E1-specific mAbs might bind to epitopes exposed at the plasma membrane (Schmaljohn et al., 1983), which may inhibit virus egress from the cell. To assess this possibility, I performed an egress inhibition assay (Fox et al., 2015). In this method, virus is added to cells prior to addition of mAb, and then supernatant is

collected at 1 hour or 6 hours after mAb addition to capture any virus that has egressed from the cell. Given that the human E1-specific mAbs do not appreciably neutralize SINV/EEEV in the standard focus reduction neutralization test (FRNT) assay (**Figures 49** and **50**), I measured egress by determining the titer of virus present in the supernatant using a focus forming assay (FFA). I observed inhibition of SINV/EEEV egress by several human anti-EEEV E1-specific mAbs (EEEV-98, -104, -109, and -126) and the 'New World' mAb EEEV-179 (**Figure 51**). This finding suggests that the standard FRNT assay is likely 'entry-biased' and does not fully capture the activity of egress inhibition even in the presence of mAb. Also, this finding suggests that epitopes are exposed prior to virus budding, enabling engagement by mAbs and blockade of virus egress.

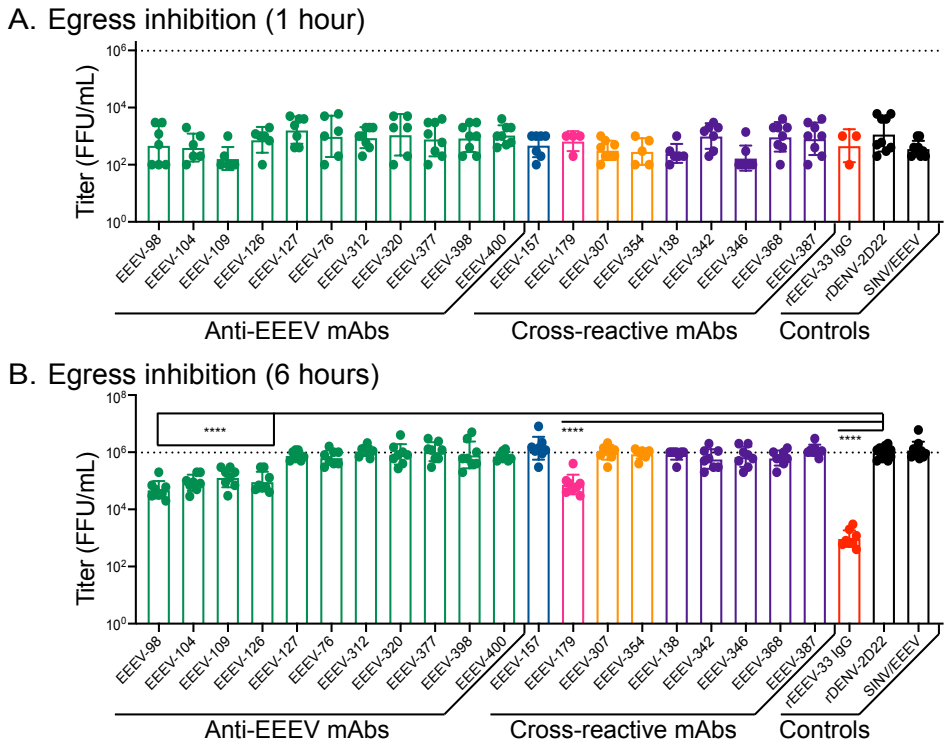

Figure 51. Anti-EEEV E1-specific mAbs inhibit viral egress. **A** and **B.** Focus-forming units (FFUs) of supernatant harvested at either 1 hour (**A**) or 6 hours (**B**) following mAb addition in an egress inhibition assay. Vero cells were inoculated with SINV/EEEV at MOI 1 and incubated at 37ºC for 2 hours. Cells were then washed extensively to remove unbound virus. Anti-EEEV or anti-alphavirus mAbs were added to the cells at 10 µg/mL and incubated for up to 6 hours at 37ºC. Reduction in SINV/EEEV FFUs were compared to the negative control mAb, rDENV-2D22, using an ordinary one-way ANOVA with Dunnett's multiple comparisons test (**** $p<0.0001$). Data in **A** and **B** represent mean ± SD of technical duplicates and of two independent experiments.

EEEV-109 exhibits Fc polyfunctionality

Abs also can exert protective effects *in vivo* via Fc-mediated effector functions. Some alphavirus antibodies were found previously to require Fc functionality for optimal *in vivo* efficacy (Earnest et al., 2019; Fox et al., 2019). In collaboration with Dr. Galit Alter's laboratory, we next evaluated whether the human E1-specific mAbs can mediate

Fc effector functions, including Ab-dependent cellular phagocytosis (ADCP), neutrophil phagocytosis (ADNP), complement deposition (ADCD), and natural killer cell activation (ADNKA), *in vitro* using bead-based assays with the recombinant EEEV E1 glycoprotein (**Figure 52**).

Overall, the mAbs exhibited a higher level of ADCP activity compared to ADNP, suggesting a greater dependence on monocytes than neutrophils for phagocytosis. Additionally, NK degranulation was observed for many mAbs (EEEV-98, -109, -138, -157, -307, -312, -368, -369, -377, -379, and -387) as observed by higher levels of MIP-1β and CD107a. Minimal IFNγ was detected was observed for all mAbs, compared to the irrelevant Ebola virus-specific negative control mAb 13C6. Two mAbs, EEEV-138 ('pan-alphavirus') and EEEV-354 ('broadly-reactive'), exhibited high levels of ADCD activity. One human anti-EEEV E1-specific mAb, EEEV-109, exhibited several Fc-mediated effector functions (ADCP, ADNP, ADCD, and ADNKA) with a >two-fold change compared to 13C6. The relatively high Fc activities observed for EEEV-109 suggests its effector functions might contribute to *in vivo* efficacy against EEEV-induced disease. The rest of the mAbs did not appear to be facilitate ADCP, ADNP, ADCD, or ADNKA activities, as they caused less than a two-fold change in phagocytic score, MFI, or % of MIP1- β, CD107a, or IFNγ, compared to the negative control mAb 13C6 (**Figure 52**).

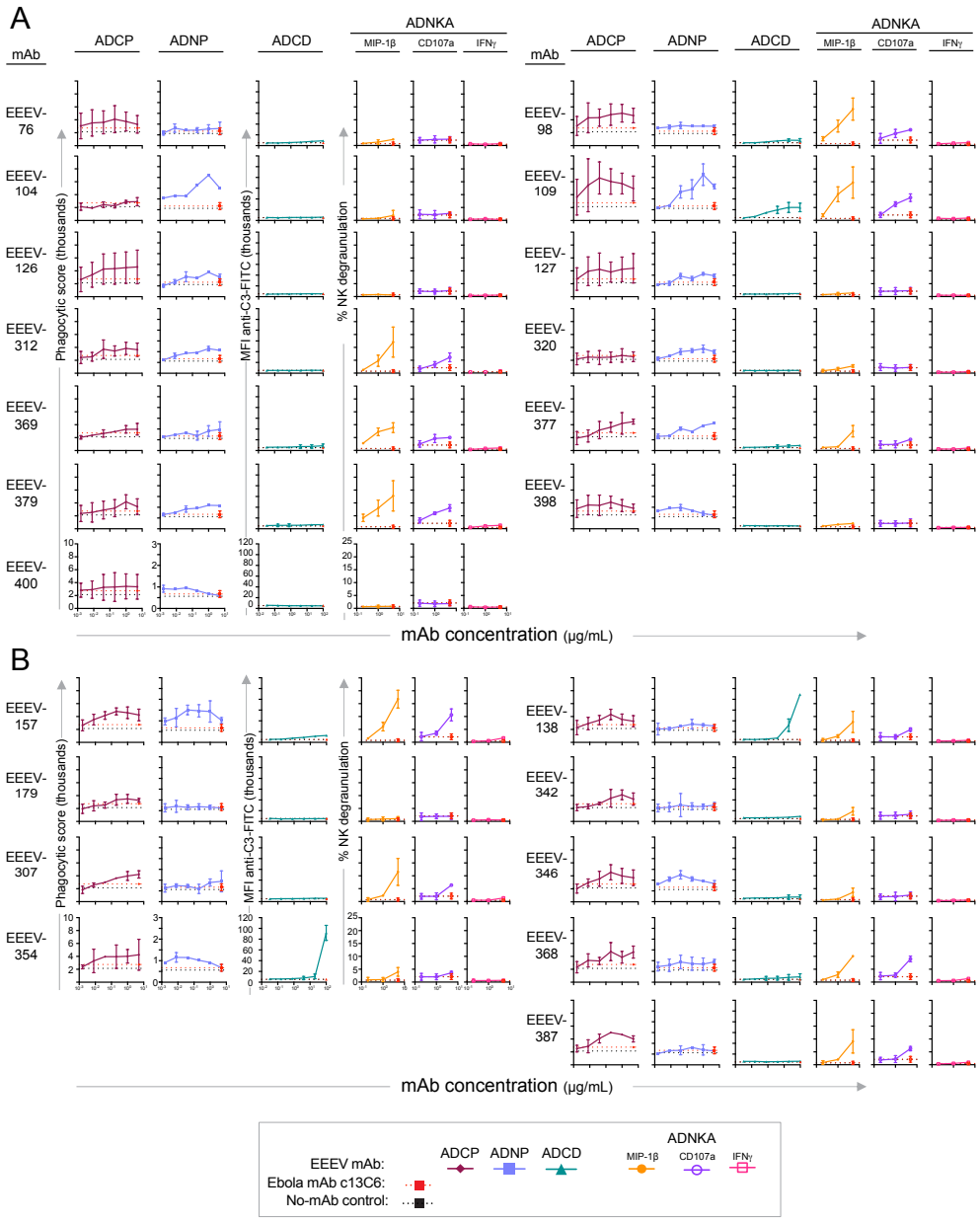

Figure 52. Fc-mediated effector function activities for human anti-EEEV and anti-alphavirus E1-specific mAbs. Monocyte and neutrophil phagocytosis (Ab-dependent cellular phagocytosis [ADCP; maroon diamonds] and Ab-dependent neutrophil phagocytosis [ADNP; light blue squares], respectively), Ab-dependent complement deposition (ADCD; teal triangles), and NK degranulation (Ab-dependent natural killer cell degranulation [ADNKA; MIP-1β (orange circles), CD107a (open purple circles), and IFNγ (open magenta squares)] activity was assessed for human anti-EEEV (**A**) or anti-alphavirus (**B**) mAbs using recombinant EEEV E1-glycoprotein-coated beads. The corresponding graphs represent mAb concentration (μg/mL) on the x-axis and phagocytic score (in thousands [ADCP and ADNP]), median fluorescence intensity of anti-C3-FITC binding (in thousands [ADCD]), or % NK degranulation (ADNKA) on the y-axis. The Ebola virus-specific negative control mAb c13C6 is shown in red squares. The red

dotted line represents the mean y-axis value. The black dotted line indicates the mean y-axis value for a no-mAb negative control. Data represent mean ± SD of two independent experiments.

EEEV-109 treats EEEV-induced disease after s.c. challenge

In collaboration with Dr. Justin Julander's laboratory, we next assessed the therapeutic efficacy of EEEV-109 in a s.c. challenge model of EEEV in mice described in chapter III. EEEV-109 was selected for study based on its high level of Fc-mediated effector functions, high level of binding to different EEEV and MADV subtypes in the cell-surface antigen display assay, and egress inhibition activity. 100% of the mice treated with EEEV-109 survived infection, whereas only 10% of the animals given rDENV-2D22 (negative isotype control) mAb survived (**Figure 53A**). Body weight measurements corresponded with the survival data (**Figure 53B**). EEEV-109 also reduced viremia to the limit of detection, whereas the majority of rDENV-2D22-treated animals had virus in the serum.

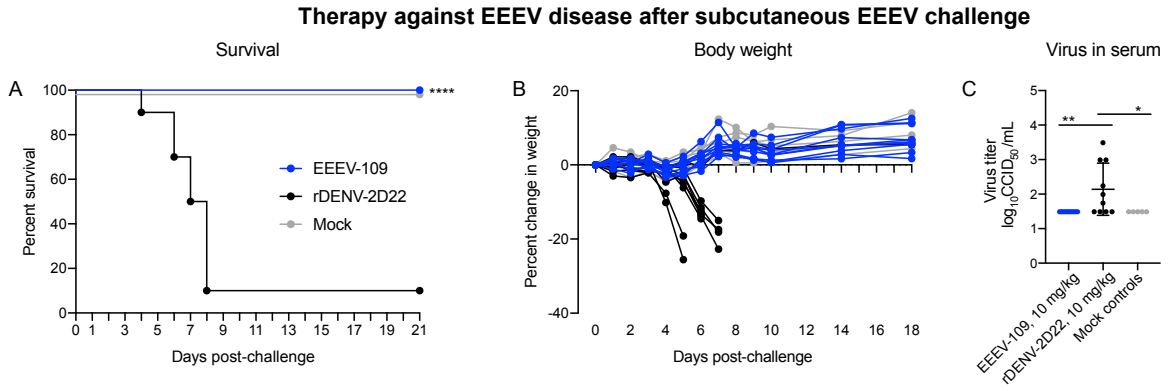

Figure 53. EEEV-109 exhibits therapeutic efficacy against EEEV-induced disease. A through **C.** C57BL/6 mice were inoculated s.c. with $10^{3.3}$ $CCID_{50}$ of EEEV (strain FL93-939) twenty-four hours prior to mAb administration i.p. at 20 or 200 µg/mouse. A mock control was included (n=5; grey). EEEV-109 (10 mg/kg; n=10; blue) mediated 100% therapeutic survival against EEEV compared to the negative control mAb rDENV-2D22 (10 mg/kg; n=10; black) (**A**). **B.** Percent body weight change of EEEV-109, rDENV-2D22, and mock-treated C57BL/6 mice over the course of 18 days after EEEV inoculation. **C.** Virus titer ($log_{10}CCID_{50}$/mL; y-axis) in serum collected three days post-inoculation was determined by an infectious cell culture assay. EEEV-109, rDENV-2D22, or mock controls are indicated on the x-axis. The negative controls, rDENV-2D22 and mock, are the same in **A** to **C** and **Figure 54A** to **54C**. The survival curves in **A** were compared using the log-rank test with Bonferroni multiple comparison correction (*p<0.05, ****p<0.0001). Virus titer in the serum for the treatment groups in **C** were compared to the negative control mAb rDENV-2D22 using an ordinary one-way ANOVA with Dunnett's multiple comparisons test (**p<0.01, *p<0.05).

EEEV-346 prevents EEEV- and CHIKV-induced disease after s.c. challenge

In collaboration with Dr. Justin Julander's laboratory, we also next assessed the *in vivo* efficacy of the human anti-alphavirus mAbs EEEV-138 and -346 against EEEV infection as described in chapter III. These two mAbs were selected for study based on their functional activities. EEEV-138 showed a high level of ADCD activity to assess the potential contribution of Fc effector function to *in vivo* efficacy. EEEV-346 was selected

because of its high level of binding to the encephalitic (EEEV, VEEV, and WEEV) and arthritogenic (CHIKV) alphaviruses and neutralizing activity against SINV/VEEV. Twenty-four hours after EEEV s.c. inoculation (dose = $10^{3.3}$ $CCID_{50}$) of C57BL/6 mice, 200 µg of EEEV-138 or 20 µg of EEEV-346 (a clone that expresses at low levels in culture) were administered by i.p. injection, and survival was monitored for 21 days. EEEV-138 and EEEV-346 resulted in 20% or 30% survival, respectively, compared to the rDENV-2D22 control (10% survival) (**Figure 54A**). The results for survival mediated by EEEV-138 were statistically significant ($p<0.05$). Again, survival results were consistent with body weights (**Figure 54B**). Viremia was observed in the serum of mice treated with EEEV-138 or EEEV-346 (**Figure 54C**) but trended lower in the EEEV-346 treatment group. This finding may be due to the lower Ab dose administered.

To determine if EEEV-346 can confer cross-protection, we collaborated with Dr. Michael S. Diamond's laboratory to assess the efficacy of this mAb against CHIKV-induced joint swelling and infection. Four-week-old C57BL/6 mice were administered a single 200 µg dose by the i.p. route 24 hours prior to inoculation with 10^3 FFU CHIKV LR 2006 OPY1. Mice were monitored for 6 days. EEEV-346 reduced joint swelling (**Figure 54D**) and viral RNA levels in the ipsilateral and contralateral muscles and ankles (**Figures 54E** to **54H**) compared to the isotype control mAb WNV E16. Thus, EEEV-346 can cross-protect against CHIKV-induced disease in mice.

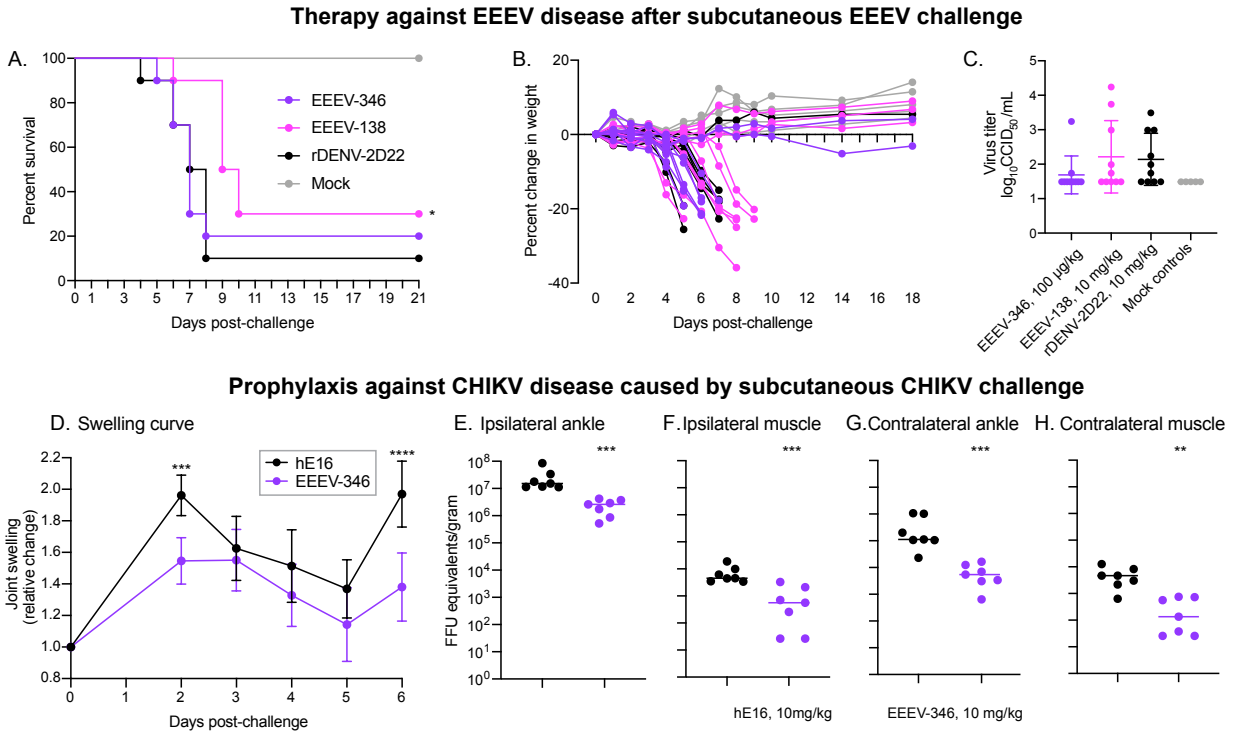

Figure 54. EEEV-346 protects against CHIKV-induced disease. A through **C.** C57BL/6 mice were inoculated s.c. with $10^{3.3}$ $CCID_{50}$ of EEEV (strain FL93-939) twenty-four hours prior to mAb administration i.p. at 20 or 200 µg/mouse. A mock control was included (n=5; grey) EEEV-138 (10 mg/kg; n=10; magenta) and EEEV-346 (100 µg/kg; n=10; purple) exhibited 30% and 20% therapeutic survival against EEEV compared to rDENV-2D22 (**A**). **B.** Percent body weight change of EEEV-138, EEEV-346, rDENV-2D22, and mock-treated C57BL/6 mice over the course of 18 days after EEEV inoculation. **C.** Virus titer ($log_{10}CCID_{50}$/mL; y-axis) in serum collected three days post-inoculation (dpi) was determined by an infectious cell culture assay. EEEV-138, EEEV-346, rDENV-2D22, or mock controls are indicated on the x-axis. The negative controls, rDENV-2D22 and mock, are the same in **A** to **C**. **D** through **H.** C57BL/6 mice (4-weeks-old) were administered 200 µg/mouse of EEEV-346 (10 mg/kg; n=7; purple) or the human West Nile virus-specific negative control mAb hE16 (10 mg/kg; n=7; black), via the i.p. route 24 hours prior to s.c. footpad inoculation with 10^3 FFU of CHIKV strain LR 2006 OPY1. EEEV-346 reduced joint swelling at 2 dpi and 6 dpi (**D**). Viral RNA levels were assessed in the ipsilateral or contralateral ankles (**E** and **G)** and muscles (**F** and **H**) 6 dpi. The survival curves in **A** were compared using the log-rank test with Bonferroni multiple comparison correction (*p<0.05, ****p<0.0001). Virus titer in the serum for the treatment groups in **C** were compared to the negative control mAb rDENV-2D22 using an ordinary one-way ANOVA with Dunnett's multiple comparisons test (**p<0.01, *p<0.05). Joint swelling (**D**) in the EEEV-346 treatment group was compared to hE16 using a two-way ANOVA with Dunnett's multiple comparisons test (***p<0.001, ****p<0.0001). Viral RNA levels present within the ipsilateral or contralateral ankles or muscles (**E** through **H**) of the EEEV-346 treatment group were compared to hE16 using a one-way ANOVA with Dunnett's multiple comparisons test (**p<0.01, ***p<0.001).

Discussion

This chapter describes human E1-specific mAbs isolated from the B cells of naturally infected EEEV-immune individuals, of which two main classes of mAbs emerged, either EEEV-specific (anti-EEEV) or cross-reactive (anti-alphavirus). Varying degrees of cross-reactivity with specificity within the encephalitic alphaviruses (EEEV-specific [anti-EEEV], 'EEEV-VEEV') and reactivity to the arthritogenic alphaviruses ('New World', 'broadly-reactive', 'pan-alphavirus') through ELISA-based and cell-surface-display antigen methods were observed. Since the E1 glycoprotein is mostly occluded by the E2 glycoprotein in the heterodimer complex, diverse binding phenotypes to virus-like particles (VLPs) and recombinant E1 glycoproteins in the presence or absence of the nonionic detergent Tween®20 was observed, which suggested differential exposure of epitopes. To mimic more native-like conditions, I tested different treatment conditions to expose potential E1 epitopes. I did not detect a difference in binding at elevated temperatures, however, acidic pH exposed epitopes for a majority of the domain II mAbs, indicating occlusion of the epitope recognized by those mAbs at neutral pH.

Several human anti-EEEEV mAbs (EEEV-104, -109, -126, -127, and -312) strongly bound EEEV and MADV subtypes in cell-surface-display antigen analyses. These mAbs (except for EEEV-312) did not depend on acidic pH or elevated temperatures for exposure of the E1 epitope on EEEV VLPs. Additionally, these mAbs

inhibited SINV/EEEV egress, which suggests that the epitope is exposed at the cell surface to allow for binding and inhibition of virus budding.

For many different subtypes that cause human and animal disease within the EEEV (EEEV and MADV), VEEV (subtypes I-VI; epizootic (IAB and IC) and enzootic (II-VI), WEEV, and SFV (CHIKV) antigenic complexes, I tested for binding reactivity of the human anti-alphavirus E1-specifc mAbs, using cell-surface-display antigen methods. Broad binding breadth for the 'pan-alphavirus' and 'broadly-reactive' mAbs to these subtypes was observed. Mapping strategies identified the epitope for these anti-alphavirus E1-specific mAbs as the highly conserved fusion loop of the E1 glycoprotein. The 'broadly-reactive' mAb EEEV-354 binds to encephalitic (EEEV and VEEV) and arthritogenic (CHIKV) alphaviruses but not to WEEV. One critical binding residue identified in EEEV alanine-scanning mutagenesis library analysis, Y93A, differs between the between the encephalitic (EEEV and VEEV) and arthritogenic (CHIKV) alphaviruses and WEEV (Q93A), which may account for the lack of binding of EEEV-354 to WEEV. EEEV-307 also does not recognize WEEV. However, Y93A was not identified as a critical residue under the conditions tested and may have a different binding angle that results in lack of binding reactivity to WEEV.

Two residues were previously identified as important factors for increased infection and transmissibility of CHIKV. An adaptive mutation within the E1 glycoprotein, A226V, was shown to increase CHIKV infection and transmissibility, leading to the Indian Ocean lineage of CHIKV (Schuffenecker et al., 2006, Tsetsarkin et al., 2007, Vazeille et al., 2007). A residue proximal to the fusion loop, V80, when mutated to V80L

or V80Q, decreased CHIKV dissemination, viral burden and fusogenic activity of CHIKV (Stapleford et al., 2014, Noval et al., 2019). Abs that recognize these residues and proximal regions (EEEV-138, -179, -307, -342, -346, -354, -368, and -387) at neutral pH might be able to block fusion and reduce viral burden in hosts, which overall may subsequently decrease transmissibility of alphaviruses.

EEEV-179 bound to EEEV, VEEV, WEEV, and CHIKV subtypes in cell-surface antigen-display methods but did not bind to CHIKV E1 glycoprotein in ELISA-based methods. Epitope mapping studies described critical alanine residues for EEEV-179 binding to residues proximal to the fusion loop (Y93A), the domain I/III linker (A286S), and domain III (N361A) of the E1 glycoprotein. Y93 and A286 are conserved among the encephalitic (EEEV, VEEV, and WEEV) and arthritogenic (CHIKV) alphaviruses, which supports the cross-reactivity binding profile of EEEV-179 to these viruses. A286 was previously identified for a moderately neutralizing CHIKV E1-reactive human mAb (DC2.315; Quiroz et al., 2019, and companion paper [Kim et al., 2020]), which suggests a common epitope recognized by human E1-specific mAbs. DC2.315, a ‘pan-alphavirus’ mAb, also was mapped to a proximal region of the fusion loop of the E1 glycoprotein (companion paper [Kim et al., 2020]), further supporting the critical alanine residues identified for EEEV-179. Competition-binding analysis suggests a similar epitope is recognized by EEEV-126. Binding reactivity to EEEV, MADV, and Pixuna virus subtypes in cell-surface antigen-display methods identified Q79 as a possible critical residue for recognition by EEEV-126. Q79 lies proximal to the fusion loop on the E1 glycoprotein. These results support the idea that EEEV-179 may recognize a quaternary

epitope within the domain I/III linker on one trimeric spike and within domain II, proximal to the fusion loop, on a neighboring trimeric spike. EEEV-179 also inhibited egress, and recognition of this epitope may lead to cross-linking of the trimeric spikes as has been observed for many neutralizing E2-specific mAbs (Williamson et al., 2020; Fox et al., 2015; Porta et al., 2014).

In addition to neutralization, Fc-mediated effector functions of Abs also may contribute to clearance of alphavirus infection *in vivo*. This mechanism has been shown for CHIKV and MAYV, since in mouse models the optimal clearance of infection and reduction of joint swelling for CHIKV and decreased MAYV-induced musculoskeletal disease required Fc-FcγR interactions primarily on monocytes (Fox et al., 2019, Earnest et al., 2019). The phagocytic activity exhibited by THP-1 monocytes described here suggests that the human E1-specific mAbs may interact with FcγRs on monocytes to aid in clearance of alphavirus infection *in vivo*. The Fc polyfunctionality observed for EEEV-109 may contribute to the therapeutic efficacy we observed for this mAb against EEEV-induced disease. Further assessment of Fc-mediated effector function involvement *in vivo* can be pursued by testing Fc variants that knock out interactions with FcγRs, such as LALA-PG, compared to WT IgG1 or use of FcγR$^{-/-}$ mice for *in vivo* efficacy against alphaviral disease.

EEEV-346, a ‘pan-alphavirus’ fusion loop mAb, moderately neutralized SINV/VEEV, with IC_{50} values of 2,044 or 3,207 ng/mL at 37ºC or 42ºC, respectively. Neutralization activity was not observed against SINV/EEEV, SINV/WEEV, CHIKV, or MAYV. The differential neutralization activity of EEEV-346 against SINV/VEEV suggests

a difference in exposure of the fusion loop between SINV/VEEV and the other alphaviruses. We selected EEEV-346 for *in vivo* mice studies, in which we observed 20% survival of the mice compared to the negative control, rDENV-2D22 (10% survival) in an EEEV s.c. challenge model. Viremia was reduced but not significantly. EEEV-346, however, reduced joint swelling and CHIKV RNA levels in a s.c. challenge model of CHIKV, thus establishing cross-protection.

This chapter describes a study that compares and contrasts the differences between E1 antigen specificity and cross-reactivity to help elucidate the molecular and biochemical basis for E1 recognition. These Abs could be used further as tools to elucidate the structural conformation states between native intact virions, cell surface, and subtype differences through structural analyses, such as cryo-EM or cryo-electron tomography (cryo-ET). Additionally, the isolation of cross-reactive mAbs described here suggests that immunization with E1 protein in particular conformations may lead to elicitation of these mAbs *in vivo* for protection against alphaviruses. Overall, these studies define the basis for molecular recognition of EEEV E1-specific and pan-alphavirus cross-reactive mAbs, which may aid in the identification of conserved targets of Ab recognition and neutralization for the encephalitic alphaviruses that is useful for future diagnostic test, vaccine, and therapeutic development.

Materials and Methods

Human subject information

Human anti-EEEV mAbs were isolated from research subjects as described in chapter III. Written informed consent was given from the subjects and protocols were approved by the Institutional Review Board (IRB) at Vanderbilt University Medical Center for the recruitment and collection of blood samples used in this study.

Mouse model

C57BL/6 mice were purchased from Jackson Laboratories. All animal procedures were carried out in accordance with the recommendations in the Guide for the Care and Use of Laboratory Animals of the National Institutes of Health. The protocols were approved by the Institutional Animal Care and Use Committee at the Washington University School of Medicine (assurance no. A3381-01) and the Utah State University IACUC protocol #10025 (also described in chapter III).

Cell lines

BHK-21, Vero, HMMA 2.5, B95.8, and Expi293F cell lines were maintained as described in chapter III. ExpiCHO-S cells (hamster, female origin; Thermo Fisher Scientific) were maintained at 37ºC in a humidified atmosphere of 8% CO_2 in ExpiCHO Expression Medium (Thermo Fisher Scientific). Routine mycoplasma detection was

performed using a universal mycoplasma detection kit (ATCC). THP-1 (human, male origin; ATCC) human monocytic cells were maintained in RPMI-1640 (Sigma) containing 10% heat-inactivated FBS (Thermo Fisher Scientific) at 37ºC in a humidified atmosphere of 5% CO_2. HEK293T (human, female origin; ATCC) cells were grown at 37ºC in DMEM supplemented with 10% FBS, 10 mM HEPES pH 7.4, 1mM Na pyruvate, and 2mM L-alanyl-L glutamine.

Viruses

The chimeric viruses Sindbis virus (SINV; TR339)/Eastern equine encephalitis virus (EEEV; strain FL93-939) was described previously (Kim et al., 2019), SINV/Venezuelan equine encephalitis virus (VEEV; strain Trinidad Donkey), and SINV/Western equine encephalitis virus (WEEV; strain McMillian) were kindly provided by Dr. William B. Klimstra. Briefly, the structural proteins genes of SINV TR339 were replaced with the structural protein genes of EEEV (FL93-939), VEEV (Trinidad Donkey), and WEEV (McMillian) under control of the SINV 26S subgenomic promoter in the cDNA clone. CHIKV (strain 181/25; UTMB) and MAYV (strain TR VL-4675; UTMB) were obtained from the World Reference Center for Emerging Viruses and Arboviruses at UTMB as previously described (Powell et al., 2020). The CHIKV LR2006 OPY1 strain for animal studies was produced from an cDNA clone as described previously (Tsetsarkin et al., 2006). The EEEV FL93-939 strain for animal studies was obtained from Dr. Robert Tesh, World Reference Center for Emerging Viruses and Arboviruses

(University of Texas Medical Branch), Galveston, TX. The virus was passaged twice in Vero cells prior to use in mice.

Plasmids

The plasmid for recombinant EEEV E1 ectodomain (strain FL93-939; amino acids Y1-S409) was described in chapter III. EEEV subtype I (strains FL93-939, PE-6), MADV (formally EEEV subtypes II-IV [strains PE-3.0815, PE-0.0155, BeAr436087, Cebus/apella/BRA/BEAN5122/1956]), VEEV subtype IAB (strains Trinidad Donkey, TC-83), VEEV subtype IC (strain P676), VEEV subtype ID (strain 3880), VEEV subtype IE (strains Mena II, MX01-22), Mosso das Pedras virus (VEEV subtype IF [strain 78V-3531]), Everglades virus (VEEV subtype II [strain Fe3-7C]), Mucambo virus (VEEV subtype IIIA [strain BeAn 8]), VEEV subtype IIIC (strain 71D-1252), Pixuna virus (VEEV subtype IV [strain BeAr 35645]), Cabassou virus (VEEV subtype V [strain CaAr 508]), Rio Negro virus (VEEV subtype VI [strain Ag80-663]), WEEV (strain McMillian), WEEV (strain Fleming), WEEV (strain Ag80-646), and CHIKV (strain 181/25) structural protein genes (capsid-E3-E2-6K-E1) were codon-optimized, synthesized and cloned into the mammalian expression vectors pcDNA3.1(+) or pTwist CMV BetaGlobin for expression of the WT EEEV or the different alphavirus structural proteins, respectively. Residues Y1-H441 of the EEEV E1 structural protein were mutated to alanine or alanine residues to serine for expression of the EEEV E1 mutants for alanine-scanning mutagenesis library analyses. Recombinant human anti-EEEV variable genes were synthesized and

cloned into either a pTwist CMV Betaglobin WPRE Neo mammalian expression vector containing the IgG1-specific constant region or a monocistronic vector, pTwist_mCis_hG1 (Zost et al., 2020) (Twist Bioscience Inc).

Recombinant proteins

Recombinant EEEV E2 glycoprotein (strain v105), CHIKV E1 protein, and EEEV virus-like particles (VLPs) were described in chapter III. Recombinant MAYV E1 protein was purchased from Meridian Life Science. VEEV and WEEV VLPs were kindly provided by Dr. John Mascola at the NIH/NIAID Vaccine Research Center (Ko et al., 2019).

Virus production

SINV/EEEV production was described in chapter III. For SINV/VEEV, SINV/WEEV, or MAYV, BHK-21 cells were inoculated at a MOI of 0.2 in DMEM/2% FBS/10 mM HEPES. After incubation at 37°C 5% CO_2 for 48 hours, virus was harvested by clarification of infected BHK-21 cell supernatants through a 0.2-μm pore size filter (Nalgene). Virus then was used fresh or stored at -80 °C until use. CHIKV was kindly provided from Dr. Michael S. Diamond's laboratory.

Recombinant EEEV E1 ectodomain expression

EEEV E1 ectodomain was produced as described in chapter III.

Human hybridoma and mAb generation

Human mAbs were generated as described in chapter III. The humanized WNV E16 mAb has been described previously (Oliphant et al., 2005) and was purified by protein A affinity chromatography.

5′ RACE nucleotide sequence analysis

Ab heavy and light-chain variable region genes were sequenced on a Pacific Biosciences Sequel system platform as described in chapter III. Gene segments and germline mutations were determined using the IMGT database or PyIR software (Soto et al., 2020).

Recombinant human IgG1 production

Recombinant human anti-EEEV mAbs were produced as described in chapter III using the ExpiFectamine 293 transfection kit (Gibco). rDENV-2D22 was produced as

previously descrbied (Zost et al., 2020) using the ExpiCHO Expression System (Gibco). Cell supernatant was purified through HiTrap MabSelect SuRe (Cytiva Life Sciences) according to the manufacturer's protocol on an ÄKTA pure 25M chromatography system. Abs were processed as described for hybridoma mAb generation above.

Protein EC_{50} ELISA

Recombinant EEEV E3E2/E2 glycoprotein (strain V105; IBT Bioservices), EEEV E1 ectodomain (strain FL93-939), CHIKV E1 protein (Meridian Life Science), MAYV E1 protein (Meridian Life Science) or EEEV, VEEV, WEEV virus-like particles (VLPs) were diluted to 2 µg/mL in 1× D-PBS to coat 384-well ELISA plates (Thermo Fisher Scientific) and incubated at 4°C overnight. A protein screening ELISA was performed as described above. However, instead of hybridoma supernatant, purified mAb was diluted to 10 µg/mL in blocking solution (1% non-fat dry milk, 1% goat serum in 1× D-PBS-T) and incubated for 2 hours at room temperature. For temperature-dependent binding ELISA, purified mAb was incubated with respective antigen for 1 hour at room temperature (~22°C), 37°C, or 42°C in blocking solution (1% non-fat dry milk, 1% goat serum in 1x D-PBS). For pH-dependent binding ELISA, purified mAb was incubated with respective antigen for 1 hour at room temperature in 1× D-PBS pH 5.4 or 7.4. Additionally, for temperature- and pH-dependent binding ELISAs, all wash and incubation steps were performed with 1× D-PBS and a suspension of secondary Abs (goat anti-human kappa-HRP (Southern Biotech) and goat anti-human lambda-HRP (Southern Biotech)) at a

1:4,000 dilution in blocking solution (1% non-fat dry milk, 1% goat serum in 1x D-PBS) was added for 1 hour at room temperature. One-step Ultra-TMB ELISA substrate solution (Thermo Fisher Scientific) was added and incubated at room temperature for 10-30 minutes. The reaction was stopped with 1N HCl (Thermo Fisher Scientific) and then read at an optical density of 450 nm with a Biotek™ plate reader.

Cell surface display alphavirus subtype binding

Transient transfection of Expi293F cells with plasmids (pcDNA3.1(+)) containing the structural proteins (capsid-E3-E2-6K-E1) of EEEV subtype I (strains FL93-939, PE-6), MADV (formally EEEV subtypes II-IV [strains PE-3.0815, PE-0.0155, BeAr436087, Cebus/apella/BRA/BEAN5122/1956]), VEEV subtype IAB (strains Trinidad Donkey, TC-83), VEEV subtype IC (strain P676), VEEV subtype ID (strain 3880), VEEV subtype IE (strains Mena II, MX01-22), Mosso das Pedras virus (VEEV subtype IF [strain 78V-3531]), Everglades virus (VEEV subtype II [strain Fe3-7C]), Mucambo virus (VEEV subtype IIIA [strain BeAn 8]), VEEV subtype IIIC (strain 71D-1252), Pixuna virus (VEEV subtype IV [strain BeAr 35645]), Cabassou virus (VEEV subtype V [strain CaAr 508]), Rio Negro virus (VEEV subtype VI [strain Ag80-663]), WEEV (strain McMilian), WEEV (strain Fleming), WEEV (strain Ag80-646), or CHIKV (strain 181/25) was performed using the ExpiFectamine 293 transfection kit (Gibco) according to the manufacturer's protocol as previously described (Williamson et al., 2020). Cells were incubated at 37°C in a humidified atmosphere of 8% CO_2 and harvested 24 hours after transfection via

centrifugation at 400 x *g* for 5 minutes. Cells were resuspended in Expi293F expression medium (Gibco) and 10% DMSO for storage at -80°C and/or in the vapor phase of liquid nitrogen. Untransfected Expi293F cells served as a negative control for non-specific mAb binding and were used fresh following incubation at 37°C in a humidified atmosphere of 8% CO_2 at 125 rpm. For analysis of mAb binding, cryopreserved cells were thawed and washed twice with FACS buffer (1x D-PBS, 2% FBS, 2 mM EDTA). Cells were plated at 25,000-50,000 cells/well in 96-well V-bottom plates (Corning). Anti-EEEV or anti-alphavirus E1-specific mAbs, positive control mAbs: 1A4B-6 (alphavirus group-reactive (Millipore)), rEEEV-97 IgG (Williamson et al., 2020), 1A3B-7 (VEEV E2-specific (Millipore)), 2A3D-5 (WEEV E1-specific (Millipore)), or the irrelevant mAb negative control, rDENV-2D22, were diluted to 10 µg/mL in FACS buffer and incubated with the cells for 30 minutes at 4°C. Cells were washed with FACS buffer and then incubated with secondary Abs (anti-human IgG-PE (Southern Biotech) or anti-mouse IgG-PE (Southern Biotech)) diluted 1:1,000 in FACS buffer for 30 minutes at 4°C. Cells were washed with FACS buffer and resuspended in 1:1,000 dilution of DAPI stain in FACS buffer at 25 to 30 µL/well. Number of events were collected on an IntelliCyt® iQue Screener PLUS flow cytometer (Sartorius). For analysis, binding of the mAb to untransfected Expi293F was subtracted to account for any non-specific mAb binding. Fold change for mAb binding to the different alphavirus subtypes was calculated by normalization of the median fluorescence relative to the irrelevant negative control mAb, rDENV-2D22.

Competition-binding ELISA

EEEV virus-like particles (VLPs) were diluted to 2 μg/mL in 1x D-PBS to coat 384-well plates (Thermo Fisher Scientific) and incubated at 4°C overnight. The plates were aspirated and blocked for 1 hour at room temperature with blocking solution (2% non-fat dry milk, 2% goat serum in 1× D-PBS-T). After blocking, the plates then were washed 3× with 1× D-PBS-T and the first Ab (10 μg/mL) in blocking solution (1% non-fat dry milk, 1% goat serum in 1x D-PBS-T) was added at 20 μL/well for 1 hour at room temperature. Biotinylated second Ab (2.5 μg/mL; final concentration of 0.5 μg/mL) was added in blocking solution (1% non-fat dry milk, 1% goat serum in 1× D-PBS-T) at 5 μL/well for 1 hour at room temperature. The plates then were washed 3× with 1x D-PBS-T and incubated with a solution of secondary Abs (mouse anti-biotin-HRP (Southern Biotech)) diluted 1:4,000 in blocking solution 1% non-fat dry milk, 1% goat serum in 1× D-PBS-T) for 1 hour at room temperature. The plates then were washed 4× with 1× D-PBS-T followed by addition of One-step Ultra-TMB ELISA substrate solution (Thermo Fisher Scientific). The reaction was stopped with 1N HCl (Thermo Fisher Scientific) and then read at an optical density of 450 nm with a Biotek™ plate reader. Percent binding of each Ab was normalized to optical density value for binding in the presence of the irrelevant negative control mAb, rDENV-2D22. Full, intermediate, or no competition of binding was defined as described above.

Alanine-scanning mutagenesis analysis

Analysis of anti-EEEV and anti-alphavirus mAb binding to WT EEEV (strain FL93-939) and EEEV E1 mutant structural proteins (capsid-E3-E2-6K-E1) was performed as described in chapter III. Residues were selected for analysis based on previously described epitopes within the Immune Epitope Database. Briefly, the WT and E1 mutant structural proteins were expressed through transient transfection of Expi293F cells according to the manufacturer's protocol. Cells were harvested 24 hours after transfection, stained with LIVE/DEAD™ Fixable Violet Dead Cell Stain Kit (Invitrogen™), and fixed with 1% PFA/PBS. Cells were washed twice with 1× D-PBS and stored at 4°C in FACS buffer until use. Cells were plated at 50,000 cells/well in 96-well V-bottom plates (Corning). Anti-EEEV, anti-alphavirus E1-specific mAbs, or the irrelevant mAb negative control, rDENV-2D22, were diluted to either 1, 0.5, 0.1 µg/mL in FACS buffer and incubated with the cells for 1 hour at 4°C. Cells were washed with FACS buffer and then incubated with secondary Abs (goat anti-human IgG-PE (Southern Biotech) or a mixture of goat anti-human kappa-PE or goat anti-human lambda-PE (Southern Biotech) diluted 1:1,000 in FACS buffer for 1 hour at 4°C. Cells were washed with FACS buffer and resuspended in 30 µL/well FACS buffer. Number of events were collected on an IntelliCyt® iQue Screener PLUS flow cytometer (Sartorius). Mock transfected Expi293F cells were included as a negative control to subtract background mAb binding to Epxi293F cells. Percent binding of each mAb to the E1 mutants was normalized to the WT EEEV structural protein control. Anti-alphavirus mAb or Fabs were screened at

1 μg/mL for binding to WT CHIKV and CHIKV E2/E1 mutant constructs expressed in HEK 293T cells with binding detected by flow cytometry as previously described (Fong et al., 2014). Ab reactivity against each mutant protein clone was calculated relative to WT protein reactivity by subtracting the signal from mock-transfected controls and normalizing to the signal from WT-transfected controls.

Focus forming assay (FFA)

Virus titration was performed as described in chapter III. However, in addition, immune EEEV, VEEV, WEEV, CHIKV, or MAYV ascites fluid (ATCC) at 1:6,000 dilution in 1× Perm Wash was added to the plates following 1% PFA fixation, 3× 1× D-PBS washes, and incubation with 1× Perm Wash (1× D-PBS, 0.1% saponin (Sigma-Aldrich), 0.1% BSA (Sigma-Aldrich)).

Temperature-dependent focus reduction neutralization test (FRNT)

Neutralization activity of anti-EEEV and anti-alphavirus E1-specific mAbs was performed as described in chapter III. For temperature-dependent FRNT, a FFA was performed as described above. However, prior to addition of virus to cells, purified mAb was diluted to 20 μg/mL (final concentration 10 μg/mL) and serially diluted three-fold in DMEM/2% FBS/10 mM HEPES. MAb-only dilutions were separated to serve as a negative control. Virus then was diluted to 2,000 FFU/mL (~50 to100 FFU/well) in

DMEM/2% FBS/10 mM HEPES and added to the mAb serial dilutions. The mAb:virus mixture was incubated at 37°C or 42°C in 5% CO_2 for 1 hour. After cells were washed 2× with 1× D-PBS, the mAb:virus mixture was then added to the cells and incubated at 37°C in 5% CO_2 for 1.5 hours. A 2% methylcellulose:2× DMEM or 2× EMEM:4% FBS:20 mM HEPES overlay was then added to the cells and incubated at 37°C in 5% CO_2 for 18 hours. Plates were fixed and immunostained as described for FFA.

Egress inhibition assay

BHK-21 cells were plated in 12-well plates (Corning) at 3 x 10^5 cells/well in DMEM/5% FBS/10 mM HEPES at 800 µL/well. Cells were incubated at 37°C in 5% CO_2 overnight. SINV/EEEV was diluted to MOI 1 in DMEM/2% FBS/10 mM HEPES and added to cells for incubation at 37°C in 5% CO_2 for 2 hours. Cells then were washed 5x with DMEM/2% FBS/10 mM HEPES followed by a wash with DMEM/2% FBS/10 mM HEPES/25 mM NH_4Cl. Purified mAb was diluted to 10 µg/mL in DMEM/2% FBS/10 mM HEPES/25 mM NH_4Cl and added to cells at 37°C in 5% CO_2 for up to 6 hours. Supernatant was harvested following 1 hour and 6 hours incubation period. Virus presence was determined through FFA at 37°C for 1 hour as described above.

Ab-dependent cellular phagocytosis (ADCP) assay

The ADCP assay was adapted from Ackerman et al. 2011. Briefly, antigen was biotinylated using sulfo-NHS LC-LC biotin, coupled to yellow-green, fluorescent Neutravidin 1 µm beads (Invitrogen™) for 2 hours at 37°C and washed two times in 0.1% BSA in PBS. 10 µL/well of coupled beads were added to 96-well plates with 100 µL/well of Abs at a concentration of 5, 1, 0.2, 0.04, 0.008 or 0.0016 µg/mL for 2 hours at 37°C to form immune complexes. After incubation, the immune complexes were spun down and the supernatant was removed. THP-1 cells were added at a concentration of 2.5 x 10^4 cells/well and incubated for 18 hours at 37˚C. After incubation, the plates were spun down, the supernatant was removed, and cells were fixed with 4% PFA for 10 minutes. Fluorescence was acquired with an Intellicyt iQue Screener. Phagocytic score was calculated using the following formula: (percentage of FITC+ cells) * (the geometric mean fluorescent intensity (gMFI) of the FITC+ cells)/10,000.

Ab-dependent neutrophil phagocytosis (ADNP) assay

The ADNP assay was adapted from Karsten et al. 2019. Antigens were coupled to beads and immune complexes were formed as described for ADCP. Neutrophils were isolated from fresh whole blood. Erythrocytes were lysed with ammonium-chloride potassium (ACK) lysis buffer (150 mM NH_4Cl, 10 mM $KHCO_3$, 0.1 mM Na_2EDTA, pH 7.4) and leukocytes were separated out by centrifugation. Leukocytes were washed with cold PBS, resuspended in R10, and added to plates at a concentration of 5 x 10^4 cells/well. The plates were incubated for 1 hour at 37°C. The neutrophil marker CD66b

(Pacific Blue conjugated anti-CD66b; BioLegend) was used to stain cells. Cells were fixed for 10 minutes in 4% PFA. Fluorescence was acquired with an Intellicyt® iQue Screener and phagocytic score was calculated as described for ADCP.

Ab-dependent complement deposition (ADCD) assay

The ADCD assay was adapted from Fischinger et al. 2019. Antigen was coupled to red fluorescent Neutravidin 1 µm beads (Invitrogen™) as described for ADCP. Immune complexes were formed by incubating 10 µL of coupled beads with 50 µL of antibody at concentrations of 100, 20, 4, 0.8, 0.16 or 0.032 µg/mL for 2 hours at 37°C. Plates were spun down, and immune complexes were washed with PBS. Lyophilized guinea pig complement (Cedarlane) was resuspended in 1 mL of cold water, diluted 1:50 in GVB^{++} (gelatin veronal buffer and additional Ca^{2+} and Mg^{2+}, Boston BioProducts) and added to the immune complexes. The plates were incubated for 20 minutes at 37°C and the reaction was stopped by washing the plates twice with 15 mM EDTA in PBS. To detect complement deposition, plates were incubated with fluorescein-conjugated goat anti-guinea pig complement C3 (MP Biomedicals) for 15 minutes in the dark. Fluorescence was acquired with an Intellicyt® iQue Screener.

Ab-dependent NK cell activation (NK activation)

Human NK cells were isolated from buffy coats using RosetteSep NK cell enrichment kit (StemCell Technologies) and Ficoll separation. The isolated NK cells were rested overnight at 1.5 x 10^6 cells/mL in IL-15 at 37°C. ELISA plates were coated with antigen at 300 ng/well and incubated for 2 hours at 37˚C. Plates were blocked with 5% BSA in PBS overnight at 4°C. The next day, 100 µL of Abs at a concentration of 5, 1 or 0.2 µg/mL, were added to the plates. Plates were incubated for 2 hours at 37°C to form immune complexes. After the incubation, NK cells were added to the plates at 5 x 10^4 cells/well in R10 supplemented with anti-CD107a PE-Cy5, BFA and GolgiStop (BD Biosciences). Plates were incubated for 5 hours at 37°C. Following the incubation, NK cells were stained for surface markers with anti-CD56 PE-Cy7, anti-CD16 APC-Cy7 and anti-CD3 Pacific Blue (BD Biosciences). NK cells were fixed and permeabilized with Fix & Perm cell permeabilization kit (Invitrogen™). Cells were incubated with anti-MIP1b PE and anti-IFNg FITC (BD Biosciences) to stain for intracellular markers. Cells were acquired on an Intellicyt® iQue Screener.

Mouse s.c. challenge with EEEV

Mice were challenged with EEEV via bilateral s.c. injections. Animals were treated with antibodies at doses of 10 mg/kg or 100 µg/kg via a single i.p. injection 24 hours post-virus challenge. Animals were monitored until 21 days post-virus inoculation (dpi) for disease signs and survival. Individual weights were recorded daily 0-10 dpi and

on 14 and 18 dpi. Serum was collected from all mice 3 dpi for assessment of serum viremia.

EEEV infectious cell culture assay

Virus titer was quantified using an infectious cell culture assay where a specific volume of either tissue homogenate or serum was added to the first tube of a series of dilution tubes. Serial dilutions were made and added to Vero cells. Three days later cytopathic effect (CPE) was used to identify the endpoint of infection. Four replicates were used to calculate the 50% cell culture infectious doses ($CCID_{50}$) per mL of plasma or gram of tissues.

Mouse s.c. challenge with CHIKV

C57BL/6 mice were housed in groups of up to 5 mice per cage. Age- and sex-matched male mice were inoculated s.c. in the footpad with 10^3 FFU of CHIKV 4 weeks of age. Joint swelling was measured using a digital caliper as described previously (Fox et al., 2019).

Measurement of CHIKV burden

CHIKV-infected mice were euthanized at 6 dpi and perfused extensively with 20 mL of PBS. Tissues were harvested, weighed, and homogenized with zirconia beads in a MagNA Lyser instrument (Roche Life Science) in 500 µL of DMEM media supplemented with 2% heat inactivated FBS. All tissue homogenates were clarified by centrifugation at 10,000 rpm for 5 min and stored at -80˚C. RNA was extracted using an Applied Biosystems 5x MagMax RNA v96 viral isolation kit (Thermo Fisher Scientific) and a Kingfisher duo prime extraction machine (Thermo Fisher Scientific). CHIKV RNA levels were determined by one-step quantitative reverse transcriptase PCR (qRT-PCR) using an Applied Biosystems Taqman RNA-to-Ct 1-step kit (Thermo Fisher Scientific) on an ABI 7500 Fast Instrument using standard cycling conditions and previously designed primer/probe sets for CHIKV (Fox et al., 2015). Viral burden was expressed on a $\log_{10}$ scale as CHIKV RNA equivalents per gram or mL after comparison with a standard curve produced using RNA isolated from viral stocks as a standard curve to determine FFU equivalents, as previously described (Fox et al., 2019).

Quantification and Statistical Analysis

Details about statistical analyses can be found in the figure legends. Half-maximal effective concentration (EC_{50}) and half-maximal inhibitory concentration (IC_{50}) values were determined after log transformation of concentration values and non-linear regression analysis using sigmoidal dose-response (variable slope). One-way ANOVA with Dunnett's multiple comparisons test was used to compare virus titer in the serum of

EEEV inoculated mice (**p<0.01, *p<0.05). Joint swelling in the CHIKV mouse model was compared using a two-way ANOVA with Dunnett's multiple comparisons test (***p<0.001, ****p<0.0001). CHIKV RNA levels were analyzed with a one-way ANOVA with Dunnett's multiple comparisons test (**p<0.01, ***p<0.001). Survival curves were compared using the log-rank test with Bonferroni multiple comparison correction (*p<0.05, ****p<0.0001). Statistical analyses were performed with GraphPad Prism v8.

Supplemental Information

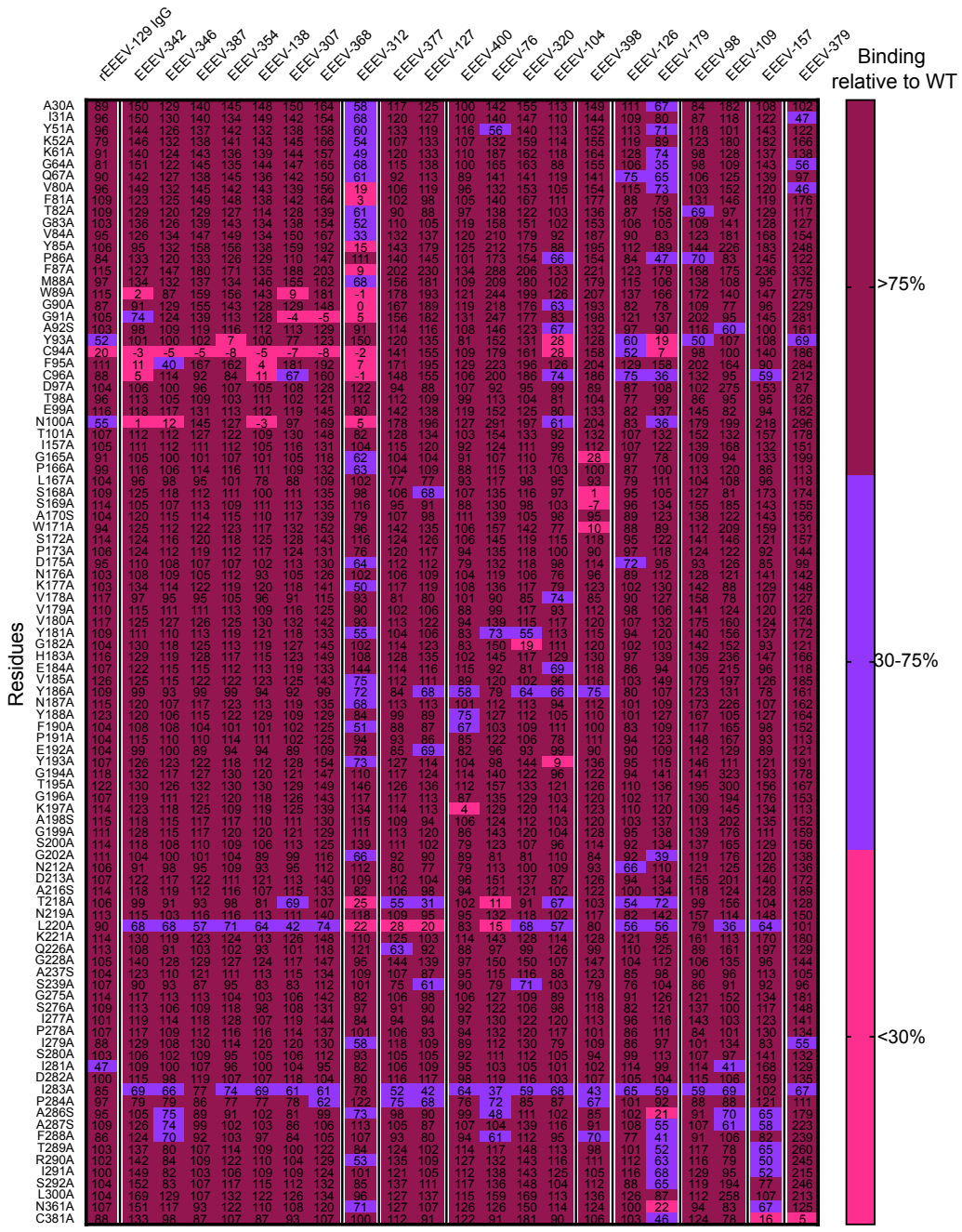

Figure 55. EEEV E1 glycoprotein alanine-scanning mutagenesis library analysis of human anti-EEEV and anti-alphavirus E1-specific mAbs. Heatmap of the EEEV E1 glycoprotein alanine mutant residues tested for human E1-specific mAbs. Residues were selected for analysis based on previously described epitopes within the Immune Epitope Database. The average percent binding is displayed as a heatmap with maroon (>70%), light blue (30-70%), or magenta (<30%) binding relative to WT. Residues are colored based on E1 domain or region (orange [domain I], purple [domain II, fusion loop]), cyan [domain II], or red [domain I/III linker or domain III]). Each mAb is ordered to correspond with the competition-binding groups as defined in **A** and residues identified for EEEV-312 or EEEV-379.

CHAPTER V

CHARACTERIZATION OF NON-NEUTRALIZING HUMAN ANTI-ALPHAVIRUS E2-SPECIFIC MONOCLONAL ANTIBODIES

Introduction

Chapters III and IV describe neutralizing human anti-EEEV E2-specific (chapter III) and neutralizing or non-neutralizing human anti-EEEV or anti-alphavirus E1-specific mAbs (chapter IV), respectively. For E2-specific mAbs, neutralization activity usually corresponds with protection (Mendoza et al., 1988). However, non-neutralizing mAbs can protect against alphaviruses (*i.e.*, VEEV, SINV, SFV) in animal models (chapters I and IV; Mendoza et al., 1988; Boere et al., 1984; Griffin, 1995). Furthermore, immunization with synthetic peptides of the N-terminus and C-terminus (residues 241-265) sequence of the VEEV E2 glycoprotein were found to elicit a non-neutralizing, protective Ab response against VEEV (Trinidad Donkey strain; subtype IAB) i.p. challenge in mice (Roehrig et al., 1991; Hunt et al., 1990; Hunt and Roehrig, 1995; Johnson et al., 1991). Further isolation of a murine mAb (1A2B-10) to the E2 N-terminus synthetic peptide (Roehrig et al., 1991), passively protected mice from VEEV (subtypes IAB, IC, and ID) challenge and was immunogenic in horses (Hunt and Roehrig, 1995).

An E2 peptide (residues 297-352) also elicited protective mAbs against SINV and SFV (Grosfeld et al., 1989; Grosfeld et al., 1992). Thus, regions of the E2 glycoprotein can induce an immune response that does not neutralize virus particles *in vitro* but may have Ab mediated mechanisms of action *in vivo*.

In addition to neutralizing activity, mAbs can induce Fc-mediated effector functions to aid in protection. This was shown for neutralizing murine anti-MAYV mAbs, in which protection did not depend on neutralizing activity but instead on the Fc domain. Regardless of neutralizing activity, reduced efficacy of mAb mediated protection in *FcγR*$^{-/-}$ mice against lethal and musculoskeletal foot swelling MAYV-induced disease. Protection was also shown to be dependent on mAb isotype and glycosylation at N297 (Earnest et al., 2019). These studies highlight the importance of Fc-mediated effector function for protection against alphaviruses.

An understanding of the non-neutralizing E2-specific mAb mediated mechanism(s) of action is lacking. To address this, I isolated a panel of thirty-nine non-neutralizing human E2-specific mAbs as described in chapter III. For this panel, I performed initial characterization studies to describe the binding reactivity, breadth, and relative epitope groups recognized by these mAbs on the EEEV E2 glycoprotein. Further characterization of this panel, however, is needed to describe the mAb mediated mechanism(s) of action for non-neutralizing human E2-specific mAbs.

For the collaborative work performed in this chapter, I would like to acknowledge Dr. William B. Klimstra's laboratory (*i.e.*, Theron Gilliland, Jr.) for performing the EEEV prophylactic and therapeutic aerosol challenge animal studies for a non-neutralizing

mAb, EEEV-30. I would also like to thank members of the iCore and TechCore teams in Dr. Crowe's laboratory for assistance with mAb expression and purification, and mAb or antigen sequencing, respectively.

Isolation of non-neutralizing human anti-alphavirus mAbs

The panel of non-neutralizing human mAbs isolated as described in chapter III was identified through a screen for potential neutralizing activity against SINV/EEEV. I tested each mAb for neutralization activity against SINV/EEEV at 10 μg/mL via FRNT and assigned neutralization activity to the mAbs tested as an arbitrary cutoff of a less than 30% reduction in relative infectivity. An example of neutralization activity against SINV/EEEV is shown for the positive control mAb, rEEEV-33 IgG, in red (**Figure 56** and chapter III). The panel of human mAbs tested discussed here did not display neutralization activity against SINV/EEEV since the relative infectivity of SINV/EEEV was >30%.

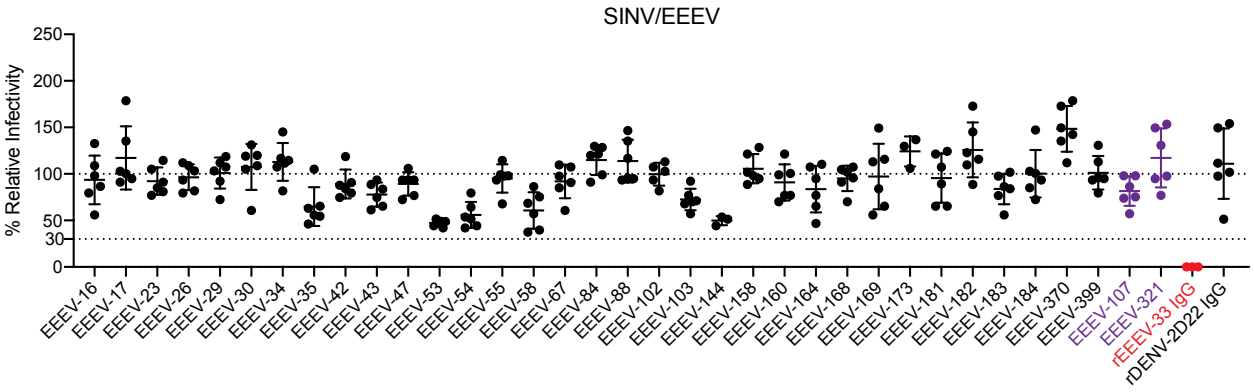

Figure 56. Non-neutralizing activity of human mAbs against SINV/EEEV. Each mAb is labeled on the x-axis and % relative SINV/EEEV infectivity is shown by the y-axis. The bottom dotted line represents an arbitrary cutoff for 30% reduction in relative SINV/EEEV infectivity and the top dotted line represents 100% relative SINV/EEEV infectivity. A positive control mAb, rEEEV-33 IgG, shown in red was included to display neutralization activity against SINV/EEEV. A negative control DENV-specific mAb, rDENV-2D22 IgG, was also included. Cross-reactive mAbs are shown in purple.

Binding reactivity of non-neutralizing human anti-EEEV E2-specific mAbs

To define binding reactivity of the non-neutralizing human E2-specific mAbs, I assessed binding to SINV/EEEV particles and recombinant EEEV E2 glycoprotein (**Table 8**). Binding to recombinant EEEV or CHIKV E1 glycoproteins was not detected. The ratio of virus/protein half-maximal EC_{50} values for binding was determined (**Table 8**) to identify differences in reactivity of mAbs recognizing epitopes more accessible on the recombinant E2 glycoprotein or virion particle-specific epitopes. A majority of the mAbs bound strongly to recombinant E2 glycoprotein by ELISA (<100 pM [<30 ng/mL] EC_{50} values). Weaker binding to SINV/EEEV particles compared to recombinant EEEV E2 glycoprotein as described by a virus/protein EC_{50} ratio of >1 suggests the epitope may

be less accessible on the surface of intact virion particles. This may contribute to the non-neutralizing activity for this panel of human E2-specific mAbs due to inability to strongly bind intact virion particles.

Group	EEEV mAb	Isotype (HC, LC)	Virus/Protein EC_{50} Ratio	EC_{50} (pM)	
				SINV/EEEV particles	EEEV E2 glycoprotein
1	EEEV-81	IgG3, λ	0.8	5.6	7.5
2	EEEV-399	IgG1, κ	1.3	20.2	15.5
	EEEV-42	IgG1, κ	1.4	31.0	22.8
	EEEV-169	IgG1, κ	1.6	40.5	26.0
	EEEV-68	IgA1, κ	1.7	111.4	65.0
	EEEV-164	IgG1, κ	1.8	412.0	234.3
	EEEV-183	IgG1, λ	1.9	33.1	17.6
	EEEV-53	IgG1, λ	2.1	32.9	15.6
	EEEV-158	IgA1, λ	2.5	3,463	1,388
	EEEV-17	IgG1, λ	2.7	33.9	12.7
	EEEV-54	IgG1, κ	3.1	25.0	8.2
	EEEV-168	IgG1, λ	3.2	65.0	20.4
	EEEV-180	IgG1, κ	3.3	35.9	10.8
	EEEV-16	IgG3, λ	3.4	44.7	13.0
	EEEV-182	IgG1, κ	3.5	38.7	11.2
	EEEV-58	IgG1, λ	3.7	29.1	7.9
	EEEV-370	IgG1, ND	3.9	100.1	25.9
	EEEV-43	IgG1, λ	4.0	28.3	7.0
	EEEV-55	IgG1, λ	4.0	52.8	13.2
	EEEV-181	IgG1, λ	4.2	25.1	6.0
	EEEV-184	IgG1, κ	4.2	57.6	13.8
	EEEV-173	IgG1, κ	4.6	46.8	10.1
	EEEV-102	ND	4.7	38.3	8.1
	EEEV-103	IgG1, κ	4.8	139.1	29.1
	EEEV-30	IgG1, λ	4.9	89.4	18.2
3	EEEV-26	IgG1, λ	5.8	59.3	10.2
	EEEV-29	IgG1, κ	6.1	46.1	7.6
	EEEV-67	IgG1, λ	6.2	108.1	17.5
	EEEV-144	IgG1, κ	6.4	2,269	354.3
	EEEV-35	IgG1, κ	6.5	103.4	15.8
	EEEV-23	IgG1, λ	6.9	121.3	17.5
	EEEV-153	IgG1, κ	7.1	112.6	15.9
	EEEV-84	IgG1, κ	9.0	379.7	42.3
4	EEEV-88	IgG1, λ	14.5	1,142	78.7
	EEEV-47	IgG1, κ	17.1	1,626	95.1
	EEEV-34	IgG1, κ	32.0	514.7	16.1
5	EEEV-160	IgG1, κ	>	>	132.6

Table 8. EC_{50} values (pM) for non-neutralizing human anti-EEEV E2-specific mAbs to SINV/EEEV particles or recombinant EEEV E2 glycoprotein. No binding to EEEV E1 or CHIKV E1 glycoproteins was detected under the conditions assessed via ELISA. Each mAb is ordered based on virus/protein EC_{50}

ratio and grouped accordingly by decreasing depth in green color (group 1 = <1 (virus > protein); group 2 = 1-5 (virus ≈ protein); group 3 = 5-10 (protein > virus); group 4 = 10-50 (protein >> virus); group 5 = >50 (protein >>> virus) virus/protein EC_{50} ratio). EC_{50} values are colored by decreasing depth in blue color (<33.3 pM [dark blue]; 33.4-333.3 pM [blue]; 333.4-3,333.3 pM [light blue]; 3,333.4-5,000 pM [lightest blue]; >5,000 pM [>]). Isotype is indicated for heavy chain as either IgG1, IgG3, or IgA1 and light chain as either κ or λ.

EEEV-107 and EEEV-321 cross-reactive with EEEV and VEEV

In addition to the panel of non-neutralizing EEEV-specific E2-specific mAbs, two mAbs. EEEV-107 and EEEV-321, cross-reacted with EEEV and VEEV VLPs or subtypes assessed via ELISA or antigen cell surface display methods, respectively (**Figure 57**). EEEV-107 and EEEV-321 bound with similar binding strength to EEEV and VEEV VLPs but strongly bound recombinant EEEV E2 glycoprotein compared to virus-particles. This suggests recognition of a conserved cryptic epitopes by these mAbs. Broad binding breadth for EEEV-107 and EEEV-321 was observed to the EEEV and VEEV subtypes tested. EEEV-321 recognized a greater number of alphavirus subtypes compared to EEEV-107. Further analysis through competition-binding studies is warranted to assess whether EEEV-107 and EEEV-321 recognize a conserved cross-reactive site on the E2 glycoprotein. However, differences in binding breadth between the two mAbs suggests two distinct epitopes are recognized by these mAbs.

A

EEEV mAb	Isotype (HC, LC)	EC_{50} (ng/mL)				
		SINV/EEEV particles	EEEV VLP	VEEV VLP	WEEV VLP	EEEV E2 glycoprotein
EEEV-107	IgG1,λ	26.6	46.1	14.2	>	2.9
EEEV-321	IgG1,λ	112.7	30.1	15.5	>	4.1

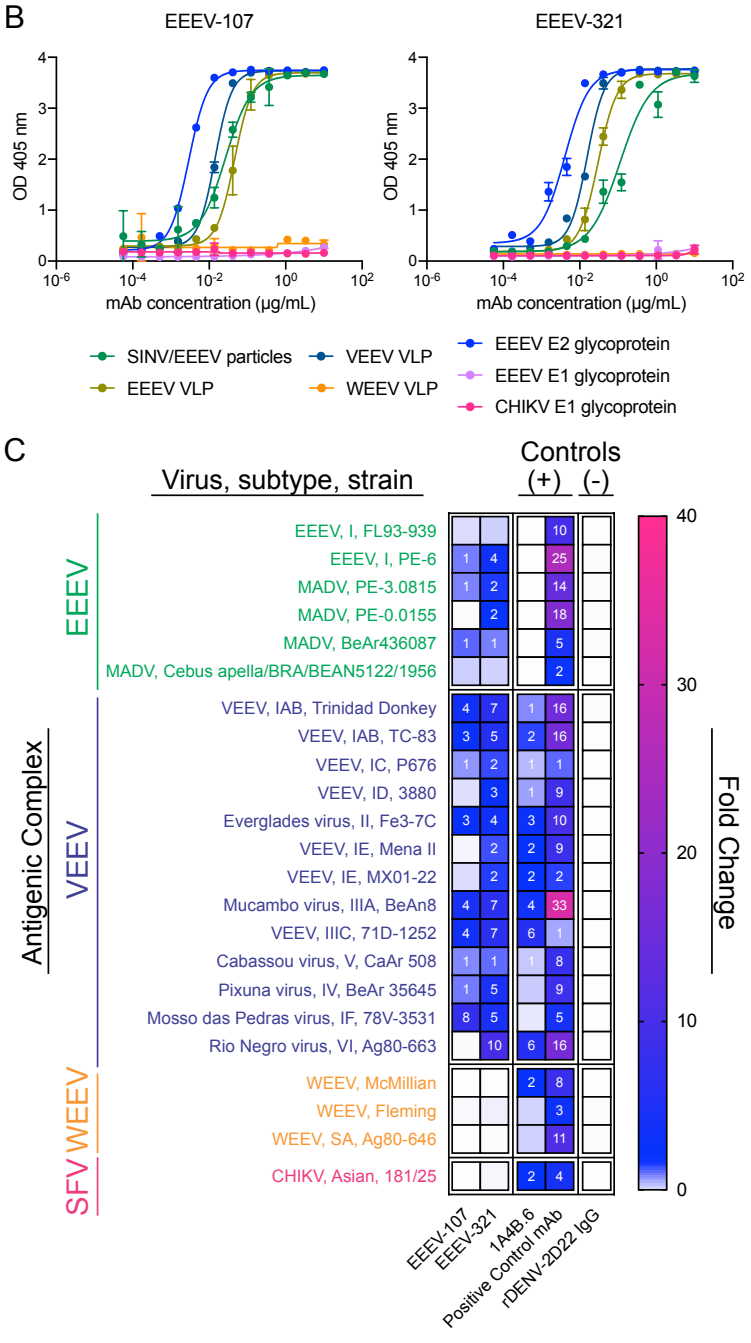

Figure 57. Binding profile of cross-reactive human anti-alphavirus E2-specific mAbs. A. EC_{50} values (ng/mL) for EEEV-107 and EEEV-321 binding to E2 antigens on EEEV or VEEV virus or virus-like particles and the E2 glycoprotein. **B.** Representative binding curves for EEEV-107 and EEEV-321 binding

to respective antigens (SINV/EEEV particles – green; EEEV VLP – light green; VEEV VLP- dark blue; WEEV VLP – orange; EEEV E2 glycoprotein – blue; EEEV E1 glycoprotein – pink; CHIKV E1 glycoprotein – magenta. **C.** EEEV-107 and EEEV-321 binding breadth to EEEV (green) and VEEV (blue) subtypes. Fold change is shown by the heat map to display strength in binding to the different alphavirus subtypes evaluated (EEEV – green; VEEV – blue; WEEV – orange; SFV – pink). Fold change indicates mAb binding to respective subtype relative to rDENV-2D22 IgG. mAb binding to untransfected Expi293F cells relative to rDENV-2D22 IgG was subtracted from subtype specific mAb binding.

Non-neutralizing antigenic determinants on the EEEV E2 glycoprotein

To determine the antigenic determinants recognized by non-neutralizing human anti-EEEV E2-specific mAbs, I performed competition-binding analyses via biolayer interferometry (BLI) with EEEV E2 glycoprotein (**Figure 58**). Neutralizing human anti-EEEV E2 domains A, B, and A/B were used as controls to aid in identification of the relative epitopes recognized by the panel of non-neutralizing human E2-specific mAbs. Interestingly, the non-neutralizing mAbs did not compete with the neutralizing mAbs. This suggests recognition of distinct antigenic sites recognized by these mAbs and may contribute to the lack of neutralization activity observed for these mAbs. Further epitope mapping studies are warranted to determine the epitopes that do not elicit neutralizing phenotypes.

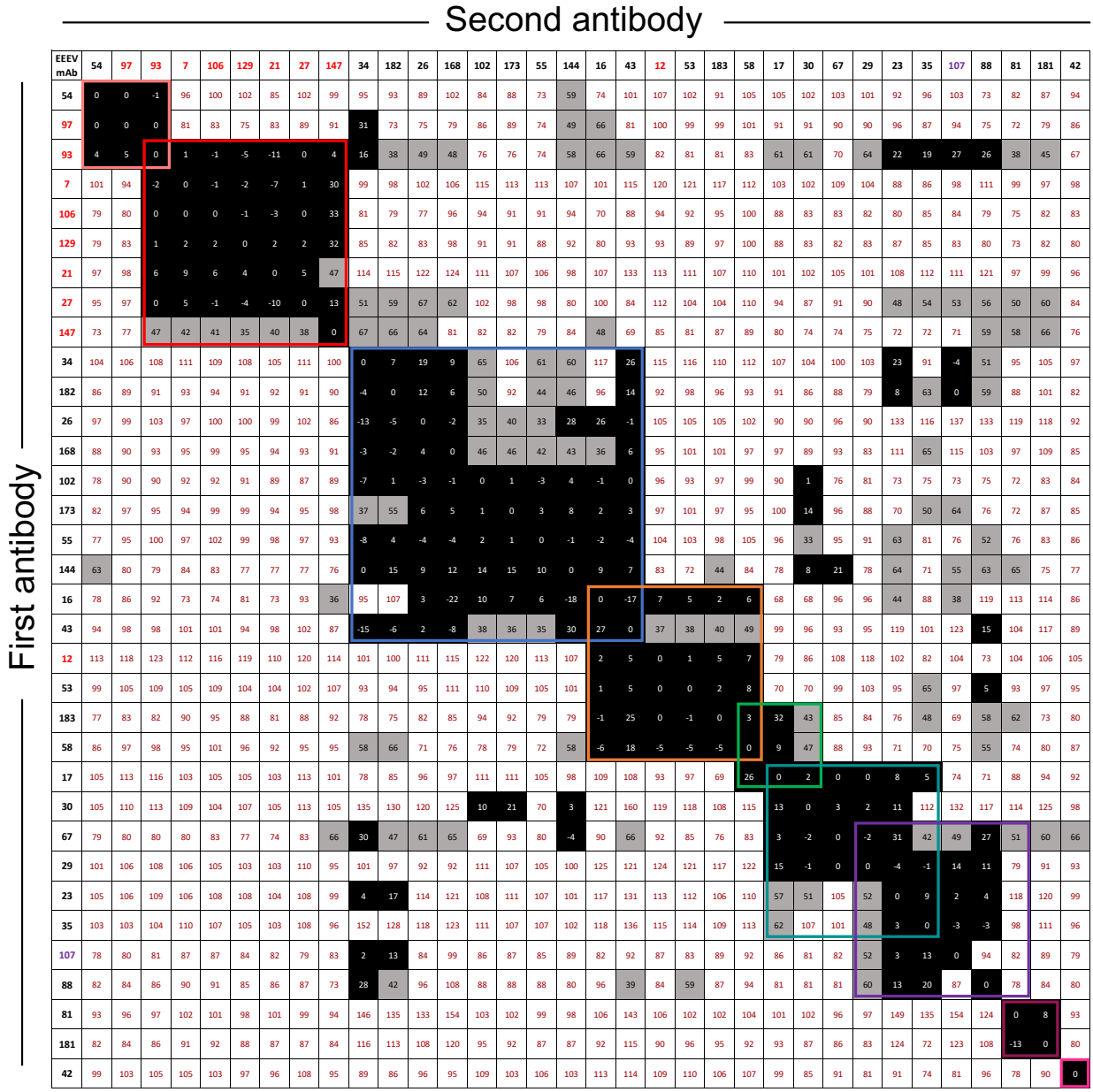

Figure 58. Non-neutralizing E2 antigenic determinants recognized by human mAbs. Competition-binding studies of human E2-specific human mAbs to recombinant EEEV E2 glycoprotein were performed through biolayer interferometry (BLI). Relative binding of the first Ab (left) in the absence of the second Ab (right) suggests competition (black boxes; < 33% maximal binding), intermediate competition (grey boxes; 33 to 67% maximal binding); no competition (white boxes; > 67% maximal binding). Competition binding groups are highlighted by the colored boxes. Neutralizing mAbs are colored in red and cross-reactive mAbs (EEEV-107) in purple.

Protection against aerosol EEEV challenge by a non-neutralizing human anti-EEEV E2-specific mAb, EEEV-30

In collaboration with Dr. William B. Klimstra's laboratory, we next assessed the *in vivo* efficacy of a non-neutralizing human anti-EEEV E2-specific mAb, EEEV-30, against aerosol EEEV challenge (**Figure 59**). In this stringent EEEV animal model, we found EEEV-30 to protect with 50% efficacy compared to the negative control treatment group, rDENV-2D22 IgG. Virus replication within the brain was limited in the EEEV-30 prophylactically treated group (**Figure 59D**). This was surprising given the stringency of this model for protection. However, this highlights the importance of non-neutralizing E2-specific mAbs for protection against alphaviruses. Assessment of potential Fc-mediated effector functions may elucidate the *in vivo* protection mechanism of EEEV-30 against EEEV aerosol challenge.

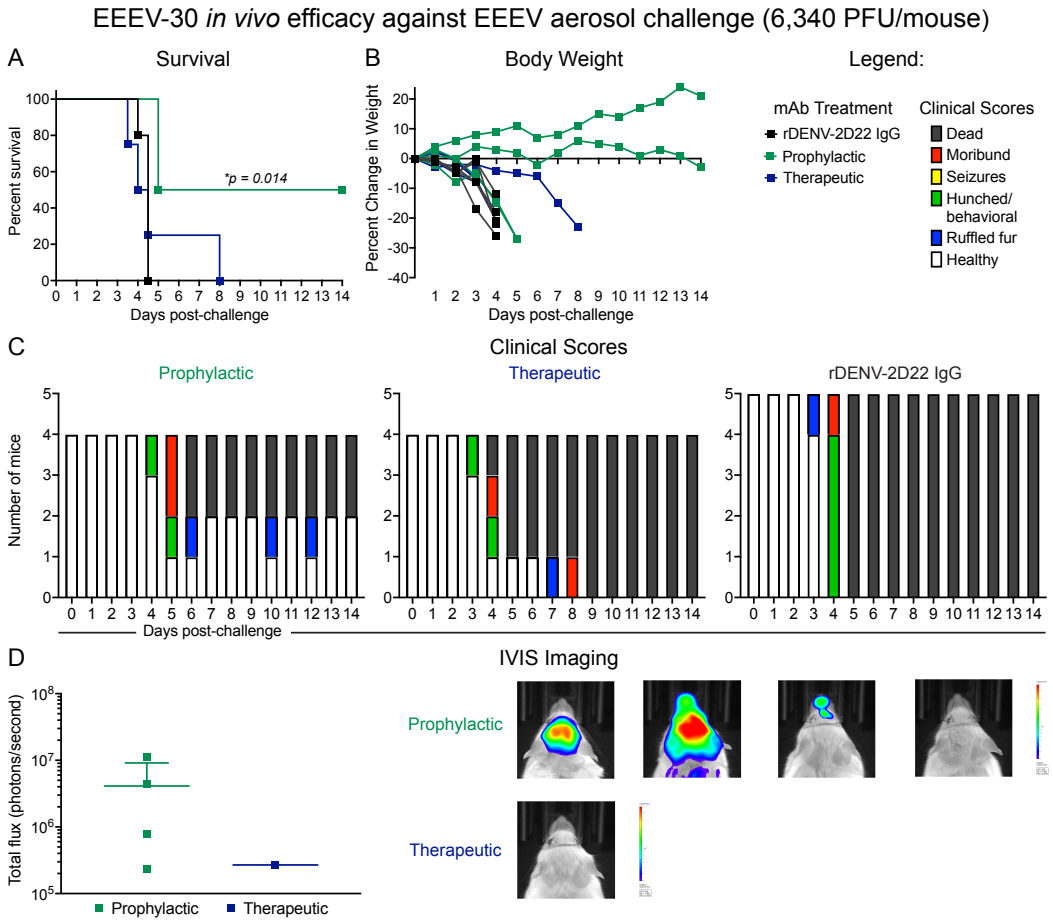

Figure 59. EEEV-30 protects against EEEV aerosol challenge. *In vivo* prophylactic (green) and therapeutic (blue) efficacy of EEEV-30 against EEEV aerosol challenge in CD-1 mice (6,340 PFU/mouse). **A.** EEEV-30 was administered prophylactically (24 h prior to virus challenge; green: n=4) or therapeutically (24 h post virus challenge; blue: n=4) at 100 µg via the IP route to CD-1 female mice (4-6-weeks old). EEEV-30 protected mice with 50% survival, respectively, against EEEV (FL93-939) aerosol challenge (1,631 to 1,825 PFU/mouse) compared to the control mAb rDENV-2D22 (black; n=5) (Fibriansah et al., 2015)**. B.** Percent body weight change of EEEV-30 and rDENV-2D22 treated CD-1 mice over the course of 14 days. **C.** Clinical scores of EEEV-30 and rDENV-2D22 treated CD-1 mice over the course of 14 days. The number of mice (y-axis) with defined clinical scores (dead (black), moribund (red), seizures/ataxia (yellow), hunched back/behavioral (blue), ruffled fur (green), healthy (white)) are indicated. **D.** *In vivo* imaging system (IVIS) images of CD-1 mice for EEEV-30 prophylactically and therapeutically treated groups at day 5 after EEEV aerosol challenge.

Discussion and Future Directions

Protective capability does not necessarily correlate with neutralization activity of anti-alphavirus mAbs (Mendoza et al., 1988; Mathews et al., 1985; Schmaljohn et al., 1982; Hunt and Roehrig, 1985; Griffin, 1995; Boere et al., 1984). The capability to protect against infection *in vivo* may be due to other Ab-dependent mechanisms, such as Fc-mediated effector functions, not assessed through *in vitro* neutralization studies. Additionally, as shown in earlier studies and in chapter IV, standard focus forming assays used in the field may not recapitulate the complete neutralization mechanisms exploited by anti-alphavirus mAbs since there appears to be a preference for inhibition of virus entry through this assay (Jin and Simmons, 2019; Jin et al., 2015). Further studies to assess egress inhibition by this panel of 'non-neutralizing' human anti-EEEV E2-specific mAbs is of interest to define a potential mechanism of neutralization by these mAbs.

A cross-protective murine E2-specifc mAb (1B2) to EEEV and VEEV was previously identified. Cross-neutralization was not observed for this mAb, which suggests an important non-neutralizing E2 epitope that confers protection against EEEV and VEEV (Pereboev et al., 1996). The isolation of two non-neutralizing human anti-EEEV and anti-VEEV cross-reactive mAbs, EEEV-107 and EEEV-321, as described in this chapter may recognize a similar epitope and protect against disease. Characterization of this panel is needed to understand the Ab-mediated mechanism(s) of action utilized by non-neutralizing E2-specific mAbs (*i.e.*, Fc-mediated effector functions, egress inhibition), identify EEEV-specific and cross-reactive E2 epitopes, and determine the additional contribution these mAbs may have for *in vivo* protection or

treatment of EEEV and VEEV infection is of interest. An understanding of non-neutralizing E2-specific mechanism(s) of action and the epitopes targeted can help inform rationale vaccine design.

Materials and Methods

All methods discussed in this chapter including human subject information, 5′ RACE sequencing, FRNT, binding EC_{50} ELISA analysis, cell surface display alphavirus subtype binding, competition-binding analysis, mouse EEEV aerosol challenge studies, IVIS imaging, and statistical analyses are described in chapters III and IV.

CHAPTER VI

NEUTRALIZATION OF VENEZUELAN EQUINE ENCEPHALITIS VIRUS BY HUMAN MONOCLONAL ANTIBODIES

Introduction

In chapters III-V, I describe human mAbs isolated from EEEV survivors of naturally acquired infection. In this chapter, I characterize human mAbs isolated from VEEV vaccinees to gain a better understanding of the human humoral response induced by immunization against Venezuelan equine encephalitis virus (VEEV).

VEEV is a mosquito-transmitted virus endemic in Central and South America, and lower regions of North America (Weaver et al., 2012). VEEV is associated with a febrile illness that in up to 15% of cases can cause encephalitis in humans with a case fatality rate of ~1% (Hunt et al., 2010; Ronca et al., 2016; Weaver et al., 2012). VEEV infection leads to a high titer viremia during infection in animal hosts, which increases the transmission potential of VEEV between mosquitos, small mammals, and large mammals (*i.e.*, equines and humans), for a high morbidity rate (Walton et al., 1973; Walton and Grayson, 1988; Wang et al., 2001; Weaver et al., 2012). The VEE antigenic complex consists of several viruses in addition to VEEV, which include six subtypes (I to

VI) and several varieties within the I (IAB and IC-IF) and III (IIIA-C) subtypes (Aguilar et al., 2011). The epizootic subtypes include IAB and IC, which have caused hundreds of thousands of VEEV human and equine disease cases, whereas, the enzootic subtypes (ID-F, II-VI) have a much lower incidence of human disease (Aguilar et al., 2011; Weaver et al., 2012; Aguilar et al., 2004).

In addition to natural transmission by mosquitos, VEEV is classified as a NIAID Category B priority pathogen and USDA/CDC Select Agent due to its previous use as a bioterrorism agent during the cold war (Weaver et al., 2012; Sidwell and Smee, 2003; Hawley and Eitzen, 2001). There are also no approved human vaccines or antiviral drugs for public use against VEEV. A live attenuated vaccine (TC-83) is available through the U.S. Army Special Immunizations Program for at-risk laboratory workers and military personnel (Berge et al., 1961). There are several concerns for this vaccine, which supports the lack of public approval. These include the possibility of *in vivo* reversion, natural transmission by mosquitos from vaccinated individuals, and the reactogenicity observed in vaccinees as 15 to 30% develop febrile symptoms (Ronca et al., 2016; McKinney et al., 1963). A formalin-inactivated vaccine (CA-84) is also available for at risk personnel. However, boosting is often needed (Jahrling and Stephenson, 1984).

The humoral response is important for alphavirus infections as described in chapters I-V. Rabbit immune serum and murine mAbs against VEEV have displayed neutralizing and non-neutralizing mechanism(s) of action for protection against VEEV infection. A critical neutralization site was defined within domain B of the E2

glycoprotein (residues 182-210) that when bound by Fab molecules appears to stabilize and prevent necessary conformational changes for virus fusion (Porta et al., 2014; Rico-Hesse et al., 1988; Roehrig et al., 1982; Roehrig and Mathews, 1985). Abs to this epitope protect against lethal VEEV infection following i.p. or aerosol challenge in mice and NHPs (Burke et al., 2019; Phillpotts, 2006; Mathews and Roehrig, 1982; Roehrig and Mathews, 1985).

A separate neutralization site was defined within domain A of the E2 glycoprotein (residues 115-119) (Hunt et al., 2010; Porta et al., 2014). Through phage display, an mAb from the B cells of VEEV TC-83 vaccinated individuals, F5, was isolated and found to target this epitope for neutralization through cross-linking E2 glycoproteins within a trimeric spike to do so (Porta et al., 2014). Administration of F5 prophylactically or therapeutically was also efficacious against VEEV infection following s.c. or aerosol challenge (Hunt et al., 2011). Thus, this epitope identifies another protective antigenic determinant on the E2 glycoprotein based on neutralization activity of mAbs.

The natural human humoral response following immunization with VEEV TC-83 remains to be elucidated. In this chapter, I describe a panel of nine human anti-VEEV mAbs isolated from VEEV TC-83 vaccinated donors to further understand this response. Of this panel, seven and two mAbs recognize the p62E1 or E1 glycoprotein, respectively. Diverse binding breadth within the VEE antigenic complex was observed by this panel of mAbs and seventeen murine anti-VEEV mAbs tested. Moreover, a number of unique human antigenic sites distinct from the epitopes recognized by neutralizing murine mAbs was observed. Structural analysis of a potent neutralizing

mAb, VEE-63, highlights a critical neutralization site within domain B of the E2 glycoprotein and may cross-link neighboring trimeric spikes as a structural mechanism of neutralization. Further characterization of this panel is needed to describe in greater detail the epitopes targeted, protective efficacy, and the mechanism(s) of action utilized by human anti-VEEV mAbs induced following VEEV TC-83 vaccination.

I would like to acknowledge Dr. William B. Klimstra at the University of Pittsburgh for providing the SINV/VEEV (Trinidad Donkey strain) cDNA clone. Additionally, I would like to acknowledge Natasha Kafai and Dr. Michael S. Diamond at Washington University for providing murine anti-VEEV mAbs isolated following mouse immunization with SINV/VEEV particles or recombinant VEEV E2 glycoprotein and performing SINV/VEEV *in vitro* neutralization studies. I would also like to acknowledge Dr. Elad Binshtein at Vanderbilt University for solving the cryo-EM reconstruction of VEEV VLPs alone and in complex with VEE-63 Fab molecules. Data collection was performed at the Stanford-SLAC Cryo-EM Center (S2C2) supported by the NIH Common Fund Transformative High Resolution Cryo-Electron Microscopy program (U24 GM129541).

Isolation of human anti-VEEV mAbs

The research subjects designated with randomly assigned Vanderbilt Vaccine Center Biorepository donor numbers, 117, 932, and 933, had a history of previous immunization with the live-attenuated vaccine strain VEEV TC-83 through an occupational health program. Vaccination history for subjects 117 and 933 is unknown.

Subject 932 was vaccinated in 2005-2006. Peripheral blood from 932 was collected 8-9 years after vaccination and PBMCs were isolated by density gradient purification and cryopreserved in liquid nitrogen until use. EBV transformation of B cells from donor blood samples was performed as described in chapter III. A panel of nine human mAbs was isolated and selected based on initial reactivity in ELISA to VEEV virus-like particles (VLPs) or recombinant VEEV E2 glycoprotein.

To further define the binding reactivity of human anti-VEEV mAbs, I assessed binding to VEEV VLPs, recombinant p62E1 protein for VEEV IAB subtypes (Trinidad Donkey and TC-83 strains), and EEEV E2 or E1 glycoproteins (**Figure 60**). Seven anti-VEEV mAbs strongly bound (<100 ng/mL half-maximal effective concentration [EC_{50}] values) VEEV VLPs and p62E1 proteins for either strain. Two mAbs, VEEV-52B and VEE-81, strongly bound (<20 ng/mL EC_{50} values) VEEV VLPs and recombinant EEEV E1 glycoprotein, which suggests recognition of cross-reactive epitopes. No binding reactivity was detected to recombinant EEEV E2 glycoprotein.

A

Binding Group	VEE mAb	Isotype (HC, LC)	EC_{50} (ng/mL)			
			VEEV VLP	VEEV p62E1 (TrD)	VEEV p62E1 (TC-83)	EEEV E1
1	VEE-63	IgG1,λ	9.3	6.3	12.0	
2	VEE-68	IgG3,κ	10.9	5.0	6.5	
	VEE-61	IgG1,κ	13.7	9.1	18.9	
	VEE-56	IgG3,κ	15.1	5.9	10.0	>
	VEE-86	IgG1,κ	17.7	9.6	17.3	
3	VEE-108	IgG1,λ	60.6	24.4	21.0	
	VEE-103	ND,κ	91.1	9.7	19.0	
4 (E1)	VEE-52B	IgG1,λ	10.2	2.4	12.5	12.0
	VEE-81	IgG3,κ	13.2	6.0	7.5	8.9

B

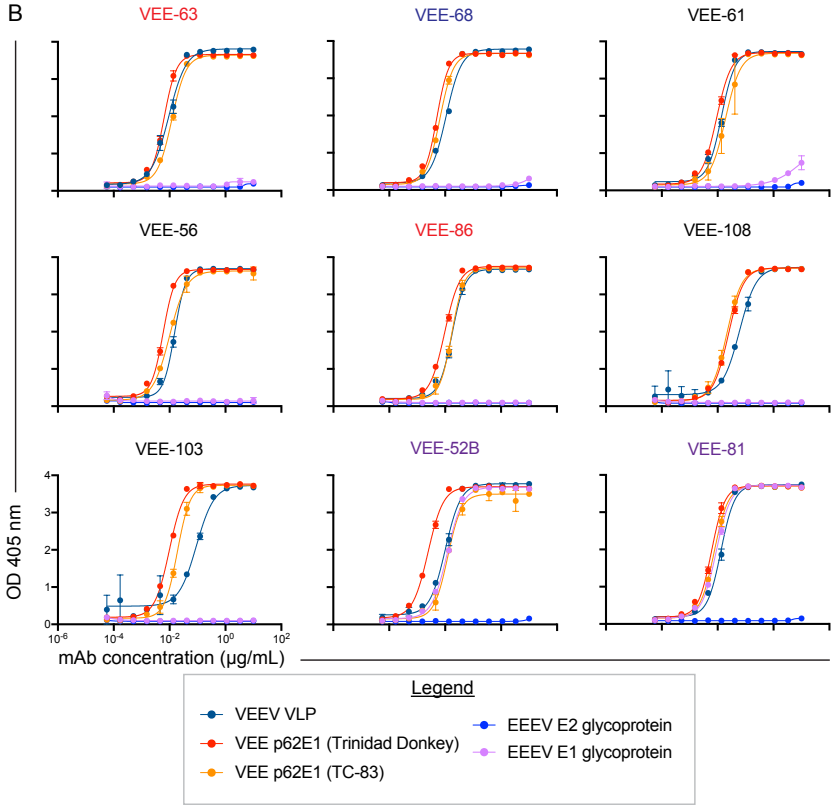

Figure 60. Binding reactivity of human anti-VEEV mAbs. A. EC_{50} values (ng/mL) for binding of human anti-VEEV mAbs to VEEV VLPs, VEEV p62E1 proteins (Trinidad Donkey or TC-83 strains), or EEEV E1 glycoproteins. Human anti-VEEV mAbs are listed in order of binding reactivity and increasing EC_{50} value for binding to VEEV VLPs. EC50 value in ng/mL is indicated by the blue heatmap (<10 [dark blue], 10.01 to 50 [medium blue], and 50.01 to 100 [light blue]). The symbol > indicates greater than 5 µg/mL EC_{50} value for binding. Isotype is indicated for each mAb as IgG1 or IgG3 for the heavy chain and κ or λ for the light chain. ND = not determined. Each mAb is labeled based on reactivity described here or in further studies: neutralizing (red) and EEEV E1 cross-reactive (purple). **B.** Representative binding curves of human anti-VEEV mAbs to VEEV VLPs (dark blue), recombinant p62E1 (Trinidad Donkey [red] or TC-83 [orange] strains) proteins, EEEV E2 glycoprotein (blue), or EEEV E1 glycoprotein (purple) with mAb concentration (µg/mL) on the x-axis and optical density at 405 nm on the y-axis. No detectable binding was observed to EEEV E2 glycoprotein. Each mAb is labeled based on reactivity described here or in further studies: neutralizing (red), EEEV E1 cross-reactive (purple), and VEE antigenic complex cross-reactive (blue). Data in **A** and **B** represent the mean ± SD of technical triplicates.

Identification of human antigenic determinants of anti-VEEV mAbs

First, to determine the number of antigenic determinants recognized by anti-VEEV mAbs, I performed competition-binding analyses via biolayer interferometry (BLI) with VEEV (TrD) p62E1 protein (**Figure 61**). Neutralizing murine anti-VEEV mAbs mapped by Dr. Michael S. Diamond's laboratory (Natasha Kafai; unpublished) to E2 domains A, B, and A/B were used as controls to aid in identification of the relative epitopes recognized by the human anti-VEEV mAbs. VEE-63 competed with murine anti-VEEV mAbs that recognize domain B of the VEEV E2 glycoprotein, which suggests VEE-63 also recognizes an epitope within this region. VEE-56 and VEE-61 did not compete and thus appear to bind unique epitopes not recognized by neutralizing murine anti-VEEV E2-specific mAbs. Several human and murine anti-VEEV mAbs did not bind with >0.2 nm shift to VEEV p62E1 protein in the BLI format. To test the full panel of human and murine anti-VEEV mAbs, I performed a competition-binding ELISA with VEEV VLPs. The neutralizing murine anti-VEEV mAbs recognized competition-binding groups corresponding to other analyses consistent with recognition of E2 domains A, B, and A/B. The human anti-VEEV mAbs identified seven competition-binding groups present on VEEV VLPs. VEE-63 again competed with murine anti-VEEV mAbs that recognize domain B of the VEEV E2 glycoprotein. Six more competition-binding groups were found and are unique from the neutralizing murine anti-VEEV mAbs since

competition was not observed with these mAbs. Two of the competition-binding groups corresponded with the EEEV E1-reactive mAbs, VEE-52B and VEE-81.

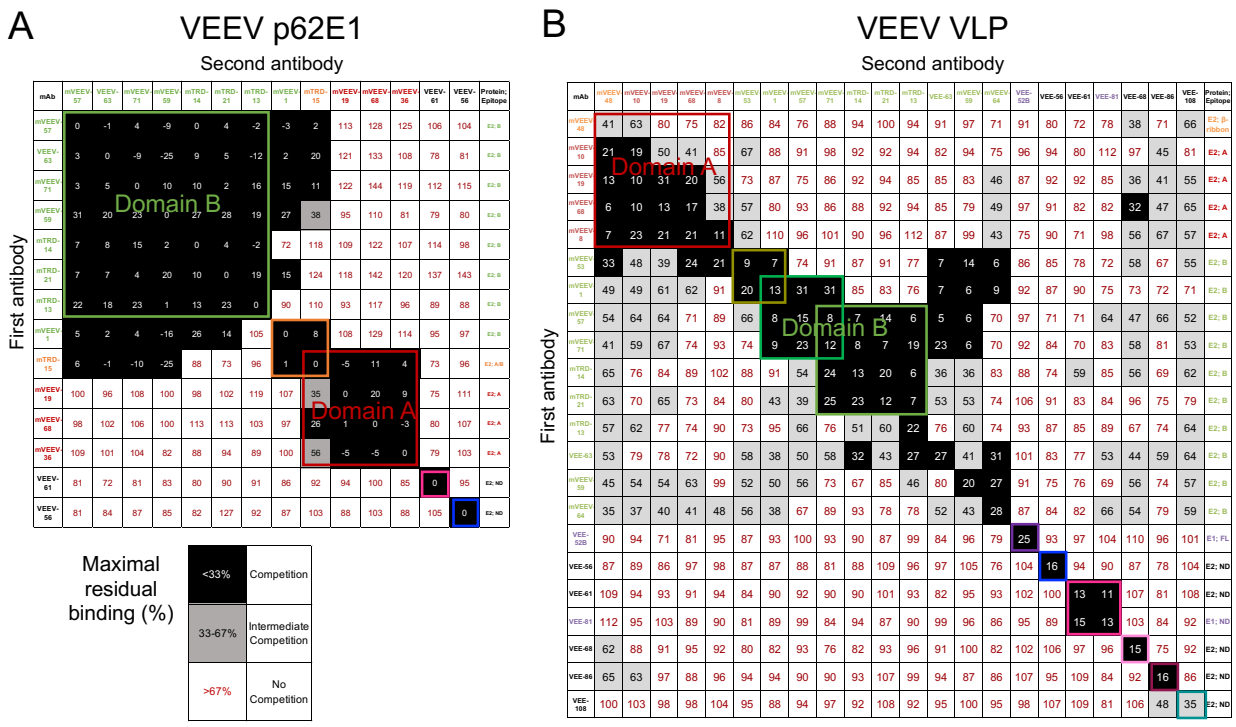

Figure 61. Human anti-VEEV mAbs recognize unique antigenic sites. Competition-binding analyses of human and murine anti-VEEV mAbs to recombinant VEEV p62E1 protein (subtype IAB; Trinidad Donkey strain; **A**) via biolayer interferometry or VEEV VLPs (**B**) via ELISA to identify the number of antigenic determinants recognized. Neutralizing murine anti-VEEV mAbs were included to group the human anti-VEEV mAbs with previously analyzed epitopes on the E2 glycoprotein (N.K. and M.S.D., unpublished data). The first mAb incubated with respective antigen (**A**: VEEV p62E1; **B**: VEEV VLP) is shown in the left-hand column and the second mAb is shown in the top column. Multiple competition binding groups were recognized by anti-VEEV mAbs to the E2 and E1 glycoproteins. Relative binding of the second mAb in the presence of the first mAb suggests competition (black boxes; < 33% maximal binding), intermediate competition (grey boxes; 33 to 67% maximal binding); no competition (white boxes; > 67% maximal binding). Competition binding groups are highlighted by the colored boxes. Anti-VEEV E2-specific mAbs appear to recognize domain A (red), domain B (green), or domain A/B (orange) of the E2 glycoprotein. Several human anti-VEEV mAbs did not compete with the murine mAbs and are highlighted by different colored boxes (blue and pink). Anti-VEEV E1-specific mAbs are colored in purple and are highlighted by the purple boxes. Data in **A** represent a dataset of biological duplicates. Data in **B** represent the mean of technical duplicates.

Binding breadth of human and murine anti-VEEV mAbs

There are six subtypes of the VEE antigenic complex, in which the epizootic subtypes consist of IAB and IC. The enzootic subtypes consist of ID-IF and II-VI. To define the binding breadth of the human and murine anti-VEEV mAbs to VEEV subtypes, I evaluated mAb binding to the structural proteins of different VEEV subtypes via a cell surface antigen display method. In this method, Expi293F cells are transfected with a plasmid encoding the structural proteins (capsid-E3-E2-6K-E1) of each subtype and mAb binding to the cell surface is assessed. Binding to at least one VEE subtype was observed as defined by a >two-fold change in mAb binding compared to the dengue virus (DENV)-specific negative control mAb, rDENV-2D22. The human anti-VEEV mAbs displayed a variety of subtype specificities and broad-reactivity compared to the neutralizing murine anti-VEEV mAbs. One human anti-VEEV mAb, VEE-68, recognized all the VEE subtypes (weak binding was observed for the VEE IE subtype strains: Mena II and MX01-22). The E2 domain B murine anti-VEEV mAbs and VEE-63 displayed less VEE subtype reactivity compared to mAbs that recognize domains A or A/B, which suggests VEE IAB subtype specific residues are recognized by these mAbs. The E1-reactive mAbs, VEE-52B and VEE-81, also recognized the WEEV and CHIKV subtypes tested, which suggests cross-reactivity for these mAbs similar to E1-specific mAbs as described in chapter IV.

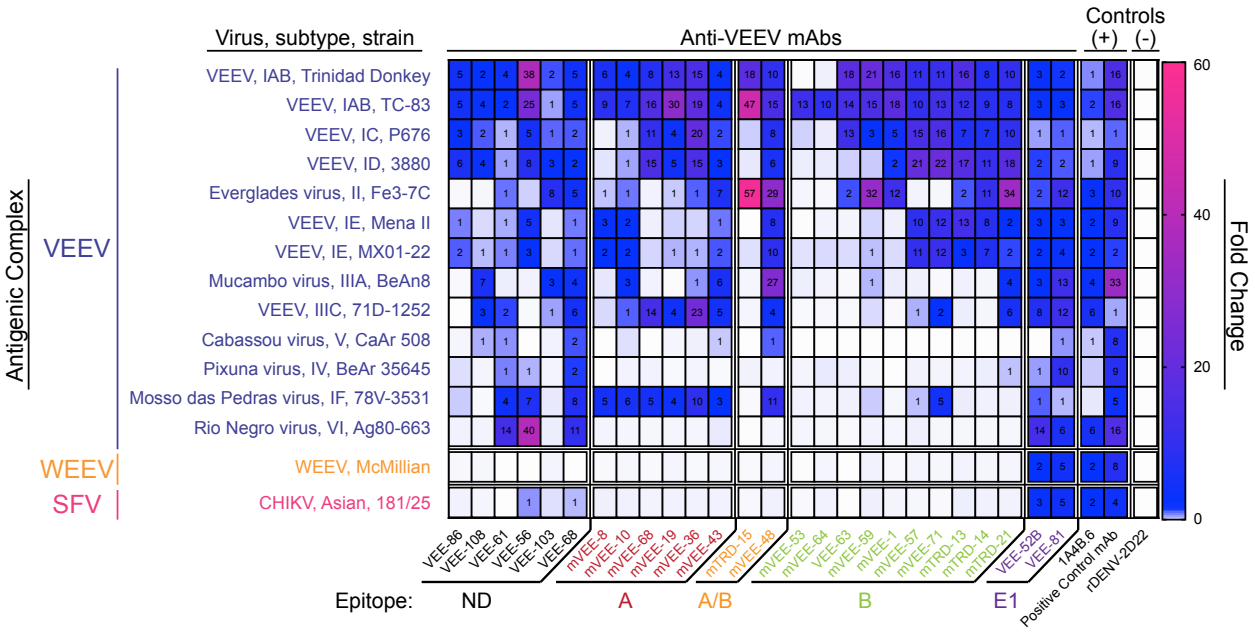

Figure 62. Binding breadth of anti-VEEV mAbs. Heatmap of fold-change for human and murine anti-VEEV mAb binding to different antigenic complexes corresponding to the structural proteins of VEEV (blue), WEEV (orange), or SFV (pink) subtypes (virus, subtype, and strain). The relative fold-change for mAb binding to each subtype was calculated after subtraction of background median fluorescence to Expi293F cells and was normalized relative to the negative control mAb rDENV-2D22. The alphavirus group E1-reactive mouse mAb,1A4B-6 (Roehrig et al., 1990) served as a positive control. The following additional positive control mAbs were used: rEEEV-97 IgG (human mAb; EEEV E2-specific; Williamson et al., 2020), 1A3B-7 (mouse mAb; VEEV E2-specific; Rico-Hesse et al., 1988, Roehrig and Mathews, 1985, Roehrig and Bolin, 1997, Goodchild et al., 2011), 2A3D-5 (mouse mAb; WEEV E1-specific; Hunt and Roehrig, 1985), and mouse anti-CHIKV ascites fluid (CHIKV; ATCC). The mAbs are shown in order based on previous analyses (N.K. and M.S.D., unpublished) and competition-binding group epitope reactivity as described in **Figure 61**. Data represent mean ± SD of technical triplicates and are representative values of two independent biological replicates.

Neutralization activity of human anti-VEEV mAbs

Next, to assess the functional activity of the human anti-VEEV mAbs, we collaborated with Dr. Diamond's laboratory to test the neutralization activity of this panel against four strains of SINV/VEEV (i.e., IAB: Trinidad Donkey and TC-83 strains; IC: INH9831; ID: ZPC738) (**Figure 63**). Of the panel of human anti-VEEV mAbs, VEE-63

potently neutralized (<2 ng/mL half-maximal inhibitory concentration (IC_{50}) values) SINV/VEEV subtypes IAB and IC. Neutralization activity was not observed against SINV/VEEV ID subtype, which may result due to sequence divergence from the IAB subtypes. VEE-52B and VEE-86 weakly neutralized SINV/VEEV (IAB: Trinidad Donkey strain).

A

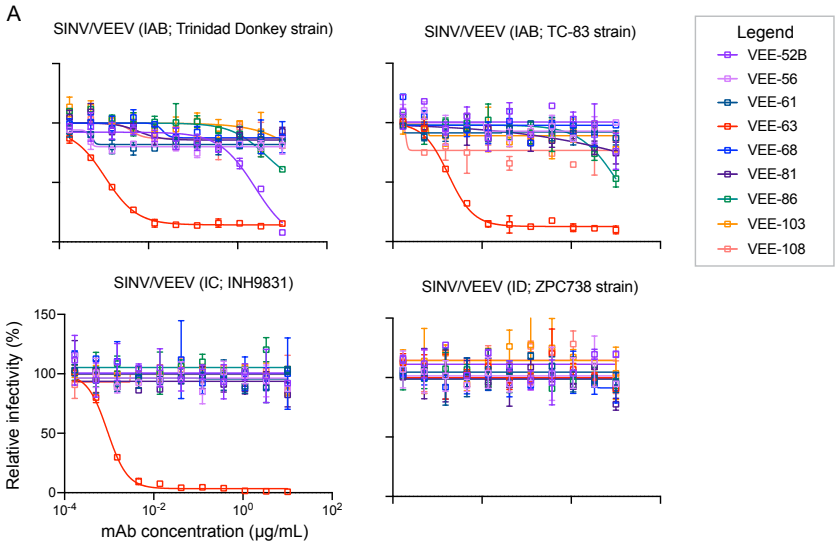

B

Binding Reactivity	IC_{50} (ng/mL)	SINV/VEEV			
		Trinidad Donkey (IAB)	TC-83 (IAB)	INH9831 (IC)	ZPC738 (ID)
p62E1	VEE-63	1.1	1.8	0.9	
	VEE-86	4,349			
	VEE-68	>	>	>	>
	VEE-61				
	VEE-56				
	VEE-108				
	VEE-103				
E1	VEE-52B	2,426			
	VEE-81	>			

Figure 63. VEE-63 potently neutralizes SINV/VEEV. A. Neutralizing activity of human anti-VEEV mAbs to SINV/VEEV (IAB: Trinidad Donkey and TC-83 strains; IC: INH9831; and ID: ZPC738) as determined by FRNT with mAb concentration (µg/mL) on the x-axis and relative infectivity (%) on the y-axis. **B.** IC_{50} values (ng/mL) of neutralization activity of human anti-VEEV mAbs to SINV/VEEVs. Neutralization potency is shown by the depth of orange color (<10 ng/mL [dark orange], >1 µg/mL [light orange], > symbol indicates >5 µg/mL).

Cryo-EM of VEE-63 in complex with VEEV VLPs

To assess the structural basis of neutralization by human anti-VEEV mAbs, I selected VEE-63 for cryo-EM complex formation with VEEV VLPs. Dr. Elad Binshtein in Dr. Crowe's laboratory performed cryo-EM analysis of the apo-form of VEEV VLPs and in complex with VEE-63 Fab molecules to a resolution of 4.4 Å and 6 Å, respectively (**Figure 64**). VEE-63 recognizes domain B of the E2 glycoprotein, which is in agreement with the competition-binding analyses as described in **Figure 61**. VEE-63 binds with high occupancy to virus particles since three Fab molecules bind per trimeric spike. Additionally, Fab constant domain contacts are observed around the 3-fold axes of the 'i3' trimeric spikes, which may help stabilize the E2 glycoprotein through inter-spike cross-linking.

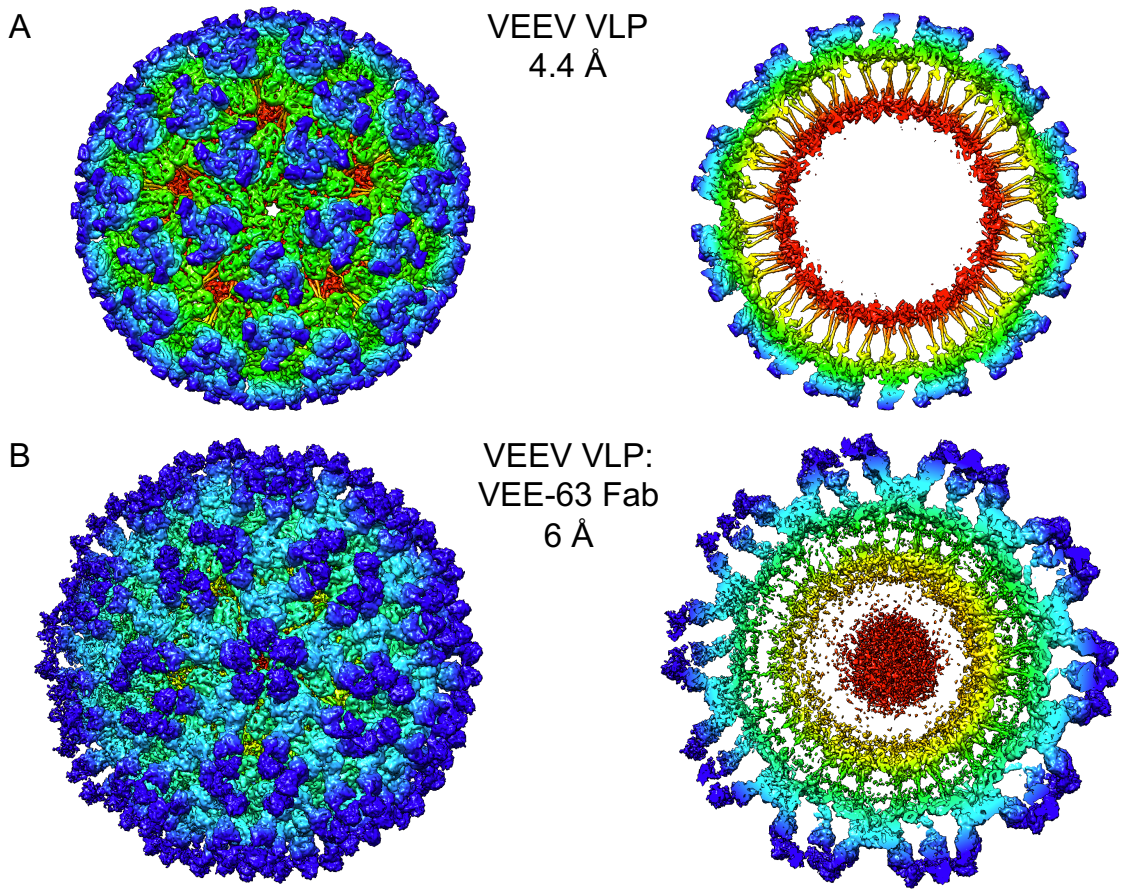

Figure 64. VEE-63 may inter-spike cross-link the trimeric spikes for neutralization of SINV/EEEV. Radially colored cryo-EM reconstruction (full view [left], cross-sectional view [right]) of VEEV VLP (**A**) and VEEV VLP in complex with the Fab form of the neutralizing mAb, VEE-63 (**B**). VEE-63 binds domain B of the E2 trimer with high occupancy and Fab constant domain contacts are observed between Fabs of neighboring spikes, which suggests inter-spike cross-linking may be a structural mechanism of neutralization for VEE-63.

Discussion and Future Directions

The studies described in this chapter begin to elucidate the human humoral response following VEEV TC-83 vaccination. A small but diverse panel of human anti-

VEEV mAbs was isolated. One potent neutralizing mAb, VEE-63, was found to target domain B of the E2 glycoprotein and may neutralize through inter-spike cross-linking on the surface of SINV/VEEV particles. Further studies are needed to describe the neutralization mechanism(s) of action of VEE-63, such as identification of a more definitive epitope mapping through alanine-scanning mutagenesis library analyses, assessment of neutralization mechanisms (*i.e.*, attachment, fusion, and egress), and in vivo efficacy of VEE-63 in mice against SINV/VEEV or VEEV challenge.

A broadly-reactive mAb, VEE-68, recognized all the VEE antigenic complex subtypes tested through cell-surface display antigen methods. It appears that human-VEEV mAbs recognize unique human antigenic determinants on VEEV particles that correspond to p62E1 or E1 glycoprotein epitopes. Human anti-VEEV mAbs that do not compete with neutralizing anti-VEEV mAbs may recognize non-neutralizing epitopes on the VEEV E2 or E1 glycoproteins. Determination of this VEE subtype cross-reactive epitope could aid in identification of a conserved region on the E2 glycoprotein for these viruses.

Through characterization of the panel of human anti-VEEV mAbs, a greater understanding of the human humoral response following VEEV TC-83 vaccination can be obtained. Comparison of the humoral response following natural VEEV infection is of interest to further describe the immunogenicity of VEEV vaccination for protection against VEEV induced disease. Furthermore, this understanding may aid in rationale VEEV vaccine design and identify Ab therapeutic candidates.

Materials and Methods

Human subject information

The subjects gave written informed consent prior to participation, and the Institutional Review Board (IRB) at Vanderbilt University Medical Center approved the protocols for the recruitment and collection of blood samples used in this study.

Cells, plasmids, and viruses

BHK-21, Vero, HMMA 2.5, B95.8, Expi293F cell lines were maintained as described in chapter III. Cells were checked for routinely mycoplasma detection using a universal mycoplasma detection kit (ATCC 30-1012K). Recombinant VEE p62E1 (strains Trinidad Donkey and TC-83) and EEEV E1 glycoprotein (strain FL93-939) with the osteonectin leader sequence and a C-terminal 6x his-tag was human codon-optimized, synthesized and cloned into the mammalian expression vectors pTwist CMV BetaGlobin or pcDNA3.1(+), respectively. VEEV subtype IAB (strains Trinidad Donkey, TC-83), VEEV subtype IC (strain P676), VEEV subtype ID (strain 3880), VEEV subtype IE (strains Mena II, MX01-22), Mosso das Pedras virus (VEEV subtype IF [strain 78V-3531]), Everglades virus (VEEV subtype II [strain Fe3-7C]), Mucambo virus (VEEV subtype IIIA [strain BeAn 8]), VEEV subtype IIIC (strain 71D-1252), Pixuna virus (VEEV subtype IV [strain BeAr 35645]), Cabassou virus (VEEV subtype V [strain CaAr 508]),

Rio Negro virus (VEEV subtype VI [strain Ag80-663]), WEEV (strain McMillian), or CHIKV (strain 181/25) structural protein genes (capsid-E3-E2-6K-E1) were codon-optimized, synthesized and cloned into the mammalian expression vectors pTwist CMV BetaGlobin for expression of the different alphavirus structural proteins. The chimeric virus Sindbis virus (SINV)/Venezuelan equine encephalitis virus (VEEV) was constructed as previously described (Paessler et al., 2003) for use in BSL-2 conditions. Briefly, the structural protein genes of SINV TR339 were replaced with the structural protein genes of VEEV Trinidad Donkey under control of the SINV 26S subgenomic promoter in the cDNA clone.

SINV/VEEV production

Plasmid DNA for SINV/VEEV was linearized with PvuI according to the manufacturer's protocols. Following linearization, the DNA was transcribed *in vitro* into RNA with the mMessage mMachine SP6 kit. SINV/VEEV RNA then was transfected into BHK-21 cells with Lipofectamine RNAiMax reagent. After 18 to 20 hours at 37°C in 5% CO_2, supernatant was harvested by clarification through a 0.2-µm pore size filter. For subsequent passaging of SINV/VEEV, BHK-21 cells were plated the day before the experiment, using 3 x 10^7 cells per T-225 cm^2 flask. The following day, cells were inoculated with SINV/VEEV at a MOI of 0.2 in DMEM/2% FBS. After incubation at 37°C in 5% CO_2 for 48 hours, SINV/VEEV was harvested by clarification of infected BHK-21

cell supernatants through a 0.2-μm pore size filter. Virus then was stored at -80 °C until use.

Recombinant protein expression

For production of VEEV p62E1 (based on strains Trinidad Donkey or TC-83), Expi293F cells were transfected transiently according to the manufacturer's protocol. Cells were incubated at 37°C in a humidified atmosphere of 8% CO_2 and supernatant was harvested by filtering through a 0.45-μm pore size filter 2 to 6 days after transfection. Cell supernatant was purified through a HisTrap Excel column using the manufacturer's protocol on an ÄKTA Pure 25M chromatography system. EEEV E1 glycoprotein was produced as described in chapter III.

Human hybridoma and mAb production

Human hybridomas and mAbs were generated as described in chapter III. In this case, 4 to 8.6 million PBMCs isolated from the research subjects were transformed with EBV.

Protein ELISA to screen hybridoma supernatants

VEEV virus-like particles (VLPs) generously provided by John Mascola of the NIH Vaccine Research Center (VRC) (Ko et al., 2019) and recombinant VEE E2 glycoprotein (Creative Diagnostics DAGA-268) were diluted to 2 µg/mL in 1× D-PBS to coat 384-well ELISA plates (Thermo Scientific #265203) at 25 µL/well and incubated at 4°C overnight. The plates were aspirated and blocked for 1 hour at room temperature with 25 µL/well blocking solution (2% non-fat dry milk (Blotting Grade Blocker Bio-Rad #170-6404), 2% goat serum (Gibco 16210-072) in D-PBS-T). After blocking, the plates then were washed 3× with D-PBS-T and a volume of 10 to 25 µL/well of supernatant from each well containing EBV-transformed B cells or hybridoma cell lines was added. Plates were incubated for 2 hours at room temperature or overnight at 4°C. Plates then were washed 3× with D-PBS-T and a suspension of secondary Abs (goat anti-human IgG Fc gamma fragment specific alkaline phosphatase conjugated; Meridian Life Science, W99008A and goat anti-human IgA-alkaline phosphatase conjugated; Southern Biotech, 2050-04) at a 1:4,000 dilution in 1% blocking solution (1% non-fat dry milk, 1% goat serum) was added at 25 µL/well for 1 hour at room temperature. Alkaline phosphatase substrate solution (phosphatase substrate tablets (Sigma #S0942) in AP substrate buffer (1M Tris aminomethane [Fisher #BP152-]), 30 mM $MgCl_2$ [Sigma #M1028]) was added at 25 µL/well following plate washing 4× with D-PBS-T. Plates were incubated at room temperature in the dark for 2 hours and then read at an optical density of 405 nm with a Biotek plate reader.

Determination of EC_{50} value for binding by protein ELISA

VEEV VLPs or recombinant VEEV p62E1 (strains Trinidad Donkey or TC-83), EEEV E3E2/E2 glycoprotein (strain V105; IBT Bioservices #0560-001), or EEEV E1 glycoprotein (strain FL93-939) were diluted to 2, 0.96, 0.5, or 2 µg/mL, respectively, in 1× D-PBS to coat 384-well ELISA plates (Thermo Scientific #265203) at 25 µL/well and incubated at 4°C overnight. A protein screening ELISA was performed as previously described above. However, instead of hybridoma supernatant, purified mAb was diluted to 10 µg/mL in blocking solution (1% non-fat dry milk, 1% goat serum) and added at 25 µL/well for 2 hours at room temperature. Additionally, plates were incubated at room temperature in the dark for 2 hours and then read at an optical density of 405 nm with a Biotek plate reader. Half-maximal effective concentration (EC_{50}) values for binding were determined after log transformation of concentration values and non-linear regression analysis using sigmoidal dose-response (variable slope) in GraphPad Prism software (version 8).

Cell surface display alphavirus subtype binding

Binding was performed as described in chapter IV. However, in this case, binding of anti-VEEV mAbs was performed to the structural proteins (capsid-E3-E2-6K-E1) of VEEV subtype IAB (strains Trinidad Donkey, TC-83), VEEV subtype IC (strain P676), VEEV subtype ID (strain 3880), VEEV subtype IE (strains Mena II, MX01-22), Mosso

das Pedras virus (VEEV subtype IF [strain 78V-3531]), Everglades virus (VEEV subtype II [strain Fe3-7C]), Mucambo virus (VEEV subtype IIIA [strain BeAn 8]), VEEV subtype IIIC (strain 71D-1252), Pixuna virus (VEEV subtype IV [strain BeAr 35645]), Cabassou virus (VEEV subtype V [strain CaAr 508]), Rio Negro virus (VEEV subtype VI [strain Ag80-663]), or WEEV (strain McMillian).

Binding of mAbs to VEE p62E1 protein detected using biolayer interferometry

Anti-penta his (HIS1K) biosensors on an Octet HTX biolayer interferometry instrument (ForteBio) were soaked for 10 minutes in 1× kinetics buffer, followed by a baseline signal measurement for 60 seconds. Recombinant VEEV p62E1 (Trinidad Donkey) monomeric glycoprotein (20 μg/mL) was immobilized onto the biosensor tips for 180 seconds. After a wash step in 1× kinetics buffer for 30 seconds, the Ab (50 μg/mL) was incubated with the antigen-containing biosensor for 600 seconds. The biosensor tips then were immersed 1× kinetics buffer for 600 seconds to account for dissociation of Ab from antigen. Abs with a relative nm shift >0.5 nm for binding were used for further competition-binding analyses via biolayer interferometry.

Competition-binding analysis via biolayer interferometry

Anti-penta his (HIS1K) biosensors on an Octet HTX biolayer interferometry instrument (ForteBio) were soaked for 10 minutes in 1× kinetics buffer, followed by a

baseline signal measurement for 60 seconds. Recombinant VEEV p62E1 (Trinidad Donkey) monomeric glycoprotein (20 μg/mL) was immobilized onto the biosensor tips for 180 seconds. After a wash step in 1× kinetics buffer for 30 seconds, the first Ab (20 μg/mL) was incubated with the antigen-containing biosensor for 600 seconds. The biosensor tips then were washed in 1× kinetics buffer for 30 seconds and then immersed in the second Ab for 600 seconds. Comparison between the maximal signal of each Ab compared to a buffer-only control was used to determine the percent binding of each Ab. A reduction in maximum signal to <33% of un-competed signal was considered full competition of binding for the second Ab in the presence of the first Ab. A reduction in maximum signal to between 33 to 67% of un-competed was of un-competed signal was considered intermediate competition of binding for the second Ab in the presence of the first Ab. Percent binding of the maximum signal >67% was considered absence of competition of binding for the second Ab in the presence of the first Ab.

Competition-binding ELISA

A competition-binding ELISA was performed as described in chapter IV. However, in this case, VEEV virus-like particles (VLPs) were diluted to 2 μg/mL in 1× D-PBS to coat 384-well plates (Thermo Fisher Scientific) and incubated at 4°C overnight.

Negative stain grid preparation and imaging

For screening and imaging of negatively stained (NS) VEEV VLP or VEEV-VLP/VEE-63 Fab samples, ~3 µL of the sample at concentrations of 10-15 µg/mL was applied to glow discharged grid with continuous carbon film on 400 square mesh copper EM grids (Electron Microscopy Sciences, Hatfield, PA). The grids were stained with 0.75% uranyl formate (UF) (Ohi et al., 2004). Images were recorded on a 4k × 4k CCD camera using an FEI TF20 (TFS) transmission electron microscope operated at 200 keV and control with SerialEM. (Mastronarde, 2005) All images were taken at 50,000× magnification with a pixel size of 2.18 A/pix in low-dose mode at a defocus of 1.5-1.8 µm. Image processing was performed using the cryoSPARC (Punjani et al., 2017).

Cryo-EM sample preparation and data collection

VEE-63 Fab molecules were produced by digesting recombinant chromatography-purified IgGs using resin-immobilized cysteine protease enzyme (FabALACTICA, Genovis). The digestion occurred in 100 mM sodium phosphate and 150 mM NaCl pH 7.2 (PBS) for around 16 h at ambient temperature. To remove cleaved Fc from intact IgG, the digestion mix was incubated with CaptureSelect Fc resin (Genovis) for 30 min at ambient temperature in PBS buffer.

For the VEEV VLP/VEE-63 Fab complex, purified VEEV VLP was concentrated to 5 mg/ml and mixed with VEE-63 Fab (4.4 mg/ml) at a molar ratio of 720:1 (Fab:VLP). The mixture was incubated for 1 hour at ambient temperature and buffer exchanged

with Amicon 100kDa (Millipore Sigma) (25mM HEPES pH 7.5, 100mM NaCl and 2mM EDTA). VEEV VLP or VEEV VLP/VEE-63 Fab (2.2 µl) samples were applied x2 to glow discharged (40 seconds at 25 milliamperes) 300 mesh Lacey grids. The grid was blotted for 2 seconds before plunging into liquid ethane using a FEI Vitrobot Mark4 (TFS) at 8°C and 100% humidity.

Grids were imaged on a Titan Krios (TFS) microsope operated at 300 keV equipped with a Falcon 4 (TFS) DED camera using counting mode. Datasets were collected for each sample (VEEV VLP or VEEV VLP/VEE-63 Fab). Movies were collected at a nominal magnification of x75,000, pixel size of 1.02775 A/pix, and defocus range of 0.5−1.6 µm. Grids were exposed at $1e^{-}/Å^2$/frame over 40 frames resulting in a total dose of ~40 $e^{-}/Å^2$ (**Table 9**).

Cryo-EM data processing

Movies were pre-processed (motioncor2 (Zheng et al., 2017), gCTF (Zhang, 2016), using Relion (Scheres, 2012; Zivanov et al., 2018). Micrographs with low resolution, high astigmatism, and defocus were removed from the data set. Further processing was done using Relion 3.1 and was the same for both dataset unless specified. A small subset of micrographs was autopicked first by Relion LoG (Fernandez-Leiro and Scheres, 2017) and 2D class averages were determined. Representative classes were selected and used as templates for another round of

autopicking. The particles were extracted in box size of 1,200 pixels and binned by 2 to a pixel size of 2.05 A/pix. The particles were then subjected to multiple rounds of 2D class averages and 3D classification (with and without symmetry) to obtain a set of clean and homogeneous particles. The particles from the selected classes were re-extracted at a pixel size of 1.806 A/pix, 3D classified and subjected to 3D autorefinement. The data was further processed with Ctfrefine, polished and final postprocessing was performed. Detailed statistics are provided in **Table 9**.

Model building

For the VEEV VLP complex, a homology model of the VEEV vaccine strain, TC-83 (PDB ID: 3J0C [Zhang et al., 2011]) was used for docking of the cryo-EM map with Chimera rigid body fit and Phenix (Pettersen et al., 2004; Adams et al., 2010). To improve the coordinate fitting, the model was subjected to iterative refinement of manual building in Coot (Emsley and Cowtan, 2004) and Phenix real-space refinement (Adams et al., 2010). The model was validated with Molprobity (Chen et al., 2010).

For the VEEV VLP/VEE-63 Fab complex, a homology model for the Fab (PDB ID: 12E8) and the refined model of the VEEV VLP was used as starting model for the VLP. The model was docked to the cryo-EM map with Chimera rigid body fit. The model was then refined in Phenix (phenix real-space refinement) and Coot. The model was validated by Molprobity (**Table 9**).

Supplemental Information

	Parameters	VEEV VLP	VEEV VLP:VEE-63 Fab
Data Deposition	EMDB		
	PDB		
Microscope setting	Microscope	Titan Krios	Titan Krios
	Voltage (kV)	300	300
	Detector	Falcon 3EC	Falcon 3EC
	Mag	x75,000	x75,000
	Pixel size	1.02775	1.02775
	Exposure (e-/Å2)	40	40
	Defocus range (μm)	0.8-1.6	0.8-1.6
Data	# Micrographs	4,565	
	# particles	13,537	
	# particle after 2D	10,000	
	Final particles #	7,514	
	Symmetry	icosahedral	icosahedral
	Resolution FSC=0.143	4.2	
Model refinement and validation	Protein residues	4,108	
	Map CC	0.8	
	RMSD		
	Bond lengths (A)	0.003	
	Bond angles	0.524	
	Ramachandran		
	Outliers (%)	0	
	Allowed (%)	5.51	
	Favored (%)	94.49	
	Poor rotamers (%)	9.08	
	MolProbity score	2.79	
	Clash score	15.27	
	CaBLAM score	3	

Table 9. Parameters used for high-resolution data collection of VEEV VLP and VEEV VLP in complex with VEE-63 Fab.

CHAPTER VII

SUMMARY AND FUTURE DIRECTIONS

SUMMARY

The body of work described here has progressed the alphavirus field forward in elucidating some of the neutralization mechanism(s) of action utilized by human mAbs against alphaviruses. Through characterization of human anti-EEEV, anti-VEEV, and anti-alphavirus mAbs, I showed that potent neutralizing mAbs target the E2 glycoprotein and inhibit at virus entry stages of the replication cycle. In contrast, E1 mAbs neutralize virus egress and display varying levels of specificity and cross-reactivity to cryptic epitopes present on this protein.

Differences in antigen recognition between E2- and E1-specific mAbs was assessed by comparing EC_{50} values for binding to virion particles and recombinant proteins. The neutralizing E2 mAbs generally bound quaternary or surface exposed epitopes as described a virus/protein EC_{50} ratio of < or ~1. In comparison, non-neutralizing mAbs may not recognize exposed epitopes since the ratio is >1, indicative of stronger binding to protein compared to intact virion particles. Recognition of non-competing epitopes by non-neutralizing mAbs with neutralizing mAbs further supports

epitope differences that may contribute to neutralization activity. Conversely, E1 mAbs generally bound cryptic epitopes as described by a virus/protein EC_{50} ratio of >1. Treatment with the nonionic detergent Tween®20 or low pH exposed some of these epitopes while elevated temperature did not. Thus, analysis of the EC_{50} ratio can quantitatively serve to assess the exposure of a mAb epitope for binding.

The neutralization phenotypes observed for E2- and E1-specific mAbs, respectively, depend on exposure of the epitope for binding and mechanism(s) of action. The standard FRNT assay to assess neutralization activity focuses on the entry steps in the alphavirus replication cycle and are primarily identify neutralizing E2-specific mAbs. In contrast, through this standard assay, E1-specific mAbs generally do not or weakly neutralize virus particles. However, when egress inhibition is assessed, E1-specific mAbs can neutralize production of virus particles. This suggests a difference in structural protein presentation between intact virions and on the surface of cellular membranes. Together, this means multiple mechanisms of action are utilized by anti-alphavirus mAbs and assessment of these mechanisms can help elucidate potential correlates of protection.

Human anti-EEEV and anti-alphavirus E1-specific mAbs were characterized to define cross-reactive features of the E1 glycoprotein. A majority of the E1-specific mAbs recognized cryptic epitopes on the surface of intact virions. ‘Broadly reactive’ and ‘pan alphavirus’ mAbs recognized the highly conserved fusion loop of the E1 glycoprotein. Exposure of this epitope appears to vary between alphaviruses due to weakly neutralizing activity of fusion loop mAbs to SINV/VEEV compared to other alphaviruses

tested (SINV/EEEV, SINV/WEEV, CHIKV, and MAYV). Cross-protection of anti-alphavirus mAb, EEEV-346, suggests Fc-mediated effector functions may contribute to protection against EEEV or CHIKV-induced disease.

All together the studies performed in this document have identified potential targets of neutralization for EEEV and VEEV, identified regions of highly conserved epitopes that confer cross-protection, and begun to identify Fc-mediated effector functions that may contribute to *in vivo* efficacy observed by neutralizing and non-neutralizing mAbs.

FUTURE DIRECTIONS

Structural studies of human anti-EEEV mAbs

Structural analyses enable a detailed view of Ab-antigen interactions. In chapter III, the structural mechanisms of neutralization for two potent mAbs, EEEV-33 and EEEV-143, were described. However, additional neutralizing mAbs were identified that target different epitopes, depend on avidity or quaternary interactions for binding or neutralization, and different potencies for *in vitro* neutralization against SINV/EEEV. Several of these neutralizing anti-EEEV mAbs showed the ability to treat against EEEV s.c. challenge, which suggests that neutralization potency measured *in vitro* does not correlate with *in vivo* efficacy. Structural analyses for a range of mAbs with various

functions can further elucidate the mechanism(s) of action for these mAbs to help inform the human humoral response against alphaviruses and aid in rationale vaccine design.

In chapter IV, I described neutralizing and potential Fc-mediated effector functions of human anti-EEEV and anti-alphavirus E1-specific mAbs. To understand how these mAbs target cryptic epitopes on the surface of intact virions, structural analyses are of extreme interest. Treatment conditions of intact virions may be required for binding of E1-specific mAbs. Additionally, cryo-ET can elucidate binding of E1-specific mAbs to infected cells to understand how these mAbs inhibit virus egress. Furthermore, differences in virus structural protein presentation can be assessed to study different virus maturation stages or display between alphaviruses. This is supported by the weak neutralization activity observed for several human anti-alphavirus E1-specific mAbs against SINV/VEEV but not other viruses.

Cooperative effects of bispecific human anti-alphavirus mAb design

Combinatorial therapy of mAbs can further enhance the *in vivo* efficacy for protection or treatment against viruses. For alphaviruses specifically, this has been shown for CHIKV and MAYV. Combination of a murine anti-CHIKV or MAYV E2-specific and E1-specific mAb has shown an increase in protective efficacy and therapeutic mAb administration window of these mAbs *in vivo* against CHIKV or MAYV in musculoskeletal foot swelling disease mouse models (Earnest et al., 2019; Pal et al., 2013). Furthermore, through combination of mAbs there is less likelihood for virus

escape from the selective pressures of both mAbs. This mimics a polyclonal Ab response that naturally occurs against viruses. The moderate neutralizing activity, Fc-mediated effector functionality, protective and therapeutic efficacy observed here suggests E1-specific mAbs may be antiviral therapeutic candidates. Ab cocktail therapies or bispecific mAbs of either two E1-specific mAbs or in combination with a potent neutralizing E2-specific mAb may further increase the efficacy of mAbs *in vivo* against alphavirus-induced disease through cooperative effects and decreased ability for viral escape mutant viruses to emerge.

Anti-E3 Abs

Abs described in this document target the E2 or E1 structural proteins. However, mAbs isolated against other structural proteins, such as the E3 protein, can neutralize and protect against VEEV infection (Parker et al., 2010). This highlights the importance of the E3 protein for alphavirus immunity. Thus, isolation and characterization of anti-E3 mAbs could serve as additional therapeutic molecules against alphavirus infections and help elucidate the involvement of the E3 protein in virus maturation, incorporation, and immune protection.

Role of mAb isotype

EEEV-33 and EEEV-143 are highly potent anti-EEEV neutralizing mAbs as described in chapter III. EEEV-33 was naturally isolated as a IgG1 molecule, whereas EEEV-143 was isolated as a IgA1 molecule. In addition, an IgM mAb has been shown to neutralize and protect against CHIKV infection in mice through blockade of virus attachment (Lam et al., 2015). The difference in Ab isotype can result in avidity interactions, differences in Fc receptor infections, and utilization of transcytosis into different tissues (see below). Thus, characterization of human anti-alphavirus mAbs as different Ab isotypes can elucidate additional mechanisms to increase *in vivo* efficacy.

The therapeutic efficacy of EEEV-143, a naturally isolated IgA mAb, observed in one study against EEEV aerosol challenge suggests that IgA molecules may serve as potential therapeutic candidates against mucosal alphavirus infection. EEEV-143 was administered i.p which may decrease the potential efficacy in comparison to other routes of mAb administration, such as i.n.. A future study to assess this could elucidate this mechanism through generation of EEEV-143 as a IgG or IgA molecule and administer both mAbs through either route.

Serology and deep sequencing studies to identify subjects for isolation of cross-neutralizing anti-alphavirus mAbs

Several alphavirus vaccines, such as VEEV TC-83, formalin-inactivated EEEV, VEEV, and WEEV vaccines, are provided through the Special Immunizations Program. Individuals that participated in this program may have elicited cross-reactive, cross-neutralizing, and cross-protective anti-alphavirus mAbs due to multiple vaccine

administrations and frequent boosting. Serology analysis of these individuals could identify potential samples with high levels of these functionalities. Furthermore, deep sequencing of these individual's B cells could identify mAbs that may not survive the *in vitro* human hybridoma method generation utilized in these studies. With this information, sibling analysis can be performed to understand the somatic hypermutations that bring about distinct Ab lineages for neutralization, cross-reactivity, or protection against alphavirus infection.

As described in chapter IV and V, the cross-reactive anti-alphavirus mAbs described are generally non-neutralizing in the classical sense but can cross-protect against alphavirus infection. Several arthritogenic cross-neutralizing E2-specific mAbs have been identified (Fox et al., 2015; Powell et al., 2020; Earnest et al., 2019). However, this remains to be undiscovered for the encephalitic alphaviruses or 'pan-alphavirus'. Utilization of samples from these individuals may provide a priceless source for mAbs with these phenotypes.

Tissue-specific targeting of human anti-alphavirus mAbs

Mucosal immunity

Aerosol exposure is one of the primary reasons EEEV is classified as a NIH Category B priority pathogen and USDA/CDC select agent. To mimic potential exposure of EEEV as a bioterrorism agent, aerosol challenge has been studied in mice and NHPs

as a model for human infection (Honnold et al., 2015; Phelps et al., 2019). The olfactory mucosa is located in the nasal cavity and consists of an olfactory neuroepithelium layer, in which olfactory receptor neurons are present (Purves et al., 2001). These nerves together form the olfactory bulb, which relays olfactory signals to the brain. During EEEV aerosol challenge, significant lesions are observed in tissues, such as the olfactory bulb (Phelps et al., 2019). The spread and course of EEEV infection within the brain parenchyma was found to correspond with the severity of olfactory bulb lesions. Detection of EEEV antigen was also observed in these tissues (Honnold et al., 2015). Additionally, in mice vaccinated with live-attenuated EEEV vaccine candidates, protection against aerosol challenge was observed even in some mice with low serum $PRNT_{80}$ values (Trobaugh et al., 2019). This suggests other immune responses may be involved such as mucosal IgA for protection against aerosol challenge. Strategies to prevent and/or treat EEEV through Ab-based methods that specifically target mucosal sites are of interest. One method to do is through utilization of naturally occurring polymeric IgA (pIgA) and IgA-like molecules for transport of the Ab across mucosal surfaces via the polymeric immunoglobulin receptor (pIgR). The pIgR can transport antibodies expressing the joining chain (J chain), such as pIgA, or be targeted specifically via an Ab or peptide. Targeting of pIgR allows for internalization of the molecule, transcytosis across the mucosal epithelium, and subsequent cleavage of the secretory component to yield secretory IgA (SIgA) in the case of pIgA (Turula and Wobus, 2018). Transcytosis of neutralizing Abs across the mucosa may block EEEV infection of the olfactory bulb to help prevent or treat infection. Design of IgA-like

molecules that specifically target both EEEV for neutralization of the virus and allow for transcytosis via pIgR can address the involvement of mucosal IgA in the protection and treatment of EEEV.

Blood-brain barrier (BBB)

One of the difficulties in treatment of EEEV is the ability of Abs to cross the blood-brain barrier (BBB) (Morens et al., 2019). Prior to viral infection, the BBB limits transport of molecules >400 Da (Neves et al., 2016). During viral infection, disruption of the BBB occurs, allowing for infiltration of immune cells and larger molecules, such as Abs (Metcalf and Griffin, 2011; Cain et al., 2017). However, the inflammatory consequences of viral replication result in neurological deterioration, making it difficult for complete recovery from infection (Metcalf and Griffin, 2011; Griffin, 2016). The limitation in therapeutic efficacy of Abs due to the BBB signifies the importance for development of molecules that can cross this barrier.

Multiple-targeting strategies are utilized for the transport of molecules across the BBB (Neves et al., 2016; Pulgar, 2018). One such strategy involves the use of receptor-mediated transcytosis to transport molecules across the BBB and into the brain parenchyma. Specific transporters, such as the transferrin receptor, insulin receptor, glucose receptor, and low-density lipoprotein receptor, have been extensively studied for drug delivery across the BBB via receptor-mediated transcytosis (Neves et al., 2016; Pulgar, 2018). Several Abs, including single domain Abs, and peptides were identified

that target these transporters to aid in delivery of drugs and other Abs, as bispecifics, across the BBB (Neves et al., 2016; Pulgar, 2018). In addition to the barrier itself, efflux pumps, such as FcRn, are present that may decrease the overall concentration of antibody in the brain parenchyma (Pulgar, 2018). Utilization of Fc variants that decrease interaction with FcRn to prevent efflux from the brain parenchyma but allow for a long-lived half-life of the Ab in circulation should be considered. Through the use of mechanisms, such as receptor-mediated transcytosis, that naturally allow for active transport of molecules across the BBB are optimal targets for Ab design (Neves et al., 2016). Design of Ab molecules that specifically target both EEEV for neutralization of the virus and receptor transport molecules for delivery of Abs across the BBB to increase the therapeutic efficacy of these molecules are of extreme interest. Treatment of EEEV by BBB targeting methods is not only important in the context for treatment against this viral encephalitic disease but also for other encephalitic agents.

Development of human anti-alphavirus mAbs for diagnostic tools and therapies

Throughout my dissertation, a number of human anti-alphavirus mAbs were isolated and characterized. The implications for the development of these mAbs can be applied as diagnostic tools and therapies. The EEEV-specific and cross-reactivity profile of the E1-specific mAbs can be utilized as diagnostic tools for clinical diagnosis and surveillance of virus presence in mosquito and animal populations. Potent neutralizing and protective human anti-EEEV mAbs were identified that could serve as a therapy for

EEEV natural disease and aerosol acquired infection. The cross-protection observed by EEEV-346 suggests potential therapeutic candidates can be studied as a one hit all alphavirus therapy. Furthermore, weakly neutralizing, egress inhibitory mAbs could limit the reactogenicity of investigational vaccines (*i.e.*, VEEV TC-83) and potentially enable a stronger induction of immunogenic responses in combination with current vaccine strategies.

LIST OF PUBLICATIONS

1. Sangha AK, Dong J, **Williamson L**, Hashiguchi T, Saphire EO, Crowe JE Jr, Meiler J. Role of non-local interactions between CDR Loops in binding affinity of MR78 antibody to Marburg virus glycoprotein. *Structure*. 2017. 25(12): 1820-1828.e2. doi: 10.1016/j.str.2017.10.005. PMID: 29153506; PMCID: PMC5718948.

2. Kim AS, Austin SK, Gardner CL, Zuiani A, Reed DS, Trobaugh DW, Sun C, Basore K, **Williamson LE**, Crowe JE Jr, Slifka MK, Fremont DH, Klimstra WB, Diamond MS. Protective antibodies against Eastern equine encephalitis virus bind to epitopes in domains A and B of the E2 glycoprotein. *Nature Microbiology.* 2019. 4(1): 187-197. doi: 10.1038/s41564-018-0286-4. PMID: 30455470; PMCID: PMC6294662.

3. **Williamson LE**, Flyak AL, Kose N, Bombardi R, Branchizio A, Reddy S, Davidson E, Doranz BJ, Fusco ML, Saphire EO, Halfmann PJ, Kawaoka Y, Piper AE, Glass PJ, Crowe JE, Jr.. Early human B cell response to Ebola virus in four U.S. survivors of infection. *Journal of Virology*. 2019. 93(8): e01439-18. doi: 10.1128/JVI.01439-18. PMID: 30728263. PMCID: PMC6450119.

4. Vogt MR, Fu J, Kose N, **Williamson LE**, Bombardi R, Setliff I, Georgiev IS, Klose T, Rossmann MG, Bochkov YA, Gern JE, Kuhn RJ, Crowe JE Jr.. Human antibodies neutralize enterovirus D68 and protect against infection and paralytic disease. *Science Immunology*. 2020. 5(49): eaba4902. doi:10.1126/sciimmunol.aba4902. PMID: 32620559; PMCID: PMC7418079.

5. Zost SJ, Gilchuk P, Case JB, Binshtein E, Chen RE, Nkolola JP, Schäfer A, Reidy JX, Trivette A, Nargi RS, Sutton RE, Suryadevara N, Martinez DR, **Williamson LE**, Chen EC, Jones T, Day S, Myers L, Hassan AO, Kafai NM, Winkler ES, Fox JM, Shrihari S, Mueller BK, Meiler J, Chandrashekar A, Mercado NB, Steinhardt JJ, Ren K, Loo YM, Kallewaard NL, McCune BT, Keeler SP, Holtzman MJ, Barouch DH, Gralinski LE, Baric RS, Thackray LB, Diamond MS, Carnahan RH, Crowe JE Jr. Potently neutralizing and protective human antibodies against SARS-CoV-2. *Nature*. 2020. 584(7821): 443-449. doi: 10.1038/s41586-020-2548-6. PMID: 32668443; PMCID: PMC7584396.

6. **Williamson LE**, Gilliland T Jr, Yadav PK, Binshtein E, Bombardi R, Kose N, Nargi RS, Sutton RE, Durie CL, Armstrong E, Carnahan RH, Walker LM, Kim AS, Fox JM, Diamond MS, Ohi MD, Klimstra WB, Crowe JE Jr. Human antibodies protect against

aerosolized Eastern equine encephalitis virus infection. *Cell*. 2020. 183(7): 1884-1900.e23. doi: 10.1016/j.cell.2020.11.011. PMID: 33301709.

7. Murin CD, Gilchuk P, Alkutkar T, Bruhn JF, **Williamson LE**, Copps J, Ilinykh PA, Huang K, Kuzmina N, Shen X, Bryan AL, Davidson E, Doranz BJ, Flyak AI, Bukreyev A, Crowe JE Jr, Ward AB. Convergence of a common solution to broad ebolavirus neutralization by glycan cap directed human antibodies. *Cell Host and Microbe.* 2020. **In review.**

8. **Williamson LE**, Reeder KM, Bailey Kevin, Roy Vicky, Fouch ME, Kose N, Trivette A, Nargi RS, Winkler ES, Kim AS, Gainza C, Rodriguez J, Armstrong E, Sutton RE, Reidy J, Carnahan RH, Klimstra WB, Diamond MS, Davidson E, Doranz BJ, Alter G, Julander JG, Crowe JE Jr.. Protective E1-specific human alphavirus antibodies recognize cryptic viral epitopes. *Cell*. 2020. **In review.** (co-submission with #9)

9. Kim AS, Kafai NM, Winkler ES, Earnest JT, Jethva P, Shah AP, Vang L, Davidson E, **Williamson LE**, Crowe JE, Boranz BJ, Lai JM, Gross ML, Klimstra WB, Fremont DH, Diamond MS. Pan-protective human monoclonal antibodies against alphaviruses target a conserved epitope in the E1 structural glycoprotein. *Cell*. 2020. **In review.** (co-submission with #8)

REFERENCES

Ackerman, M.E., Moldt, B., Wyatt, R.T., Dugast, A-S., McAndrew, E., Tsoukas, S., Jost, S., Berger, C.T., Sciaranghella, G., Liu, Q., Irvine, D.J., Burton, D.R., and Alter, G. (2011). A robust, high-throughput assay to determine the phagocytic activity of clinical antibody samples. J Immunol Methods *366*, 8-19.

Adams, P.D., Afonine, P.V., Bunkoczi, G., Chen, V.B., Davis, I.W., Echols, N., Headd, J.J., Hung, L.W., Kapral, G.J., Grosse-Kunstleve, R.W.*, et al.* (2010). PHENIX: a comprehensive Python-based system for macromolecular structure solution. Acta Crystallogr D Biol Crystallogr *66*, 213-221.

Agapov, E.V., Razumov, I.A., Frolov, I.V., Kolykhalov, A.A., Netesov, S.V., and Loktev, V.B. (1994). Localization of four antigenic sites involved in Venezuelan equine encephalomyelitis virus protection. Arch Virol *139*, 173-181.

Aguilar PV, Greene IP, Coffey LL, Medina G, Moncayo AC, Anishchenko M, Ludwig GV, Turell MJ, O'Guinn ML, Lee J, Tesh RB, Watts DM, Russell KL, Hice C, Yanoviak S, Morrison AC, Klein TA, Dohm DJ, Guzman H, Travassos da Rosa AP, Guevara C, Kochel T, Olson J, Cabezas C, Weaver SC (2004). Endemic Venezuelan equine encephalitis in northern Peru. Emerging Infectious Diseases *10*: 880–888.

Aguilar PV, Robich RM, Turell MJ, O'Guinn ML, Klein TA, Huaman A, Guevara C, Rios Z, Tesh RB, Watts DM, Olson J, Weaver SC (2007). Endemic eastern equine encephalitis in the Amazon region of Peru. Am J Trop Med Hyg *76(2)*: 293-8.

Aguilar, P.V., Estrada-Franco, J.G., Navarro-Lopez, R., Ferro, C., Haddow, A.D., and Weaver, S.C. (2011). Endemic Venezuelan equine encephalitis in the Americas: hidden under the dengue umbrella. Future Virol *6*, 721-740.

Aguilar-Luis, M.A., Del Valle-Mendoza, J., Silva-Caso, W., Gil-Ramirez, T., Levy-Blitchtein, S., Bazan-Mayra, J., Zavaleta-Gavidia, V., Cornejo-Pacherres, D., Palomares-Reyes, C., and Del Valle, L.J. (2020). An emerging public health threat: Mayaro virus increases its distribution in Peru. Int J Infect Dis *92*, 253-258.

Ahn A, Klimjack MR, Chatterjee PK, Kielian M (1999). An epitope of the Semliki Forest virus fusion protein exposed during virus-membrane fusion. J Virol *73(12)*: 10029-39.

Ahn A, Gibbons DL, Kielian M (2002). The fusion peptide of Semliki Forest virus associates with sterol-rich membrane domains. J Virol *76(7)*: 3267-75.

Akahata W, Yang ZY, Andersen H, Sun S, Holdaway HA, Kong WP, Lewis MG, Higgs S, Rossmann MG, Rao S, Nabel GJ (2010). A virus-like particle vaccine for epidemic

Chikungunya virus protects nonhuman primates against infection. Nat Med *16(3)*: 334-8.

Akhrymuk I, Frolov I, Frolova EI (2016). Both RIG-I and MDA5 detect alphavirus replication in concentration-dependent mode. Virology *487*: 230-41.

Akkina R (2014). Humanized mice for studying human immune responses and generating human monoclonal antibodies. Microbiol Spectr *2(2)*.

Allison AB, Stallknecht DE (2009). Genomic sequencing of Highlands J virus: a comparison to western and eastern equine encephalitis viruses. Virus Res *145(2)*: 334-40.

Anderson CR, Downs WG, Wattley GH, Ahin NW, Reese AA (1957). Mayaro virus: a new human disease agent. II. Isolation from blood of patients in Trinidad, B.W.I. Am J Trop Med Hyg *6(6)*: 1012-6.

Arenívar C, Rodríguez Y, Rodríguez-Morales AJ, Anaya JM (2019). Osteoarticular manifestations of Mayaro virus infection. Curr Opin Rheumatol *31(5)*: 512-516.

Armstrong, P.M., and Andreadis, T.G. (2010). Eastern equine encephalitis virus in mosquitoes and their role as bridge vectors. Emerg Infect Dis *16*, 1869-1874.

Armstrong, P.M., and Andreadis, T.G. (2013). Eastern equine encephalitis virus--old enemy, new threat. N Engl J Med *368*, 1670-1673.

Arrigo NC, Adams AP, Weaver SC (2010). Evolutionary patterns of eastern equine encephalitis virus in North versus South America suggest ecological differences and taxonomic revision. J Virol *84*: 1014–1025.

Assunção-Miranda I, Cruz-Oliveira C, Da Poian AT (2013). Molecular mechanisms involved in the pathogenesis of alphavirus-induced arthritis. Biomed Res Int *2013*: 973516.

Atasheva S, Wang E, Adams AP, Plante KS, Ni S, Taylor K, Miller ME, Frolov I, Weaver SC (2009). Chimeric alphavirus vaccine candidates protect mice from intranasal challenge with western equine encephalitis virus. Vaccine *27(32)*: 4309-19.

Audet J, Wong G, Wang H, Lu G, Gao GF, Kobinger G, Qiu X (2014). Molecular characterization of the monoclonal antibodies composing ZMAb: a protective cocktail against Ebola virus. Sci Rep *4*: 6881.

Ayres, J.C., and Feemster, R.F. (1949). The sequelae of eastern equine encephalomyelitis. N Engl J Med *240*, 960-962.

Barbey-Martin C, Gigant B, Bizebard T, Calder LJ, Wharton SA, Skehel JJ, Knossow M (2002). An antibody that prevents the hemagglutinin low pH fusogenic transition. Virology. *294(1)*: 70-4.

Baxter, V.K., and Griffin, D.E. (2016). Interferon gamma modulation of disease manifestation and the local antibody response to alphavirus encephalomyelitis. J Gen Virol *97*, 2908-2925.

Berge TO, Banks IS, Tigertt WD (1961). Attenuation of Venezuelan equine encephalomyelitis virus by *in vitro* cultivation in guinea pig heart cells. Am J Hyg *73*: 209–218.

Bergren, N.A., Auguste, A.J., Forrester, N.L., Negi, S.S., Braun, W.A., and Weaver, S.C. (2014). Western equine encephalitis virus: evolutionary analysis of a declining alphavirus based on complete genome sequences. J Virol *88*, 9260-9267.

Bergren, N.A., Haller, S., Rossi, S.L., Seymour, R.L., Huang, J., Miller, A.L., Bowen, R.A., Hartman, D.A., Brault, A.C., and Weaver, S.C. (2020). "Submergence" of Western equine encephalitis virus: Evidence of positive selection argues against genetic drift and fitness reductions. PLoS Pathog *16*, e1008102.

Bernard, E., Solignat, M., Gay, B., Chazal, N., Higgs, S., Devaux, C., and Briant, L. (2010). Endocytosis of chikungunya virus into mammalian cells: role of clathrin and early endosomal compartments. PLoS One *5*, e11479.

Bernard KA, Klimstra WB, Johnston RE (2000). Mutations in the E2 glycoprotein of Venezuelan equine encephalitis virus confer heparan sulfate interaction, low morbidity, and rapid clearance from blood of mice. Virology *276(1)*: 93-103.

Bick MJ, Carroll JW, Gao G, Goff SP, Rice CM, MacDonald MR (2003). Expression of the zinc-finger antiviral protein inhibits alphavirus replication. J Virol *77(21)*: 11555-62.

Bigler WJ, Lassing EB, Buff EE, Prather EC, Beck EC, Hoff GL (1976). Endemic eastern equine encephalomyelitis in Florida: a twenty-year analysis, 1955-1974. Am J Trop Med Hyg *25(6)*: 884-90.

Binder GK, Griffin DE (2001). Interferon-gamma-mediated site-specific clearance of alphavirus from CNS neurons. Science. *293(5528)*: 303-6.

Boere, W.A., Harmsen, T., Vinje, J., Benaissa-Trouw, B.J., Kraaijeveld, C.A., and Snippe, H. (1984). Identification of distinct antigenic determinants on Semliki Forest virus by using monoclonal antibodies with different antiviral activities. J Virol *52*, 575-582.

Bornholdt ZA, Turner HL, Murin CD, Li W, Sok D, Souders CA, Piper AE, Goff A, Shamblin JD, Wollen SE, Sprague TR, Fusco ML, Pommert KB, Cavacini LA, Smith HL, Klempner M, Reimann KA, Krauland E, Gerngross TU, Wittrup KD, Saphire EO, Burton DR, Glass PJ, Ward AB, Walker LM 2016. Isolation of potent neutralizing antibodies from a survivor of the 2014 Ebola virus outbreak. Science *351*: 1078–1083.

Bornholdt ZA, Ndungo E, Fusco ML, Bale S, Flyak AI, Crowe JE Jr, Chandran K, Saphire EO (2016). Host-primed Ebola virus GP exposes a hydrophobic NPC1 receptor-binding pocket, revealing a target for broadly neutralizing antibodies. mBio *7*: e02154-15.

Bray M, Davis K, Geisbert T, Schmaljohn C, Huggins J (1999). A mouse model for evaluation of prophylaxis and therapy of Ebola hemorrhagic fever. J Infect Dis *179*: S248–S258.

Bréhin AC, Casadémont I, Frenkiel MP, Julier C, Sakuntabhai A, Desprès P (2009). The large form of human 2',5'-Oligoadenylate Synthetase (OAS3) exerts antiviral effect against Chikungunya virus. Virology. 384(1): 216-22.

Brochet, X., Lefranc, M.P., and Giudicelli, V. (2008). IMGT/V-QUEST: the highly customized and integrated system for IG and TR standardized V-J and V-D-J sequence analysis. Nucleic Acids Res *36*, W503-508.

Broeck GT, Merrill MH (1933). A serological difference between Eastern and Western equine encephalomyelitis virus. Proceedings of the Society for Experimental Biology and Medicine *31(2)*: 217-220.

Broeckel, R., Fox, J.M., Haese, N., Kreklywich, C.N., Sukulpovi-Petty, S., Legasse, A., Smith, P.P., Denton, M., Corvey, C., Krishnan, S*., et al.* (2017). Therapeutic administration of a recombinant human monoclonal antibody reduces the severity of chikungunya virus disease in rhesus macaques. PLoS Negl Trop Dis *11*, e0005637.

Brown, R.S., Wan, J.J., and Kielian, M. (2018). The alphavirus exit pathway: what we know and what we wish we knew. Viruses *10*: 89.

Brustolin M, Pujhari S, Henderson CA, Rasgon JL (2018). *Anopheles* mosquitoes may drive invasion and transmission of Mayaro virus across geographically diverse regions. PLOS Neglected Tropical Diseases *12(11)*: e0006895.

Burke, C.W., Froude, J.W., Miethe, S., Hulseweh, B., Hust, M., and Glass, P.J. (2018). Human-like neutralizing antibodies protect mice from aerosol exposure with Western equine encephalitis virus. Viruses *10*, 147.

Burke, C.W., Froude, J.W., Rossi, F., White, C.E., Moyer, C.L., Ennis, J., Pitt, M.L., Streatfield, S., Jones, R.M., Musiychuk, K.*, et al.* (2019). Therapeutic monoclonal antibody treatment protects nonhuman primates from severe Venezuelan equine encephalitis virus disease after aerosol exposure. PLoS Pathog *15*, e1008157.

Byrd EA, Kielian M (2017). An *Alphavirus* E2 membrane-proximal domain promotes envelope protein lateral interactions and virus budding. mBio. *8(6)*: e01564-17.

Byrd EA, Kielian M (2019). The Alphavirus E2 membrane-proximal domain impacts capsid interaction and glycoprotein lattice formation. J Virol *93(4)*: e01881-18.

Byrnes AP, Griffin DE (2000). Large-plaque mutants of Sindbis virus show reduced binding to heparan sulfate, heightened viremia, and slower clearance from the circulation. J Virol *74(2)*: 644-51.

Cagno V, Tseligka ED, Jones ST, Tapparel C (2019). Heparan sulfate proteoglycans and viral attachment: true receptors or adaptation bias? Viruses. *11(7)*: 596.

Cain MD, Salimi H, Gong Y, Yang L, Hamilton SL, Heffernan JR, Hou J, Miller MJ, Klein RS (2017). Virus entry and replication in the brain precedes blood-brain barrier disruption during intranasal alphavirus infection. J Neuroimmunol *308*: 118-130.

Calisher CH, Shope RE, Brandt W, Casals J, Karabatsos N, Murphy FA, Tesh RB, Wiebe ME (1980). Proposed antigenic classification of registered arboviruses I. Togaviridae, Alphavirus. Intervirology *14(5-6)*: 229-32.

Calisher CH, Meurman O, Brummer-Korvenkontio M, Halonen PE, Muth DJ (1985). Sensitive enzyme immunoassay for detecting immunoglobulin M antibodies to Sindbis virus and further evidence that Pogosta disease is caused by a western equine encephalitis complex virus. J Clin Microbiol *22(4)*: 566-71.

Calisher CH, Karabatsos N, Lazuick JS, Monath TP, Wolff KL (1988). Reevaluation of the western equine encephalitis antigenic complex of alphaviruses (family Togaviridae) as determined by neutralization tests. Am J Trop Med Hyg. *38(2)*: 447-52.

Calisher CH (1994). Medically important arboviruses of the United States and Canada. Clin Microbiol Rev. *7(1)*: 89-116.

Cardoso, F.D., Rezende, I.M., Barros, E.L.T., Sacchetto, L., Garces, T., Silva, N.I.O., Alves, P.A., Soares, J.O., Kroon, E.G., Pereira, A.*, et al.* (2019). Circulation of

Chikungunya virus East-Central-South Africa genotype during an outbreak in 2016-17 in Piaui State, Northeast Brazil. Rev Inst Med Trop Sao Paulo *61*, e57.

Carpentier KS, Morrison TE (2018). Innate immune control of alphavirus infection. Curr Opin Virol *28*: 53-60.

Carragher, B., Kisseberth, N., Kriegman, D., Milligan, R.A., Potter, C.S., Pulokas, J., and Reilein, A. (2000). Leginon: an automated system for acquisition of images from vitreous ice specimens. J Struct Biol *132*, 33-45.

Carrera JP, Forrester N, Wang E, Vittor AY, Haddow AD, López-Vergès S, Abadía I, Castaño E, Sosa N, Báez C, Estripeaut D, Díaz Y, Beltrán D, Cisneros J, Cedeño HG, Travassos da Rosa AP, Hernandez H, Martínez-Torres AO, Tesh RB, Weaver SC (2013). Eastern equine encephalitis in Latin America. N Engl J Med *369(8)*: 732-44.

Carrera, J., Cucunubá, Z. M., Neira, K., Lambert, B., Pittí, Y., Liscano, J., Garzón, J. L., Beltran, D., Collado-Mariscal, L., Saenz, L., Sosa, N., Rodriguez-Guzman, L. D., González, P., Lezcano, A. G., Pereyra-Elías, R., Valderrama, A., Weaver, S. C., Vittor, A. Y., Armién, B., Pascale, J., & Donnelly, C. A. (2020). Endemic and epidemic human alphavirus infections in Eastern Panama: an analysis of population-based cross-sectional surveys. The American Journal of Tropical Medicine and Hygiene *103*(6), 2429-2437.

Casals, J. (1963). New developments in the classification of arthropod-borne animal viruses. *An. Microbiol 11*:13.

Centers for Disease Control and Prevention (CDC) website, www.cdc.gov/easternequineencephalitis/tech/epi.html, accessed on January 31st, 2021.

Centers for Disease Control and Prevention (CDC) website, https://www.cdc.gov/easternequineencephalitis/index.html, accessed on January 31st, 2021.

Chang LJ, Dowd KA, Mendoza FH, Saunders JG, Sitar S, Plummer SH, Yamshchikov G, Sarwar UN, Hu Z, Enama ME, Bailer RT, Koup RA, Schwartz RM, Akahata W, Nabel GJ, Mascola JR, Pierson TC, Graham BS, Ledgerwood JE; VRC 311 Study Team (2014). Safety and tolerability of chikungunya virus-like particle vaccine in healthy adults: a phase 1 dose-escalation trial. Lancet. *384(9959)*: 2046-52.

Charles PC, Walters E, Margolis F, Johnston RE (1995). Mechanism of neuroinvasion of Venezuelan equine encephalitis virus in the mouse. Virology *208(2)*: 662-71.

Chatterjee PK, Eng CH, Kielian M (2002). Novel mutations that control the sphingolipid and cholesterol dependence of the Semliki Forest virus fusion protein. J Virol *76(24)*: 12712-22.

Chen, V.B., Arendall, W.B., 3rd, Headd, J.J., Keedy, D.A., Immormino, R.M., Kapral, G.J., Murray, L.W., Richardson, J.S., and Richardson, D.C. (2010). MolProbity: all-atom structure validation for macromolecular crystallography. Acta Crystallogr D Biol Crystallogr *66*: 12-21.

Chen L, Wang M, Zhu D, Sun Z, Ma J, Wang J, Kong L, Wang S, Liu Z, Wei L, He Y, Wang J, Zhang X (2018). Implication for alphavirus host-cell entry and assembly indicated by a 3.5Å resolution cryo-EM structure. Nat Commun *9(1)*: 5326.

Chen, C.L., Hasan, S.S., Klose, T., Sun, Y., Buda, G., Sun, C., Klimstra, W.B., and Rossmann, M.G. (2020). Cryo-EM structure of eastern equine encephalitis virus in complex with heparan sulfate analogues. Proc Natl Acad Sci USA *117*: 8890-8899.

Choi HK, Tong L, Minor W, Dumas P, Boege U, Rossmann MG, Wengler G (1991). Structure of Sindbis virus core protein reveals a chymotrypsin-like serine proteinase and the organization of the virion. Nature. *354(6348)*: 37-43.

Cirimotich CM, Vela EM, Garver J, Barnewall RE, Miller BD, Meister GT, Rogers JV (2017). Chikungunya virus infection in cynomolgus macaques following intradermal and aerosol exposure. Virol J *14(1)*: 135.

Clackson T, Hoogenboom HR, Griffiths AD, Winter G (1991). Making antibody fragments using phage display libraries. Nature *352(6336)*: 624-8.

Corthésy B, Benureau Y, Perrier C, Fourgeux C, Parez N, Greenberg H, Schwartz-Cornil I (2006). Rotavirus anti-VP6 secretory immunoglobulin A contributes to protection via intracellular neutralization but not via immune exclusion. J Virol *80(21)*: 10692-9.

Corti D, Voss J, Gamblin SJ, Codoni G, Macagno A, Jarrossay D, Vachieri SG, Pinna D, Minola A, Vanzetta F, Silacci C, Fernandez-Rodriguez BM, Agatic G, Bianchi S, Giacchetto-Sasselli I, Calder L, Sallusto F, Collins P, Haire LF, Temperton N, Langedijk JP, Skehel JJ, Lanzavecchia A (2011). A neutralizing antibody selected from plasma cells that binds to group 1 and group 2 influenza A hemagglutinins. Science 333(6044): 850-6.

Corti D, Lanzavecchia A (2014). Efficient methods to isolate human monoclonal antibodies from memory B cells and plasma cells. Microbiol Spectr *2(5)*.

Corti D, Misasi J, Mulangu S, Stanley DA, Kanekiyo M, Wollen S, Ploquin A, Doria-Rose NA, Staupe RP, Bailey M, Shi W, Choe M, Marcus H, Thompson EA, Cagigi A, Silacci C, Fernandez-Rodriguez B, Perez L, Sallusto F, Vanzetta F, Agatic G, Cameroni E, Kisalu N, Gordon I, Ledgerwood JE, Mascola JR, Graham BS, Muyembe-Tamfun J-JJ, Trefry JC, Lanzavecchia A, Sullivan NJ (2016). Protective monotherapy against lethal Ebola virus infection by a potently neutralizing antibody. Science *351*: 1339–1342.

Couderc T, Chrétien F, Schilte C, Disson O, Brigitte M, Guivel-Benhassine F, Touret Y, Barau G, Cayet N, Schuffenecker I, Desprès P, Arenzana-Seisdedos F, Michault A, Albert ML, Lecuit M (2008). A mouse model for chikungunya: young age and inefficient type-I interferon signaling are risk factors for severe disease. PLoS Pathog *4(2)*: e29.

Couderc T, Khandoudi N, Grandadam M, Visse C, Gangneux N, Bagot S, Prost JF, Lecuit M (2009). Prophylaxis and therapy for chikungunya virus infection. J Infect Dis *200(4)*: 516-23.

Crans WJ, McNelly J, Schulze TL, Main A (1986). Isolation of eastern equine encephalitis virus from Aedes sollicitans during an epizootic in southern New Jersey. J Am Mosq Control Assoc *2(1)*: 68-72.

Crowe JE Jr. (2017). Principles of broad and potent antiviral human antibodies: insights for vaccine design. Cell Host Microbe *22(2)*: 193-206.

Daneman R, Prat A (2015). The blood-brain barrier. Cold Spring Harb Perspect Biol *7(1)*: a020412.

Davidson E, Doranz BJ. 2014. A high-throughput shotgun mutagenesis approach to mapping B-cell antibody epitopes. Immunology *143*: 13–20.

Davidson E, Bryan C, Fong RH, Barnes T, Pfaff JM, Mabila M, Rucker JB, Doranz BJ. 2015. Mechanism of binding to Ebola virus glycoprotein by the ZMapp, ZMAb, and MB-003 cocktail antibodies. J Virol *89*: 10982–10992.

de la Rosa-Trevin, J.M., Oton, J., Marabini, R., Zaldivar, A., Vargas, J., Carazo, J.M., and Sorzano, C.O. (2013). Xmipp 3.0: an improved software suite for image processing in electron microscopy. J Struct Biol *184*: 321-328.

de la Rosa-Trevin, J.M., Quintana, A., Del Cano, L., Zaldivar, A., Foche, I., Gutierrez, J., Gomez-Blanco, J., Burguet-Castell, J., Cuenca-Alba, J., Abrishami, V*., et al.* (2016). Scipion: A software framework toward integration, reproducibility and validation in 3D electron microscopy. J Struct Biol *195*: 93-99.

DeTulleo, L., and Kirchhausen, T. (1998). The clathrin endocytic pathway in viral infection. EMBO J *17*: 4585-4593.

Diagne CT, Bengue M, Choumet V, Hamel R, Pompon J, Missé D (2020). Mayaro virus pathogenesis and transmission mechanisms. Pathogens *9(9)*: 738.

Doxsey SJ, Brodsky FM, Blank GS, Helenius A (1987). Inhibition of endocytosis by anti-clathrin antibodies. Cell *50(3)*: 453-63.

Dupuy LC, Richards MJ, Livingston BD, Hannaman D, Schmaljohn CS (2018). A multiagent alphavirus DNA vaccine delivered by intramuscular electroporation elicits robust and durable virus-specific immune responses in mice and rabbits and completely protects mice against lethal Venezuelan, Western, and Eastern equine encephalitis virus aerosol challenges. J Immunol Res *2018*: 8521060.

Earnest, J.T., Basore, K., Roy, V., Bailey, A.L., Wang, D., Alter, G., Fremont, D.H., and Diamond, M.S. (2019). Neutralizing antibodies against Mayaro virus require Fc effector functions for protective activity. J Exp Med *216*: 2282-2301.

Edelman R, Tacket CO, Wasserman SS, Bodison SA, Perry JG, Mangiafico JA (2000). Phase II safety and immunogenicity study of live chikungunya virus vaccine TSI-GSD-218. Am J Trop Med Hyg *62(6)*: 681-5.

Edwards MJ, Dimmock NJ (2001). Hemagglutinin 1-specific immunoglobulin G and Fab molecules mediate postattachment neutralization of influenza A virus by inhibition of an early fusion event. J Virol *75(21)*: 10208-18.

Emsley, P., and Cowtan, K. (2004). Coot: model-building tools for molecular graphics. Acta Crystallogr D Biol Crystallogr *60*: 2126-2132.

EnCheng, S., Jing, Z., Tao, Y., QingYuan, X., Yongli, Q., WenShi, W., Peng, W., Liang, S., Jing, S., and DongLai, W. (2013). Analysis of murine B-cell epitopes on Eastern equine encephalitis virus glycoprotein E2. Appl Microbiol Biotechnol *97*: 6359-6372.

Erasmus JH, Seymour RL, Kaelber JT, Kim DY, Leal G, Sherman MB, Frolov I, Chiu W, Weaver SC, Nasar F (2018). Novel insect-specific Eilat virus-based chimeric vaccine candidates provide durable, mono- and multivalent, single-dose protection against lethal alphavirus challenge. J Virol *92(4)*: e01274-17.

Fernandez-Leiro, R., and Scheres, S.H.W. (2017). A pipeline approach to single-particle processing in RELION. Acta Crystallogr D Struct Biol *73*: 496-502.

Fibriansah, G., Ibarra, K.D., Ng, T.S., Smith, S.A., Tan, J.L., Lim, X.N., Ooi, J.S., Kostyuchenko, V.A., Wang, J., de Silva, A.M*., et al.* (2015). DENGUE VIRUS. Cryo-EM

structure of an antibody that neutralizes dengue virus type 2 by locking E protein dimers. Science *349*: 88-91.

Fields W, Kielian M (2013). A key interaction between the alphavirus envelope proteins responsible for initial dimer dissociation during fusion. J Virol *87(7)*: 3774-81.

Firth AE, Chung BY, Fleeton MN, Atkins JF (2008). Discovery of frameshifting in Alphavirus 6K resolves a 20-year enigma. J Virol *5*: 108.

Fischinger, S., Fallon, J.K., Michell, A.R., Broge, T., Suscovich, T.J., Streeck, H., and Alter G. (2019). A high-throughput, bead-based, antigen-specific assay to assess the ability of antibodies to induce complement activation. J Immunol Methods *473*: 112630.

Flyak AI, Ilinykh PA, Murin CD, Garron T, Shen X, Fusco ML, Hashiguchi T, Bornholdt ZA, Slaughter JC, Sapparapu G, Klages C, Ksiazek TG, Ward AB, Saphire EO, Bukreyev A, Crowe JE Jr. (2015). Mechanism of human antibody-mediated neutralization of Marburg virus. Cell. *160*: 893-903.

Flyak AI, Shen X, Murin CD, Turner HL, David JA, Fusco ML, Lampley R, Kose N, Ilinykh PA, Kuzmina N, Branchizio A, King H, Brown L, Bryan C, Davidson E, Doranz BJ, Slaughter JC, Sapparapu G, Klages C, Ksiazek TG, Saphire EO, Ward AB,

Bukreyev A, Crowe JE Jr. (2016). Cross-reactive and potent neutralizing antibody responses in human survivors of natural ebolavirus infection. Cell *164*: 392–405.

Flyak AI, Kuzmina N, Murin CD, Bryan C, Davidson E, Gilchuk P, Gulka CP, Ilinykh PA, Shen X, Huang K, Ramanathan P, Turner H, Fusco ML, Lampley R, Kose N, King H, Sapparapu G, Doranz BJ, Ksiazek TG, Wright DW, Saphire EO, Ward AB, Bukreyev A, Crowe JE Jr. (2018). Broadly neutralizing antibodies from human survivors target a conserved site in the Ebola virus glycoprotein HR2-MPER region. Nat Microbiol *3*: 670–677.

Flynn, D.C., Meyer, W.J., Mackenzie, J.M., Jr., and Johnston, R.E. (1990). A conformational change in Sindbis virus glycoproteins E1 and E2 is detected at the plasma membrane as a consequence of early virus-cell interaction. J Virol *64*, 3643-3653.

Fong, R.H., Banik, S.S., Mattia, K., Barnes, T., Tucker, D., Liss, N., Lu, K., Selvarajah, S., Srinivasan, S., Mabila, M.*, et al.* (2014). Exposure of epitope residues on the outer face of the chikungunya virus envelope trimer determines antibody neutralizing efficacy. J Virol *88*, 14364-14379.

Fong SW, Kini RM, Ng LFP (2018). Mosquito saliva reshapes alphavirus infection and immunopathogenesis. J Virol *92(12)*: e01004-17.

Forsell K, Griffiths G, Garoff H (1996). Preformed cytoplasmic nucleocapsids are not necessary for alphavirus budding. EMBO J *15(23)*: 6495-505.

Forsell K, Xing L, Kozlovska T, Cheng RH, Garoff H (2000). Membrane proteins organize a symmetrical virus. EMBO J. *19(19)*: 5081-91.

Forshey BM, Guevara C, Laguna-Torres VA, Cespedes M, Vargas J, Gianella A, Vallejo E, Madrid C, Aguayo N, Gotuzzo E, Suarez V, Morales AM, Beingolea L, Reyes N, Perez J, Negrete M, Rocha C, Morrison AC, Russell KL, Blair PJ, Olson JG, Kochel TJ (2010). Arboviral etiologies of acute febrile illnesses in Western South America, 2000–2007. PLoS Neglected Tropical Diseases *4*: e787.

Forthal DN (2014). Functions of Antibodies. Microbiol Spectr *2(4)*: AID-0019-2014.

Fox, J.M., Long, F., Edeling, M.A., Lin, H., van Duijl-Richter, M.K.S., Fong, R.H., Kahle, K.M., Smit, J.M., Jin, J., Simmons, G.*, et al.* (2015). Broadly Neutralizing Alphavirus Antibodies Bind an Epitope on E2 and Inhibit Entry and Egress. Cell *163*: 1095-1107.

Fox, J.M., Roy, V., Gunn, B.M., Huang, L., Edeling, M.A., Mack, M., Fremont, D.H., Doranz, B.J., Johnson, S., Alter, G.*, et al.* (2019). Optimal therapeutic activity of

monoclonal antibodies against chikungunya virus requires Fc-FcgammaR interaction on monocytes. Sci Immunol *4*: eaav5062.

Fragkoudis R, Dixon-Ballany CM, Zagrajek AK, Kedzierski L, Fazakerley JK (2018). Following acute encephalitis, Semliki Forest virus is undetectable in the brain by infectivity assays but functional virus RNA capable of generating infectious virus persists for life. Viruses *10(5)*: 273.

Fuller, S.D., Berriman, J.A., Butcher, S.J., and Gowen, B.E. (1995). Low pH induces swiveling of the glycoprotein heterodimers in the Semliki Forest virus spike complex. Cell *81*, 715-725.

Ganesan VK, Duan B, Reid SP (2017). Chikungunya virus: pathophysiology, mechanism, and modeling. Viruses. *9(12)*: 368.

Gardner CL, Burke CW, Tesfay MZ, Glass PJ, Klimstra WB, Ryman KD (2008). Eastern and Venezuelan equine encephalitis viruses differ in their ability to infect dendritic cells and macrophages: impact of altered cell tropism on pathogenesis. J Virol *82(21)*: 10634-46.

Gardner J, Anraku I, Le TT, Larcher T, Major L, Roques P, Schroder WA, Higgs S, Suhrbier A (2010). Chikungunya virus arthritis in adult wild-type mice. J Virol *84(16)*: 8021-32.

Gardner, C.L., Ebel, G.D., Ryman, K.D., and Klimstra, W.B. (2011). Heparan sulfate binding by natural eastern equine encephalitis viruses promotes neurovirulence. Proc Natl Acad Sci U S A *108*: 16026-16031.

Gardner CL, Burke CW, Higgs ST, Klimstra WB, Ryman KD (2012). Interferon-alpha/beta deficiency greatly exacerbates arthritogenic disease in mice infected with wild-type chikungunya virus but not with the cell culture-adapted live-attenuated 181/25 vaccine candidate. Virology *425(2)*: 103-12.

Gardner CL, Choi-Nurvitadhi J, Sun C, Bayer A, Hritz J, Ryman KD, Klimstra WB (2013). Natural variation in the heparan sulfate binding domain of the eastern equine encephalitis virus E2 glycoprotein alters interactions with cell surfaces and virulence in mice. J Virol *87(15)*: 8582-90.

Gardner, C.L., Sun, C., Luke, T., Raviprakash, K., Wu, H., Jiao, J.A., Sullivan, E., Reed, D.S., Ryman, K.D., and Klimstra, W.B. (2017). Antibody preparations from human transchromosomic cows exhibit prophylactic and therapeutic efficacy against Venezuelan equine encephalitis virus. J Virol *91*: e00226-17.

Gérardin P, Couderc T, Bintner M, Tournebize P, Renouil M, Lémant J, Boisson V, Borgherini G, Staikowsky F, Schramm F, Lecuit M, Michault A; Encephalchik Study Group (2016). Chikungunya virus-associated encephalitis: a cohort study on La Réunion Island, 2005-2009. Neurology *86(1)*: 94-102.

Gibbons, D.L., Ahn, A., Chatterjee, P.K., and Kielian, M. (2000). Formation and characterization of the trimeric form of the fusion protein of Semliki Forest virus. J Virol *74*: 7772-7780.

Gibbons, D.L., Ahn, A., Liao, M., Hammar, L., Cheng, R.H., and Kielian, M. (2004). Multistep regulation of membrane insertion of the fusion peptide of Semliki Forest virus. J Virol *78*: 3312-3318.

Gilchuk P, Kuzmina N, Ilinykh PA, Huang K, Gunn BM, Bryan A, Davidson E, Doranz BJ, Turner HL, Fusco ML, Bramble MS, Hoff NA, Binshtein E, Kose N, Flyak AI, Flinko R, Orlandi C, Carnahan R, Parrish EH, Sevy AM, Bombardi RG, Singh PK, Mukadi P, Muyembe-Tamfum JJ, Ohi MD, Saphire EO, Lewis GK, Alter G, Ward AB, Rimoin AW, Bukreyev A, Crowe JE Jr. 2018. Multifunctional pan-ebolavirus antibody recognizes a site of broad vulnerability on the Ebolavirus glycoprotein. Immunity *49*: 363–374.e10.

Gilchuk P, Mire CE, Geisbert JB, Agans KN, Deer DJ, Cross RW, Slaughter JC, Flyak AI, Mani J, Pauly MH, Velasco J, Whaley KJ, Zeitlin L, Geisbert TW, Crowe JE Jr. (2018). Efficacy of human monoclonal antibody monotherapy against bundibugyo virus infection in nonhuman primates. J Infect Dis *218*: S565–S573.

Gilchuk IM, Bangaru S, Gilchuk P, Irving RP, Kose N, Bombardi RG, Thornburg NJ, Creech CB, Edwards KM, Li S, Turner HL, Yu W, Zhu X, Wilson IA, Ward AB, Crowe JE Jr. (2019). Influenza H7N9 virus neuraminidase-specific human monoclonal antibodies inhibit viral egress and protect from lethal influenza infection in mice. Cell Host Microbe *26(6)*: 715-728.e8.

Giudicelli, V., and Lefranc, M.P. (2011). IMGT/junctionanalysis: IMGT standardized analysis of the V-J and V-D-J junctions of the rearranged immunoglobulins (IG) and T cell receptors (TR). Cold Spring Harb Protoc *2011*: 716-725.

Goodchild, S.A., O'Brien, L.M., Steven, J., Muller, M.R., Lanning, O.J., Logue, C.H., D'Elia, R.V., Phillpotts, R.J., and Perkins, S.D. (2011). A humanised murine monoclonal antibody with broad serogroup specificity protects mice from challenge with Venezuelan equine encephalitis virus. Antiviral Res *90*: 1-8.

Grant, T., Rohou, A., and Grigorieff, N. (2018). cisTEM, user-friendly software for single-particle image processing. Elife *7*: e35383.

Grieder FB, Vogel SN (1999). Role of interferon and interferon regulatory factors in early protection against Venezuelan equine encephalitis virus infection. Virology *257(1)*: 106-18.

Griffin, D. (1995). Roles and reactivities of antibodies to alphaviruses. Seminars in Virology *6*: 249-255.

Griffin, D., Levine, B., Tyor, W., Ubol, S., and Despres, P. (1997). The role of antibody in recovery from alphavirus encephalitis. Immunol Rev *159*: 155-161.

Griffin DE (2010). Recovery from viral encephalomyelitis: immune-mediated noncytolytic virus clearance from neurons. Immunol Res *47(1-3)*: 123-33.

Griffin, D.E. (2016). Alphavirus Encephalomyelitis: Mechanisms and approaches to prevention of neuronal damage. Neurotherapeutics *13*: 455-460.

Griffin, D.E. (2016). Neurotropic viral infections (Springer International Publishing).

Grosfeld H, Velan B, Leitner M, Cohen S, Lustig S, Lachmi BE, Shafferman A (1989). Semliki Forest virus E2 envelope epitopes induce a nonneutralizing humoral response which protects mice against lethal challenge. J Virol *63(8)*: 3416-22.

Grosfeld H, Lustig S, Gozes Y, Velan B, Cohen S, Leitner M, Lachmi B, Katz D, Olshevski U, Shafferman A (1992). Divergent envelope E2 alphavirus sequences spanning amino acids 297 to 352 induce in mice virus-specific protective immunity and antibodies with complement-mediated cytolytic activity. J Virol *66(2)*: 1084-90.

Hahn CS, Lustig S, Strauss EG, Strauss JH (1988). Western equine encephalitis virus is a recombinant virus. Proc Natl Acad Sci USA *85*: 5997–6001.

Halfmann P, Kim JH, Ebihara H, Noda T, Neumann G, Feldmann H, Kawaoka Y. 2008. Generation of biologically contained Ebola viruses. Proc Natl Acad Sci USA *105*: 1129–1133.

Hanson, RP, Sulkin, SE, Beuscher, EL, Hammon, WM, McKinney, RW, Work, TH (1967). Arbovirus infections of laboratory workers. Extent of problem emphasizes the need for more effective measures to reduce hazards. Science *158*: 1283–1286.

Hardy WR, Strauss JH (1989). Processing the nonstructural polyproteins of sindbis virus: nonstructural proteinase is in the C-terminal half of nsP2 and functions both in cis and in trans. J Virol *63(11)*: 4653-64.

Hasan SS, Sun C, Kim AS, Watanabe Y, Chen CL, Klose T, Buda G, Crispin M, Diamond MS, Klimstra WB, Rossmann MG (2018). Cryo-EM structures of Eastern equine encephalitis virus reveal mechanisms of virus disassembly and antibody neutralization. Cell Rep *25(11)*: 3136-3147.e5.

Hashiguchi T, Fusco ML, Bornholdt ZA, Lee JE, Flyak AI, Matsuoka R, Kohda D, Yanagi Y, Hammel M, Crowe JE Jr, Saphire EO. 2015. Structural basis for Marburg virus neutralization by a cross-reactive human antibody. Cell *160*: 904–912.

Hawley RJ, Eitzen EM Jr. (2001). Biological weapons--a primer for microbiologists. Annu Rev Microbiol 55: 235-53.

Hawman DW, Stoermer KA, Montgomery SA, Pal P, Oko L, Diamond MS, Morrison TE (2013). Chronic joint disease caused by persistent chikungunya virus infection is controlled by the adaptive immune response. J Virol *87(24)*: 13878-88.

Helenius A, Marsh M, White J (1982). Inhibition of Semliki forest virus penetration by lysosomotropic weak bases. J Gen Virol 58 Pt 1:47-61.

Henderson, R., Sali, A., Baker, M.L., Carragher, B., Devkota, B., Downing, K.H., Egelman, E.H., Feng, Z., Frank, J., Grigorieff, N.*, et al.* (2012). Outcome of the first electron microscopy validation task force meeting. Structure *20*: 205-214.

Her Z, Teng TS, Tan JJ, Teo TH, Kam YW, Lum FM, Lee WW, Gabriel C, Melchiotti R, Andiappan AK, Lulla V, Lulla A, Win MK, Chow A, Biswas SK, Leo YS, Lecuit M, Merits A, Rénia L, Ng LF (2015). Loss of TLR3 aggravates CHIKV replication and pathology due to an altered virus-specific neutralizing antibody response. EMBO Mol Med *7(1)*: 24-41.

Hoch AL, Peterson NE, LeDuc JW, Pinheiro FP (1981). An outbreak of Mayaro virus disease in Belterra, Brazil. III. Entomological and ecological studies. Am J Trop Med Hyg *30(3)*: 689-98.

Holmes, A.C., Basore, K., Fremont, D.H., and Diamond, M.S. (2020). A molecular understanding of alphavirus entry. PLoS Pathog *16*, e1008876.

Hong EM, Perera R, Kuhn RJ (2006). Alphavirus capsid protein helix I controls a checkpoint in nucleocapsid core assembly. J Virol *80(18)*: 8848-55.

Honnold SP, Mossel EC, Bakken RR, Lind CM, Cohen JW, Eccleston LT, Spurgers KB, Erwin-Cohen R, Glass PJ, Maheshwari RK (2015). Eastern equine encephalitis virus in mice II: pathogenesis is dependent on route of exposure. J Virol *12*: 154.

Hoogenboom HR (2002). Overview of antibody phage-display technology and its applications. Methods Mol Biol *178*: 1-37.

Hulseweh, B., Rulker, T., Pelat, T., Langermann, C., Frenzel, A., Schirrmann, T., Dubel, S., Thullier, P., and Hust, M. (2014). Human-like antibodies neutralizing Western equine encephalitis virus. MAbs *6*: 718-727.

Hunt, A.R., and Roehrig, J.T. (1985). Biochemical and biological characteristics of epitopes on the E1 glycoprotein of western equine encephalitis virus. Virology *142*: 334-346.

Hunt, A.R., Johnson, A.J., and Roehrig, J.T. (1990). Synthetic peptides of Venezuelan equine encephalomyelitis virus E2 glycoprotein. I. Immunogenic analysis and identification of a protective peptide. Virology *179*: 701-711.

Hunt, A.R., Short, W.A., Johnson, A.J., Bolin, R.A., and Roehrig, J.T. (1991). Synthetic peptides of the E2 glycoprotein of Venezuelan equine encephalomyelitis virus. II. Antibody to the amino terminus protects animals by limiting viral replication. Virology *185*: 281-290.

Hunt, A.R., and Roehrig, J.T. (1995). Localization of a protective epitope on a Venezuelan equine encephalomyelitis (VEE) virus peptide that protects mice from both

epizootic and enzootic VEE virus challenge and is immunogenic in horses. Vaccine *13*: 281-288.

Hunt, A.R., Frederickson, S., Hinkel, C., Bowdish, K.S., and Roehrig, J.T. (2006). A humanized murine monoclonal antibody protects mice either before or after challenge with virulent Venezuelan equine encephalomyelitis virus. J Gen Virol *87*: 2467-2476.

Hunt, A.R., Frederickson, S., Maruyama, T., Roehrig, J.T., and Blair, C.D. (2010). The first human epitope map of the alphaviral E1 and E2 proteins reveals a new E2 epitope with significant virus neutralizing activity. PLoS Negl Trop Dis *4*: e739.

Hunt, A.R., Bowen, R.A., Frederickson, S., Maruyama, T., Roehrig, J.T., and Blair, C.D. (2011). Treatment of mice with human monoclonal antibody 24h after lethal aerosol challenge with virulent Venezuelan equine encephalitis virus prevents disease but not infection. Virology *414*: 146-152.

Hyde JL, Gardner CL, Kimura T, White JP, Liu G, Trobaugh DW, Huang C, Tonelli M, Paessler S, Takeda K, Klimstra WB, Amarasinghe GK, Diamond MS (2014). A viral RNA structural element alters host recognition of nonself RNA. Science *343(6172)*: 783-7.

Jacobs SE, Lamson DM, St George K, Walsh TJ (2013). Human rhinoviruses. Clin Microbiol Rev. *26(1)*: 135-62.

Jahrling PB, Stephenson EH (1984). Protective efficacies of live attenuated and formaldehyde-inactivated Venezuelan equine encephalitis virus vaccines against aerosol challenge in hamsters. J Clin Microbiol *19(3)*: 429-31.

Jemielity S, Wang JJ, Chan YK, Ahmed AA, Li W, Monahan S, Bu X, Farzan M, Freeman GJ, Umetsu DT, Dekruyff RH, Choe H (2013). TIM-family proteins promote infection of multiple enveloped viruses through virion-associated phosphatidylserine. PLoS Pathog *9(3)*: e1003232.

Jennewein MF, Alter G (2017). The immunoregulatory roles of antibody glycosylation. Trends Immunol *38(5)*: 358-372.

Jin, J., Liss, N.M., Chen, D.H., Liao, M., Fox, J.M., Shimak, R.M., Fong, R.H., Chafets, D., Bakkour, S., Keating, S.*, et al.* (2015). Neutralizing monoclonal antibodies block chikungunya virus entry and release by targeting an epitope critical to viral pathogenesis. Cell Rep *13*: 2553-2564.

Jin J, Galaz-Montoya JG, Sherman MB, Sun SY, Goldsmith CS, O'Toole ET, Ackerman L, Carlson LA, Weaver SC, Chiu W, Simmons G (2018). Neutralizing antibodies inhibit

chikungunya virus budding at the plasma membrane. Cell Host Microbe *24(3)*: 417-428.e5.

Jin, J. and Simmons, G. (2019). Antiviral functions of monoclonal antibodies against Chikungunya virus. Viruses *11*: 305.

Johnson AJ, Hunt AR, Roehrig JT (1991). Synthetic peptides of Venezuelan equine encephalomyelitis virus E2 glycoprotein. III. Identification of a protective peptide derived from the carboxy-terminal extramembranal one-third of the protein. Virology *185(2)*: 840-2.

Jose J, Snyder JE, Kuhn RJ (2009). A structural and functional perspective of alphavirus replication and assembly. Future Microbiol *4(7)*: 837-56.

Jose J, Taylor AB, Kuhn RJ (2017). Spatial and temporal analysis of alphavirus replication and assembly in mammalian and mosquito cells. mBio *8(1)*: e02294-16.

Jupp PG, McIntosh BM, Dos Santos I, DeMoor P (1981). Laboratory vector studies on six mosquito and one tick species with chikungunya virus. Trans R Soc Trop Med Hyg *75(1)*: 15-9.

Jupp PG, McIntosh BM (1990). Aedes furcifer and other mosquitoes as vectors of chikungunya virus at Mica, northeastern Transvaal, South Africa. J Am Mosq Control Assoc *6(3)*: 415-20.

Justman J., Klimjack, M.R., and Kielian, M. (1993). Role of spike protein conformational changes in fusion of Semliki Forest virus. J Virol *67*: 7597-607.

Kam YW, Ong EK, Rénia L, Tong JC, Ng LF (2009). Immuno-biology of chikungunya and implications for disease intervention. Microbes Infect *11(14-15)*: 1186-96.

Karsten, C.B., Mehta, N., Shin, S.A., Diefenbach, T.J., Slein, M.D., Karpinski, W., Irvine, E.B., Broge, T., Suscovich, T.J., and Alter, G. (2019). A versatile high-throughput assay to characterize antibody-mediated neutrophil phagocytosis. J Immunol Methods *471*: 46-56.

Kaufmann B, Nybakken GE, Chipman PR, Zhang W, Diamond MS, Fremont DH, Kuhn RJ, Rossmann MG (2006). West Nile virus in complex with the Fab fragment of a neutralizing monoclonal antibody. Proc Natl Acad Sci USA *103(33)*: 12400-4.

Kielian M, Chanel-Vos C, Liao M (2010). Alphavirus entry and membrane fusion. Viruses *2(4)*: 796-825.

Kielian M, Rey FA (2006). Virus membrane-fusion proteins: more than one way to make a hairpin. Nat Rev Microbiol *4(1)*: 67-76.

Kielian M (2014). Mechanisms of virus membrane fusion proteins. Annu Rev Virol *1(1)*: 171-89.

Kim, A.S., Austin, S.K., Gardner, C.L., Zuiani, A., Reed, D.S., Trobaugh, D.W., Sun, C., Basore, K., Williamson, L.E., Crowe, J.E., Jr.*, et al.* (2019). Protective antibodies against Eastern equine encephalitis virus bind to epitopes in domains A and B of the E2 glycoprotein. Nat Microbiol *4*: 187-197.

Klimstra WB, Ryman KD, Johnston RE (1998). Adaptation of Sindbis virus to BHK cells selects for use of heparan sulfate as an attachment receptor. J Virol 72(9): 7357-66.

Klimstra, W.B., Nangle, E.M., Smith, M.S., Yurochko, A.D., and Ryman, K.D. (2003). DC-SIGN and L-SIGN can act as attachment receptors for alphaviruses and distinguish between mosquito cell- and mammalian cell-derived viruses. J Virol *77*: 12022-12032.

Ko, S.Y., Akahata, W., Yang, E.S., Kong, W.P., Burke, C.W., Honnold, S.P., Nichols, D.K., Huang, Y.S., Schieber, G.L., Carlton, K.*, et al.* (2019). A virus-like particle vaccine prevents equine encephalitis virus infection in nonhuman primates. Sci Transl Med *11*: eaav3113.

Kose, N., Fox, J.M., Sapparapu, G., Bombardi, R., Tennekoon, R.N., de Silva, A.D., Elbashir, S.M., Theisen, M.A., Humphris-Narayanan, E., Ciaramella, G.*, et al.* (2019). A lipid-encapsulated mRNA encoding a potently neutralizing human monoclonal antibody protects against chikungunya infection. Sci Immunol *4*: eaaw6647.

Krammer F (2019). The human antibody response to influenza A virus infection and vaccination. Nat Rev Immunol *19(6)*: 383-397.

Krzywinski M, Schein J, Birol I, Connors J, Gascoyne R, Horsman D, Jones SJ, Marra MA. 2009. Circos: an information aesthetic for comparative genomics. Genome Res *19*: 1639–1645.

Kulcsar KA, Baxter VK, Greene IP, Griffin DE (2014). Interleukin 10 modulation of pathogenic Th17 cells during fatal alphavirus encephalomyelitis. Proc Natl Acad Sci USA *111(45)*: 16053-8.

Kulcsar KA, Baxter VK, Abraham R, Nelson A, Griffin DE (2015). Distinct Immune Responses in Resistant and Susceptible Strains of Mice during Neurovirulent Alphavirus Encephalomyelitis. J Virol *89(16)*: 8280-91.

Kuhn JH, Andersen KG, Bào Y, Bavari S, Becker S, Bennett RS, Bergman NH, Blinkova O, Bradfute S, Brister JR, Bukreyev A, Chandran K, Chepurnov AA, Davey RA, Dietzgen RG, Doggett NA, Dolnik O, Dye JM, Enterlein S, Fenimore PW, Formenty P, Freiberg AN, Garry RF, Garza NL, Gire SK, Gonzalez J-PP, Griffiths A, Happi CT, Hensley LE, Herbert AS, Hevey MC, Hoenen T, Honko AN, Ignatyev GM, Jahrling PB, Johnson JC, Johnson KM, Kindrachuk J, Klenk H-DD, Kobinger G, Kochel TJ, Lackemeyer MG, Lackner DF, Leroy EM, Lever MS, Mühlberger E, Netesov SV, Olinger GG, Omilabu SA, Palacios G, et al. 2014. Filovirus RefSeq entries: evaluation and selection of filovirus type variants, type sequences, and names. Viruses *6*: 3663–3682.

Lam S, Nyo M, Phuektes P, Yew CW, Tan YJ, Chu JJ (2015). A potent neutralizing IgM mAb targeting the N218 epitope on E2 protein protects against Chikungunya virus pathogenesis. MAbs *7(6)*: 1178-94.

Langsjoen, R.M., Haller, S.L., Roy, C.J., Vinet-Oliphant, H., Bergren, N.A., Erasmus, J.H., Livengood, J.A., Powell, T.D., Weaver, S.C., and Rossi, S.L. (2018). Chikungunya virus strains show lineage-specific variations in virulence and cross-protective ability in murine and nonhuman primate models. mBio *9*.

Lanzavecchia A (2018). Dissecting human antibody responses: useful, basic and surprising findings. EMBO Mol Med *10(3)*: e8879.

Larrick, J., Danielsson, L., Brenner, C. *et al.* (1989). Polymerase chain reaction using mixed primers: cloning of human monoclonal antibody variable region genes from single hybridoma cells. Nat Biotechnol 7: 934–938.

Lednicky, J.A., White, S.K., Mavian, C.N., El Badry, M.A., Telisma, T., Salemi, M., BA, O.K., Beau De Rochars, V.M., and Morris, J.G., Jr. (2019). Emergence of Madariaga virus as a cause of acute febrile illness in children, Haiti, 2015-2016. PLoS Negl Trop Dis *13*: e0006972.

Lee CY, Kam YW, Fric J, Malleret B, Koh EG, Prakash C, Huang W, Lee WW, Lin C, Lin RT, Renia L, Wang CI, Ng LF, Warter L (2011). Chikungunya virus neutralization antigens and direct cell-to-cell transmission are revealed by human antibody-escape mutants. PLoS Pathog *7(12)*: e1002390.

Lee JE, Fusco ML, Hessell AJ, Oswald WB, Burton DR, Saphire EO (2008). Structure of the Ebola virus glycoprotein bound to an antibody from a human survivor. Nature *454*: 177–182.

Lemm JA, Rümenapf T, Strauss EG, Strauss JH, Rice CM (1994). Polypeptide requirements for assembly of functional Sindbis virus replication complexes: a model for the temporal regulation of minus- and plus-strand RNA synthesis. EMBO J *13(12)*: 2925-34.

Lescar, J., Roussel, A., Wien, M.W., Navaza, J., Fuller, S.D., Wengler, G., Wengler, G., and Rey, F.A. (2001). The Fusion glycoprotein shell of Semliki Forest virus: an icosahedral assembly primed for fusogenic activation at endosomal pH. Cell *105*: 137-148.

Leung JY, Ng MM, Chu JJ (2011). Replication of alphaviruses: a review on the entry process of alphaviruses into cells. Adv Virol 2011: 249640.

Levine, B., Hardwick, J.M., Trapp, B.D., Crawford, T.O., Bollinger, R.C., and Griffin, D.E. (1991). Antibody-mediated clearance of alphavirus infection from neurons. Science *254*: 856-860.

Levitt NH, Ramsburg HH, Hasty SE, Repik PM, Cole FE Jr, Lupton HW (1986). Development of an attenuated strain of chikungunya virus for use in vaccine production. Vaccine *4(3)*: 157-62.

Li, L., Jose, J., Xiang, Y., Kuhn, R.J., and Rossmann, M.G. (2010). Structural changes of envelope proteins during alphavirus fusion. Nature *468*: 705-708.

Lidbury BA, Rulli NE, Suhrbier A, Smith PN, McColl SR, Cunningham AL, Tarkowski A, van Rooijen N, Fraser RJ, Mahalingam S (2008). Macrophage-derived proinflammatory

factors contribute to the development of arthritis and myositis after infection with an arthrogenic alphavirus. J Infect Dis *197(11)*: 1585-93.

Liljeström P, Lusa S, Huylebroeck D, Garoff H (1991). In vitro mutagenesis of a full-length cDNA clone of Semliki Forest virus: the small 6,000-molecular-weight membrane protein modulates virus release. J Virol *65(8)*: 4107-13.

Lindsey, N.P., Staples, J.E., and Fischer, M. (2018). Eastern equine encephalitis virus in the United States, 2003-2016. Am J Trop Med Hyg *98*: 1472-1477.

Lindsey, N.P., Martin, S.W., Staples, J.E., and Fischer, M. (2020). Notes from the field: multistate outbreak of Eastern equine encephalitis virus - United States, 2019. MMWR Morb Mortal Wkly Rep *69*: 50-51.

Liu JL, Shriver-Lake LC, Zabetakis D, Goldman ER, Anderson GP (2018). Selection of single-domain antibodies towards Western equine encephalitis virus. Antibodies (Basel) *7(4)*: 44.

Loewy A, Smyth J, von Bonsdorff CH, Liljeström P, Schlesinger MJ (1995). The 6-kilodalton membrane protein of Semliki Forest virus is involved in the budding process. J Virol *69(1)*: 469-75.

Lonberg N (2005). Human antibodies from transgenic animals. Nat Biotechnol *23(9)*: 1117-25.

Long, F., Fong, R.H., Austin, S.K., Chen, Z., Klose, T., Fokine, A., Liu, Y., Porta, J., Sapparapu, G., Akahata, W.*, et al.* (2015). Cryo-EM structures elucidate neutralizing mechanisms of anti-chikungunya human monoclonal antibodies with therapeutic activity. Proc Natl Acad Sci USA *112*: 13898-13903.

Lu LL, Suscovich TJ, Fortune SM, Alter G (2018). Beyond binding: antibody effector functions in infectious diseases. Nat Rev Immunol 18(1): 46-61.

Lu RM, Hwang YC, Liu IJ, Lee CC, Tsai HZ, Li HJ, Wu HC (2020). Development of therapeutic antibodies for the treatment of diseases. J Biomed Sci *27(1)*: 1.

Lu YE, Kielian M (2000). Semliki forest virus budding: assay, mechanisms, and cholesterol requirement. J Virol 74(17): 7708-19.

Ludwig GV, Kondig JP, Smith JF (1996). A putative receptor for Venezuelan equine encephalitis virus from mosquito cells. J Virol *70(8)*: 5592-9.

Lum FM, Teo TH, Lee WW, Kam YW, Rénia L, Ng LF (2013). An essential role of antibodies in the control of chikungunya virus infection. J Immunol 190(12): 6295-302.

Lum FM, Couderc T, Chia BS, Ong RY, Her Z, Chow A, Leo YS, Kam YW, Rénia L, Lecuit M, Ng LFP (2018). Antibody-mediated enhancement aggravates chikungunya virus infection and disease severity. Sci Rep *8(1)*: 1860.

Lynch RM, Tran L, Louder MK, Schmidt SD, Cohen M; CHAVI 001 Clinical Team Members, Dersimonian R, Euler Z, Gray ES, Abdool Karim S, Kirchherr J, Montefiori DC, Sibeko S, Soderberg K, Tomaras G, Yang ZY, Nabel GJ, Schuitemaker H, Morris L, Haynes BF, Mascola JR (2012). The development of CD4 binding site antibodies during HIV-1 infection. J Virol *86(14)*: 7588-95.

Lyon MG, Mehta AK, Varkey JB, Brantly K, Plyler L, McElroy AK, Kraft CS, Towner JS, Spiropoulou C, Ströher U, Uyeki TM, Ribner BS, Emory Serious Communicable Diseases Unit. 2014. Clinical care of two patients with Ebola virus disease in the United States. N Engl J Med *371*: 2402–2409.

Ma, H., Kim, A.S., Kafai, N.M., Earnest, J.T., Shah, A.P., Case, J.B., Basore, K., Gilliland, T.C., Sun, C., Nelson, C.A.*, et al.* (2020). LDLRAD3 is a receptor for Venezuelan equine encephalitis virus. Nature *588*: 308-314.

Mallilankaraman K, Shedlock DJ, Bao H, Kawalekar OU, Fagone P, Ramanathan AA, Ferraro B, Stabenow J, Vijayachari P, Sundaram SG, Muruganandam N, Sarangan G,

Srikanth P, Khan AS, Lewis MG, Kim JJ, Sardesai NY, Muthumani K, Weiner DB (2011). A DNA vaccine against chikungunya virus is protective in mice and induces neutralizing antibodies in mice and nonhuman primates. PLoS Negl Trop Dis *5(1)*: e928.

Marks JD, Hoogenboom HR, Bonnert TP, McCafferty J, Griffiths AD, Winter G (1991). By-passing immunization. Human antibodies from V-gene libraries displayed on phage. J Mol Biol 222(3): 581-97.

Marquardt MT, Phalen T, Kielian M (1993). Cholesterol is required in the exit pathway of Semliki Forest virus. J Cell Biol *123(1)*: 57-65.

Marston HD, Paules CI, Fauci AS (2018). Monoclonal antibodies for emerging infectious diseases - borrowing from history. N Engl J Med 378(16): 1469-1472.

Martinez MG, Kielian M (2016). Intercellular extensions are induced by the alphavirus structural proteins and mediate virus transmission. PLoS Pathog *12(12)*: e1006061.

Masrinoul P, Puiprom O, Tanaka A, Kuwahara M, Chaichana P, Ikuta K, Ramasoota P, Okabayashi T (2014). Monoclonal antibody targeting chikungunya virus envelope 1 protein inhibits virus release. Virology 464-465: 111-117.

Mastronarde, D.N. (2005). Automated electron microscope tomography using robust prediction of specimen movements. J Struct Biol *152*: 36-51.

Mathews JH, Roehrig JT (1982). Determination of the protective epitopes on the glycoproteins of Venezuelan equine encephalomyelitis virus by passive transfer of monoclonal antibodies. J Immunol *129(6)*: 2763-7.

Mavalankar D, Shastri P, Bandyopadhyay T, Parmar J, Ramani KV (2008). Increased mortality rate associated with chikungunya epidemic, Ahmedabad, India. Emerg Infect Dis *14(3)*: 412-5.

Mazanec MB, Coudret CL, Fletcher DR (1995). Intracellular neutralization of influenza virus by immunoglobulin A anti-hemagglutinin monoclonal antibodies. J Virol *69(2)*: 1339-43.

McClain DJ, Pittman PR, Ramsburg HH, Nelson GO, Rossi CA, Mangiafico JA, et al. (1998). Immunologic interference from sequential administration of live attenuated alphavirus vaccines. J Infect Dis 177: 634–41.

McElroy AK, Akondy RS, Davis CW, Ellebedy AH, Mehta AK, Kraft CS, Lyon GM, Ribner BS, Varkey J, Sidney J, Sette A, Campbell S, Ströher U, Damon I, Nichol ST,

Spiropoulou CF, Ahmed R (2015). Human Ebola virus infection results in substantial immune activation. Proc Natl Acad Sci USA *112*: 4719–4724.

Mckinney R. W. et al. (1963) 'Use of an Attenuated Strain of Venezuelan Equine Encephalo-Myelitis Virus for Immunization in Man', The American Journal of Tropical Medicine Hygiene, 12: 597–603.

Meissner JD, Huang CY, Pfeffer M, Kinney RM (1999). Sequencing of prototype viruses in the Venezuelan equine encephalitis antigenic complex. Virus Res *64(1)*: 43-59.

Mendes, A., & Kuhn, R. J. (2018). Alphavirus Nucleocapsid Packaging and Assembly. Viruses *10*(3): 138.

Mendoza, Q.P., Stanley, J., and Griffin, D.E. (1988). Monoclonal antibodies to the E1 and E2 glycoproteins of Sindbis virus: definition of epitopes and efficiency of protection from fatal encephalitis. J Gen Virol *69(Pt 12)*: 3015-3022.

Mestas J, Hughes CC (2004). Of mice and not men: differences between mouse and human immunology. J Immunol *172(5)*: 2731-8.

Metcalf, T.U., and Griffin, D.E. (2011). Alphavirus-induced encephalomyelitis: antibody-secreting cells and viral clearance from the nervous system. J Virol *85*: 11490-11501.

Metcalf, T.U., Baxter, V.K., Nilaratanakul, V., and Griffin, D.E. (2013). Recruitment and retention of B cells in the central nervous system in response to alphavirus encephalomyelitis. J Virol *87*: 2420-2429.

Metz SW, Gardner J, Geertsema C, Le TT, Goh L, Vlak JM, Suhrbier A, Pijlman GP (2013). Effective chikungunya virus-like particle vaccine produced in insect cells. PLoS Negl Trop Dis *7(3)*: e2124.

Meyer, W.J., Gidwitz, S., Ayers, V.K., Schoepp, R.J., and Johnston, R.E. (1992). Conformational alteration of Sindbis virion glycoproteins induced by heat, reducing agents, or low pH. J Virol *66*: 3504-3513.

Meyer, W.J., and Johnston, R.E. (1993). Structural rearrangement of infecting Sindbis virions at the cell surface: mapping of newly accessible epitopes. J Virol *67*: 5117-5125.

Misasi J, Gilman MS, Kanekiyo M, Gui M, Cagigi A, Mulangu S, Corti D, Ledgerwood JE, Lanzavecchia A, Cunningham J, Muyembe-Tamfun JJ, Baxa U, Graham BS, Xiang Y, Sullivan NJ, McLellan JS (2016). Structural and molecular basis for Ebola virus neutralization by protective human antibodies. Science *351*: 1343–1346.

Mitchell, C.J., Niebylski, M.L., Smith, G.C., Karabatsos, N., Martin, D., Mutebi, J.P., Craig, G.B., Jr., and Mahler, M.J. (1992). Isolation of eastern equine encephalitis virus from Aedes albopictus in Florida. Science *257*: 526-527.

Morens, D.M., Folkers, G.K., and Fauci, A.S. (2019). Eastern equine encephalitis virus - another emergent arbovirus in the United States. N Engl J Med *381*: 1989-1992.

Mostafavi H, Abeyratne E, Zaid A, Taylor A (2019). Arthritogenic alphavirus-induced immunopathology and targeting host inflammation as a therapeutic strategy for alphaviral disease. Viruses *11(3)*: 290.

Mukhopadhyay, S., Zhang, W., Gabler, S., Chipman, P.R., Strauss, E.G., Strauss, J.H., Baker, T.S., Kuhn, R.J., and Rossmann, M.G. (2006). Mapping the structure and function of the E1 and E2 glycoproteins in alphaviruses. Structure *14*: 63-73.

Murin CD, Fusco ML, Bornholdt ZA, Qiu X, Olinger GG, Zeitlin L, Kobinger GP, Ward AB, Saphire EO (2014). Structures of protective antibodies reveal sites of vulnerability on Ebola virus. Proc Natl Acad Sci USA *111*: 17182–17187.

Muthumani K, Lankaraman KM, Laddy DJ, Sundaram SG, Chung CW, Sako E, Wu L, Khan A, Sardesai N, Kim JJ, Vijayachari P, Weiner DB (2008). Immunogenicity of novel consensus-based DNA vaccines against chikungunya virus. Vaccine *26(40)*: 5128-34.

Narayan R, Tripathi S (2020). Intrinsic ADE: The dark side of antibody dependent enhancement during dengue infection. Front Cell Infect Microbiol *10*: 580096.

Neighbours LM, Long K, Whitmore AC, Heise MT (2012). Myd88-dependent toll-like receptor 7 signaling mediates protection from severe Ross River virus-induced disease in mice. J Virol *86(19)*: 10675-85.

Neves V, A.-d.-S.F., Corte-Real S, A.R.B. Castanho M (2016). Antibody approaches to treat brain diseases. Trends in Biotechnology *34*: 36-48.

Nilaratanakul, V., Chen, J., Tran, O., Baxter, V.K., Troisi, E.M., Yeh, J.X., and Griffin, D.E. (2018). Germ line IgM is sufficient, but not required, for antibody-mediated alphavirus clearance from the central nervous system. J Virol *92*: e02081-17.

Noranate N, Takeda N, Chetanachan P, Sittisaman P, A-Nuegoonpipat A, Anantapreecha S (2014). Characterization of chikungunya virus-like particles. PLoS One 9(9): e108169.

Noval, M.G., Rodriguez-Rodriguez, B.A., Rangel, M.V., and Stapleford, K.A. (2019). Evolution-driven attenuation of alphaviruses highlights key glycoprotein determinants regulating viral infectivity and dissemination. Cell Rep *28*: 460-471.

Ohi, M., Li, Y., Cheng, Y., and Walz, T. (2004). Negative staining and image classification - powerful tools in modern electron microscopy. Biol Proced Online *6*: 23-34.

Oliphant, T., Engle, M., Nybakken, G.E., Doane, C., Johnson, S., Huang, L., Gorlatov, S., Mehlhop, E., Marri, A., Chung, K.M., Ebel, G.D., Kramer, L.D., Fremont, D.H., and Diamond, M.S. (2005) Development of a humanized monoclonal antibody with therapeutic potential against West Nile virus. Nat Med *11*: 522-30.

Owen KE, Kuhn RJ (1996). Identification of a region in the Sindbis virus nucleocapsid protein that is involved in specificity of RNA encapsidation. J Virol *70(5)*: 2757-63.

Paes C, Ingalls J, Kampani K, Sulli C, Kakkar E, Murray M, Kotelnikov V, Greene TA, Rucker JB, Doranz BJ (2009). Atomic-level mapping of antibody epitopes on a GPCR. J Am Chem Soc *131*: 6952–6954.

Paessler S, Fayzulin RZ, Anishchenko M, Greene IP, Weaver SC, Frolov I (2003). Recombinant Sindbis/Venezuelan equine encephalitis virus is highly attenuated and immunogenic. J Virol *77(17)*: 9278-86.

Paessler S, Weaver SC (2009). Vaccines for Venezuelan equine encephalitis. Vaccine *27 (Suppl 4)*: D80-5.

Pal, P., Dowd, K.A., Brien, J.D., Edeling, M.A., Gorlatov, S., Johnson, S., Lee, I., Akahata, W., Nabel, G.J., Richter, M.K.*, et al.* (2013). Development of a highly protective combination monoclonal antibody therapy against chikungunya virus. PLoS Pathog *9*: e1003312.

Pallesen J, Murin CD, de Val N, Cottrell CA, Hastie KM, Turner HL, Fusco ML, Flyak AI, Zeitlin L, Crowe JE Jr, Andersen KG, Saphire EO, Ward AB (2016). Structures of Ebola virus GP and sGP in complex with therapeutic antibodies. Nat Microbiol *1*: 16128.

Parker MD, Buckley MJ, Melanson VR, Glass PJ, Norwood D, Hart MK (2010). Antibody to the E3 glycoprotein protects mice against lethal Venezuelan equine encephalitis virus infection. J Virol *84(24)*: 12683-90.

Pereboev, A.V., Razumov, I.A., Svyatchenko, V.A., and Loktev, V.B. (1996). Glycoproteins E2 of the Venezuelan and eastern equine encephalomyelitis viruses contain multiple cross-reactive epitopes. Arch Virol *141*: 2191-2205.

Pettersen, E.F., Goddard, T.D., Huang, C.C., Couch, G.S., Greenblatt, D.M., Meng, E.C., and Ferrin, T.E. (2004). UCSF Chimera--a visualization system for exploratory research and analysis. J Comput Chem *25*: 1605-1612.

Phelps, A.L., O'Brien, L.M., Eastaugh, L.S., Davies, C., Lever, M.S., Ennis, J., Zeitlin, L., Nunez, A., and Ulaeto, D.O. (2019). Aerosol infection of Balb/c mice with eastern equine encephalitis virus; susceptibility and lethality. Virol J *16*: 2.

Phillpotts RJ (2006). Venezuelan equine encephalitis virus complex-specific monoclonal antibody provides broad protection, in murine models, against airborne challenge with viruses from serogroups I, II and III. Virus Res *120(1-2)*: 107-12.

Pierson TC, Diamond MS (2008). Molecular mechanisms of antibody-mediated neutralization of flavivirus infection. Expert Rev Mol Med *10*: e12.

Pittman PR, Makuch RS, Mangiafico JA, Cannon TL, Gibbs PH, Peters CJ (1996). Long-term duration of detectable neutralizing antibodies after administration of live-attenuated VEE vaccine and following booster vaccination with inactivated VEE vaccine. Vaccine *14*: 337–343.

Poddar S, Hyde JL, Gorman MJ, Farzan M, Diamond MS (2016). The interferon-stimulated gene IFITM3 restricts infection and pathogenesis of arthritogenic and encephalitic alphaviruses. J Virol *90(19)*: 8780-94.

Porta, J., Jose, J., Roehrig, J.T., Blair, C.D., Kuhn, R.J., and Rossmann, M.G. (2014). Locking and blocking the viral landscape of an alphavirus with neutralizing antibodies. J Virol *88*: 9616-9623.

Porta J, Mangala Prasad V, Wang CI, Akahata W, Ng LF, Rossmann MG (2015). Structural studies of chikungunya virus-like particles complexed with human antibodies: neutralization and cell-to-cell transmission. J Virol *90(3)*: 1169-77.

Powell, L.A., Fox, J.M., Kose, N., Kim, A.S., Majedi, M., Bombardi, R., Carnahan, R.H., Slaughter, J.C., Morrison, T.E., Diamond, M.S.*, et al.* (2020). Human monoclonal antibodies against Ross River virus target epitopes within the E2 protein and protect against disease. PLoS Pathog *16*: e1008517.

Powell LA, Miller A, Fox JM, Kose N, Klose T, Kim AS, Bombardi R, Tennekoon RN, Dharshan de Silva A, Carnahan RH, Diamond MS, Rossmann MG, Kuhn RJ, Crowe JE Jr. (2020). Human mAbs broadly protect against arthritogenic alphaviruses by recognizing conserved elements of the mxra8 receptor-binding site. Cell Host Microbe *28(5)*: 699-711.e7.

Powers AM, Brault AC, Tesh RB, Weaver SC (2000). Re-emergence of chikungunya and O'nyong-nyong viruses: evidence for distinct geographical lineages and distant evolutionary relationships. J Gen Virol *81(Pt 2)*: 471-9.

Powers AM, Aguilar PV, Chandler LJ, Brault AC, Meakins TA, Watts D, Russell KL, Olson J, Vasconcelos PF, Da Rosa AT, Weaver SC, Tesh RB (2006). Genetic relationships among Mayaro and Una viruses suggest distinct patterns of transmission. Am J Trop Med Hyg *75(3)*: 461-9.

Powers AM (2015). Risks to the Americas associated with the continued expansion of chikungunya virus. J Gen Virol *96(Pt 1)*: 1-5.

Pulgar, V.M. (2018). Transcytosis to cross the blood brain barrier, new advancements and challenges. Front Neurosci *12*: 1019.

Punjani A, Rubinstein JL, Fleet DJ, Brubaker MA (2017). cryoSPARC: algorithms for rapid unsupervised cryo-EM structure determination. Nat Methods *14(3)*: 290-296.

Purves D, Augustine GJ, Fitzpatrick D, et al., editors. Neuroscience. 2nd edition. Sunderland (MA): Sinauer Associates; 2001. The olfactory bulb. Available from: https://www.ncbi.nlm.nih.gov/books/NBK11158/

Qin ZL, Zheng Y, Kielian M (2009). Role of conserved histidine residues in the low-pH dependence of the Semliki Forest virus fusion protein. J Virol *83(9)*: 4670-7.

Qiu X, Wong G, Audet J, Bello A, Fernando L, Alimonti JB, Fausther-Bovendo H, Wei H, Aviles J, Hiatt E, Johnson A, Morton J, Swope K, Bohorov O, Bohorova N, Goodman C, Kim D, Pauly MH, Velasco J, Pettitt J, Olinger GG, Whaley K, Xu B, Strong JE, Zeitlin L, Kobinger GP (2014). Reversion of advanced Ebola virus disease in nonhuman primates with ZMapp. Nature *514*: 47–53.

Quiroz E, Aguilar PV, Cisneros J, Tesh RB, Weaver SC (2009). Venezuelan equine encephalitis in Panama: fatal endemic disease and genetic diversity of etiologic viral strains. PLoS Negl Trop Dis *3(6)*: e472.

Quiroz, J.A., Malonis, R.J., Thackray, L.B., Cohen, C.A., Pallesen, J., Jangra, R.K., Brown, R.S., Hofmann, D., Holtsberg, F.W., Shulenin, S.*, et al.* (2019). Human monoclonal antibodies against chikungunya virus target multiple distinct epitopes in the E1 and E2 glycoproteins. PLoS Pathog *15*: e1008061.

Rabinowitz SG, Adler WH (1973). Host defenses during primary Venezuelan equine encephalomyelitis virus infection in mice. I. Passive transfer of protection with immune serum and immune cells. J Immunol *110(5)*: 1345-53.

Reed DS, Lind CM, Sullivan LJ, Pratt WD, Parker MD (2004). Aerosol infection of cynomolgus macaques with enzootic strains of Venezuelan equine encephalitis viruses. J Infect Dis *189(6)*: 1013-7.

Reichert, E., Clase, A., Bacetty, A., and Larsen, J. (2009). Alphavirus antiviral drug development: scientific gap analysis and prospective research areas. Biosecur Bioterror *7*: 413-427.

Reynaud JM, Kim DY, Atasheva S, Rasalouskaya A, White JP, et al. (2015). IFIT1 differentially interferes with translation and replication of alphavirus genomes and promotes induction of type I interferon. PLOS Pathogens *11(4)*: e1004863.

Rico-Hesse, R., Roehrig, J.T., and Dickerman, R.W. (1988). Monoclonal antibodies define antigenic variation in the ID variety of Venezuelan equine encephalitis virus. Am J Trop Med Hyg *38*: 187-94.

Robinson MC (1955). An epidemic of virus disease in Southern Province, Tanganyika Territory, in 1952–53. I. Clinical features. Trans R Soc Trop Med Hyg *49(1)*: 28–32.

Roehrig, J.T., Day, J.W., and Kinney, R.M. (1982). Antigenic analysis of the surface glycoproteins of a Venezuelan equine encephalomyelitis virus (TC-83) using monoclonal antibodies. Virology *118*: 269-278.

Roehrig, J.T., and Mathews, J.H. (1985). The neutralization site on the E2 glycoprotein of Venezuelan equine encephalomyelitis (TC-83) virus is composed of multiple conformationally stable epitopes. Virology *142*: 347-356.

Roehrig, J.T., Hunt, A.R., Kinney, R.M., and Mathews, J.H. (1988). In vitro mechanisms of monoclonal antibody neutralization of alphaviruses. Virology *165*: 66-73.

Roehrig, J.T., Hunt, A.R., Chang, G.J., Sheik, B., Bolin, R.A., Tsai, T.F., and Trent, D.W. (1990) Identification of monoclonal antibodies capable of differentiating antigenic varieties of eastern equine encephalitis viruses. Am J Trop Med Hyg *42*: 394-8.

Roehrig, J.T., and Bolin, R.A. (1997). Monoclonal antibodies capable of distinguishing epizootic from enzootic varieties of subtype 1 Venezuelan equine encephalitis viruses in a rapid indirect immunofluorescence assay. J Clin Microbiol *35*: 1887-1890.

Rohou, A., and Grigorieff, N. (2015). CTFFIND4: Fast and accurate defocus estimation from electron micrographs. J Struct Biol *192*: 216-221.

Ronca, S.E., Dineley, K.T., and Paessler, S. (2016). Neurological sequelae resulting from encephalitic alphavirus infection. Front Microbiol *7*: 959.

Rose, P.P., Hanna, S.L., Spiridigliozzi, A., Wannissorn, N., Beiting, D.P., Ross, S.R., Hardy, R.W., Bambina, S.A., Heise, M.T., and Cherry, S. (2011). Natural resistance-associated macrophage protein is a cellular receptor for sindbis virus in both insect and mammalian hosts. Cell Host Microbe *10*: 97-104.

Roussel, A., Lescar, J., Vaney, M.C., Wengler, G., Wengler, G., and Rey, F.A. (2006). Structure and interactions at the viral surface of the envelope protein E1 of Semliki Forest virus. Structure *14*: 75-86.

Rowell JF, Griffin DE (2002). Contribution of T cells to mortality in neurovirulent Sindbis virus encephalomyelitis. J Neuroimmunol *127(1-2)*: 106-14.

Roy CJ, Adams AP, Wang E, Leal G, Seymour RL, Sivasubramani SK, Mega W, Frolov I, Didier PJ, Weaver SC (2013). A chimeric Sindbis-based vaccine protects cynomolgus macaques against a lethal aerosol challenge of eastern equine encephalitis virus. Vaccine *31(11)*: 1464-70.

Rudd PA, Wilson J, Gardner J, Larcher T, Babarit C, Le TT, Anraku I, Kumagai Y, Loo YM, Gale M Jr, Akira S, Khromykh AA, Suhrbier A (2012). Interferon response factors 3 and 7 protect against chikungunya virus hemorrhagic fever and shock. J Virol *86(18)*: 9888-98.

Rupp JC, Sokoloski KJ, Gebhart NN, Hardy RW (2015). Alphavirus RNA synthesis and non-structural protein functions. J Gen Virol *96(9)*: 2483-2500.

Ryman KD, Klimstra WB, Nguyen KB, Biron CA, Johnston RE (2000). Alpha/beta interferon protects adult mice from fatal Sindbis virus infection and is an important determinant of cell and tissue tropism. J Virol *74(7)*: 3366-78.

Ryman KD, Gardner CL, Burke CW, Meier KC, Thompson JM, Klimstra WB (2007). Heparan sulfate binding can contribute to the neurovirulence of neuroadapted and nonneuroadapted Sindbis viruses. J Virol *81(7)*: 3563-73.

Ryzhikov, AB, Ryabchikova, EI, Sergeev, AN, Tkacheva, NV (1995). Spread of Venezuelan equine encephalitis virus in mice olfactory tract. Arch Virol *140*: 2243–2254.

Sahoo, B., Gudigamolla, N.K., and Chowdary, T.K. (2020). Acidic pH-induced conformational changes in chikungunya virus fusion protein E1: a spring-twisted region in the domain I-III linker acts as a hinge point for swiveling motion of domains. J Virol *94*.

Salimi H, Cain MD, Jiang X, Roth RA, Beatty WL, Sun C, Klimstra WB, Hou J, and Klein RS (2020). Encephalitic alphaviruses exploit caveola-mediated transcytosis at the blood-brain barrier for central nervous system entry. *mBio* 11: e02731-19.

Sánchez-San Martín C, Sosa H, Kielian M (2008). A stable prefusion intermediate of the alphavirus fusion protein reveals critical features of class II membrane fusion. Cell Host Microbe *4(6)*: 600-8.

Sangha AK, Dong J, Williamson L, Hashiguchi T, Saphire EO, Crowe JE Jr, Meiler J (2017). Role of non-local interactions between CDR loops in binding affinity of MR78 antibody to Marburg virus glycoprotein. Structure *25(12)*: 1820-1828.e2.

Saphire EO, Schendel SL, Fusco ML, Gangavarapu K, Gunn BM, Wec AZ, Halfmann PJ, Brannan JM, Herbert AS, Qiu X, Wagh K, He S, Giorgi EE, Theiler J, Pommert KBJB, Krause TB, Turner HL, Murin CD, Pallesen J, Davidson E, Ahmed R, Aman MJ, Bukreyev A, Burton DR, Crowe JE Jr, Davis CW, Georgiou G, Krammer F, Kyratsous CA, Lai JR, Nykiforuk C, Pauly MH, Rijal P, Takada A, Townsend AR, Volchkov V, Walker LM, Wang C-I, Zeitlin L, Doranz BJ, Ward AB, Korber B, Kobinger GP, Andersen KG, Kawaoka Y, Alter G, Chandran K, Dye JM, Viral Hemorrhagic Fever Immunotherapeutic Consortium. 2018. Systematic analysis of monoclonal antibodies against ebola virus GP defines features that contribute to protection. Cell *174*: 938–952.e13.

Scheres, S.H. (2012). RELION: implementation of a Bayesian approach to cryo-EM structure determination. J Struct Biol *180*: 519-530.

Scheres, S.H., and Chen, S. (2012). Prevention of overfitting in cryo-EM structure determination. Nat Methods *9*: 853-854.

Schilte C, Buckwalter MR, Laird ME, Diamond MS, Schwartz O, Albert ML (2012). Cutting edge: independent roles for IRF-3 and IRF-7 in hematopoietic and nonhematopoietic cells during host response to chikungunya infection. J Immunol *188(7)*: 2967-71.

Schmaljohn, A.L., Kokubun, K.M., and Cole, G.A. (1983). Protective monoclonal antibodies define maturational and pH-dependent antigenic changes in Sindbis virus E1 glycoprotein. Virology *130*: 144-154.

Schneider AB, Ochsenreiter R, Hostager R, Hofacker IL, Janies D, Wolfinger MT (2019). Updated phylogeny of chikungunya virus suggests lineage-specific rna architecture. Viruses *11(9)*: 798.

Schnierle BS (2019). Cellular Attachment and Entry Factors for Chikungunya Virus. Viruses *11(11)*: 1078.

Schuffenecker, I., Iteman, I., Michault, A., Murri, S., Frangeul, L., Vaney, M-C., Lavenir, R., Pardigon, N., Reynes, J-M, Pettinelli, F., *et al*. (2006). Genome microevolution of chikungunya viruses causing the Indian Ocean outbreak. PLoS Med *3*: e263.

Schwartz O, Albert ML (2010). Biology and pathogenesis of chikungunya virus. Nat Rev Microbiol *8(7)*: 491-500.

Selvarajah, S., Sexton, N.R., Kahle, K.M., Fong, R.H., Mattia, K.A., Gardner, J., Lu, K., Liss, N.M., Salvador, B., Tucker, D.F*., et al.* (2013). A neutralizing monoclonal antibody targeting the acid-sensitive region in chikungunya virus E2 protects from disease. PLoS Negl Trop Dis *7*: e2423.

Setliff I, Shiakolas AR, Pilewski KA, Murji AA, Mapengo RE, Janowska K, Richardson S, Oosthuysen C, Raju N, Ronsard L, Kanekiyo M, Qin JS, Kramer KJ, Greenplate AR, McDonnell WJ, Graham BS, Connors M, Lingwood D, Acharya P, Morris L, Georgiev IS (2019). High-throughput mapping of b cell receptor sequences to antigen specificity. Cell *179(7)*: 1636-1646.e15.

Shaw C, Panther L, August A, Zaks T, Smolenov I, Bart S, Watson M (2019). Safety and immunogenicity of a mRNA-based chikungunya vaccine in a phase 1 dose-ranging trial. International Journal of Infectious Disease *79(Suppl 1)*: 17.

Sheehan J, Marasco WA (2015). Phage and yeast display. Microbiol Spectr *3(1)*: AID-0028-2014.

Sherwood, J.A., Stehman, S.V., Howard, J.J., and Oliver, J. (2020). Cases of Eastern equine encephalitis in humans associated with Aedes canadensis, Coquillettidia perturbans and Culiseta melanura mosquitoes with the virus in New York State from 1971 to 2012 by analysis of aggregated published data. Epidemiol Infect *148*: e72.

Shi B, Ma L, He X, Wang X, Wang P, Zhou L, Yao X (2014). Comparative analysis of human and mouse immunoglobulin variable heavy regions from IMGT/LIGM-DB with IMGT/HighV-QUEST. Theor Biol Med Model *11*: 30.

Shields RL, Lai J, Keck R, O'Connell LY, Hong K, Meng YG, Weikert SH, Presta LG (2002). Lack of fucose on human IgG1 N-linked oligosaccharide improves binding to human Fcgamma RIII and antibody-dependent cellular toxicity. J Biol Chem *277(30)*: 26733-40.

Shirako Y, Strauss JH (1994). Regulation of Sindbis virus RNA replication: uncleaved P123 and nsP4 function in minus-strand RNA synthesis, whereas cleaved products from P123 are required for efficient plus-strand RNA synthesis. J Virol *68(3)*: 1874-85.

Shultz, L. D., Brehm, M. A., Bavari, S., & Greiner, D. L. (2011). Humanized mice as a preclinical tool for infectious disease and biomedical research. Annals of the New York Academy of Sciences *1245*: 50–54.

Sidwell, R.W., and Smee, D.F. (2003). Viruses of the Bunya- and Togaviridae families: potential as bioterrorism agents and means of control. Antiviral Res *57*: 101-111.

Singh I, Helenius A (1992). Role of ribosomes in Semliki Forest virus nucleocapsid uncoating. J Virol *66(12)*: 7049-58.

Sjöberg M, Lindqvist B, Garoff H (2011). Activation of the alphavirus spike protein is suppressed by bound E3. J Virol *85(11)*: 5644-50.

Smit JM, Waarts BL, Kimata K, Klimstra WB, Bittman R, Wilschut J (2002). Adaptation of alphaviruses to heparan sulfate: interaction of Sindbis and Semliki forest viruses with liposomes containing lipid-conjugated heparin. J Virol *76(20)*: 10128-37.

Smith JL, Pugh CL, Cisney ED, Keasey SL, Guevara C, Ampuero JS, Comach G, Gomez D, Ochoa-Diaz M, Hontz RD, Ulrich RG (2018). Human antibody responses to emerging Mayaro virus and cocirculating alphavirus infections examined by using structural proteins from nine New and Old world lineages. mSphere *3(2)*: e00003-18.

Smith, S.A., Silva, L.A., Fox, J.M., Flyak, A.I., Kose, N., Sapparapu, G., Khomandiak, S., Ashbrook, A.W., Kahle, K.M., Fong, R.H.*, et al.* (2015). Isolation and characterization of broad and ultrapotent human monoclonal antibodies with therapeutic activity against chikungunya virus. Cell Host Microbe *18*: 86-95.

Smith SA, Crowe JE Jr. (2015). Use of human hybridoma technology to isolate human monoclonal antibodies. Microbiol Spectr *3(1)*: AID-0027-2014.

Smith TJ, Olson NH, Cheng RH, Liu H, Chase ES, Lee WM, Leippe DM, Mosser AG, Rueckert RR, Baker TS (1993). Structure of human rhinovirus complexed with Fab fragments from a neutralizing antibody. J Virol *67(3)*: 1148-58.

Snyder JE, Kulcsar KA, Schultz KL, Riley CP, Neary JT, Marr S, Jose J, Griffin DE, Kuhn RJ (2013). Functional characterization of the alphavirus TF protein. J Virol *87(15)*: 8511-23.

Sok D, Burton DR (2018). Recent progress in broadly neutralizing antibodies to HIV. Nat Immunol *19(11)*: 1179-1188.

Soonsawad P, Xing L, Milla E, Espinoza JM, Kawano M, Marko M, Hsieh C, Furukawa H, Kawasaki M, Weerachatyanukul W, Srivastava R, Barnett SW, Srivastava IK, Cheng

RH (2010). Structural evidence of glycoprotein assembly in cellular membrane compartments prior to Alphavirus budding. J Virol *84(21)*: 11145-51.

Sorzano, C.O., de la Rosa Trevin, J.M., Oton, J., Vega, J.J., Cuenca, J., Zaldivar-Peraza, A., Gomez-Blanco, J., Vargas, J., Quintana, A., Marabini, R.*, et al.* (2013). Semiautomatic, high-throughput, high-resolution protocol for three-dimensional reconstruction of single particles in electron microscopy. Methods Mol Biol *950*: 171-193.

Soto, C., Finn, J.A., Willis, J.R., Day, S.B., Sinkovits, R.S., Jones, T., Schmitz, S., Meiler, J., Branchizio, A., and Crowe, J.E. (2020). PyIR: a scalable wrapper for processing billions of immunoglobulin and T cell receptor sequences using IgBLAST. BMC Bioinformatics *21*: 314.

Sourisseau M, Schilte C, Casartelli N, Trouillet C, Guivel-Benhassine F, Rudnicka D, Sol-Foulon N, Le Roux K, Prevost MC, Fsihi H, Frenkiel MP, Blanchet F, Afonso PV, Ceccaldi PE, Ozden S, Gessain A, Schuffenecker I, Verhasselt B, Zamborlini A, Saïb A, Rey FA, Arenzana-Seisdedos F, Desprès P, Michault A, Albert ML, Schwartz O (2007). Characterization of reemerging chikungunya virus. PLoS Pathog *3(6)*: e89.

Stapleford, K.A., Coffey, L.L., Lay, S., Bordería, A.V., Duong, V., Isakov, O., Rozen-Gagnon, K., Arias-Goeta, C., Blanc, H., Beaucourt, S., *et al.* (2014). Emergence and

transmission of arbovirus evolutionary intermediates with epidemic potential. Cell Host Microbe *15*: 706-16.

Strauss JH, Strauss EG (1994). The alphaviruses: gene expression, replication, and evolution. Microbiol Rev *58(3)*: 491-562.

Suhrbier A, Mahalingam S (2009). The immunobiology of viral arthritides. Pharmacol Ther *124(3)*: 301-8.

Suhrbier, A., Jaffar-Bandjee, M.C., and Gasque, P. (2012). Arthritogenic alphaviruses--an overview. Nat Rev Rheumatol *8*, 420-429.

Sun, E., Zhao, J., Sun, L., Xu, Q., Yang, T., Qin, Y., Wang, W., Wei, P., Sun, J., and Wu, D. (2013a). Comprehensive mapping of common immunodominant epitopes in the eastern equine encephalitis virus E2 protein recognized by avian antibody responses. PLoS One *8*: e69349.

Sun, S., Xiang, Y., Akahata, W., Holdaway, H., Pal, P., Zhang, X., Diamond, M.S., Nabel, G.J., and Rossmann, M.G. (2013b). Structural analyses at pseudo atomic resolution of Chikungunya virus and antibodies show mechanisms of neutralization. Elife *2*: e00435.

Sun C, Gardner CL, Watson AM, Ryman KD, and Klimstra WB (2014). Stable, high-level expression of reporter proteins from improved alphavirus expression vectors to track replication and dissemination during encephalitic and arthritogenic disease. J Virol *88*: 2035-2046.

Suomalainen M, Liljeström P, Garoff H (1992). Spike protein-nucleocapsid interactions drive the budding of alphaviruses. J Virol *66(8)*: 4737-47.

Tan, Y., Lam, T.T-Y., Heberlein-Larson, L.A., Smole, S.C., Auguste, A.J., Hennigan, S., Halpin, R.A., Fedorova, N., Puri, V., Stockwell, T.B., *et al.* (2018). Large-scale complete-genome sequencing and phylodynamic analysis of eastern equine encephalitis virus reveals source-sink transmission dynamics in the United States. J Virol *92*: e00074-18.

Teo TH, Lum FM, Claser C, Lulla V, Lulla A, Merits A, Rénia L, Ng LF (2013). A pathogenic role for CD4+ T cells during chikungunya virus infection in mice. J Immunol 190(1): 259-69.

Thomas AA, Vrijsen R, Boeyé A (1986). Relationship between poliovirus neutralization and aggregation. J Virol *59(2)*: 479-85.

Tiwari M, Parida M, Santhosh SR, Khan M, Dash P, Rao PV (2009). Assessment of immunogenic potential of Vero adapted formalin inactivated vaccine derived from novel ECSA genotype of chikungunya virus. Vaccine *27*: 2513–2522.

Traggiai E, Becker S, Subbarao K, Kolesnikova L, Uematsu Y, Gismondo MR, Murphy BR, Rappuoli R, Lanzavecchia A (2004). An efficient method to make human monoclonal antibodies from memory B cells: potent neutralization of SARS coronavirus. Nat Med *10(8)*: 871-5.

Trobaugh, D.W., Sun, C., Dunn, M.D., Reed, D.S., and Klimstra, W.B. (2019). Rational design of a live-attenuated Eastern equine encephalitis virus vaccine through informed mutation of virulence determinants. PLoS Pathog *15*: e1007584.

Tsetsarkin, K., Higgs, S., McGee, C.E., De Lamballerie, X., Charrel, R.N., and Vanlandingham, D.L. (2006). Infectious clones of chikungunya virus (La Réunion isolate) for vector competence studies. Vector Borne Zoonotic Dis *6*: 325-337.

Tsetsarkin KA, Vanlandingham DL, McGee CE, Higgs S (2007). A single mutation in chikungunya virus affects vector specificity and epidemic potential. PLOS Pathogens *3(12)*: e201.

Tsetsarkin KA, Weaver SC (2011). Sequential adaptive mutations enhance efficient

vector switching by chikungunya virus and its epidemic emergence. PLOS Pathogens *7(12)*: e1002412.

Turchaninova, M.A., Davydov, A., Britanova, O.V., Shugay, M., Bikos, V., Egorov, E.S., Kirgizova, V.I., Merzlyak, E.M., Staroverov, D.B., Bolotin, D.A.*, et al.* (2016). High-quality full-length immunoglobulin profiling with unique molecular barcoding. Nat Protoc *11*: 1599-1616.

Turula, H., and Wobus, C.E. (2018). The role of the polymeric immunoglobulin receptor and secretory immunoglobulins during mucosal infection and immunity. Viruses *10*: 237.

Tyor W. R., Wesselingh S., Levine B., Griffin D. E. (1992). Long-term intraparenchymal Ig secretion after acute viral encephalitis in mice. J. Immunol *149*: 4016–4020.

Tyor WR, Griffin DE (1993). Virus specificity and isotype expression of intraparenchymal antibody-secreting cells during Sindbis virus encephalitis in mice. J Neuroimmunol *48(1)*: 37-44.

Ubol S, Tucker PC, Griffin DE, Hardwick JM (1994). Neurovirulent strains of alphavirus induce apoptosis in bcl-2-expressing cells: role of a single amino acid change in the E2 glycoprotein. Proc Natl Acad Sci USA *91(11)*: 5202-6.

Uchime O, Fields W, Kielian M (2013). The role of E3 in pH protection during alphavirus assembly and exit. J Virol *87(18)*: 10255-62.

Vazeille, M., Moutailler, S., Coudrier, D., Rousseaux, C., Khun, H., Huerre, M., Thiria, J., Dehecq, J-S., Fontenille, D., Schuffenecker, I., *et al*. (2007). Two chikungunya isolates from the outbreak of La Reunion (Indian Ocean) exhibit different patterns of infection in the mosquito, Aedes albopictus. PLoS One *2*: e1168.

Vinuela-Berni, V., Gomez-Gonzalez, B., and Quintanar-Stephano, A. (2020). Blockade of Arginine Vasopressin receptors prevents blood-brain barrier breakdown in Experimental Autoimmune Encephalomyelitis. Sci Rep *10*: 467.

Vogel P, Kell WM, Fritz DL, Parker MD, Schoepp RJ (2005). Early events in the pathogenesis of eastern equine encephalitis virus in mice. Am J Pathol *166(1)*: 159-71.

Vogt MR, Fu J, Kose N, Williamson LE, Bombardi R, Setliff I, Georgiev IS, Klose T, Rossmann MG, Bochkov YA, Gern JE, Kuhn RJ, Crowe JE Jr. (2020). Human antibodies neutralize enterovirus D68 and protect against infection and paralytic disease. Sci Immunol *5(49)*: eaba4902.

Voss, J.E., Vaney, M.C., Duquerroy, S., Vonrhein, C., Girard-Blanc, C., Crublet, E., Thompson, A., Bricogne, G., and Rey, F.A. (2010). Glycoprotein organization of chikungunya virus particles revealed by X-ray crystallography. Nature *468*: 709-712.

Wahlberg, J.M. and Garoff, H. (1992). Membrane fusion process of Semliki Forest virus. I: Low pH-induced rearrangement in spike protein quaternary structure precedes virus penetration into cells. J Cell Biol *116*: 339-48.

Wahlberg, J.M., Bron R., Wilschut, J., and Garoff, H. (1992). Membrane fusion of Semliki Forest virus involves homotrimers of the fusion protein. J Virol *66*: 7309-18.

Walton TE, Alvarez O, Jr., Buckwalter RM, Johnson KM (1973). Experimental infection of horses with enzootic and epizootic strains of Venezuelan equine encephalomyelitis virus. Journal of Infectious Diseases *128*: 271–282.

Walton TE, Grayson MA. Venezuelan equine encephalomyelitis. In: Monath TP, editor. The Arboviruses: Epidemiology and Ecology. vol. IV. CRC Press; Boca Raton, FL: 1988. pp. 203–231.

Wang E, Bowen RA, Medina G, Powers AM, Kang W, Chandler LM, Shope RE, Weaver SC (2001). Virulence and viremia characteristics of 1992 epizootic subtype IC

Venezuelan equine encephalitis viruses and closely related enzootic subtype ID strains. American Journal of Tropical Medicine and Hygiene *65*: 64–69.

Wang E, Volkova E, Adams AP, Forrester N, Xiao SY, Frolov I, Weaver SC (2008). Chimeric alphavirus vaccine candidates for chikungunya. Vaccine *26(39)*: 5030-9.

Wang E, Kim DY, Weaver SC, Frolov I (2011). Chimeric chikungunya viruses are nonpathogenic in highly sensitive mouse models but efficiently induce a protective immune response. J Virol *85(17)*: 9249-52.

Weaver SC, Kang W, Shirako Y, Rumenapf T, Strauss EG, Strauss JH (1997). Recombinational history and molecular evolution of western equine encephalomyelitis complex alphaviruses. Journal of Virology *71*: 613–623.

Weaver SC, Ferro C, Barrera R, Boshell J, Navarro JC (2004). Venezuelan equine encephalitis. Annual Review of Entomology *49*: 141–174.

Weaver SC, Frey TK, Huang HV, Kinney RM, Rice CM, Roehrig JT, Shope RE, Strauss EG. Togaviridae. In: Fauquet CM, Mayo MA, Maniloff J, Desselberger U, Ball LA, editors. Virus Taxonomy, VIII Report of the ICTV. Elsevier/Academic Press; London: 2005. pp. 999–1008.

Weaver SC (2006). Evolutionary influences in arboviral disease. Current Topics in Microbiology and Immunology *299*: 285–314.

Weaver SC, Winegar R, Manger ID, Forrester NL (2012). Alphaviruses: population genetics and determinants of emergence. Antiviral Res *94(3)*: 242-57.

Weaver S. C. (2014). Arrival of chikungunya virus in the new world: prospects for spread and impact on public health. PLoS neglected tropical diseases *8(6)*: e2921.

Weaver SC, Forrester NL (2015). Chikungunya: evolutionary history and recent epidemic spread. Antiviral Res *120*: 32-9.

Webster RG, Laver WG (1967). Preparation and properties of antibody directed specifically against the neuraminidase of influenza virus. J Immunol *99(1)*: 49-55.

Wec AZ, Nyakatura EK, Herbert AS, Howell KA, Holtsberg FW, Bakken RR, Mittler E, Christin JR, Shulenin S, Jangra RK, Bharrhan S, Kuehne AI, Bornholdt ZA, Flyak AI, Saphire EO, Crowe JE Jr, Aman MJ, Dye JM, Lai JR, Chandran K (2016). A “Trojan horse” bispecific-antibody strategy for broad protection against ebolaviruses. Science *354*: 350–354.

Wec AZ, Herbert AS, Murin CD, Nyakatura EK, Abelson DM, Fels JM, He S, James RM, La Vega M-AA, de Zhu W, Bakken RR, Goodwin E, Turner HL, Jangra RK, Zeitlin L, Qiu X, Lai JR, Walker LM, Ward AB, Dye JM, Chandran K, Bornholdt ZA (2017). Antibodies from a human survivor define sites of vulnerability for broad protection against ebolaviruses. Cell *169*: 878–890.e15.

Wengler G, Würkner D, Wengler G (1992). Identification of a sequence element in the alphavirus core protein which mediates interaction of cores with ribosomes and the disassembly of cores. Virology *191(2)*: 880-8.

Wengler, G., Wengler, G., and Rey, F.A. (1999). The isolation of the ectodomain of the alphavirus E1 protein as a soluble hemagglutinin and its crystallization. Virology *257*: 472-482.

White L.J., Wang J.G., Davis N.L., Johnston R.E. (2001). Role of alpha/beta interferon in Venezuelan equine encephalitis virus pathogenesis: effect of an attenuating mutation in the 5′ untranslated region. J. Virol *75*: 3706–3718.

Williamson LE, Flyak AI, Kose N, Bombardi R, Branchizio A, Reddy S, Davidson E, Doranz BJ, Fusco ML, Saphire EO, Halfmann PJ, Kawaoka Y, Piper AE, Glass PJ, Crowe JE Jr. (2019). Early human B cell response to Ebola virus in four U.S. survivors of infection. J Virol *93(8)*: e01439-18.

Williamson, L.E., Gilliland, T., Yadav, P.K., Binshtein, E., Bombardi, R., Kose, N., Nargi, R.S., Sutton, R.E., Durie, C.L., Armstrong, E., *et al.* (2020). Human antibodies protect against aerosolized Eastern equine encephalitis virus infection. Cell *S0092-8674*: 31528-2.

Williamson LE, Reeder KM, Bailey K, Roy V, Fouch ME, Kose N, Trivette A, Nargi RS, Winkler ES, Kim AS, Gainza C, Rodriguez J, Armstrong E, Sutton RE, Reidy J, Carnahan R, Klimstra WB, Diamond MS, Davidson E, Doranz BJ, Alter G, Julander JG, Crowe JE Jr. (2020). Protective E1-specific human alphavirus antibodies recognize cryptic viral epitopes. Cell. In review.

World health organization (WHO) website, https://www.who.int/news-room/fact-sheets/detail/chikungunya, accessed on January 31st, 2021.

Yactayo, S., Staples, J.E., Millot, V., Cibrelus, L., and Ramon-Pardo, P. (2016). Epidemiology of chikungunya in the Americas. J Infect Dis *214*, S441-S445.

Yap, M.L., Klose, T., Urakami, A., Hasan, S.S., Akahata, W., and Rossmann, M.G. (2017). Structural studies of Chikungunya virus maturation. Proc Natl Acad Sci USA *114*: 13703-13707.

Young NA, Johnson KM (1969a). Antigenic variants of Venezuelan equine encephalitis virus: their geographic distribution and epidemiologic significance. American Journal of Epidemiology. *89*:286–307.

Yu, X., McGraw, P.A., House, F.S., and Crowe, J.E., Jr. (2008a). An optimized electrofusion-based protocol for generating virus-specific human monoclonal antibodies. J Immunol Methods *336*: 142-151.

Yu, X., Tsibane, T., McGraw, P.A., House, F.S., Keefer, C.J., Hicar, M.D., Tumpey, T.M., Pappas, C., Perrone, L.A., Martinez, O.*, et al.* (2008b). Neutralizing antibodies derived from the B cells of 1918 influenza pandemic survivors. Nature *455*: 532-536.

Yuan M, Wu NC, Zhu X, Lee CD, So RTY, Lv H, Mok CKP, Wilson IA (2020). A highly conserved cryptic epitope in the receptor binding domains of SARS-CoV-2 and SARS-CoV. Science *368(6491)*: 630-633.

Yun NE, Peng BH, Bertke AS, Borisevich V, Smith JK, Smith JN, Poussard AL, Salazar M, Judy BM, Zacks MA, Estes DM, Paessler S (2009). CD4+ T cells provide protection against acute lethal encephalitis caused by Venezuelan equine encephalitis virus. Vaccine *27(30)*: 4064-73.

Zeng X, Mukhopadhyay S, Brooks CL 3rd. Residue-level resolution of alphavirus envelope protein interactions in pH-dependent fusion. Proc Natl Acad Sci USA. 2015 *112(7)*: 2034-9.

Zhang, K. (2016). Gctf: Real-time CTF determination and correction. J Struct Biol *193*: 1-12.

Zhang, R., Hryc, C.F., Cong, Y., Liu, X., Jakana, J., Gorchakov, R., Baker, M.L., Weaver, S.C., and Chiu, W. (2011). 4.4 A cryo-EM structure of an enveloped alphavirus Venezuelan equine encephalitis virus. EMBO J *30*: 3854-3863.

Zhang, R., Kim, A.S., Fox, J.M., Nair, S., Basore, K., Klimstra, W.B., Rimkunas, R., Fong, R.H., Lin, H., Poddar, S.*, et al.* (2018). Mxra8 is a receptor for multiple arthritogenic alphaviruses. Nature *557*: 570-574.

Zhang S, Loy T, Ng TS, Lim XN, Chew SV, Tan TY, Xu M, Kostyuchenko VA, Tukijan F, Shi J, Fink K, Lok SM (2020). A human antibody neutralizes different flaviviruses by using different mechanisms. Cell Rep *31(4)*: 107584.

Zhang X, Fugère M, Day R, Kielian M (2003). Furin processing and proteolytic activation of Semliki Forest virus. J Virol *77(5)*: 2981-9.

Zhao H, Lindqvist B, Garoff H, von Bonsdorff CH, Liljeström P (1994). A tyrosine-based motif in the cytoplasmic domain of the alphavirus envelope protein is essential for budding. EMBO J *13(18)*: 4204-11.

Zhao, J., Sun, E.C., Liu, N.H., Yang, T., Xu, Q.Y., Qin, Y.L., Yang, Y.H., and Wu, D.L. (2012). Phage display identifies an Eastern equine encephalitis virus glycoprotein E2-specific B cell epitope. Vet Immunol Immunopathol *148*: 364-368.

Zhao Y, Ren J, Harlos K, Jones DM, Zeltina A, Bowden TA, Padilla-Parra S, Fry EE, Stuart DI. 2016. Toremifene interacts with and destabilizes the Ebola virus glycoprotein. Nature *535*: 169–172.

Zheng, S.Q., Palovcak, E., Armache, J.P., Verba, K.A., Cheng, Y., and Agard, D.A. (2017). MotionCor2: anisotropic correction of beam-induced motion for improved cryo-electron microscopy. Nat Methods *14*: 331-332.

Zheng Y, Sánchez-San Martín C, Qin ZL, Kielian M (2011). The domain I-domain III linker plays an important role in the fusogenic conformational change of the alphavirus membrane fusion protein. J Virol *85(13)*: 6334-42.

Zhou QF, Fox JM, Earnest JT, Ng TS, Kim AS, Fibriansah G, Kostyuchenko VA, Shi J, Shu B, Diamond MS, Lok SM (2020). Structural basis of chikungunya virus inhibition by monoclonal antibodies. Proc Natl Acad Sci USA *117(44)*: 27637-27645.

Zivanov, J., Nakane, T., Forsberg, B.O., Kimanius, D., Hagen, W.J., Lindahl, E., and Scheres, S.H. (2018). New tools for automated high-resolution cryo-EM structure determination in RELION-3. Elife *7*.

Zost, S.J., Gilchuk, P., Case, J.B., Binshtein, E., Chen, R.E., Nkolola, J.P., Shafer, A., Reidy, J.X., Trivette, A., Nargi, R.S., *et al.* (2020). Potently neutralizing and protective human antibodies against SARS-CoV-2. Nature *584*: 443-449.